

# Porewater Geochemistry, Method Comparison and Opalinus Clay – Passwang Formation Interface Study at the Mont Terri URL

**NWMO-TR-2017-10**

**June 2017**

**H.Niklaus Waber and Daniel Rufer**

Rock-Water Interaction, Institute of Geological Sciences  
University of Bern, Switzerland

**nwmo**

NUCLEAR WASTE  
MANAGEMENT  
ORGANIZATION

SOCIÉTÉ DE GESTION  
DES DÉCHETS  
NUCLÉAIRES



**Nuclear Waste Management Organization**  
22 St. Clair Avenue East, 6<sup>th</sup> Floor  
Toronto, Ontario  
M4T 2S3  
Canada

Tel: 416-934-9814  
Web: [www.nwmo.ca](http://www.nwmo.ca)

# **Porewater Geochemistry, Method Comparison and Opalinus Clay – Passwang Formation Interface Study at the Mont Terri URL**

**NWMO-TR-2017-10**

June 2017

**H. Niklaus Waber and Daniel Rufer**

Water-Rock Interaction, Institute of Geological Sciences, University of  
Bern, Switzerland

This report has been prepared at the University of Bern, under contract to the NWMO, as part of a joint project between the following members of the Mont Terri Consortium: NWMO, NAGRA, IRSN and Swisstopo. The report has been reviewed by the NWMO and contributing authors. The views and conclusions are those of the author(s) and do not necessarily represent those of the NWMO.

### Document History

Title:	Porewater Geochemistry, Method Comparison and Opalinus Clay – Passwang Formation Interface Study at the Mont Terri URL		
Report Number:	NWMO-TR-2017-10		
Revision:	R000	Date:	June 2017
Report Contributors			
Authored by:	H.N. Waber and D. Rufer (Rock-Water Interaction, Institute of Geological Sciences, University of Bern, Switzerland)		
Reviewed by:	D. Traber (Nagra), M. Mazurek (University of Bern)		
Approved by:	H.N. Waber		
Nuclear Waste Management Organization			
Reviewed by:	Laura Kennell-Morrison		
Accepted by:	Mark Jensen		

**ABSTRACT**

**Title:** Porewater Geochemistry, Method Comparison and Opalinus Clay–Passwang Formation Interface Study at the Mont Terri URL  
**Report No.:** NWMO-TR-2017-10  
**Author(s):** H. Niklaus Waber & D. Rufer  
**Company:** Rock-Water Interaction, Institute of Geological Sciences, University of Bern, Switzerland  
**Date:** June 2017

**Abstract**

The present study focuses on the geochemical characterisation of porewater solutes in the Opalinus Clay at the Mont Terri URL. The investigations were carried out within the Mont Terri Project DB-A Experiment (Deep inclined borehole across the Opalinus Clay) conducted by an international consortium. At the Mont Terri URL, borehole BDB-1 is the first borehole that crosscuts the Opalinus Clay in its entire thickness. Borehole BDB-1 cuts across the Jurassic sediment sequence of low-permeability rock, from the Hauptrogenstein, across the Passwang Formation (Fm) and the Opalinus Clay, and into the rocks of the Staffelegg Formation (Fm). This allowed, for the first time, collection of porewater samples at a high spatial frequency. Furthermore, all samples experienced the same history in drilling, sampling and laboratory treatment. This facilitates identification of artefacts induced by indirect porewater characterisation techniques and allows improved interpretation of the data in terms of porewater evolution as a function of space and time. In addition, groundwater could be collected from a water-conducting zone in the Passwang Fm at 58.6m BHL, but was not encountered in the lithologies in the footwall of the Opalinus Clay.

The different natural tracers in the porewater ( $\text{Cl}^-$ ,  $\delta^{37}\text{Cl}$ ,  $\text{Br}^-$ ,  $\delta^{18}\text{O}$ ,  $\delta^2\text{H}$ , He,  $^3\text{He}/^4\text{He}$ , Ar) all describe well-defined concentration profiles from the Staffelegg Fm across the Opalinus Clay into the Passwang Fm. The concentration profiles of all tracers indicate diffusion as the dominant solute transport process across the Opalinus Clay. These findings are in accordance with previous work conducted at the Mont Terri URL (Pearson et al. 2003; Mazurek et al. 2009, 2011). In the rocks of the Passwang Fm, the tracer concentrations display more complex profiles that are, at least, partly due to the poor knowledge about anion-accessible porosity in the low clay-content rocks. Chemical compounds and noble gas concentrations indicate local minima at locations closer to the Opalinus Clay than the present-day water-conducting zone. These local minima are also observed in isotope and ion-ion ratios, independent of any porosity value, and are interpreted to have acted at some time in the past as boundary conditions for the solute exchange between the Opalinus Clay and the Passwang Fm. Quantification of the  $^4\text{He}$  concentration profile suggest that these old boundaries may have been active until a few tens to a hundred thousand of years ago.

Ion-ion ratios in aqueous extract solutions reveal similarly well-defined profiles across the Opalinus Clay into the Passwang Fm. Ratios of  $\text{Br}/\text{Cl}$  and  $\text{SO}_4/\text{Cl}$  are below and above, respectively, those of modern seawater. Consistent with all natural porewater tracers, these ratios are best explained by long-term exchange between porewater in the Opalinus Clay with porewater or groundwater in the Triassic evaporite sequences underlying the Opalinus Clay. This contrasts previous interpretations, which assumed residual seawater as the main origin of solutes in porewater of the Opalinus Clay (e.g., Pearson and Waber 2001; Pearson et al. 2003; Mazurek and de Haller 2017). It is, however, not in conflict with the most recent history of tracer profile evolution over the last few millions of years (e.g., Mazurek et al. 2009, 2011).

The present data, combined with geochemical modelling, indicate that the  $\text{SO}_4^{2-}$  concentrations obtained by aqueous extraction are compatible with the geochemical properties of the Opalinus Clay rocks (such as the cation exchange properties and mineral equilibria) when compared to  $\text{SO}_4^{2-}$  concentrations obtained by high-pressure squeezing and water accumulated over long time periods from boreholes, where potential for oxidation exists prior to analysis. It is concluded that the  $\text{SO}_4^{2-}$  concentration obtained from aqueous extraction serves as a suitable proxy for the in-situ porewater  $\text{SO}_4^{2-}$  concentration. For future modelling of the porewater composition of the Opalinus Clay at Mont Terri, it is recommended to use the  $\text{SO}_4/\text{Cl}$  ratio obtained in cautiously prepared aqueous extract solutions instead of the seawater  $\text{SO}_4/\text{Cl}$  ratio or fixation of the  $\text{SO}_4^{2-}$  concentration by mineral solubility controls.

**TABLE OF CONTENTS**

	<b><u>Page</u></b>
<b>ABSTRACT .....</b>	<b>iii</b>
<b>1. INTRODUCTION.....</b>	<b>1</b>
<b>2. DRILLING OPERATIONS.....</b>	<b>5</b>
<b>3. DRILL-CORE SAMPLING FOR POREWATER INVESTIGATIONS .....</b>	<b>6</b>
<b>3.1 Core Sampling Strategy and Sample Types .....</b>	<b>6</b>
<b>3.2 Core Handling, Sampling Procedures and Laboratory Analyses .....</b>	<b>7</b>
3.2.1 Porewater Chemistry Samples .....	10
3.2.2 Porewater Noble Gas Samples .....	13
<b>4. GROUNDWATER SAMPLING .....</b>	<b>18</b>
<b>5. ANALYTICAL METHODS.....</b>	<b>20</b>
<b>5.1 MINERALOGICAL ANALYSES.....</b>	<b>20</b>
5.1.1 Whole Rock Mineralogy.....	20
5.1.2 Inorganic Carbon, Organic Carbon and Total Sulphur of Whole Rock.....	20
5.1.3 Clay Mineralogy.....	21
<b>5.2 PETROPHYSICAL PARAMETERS.....</b>	<b>21</b>
5.2.1 Water Loss, Mass of Porewater and Gravimetric Water Content.....	21
5.2.2 Bulk and Grain Density.....	23
5.2.3 Pycnometer Porosity and Water-Loss Porosity.....	24
5.2.4 Specific Surface Area (BET).....	26
<b>5.3 AQUEOUS EXTRACTION .....</b>	<b>26</b>
5.3.1 Chemical Analyses of extract solutions .....	27
5.3.2 Chloride Isotope Analyses of Extract Solutions and Groundwater .....	27
5.3.3 Conversion of Aqueous Extract Data to Porewater Concentrations .....	28
<b>5.4 ISOTOPE DIFFUSIVE EXCHANGE TECHNIQUE .....</b>	<b>29</b>
5.4.1 Water Content by the Isotope Diffusive Exchange Technique .....	31
5.4.1.1 Uncertainty .....	32
5.4.2 Derivation of Isotope Porewater Isotope Composition .....	32
5.4.2.1 Uncertainty .....	32
<b>5.5 NOBLE GAS ANALYSES.....</b>	<b>33</b>
5.5.1 Uncertainty on Noble Gas Measurements.....	36
5.5.2 Analytical Uncertainty Versus Total Uncertainty.....	37
5.5.3 Analytical Limits and Accuracy .....	38
5.5.4 Monitoring Analytical Accuracy and Precision Using Reference Gases.....	39
5.5.5 A Note Concerning the <sup>40</sup> Ar/ <sup>36</sup> Ar Reference Value for Air.....	43
<b>5.6 NOBLE GAS AND PARENT RADIONUCLIDE ANALYSES ON ROCK         SAMPLES. ....</b>	<b>43</b>
<b>5.7 GROUNDWATER ANALYSES.....</b>	<b>43</b>
5.7.1 On-site measurements .....	43
5.7.2 Chemical and Isotope Analyses .....	44
<b>6. ROCK COMPOSITION AND WATER-CONDUCTING FEATURES .....</b>	<b>45</b>
<b>6.1 WHOLE ROCK MINERALOGY .....</b>	<b>45</b>
<b>6.2 CLAY MINERALOGY .....</b>	<b>49</b>

6.3	<b>OPEN FRACTURES, WATER-CONDUCTING FEATURES AND WET SPOTS</b>	<b>51</b>
7.	<b>PETROPHYSICAL PARAMETERS</b>	<b>58</b>
7.1	<b>GRAIN AND BULK DENSITY</b>	<b>58</b>
7.2	<b>PYCNOMETER POROSITY</b>	<b>60</b>
7.3	<b>WATER CONTENT</b>	<b>61</b>
7.3.1	Water Content from Water Loss	61
7.3.2	Water Content from Isotope Mass Balance	63
7.4	<b>WATER-LOSS POROSITY</b>	<b>66</b>
7.5	<b>WATER CONTENT AND POROSITY OF POREWATER NOBLE GAS SAMPLES</b>	<b>69</b>
7.6	<b>SPECIFIC SURFACE AREA (N<sub>2</sub>-BET)</b>	<b>72</b>
8.	<b>AQUEOUS EXTRACTION DATA</b>	<b>80</b>
8.1	<b>PASSWANG FORMATION ROCKS</b>	<b>81</b>
8.2	<b>OPALINUS CLAY ROCKS</b>	<b>83</b>
8.3	<b>STAFFELEGG FORMATION ROCKS</b>	<b>86</b>
8.4	<b>GENERAL FEATURES OF AQUEOUS EXTRACT SOLUTIONS</b>	<b>87</b>
8.5	<b>MOBILE ELEMENTS (Cl, Br)</b>	<b>88</b>
8.6	<b>ORIGIN OF SULPHATE</b>	<b>92</b>
8.6.1	Sulphur Inventory in the Rock	93
8.6.2	Sulphate in Borehole Water and Squeezed Water	93
8.6.3	Sulphate in Aqueous Extract Solutions	96
8.6.4	Summary About Origin of Sulphate	105
9.	<b>POREWATER CHEMICAL CONCENTRATIONS</b>	<b>110</b>
9.1	<b>CHLORIDE CONCENTRATIONS IN POREWATER</b>	<b>111</b>
9.2	<b>CHLORINE STABLE ISOTOPES (<math>\delta^{37}\text{Cl}</math>) IN POREWATER</b>	<b>117</b>
9.2.1	Chlorine Isotopes During High-pressure Squeezing	117
9.2.2	Spatial Distribution of $\delta^{37}\text{Cl}$ in Porewater Across the Opalinus Clay	119
9.2.3	Evolution of $\delta^{37}\text{Cl}$ in Porewater Across the Opalinus Clay	121
9.3	<b>BROMIDE CONCENTRATIONS IN POREWATER</b>	<b>123</b>
9.4	<b>Cl<sup>-</sup> AND Br<sup>-</sup> ACROSS THE PASSWANG FM – OPALINUS CLAY INTERFACE</b>	<b>125</b>
10.	<b><math>\delta^{18}\text{O}</math> and <math>\delta^2\text{H}</math> IN POREWATER</b>	<b>130</b>
10.1	<b>ORIGIN OF WATER COMPONENT</b>	<b>130</b>
10.2	<b>SPATIAL DISTRIBUTION OF WATER ISOTOPES</b>	<b>132</b>
10.3	<b><math>\delta^{18}\text{O}</math> AND <math>\delta^2\text{H}</math> ACROSS THE PASSWANG FM – OPALINUS CLAY INTERFACE</b>	<b>134</b>
11.	<b>NOBLE GAS CONCENTRATIONS AND ISOTOPES IN POREWATER</b>	<b>139</b>
11.1	<b>EVALUATION OF AIR CONTAMINATION</b>	<b>139</b>
11.1.1	Samples with Elevated Gas Concentrations	144
11.1.2	Samples From Below 83.78 m and From 90.68 m, 101.63 m and 120.86 m BHL	148
11.2	<b><math>^4\text{He}</math> CONCENTRATION AND <math>^3\text{He}/^4\text{He}</math> RATIO IN POREWATER</b>	<b>152</b>
11.3	<b>EVOLUTION OF THE <math>^4\text{He}</math> POREWATER PROFILE</b>	<b>155</b>
11.3.1	In-situ Production of He in the Rock and Transfer to the Porewater	155

11.3.2	Quantitative Assessment of the He Porewater Profile.....	157
11.3.2.1	Assessment of Steady-state of the Porewater – Groundwater System.....	159
11.3.2.2	1D Diffusion Model for the Evolution of the Porewater Helium Profile .....	161
11.4	<b>Ar CONCENTRATION AND <sup>40</sup>Ar/<sup>36</sup>Ar ISOTOPE RATIO IN POREWATER ....</b>	<b>165</b>
12.	<b>GROUNDWATER COMPOSITION AND EVOLUTION .....</b>	<b>167</b>
13.	<b>SUMMARY AND CONCLUSIONS.....</b>	<b>172</b>
	<b>ACKNOWLEDGEMENTS .....</b>	<b>176</b>
	<b>REFERENCES .....</b>	<b>177</b>
	<b>APPENDIX A:.....</b>	<b>187</b>
	<b>APPENDIX B:.....</b>	<b>209</b>

**LIST OF TABLES**

	<b><u>Page</u></b>
Table 3-1: Sample Type Designations, Participating Research Groups and Analyses for BDB-1 Samples.....	6
Table 3-2: Teams and Persons Involved in On-site Sampling.....	8
Table 3-3: List of Porewater Chemistry (-RWI-AQ) Samples and Analysed Parameters .....	14
Table 3-4: List of Porewater Noble Gas (-RWI-NG) Samples and Analysed Parameters .....	17
Table 5-1: Limits of Detection (LOD) and Limits of Calibration (LOC) Valid for the BDB-1 Analyses.....	39
Table 5-2: Analytical Accuracy and Precision of Reference Gases Measured with BDB-1 Samples .....	40
Table 6-1: Mineralogical Composition of Porewater Chemistry Samples .....	57
Table 7-1: Petrophysical Data of Porewater Chemistry Samples .....	75
Table 7-2: Petrophysical Data of Noble Gas Samples.....	79
Table 9-1: Concentrations of Cl <sup>-</sup> and Br <sup>-</sup> from Aqueous Extract Solutions Calculated to the Water-loss Porosity and to Porewater Concentrations Using Facies-specific Anion-accessible Porosity .....	115
Table 9-2: Concentrations of Cl <sup>-</sup> , Br <sup>-</sup> and I <sup>-</sup> and $\delta^{37}\text{Cl}$ of Water Squeezed at Different Pressures from Shaly Facies Opalinus Clay in Borehole BPC-C1.....	119
Table 10-1: Porewater $\delta^{18}\text{O}$ and $\delta^2\text{H}$ Derived by the Isotope Diffusive Exchange Technique ..	137
Table 11-1: Representative He and Ar Compositions of a BDB-1 Porewater Gas and Air.....	140
Table 11-2: Gas Pressure in Sample Containers, Ne and Gas Concentration in Porewater, He, Ne and Ar Concentration in Gas and $^{20}\text{Ne}/^{22}\text{Ne}$ Ratio in Gas of BDB-1 Samples .....	151
Table 11-3: $^4\text{He}$ and Ar Concentration and $^3\text{He}/^4\text{He}$ and $^{40}\text{Ar}/^{36}\text{Ar}$ Isotope Ratio in Porewater of BDB-1 Samples.....	154
Table 11-4: Radionuclide and $^4\text{He}$ Concentration, $^3\text{He}/^4\text{He}$ Isotope Ratio and Helium Production Rates and Ratios in the Rock Matrix of BDB-1 Samples .....	158
Table 11-5: Overview of Best-fit Model Parameters for Modelling the He Concentration Profile over the Opalinus Clay and Bounding Units at Mont Terri Obtained in this Work and by Mazurek et al. (2011) .....	163
Table 12-1: Chemical and Isotope Composition of Groundwater Sampled from the Water-conducting Zone in the Passwang Fm of Borehole BDB-1 .....	170
Table 12-2: Modelled Parameters of Groundwater Sampled from the Water-conducting Zone in the Passwang Fm of Borehole BDB-1 .....	171

**LIST OF FIGURES**

	<b><u>Page</u></b>
Figure 1-1: Detailed Lithostratigraphy and Biostratigraphy of the Early and Middle Jurassic Strata Encountered by Borehole BDB-1 at the Mont Terri URL (from Hostettler et al. 2017). .....	3
Figure 3-1: Adjacency Criteria for Comparative Samples. ....	7
Figure 3-2: Schematic Workflow of Core Processing Prior to Individual Sampling. ....	9
Figure 3-3: Removal of the “Stratigraphy-slab” by Dry Cutting on Site Immediately after Core Recovery. ....	10
Figure 3-4: Exposure Durations to Air for the AQ and SQ Samples (top) and for the NG Samples (bottom) Over the Course of the Sampling Campaign. ....	11
Figure 3-5: Distribution of Exposure Durations to Air for the AQ and SQ Samples (top) and for the NG Samples (bottom). ....	12
Figure 3-6: Central Core Section Used for Porewater Noble Gas Extraction (left) and the Assembled Porewater Noble Gas Sampling Apparatus at RWI, Uni Bern (right). ....	16
Figure 4-1: Groundwater Samples Collected in Appropriate Sample Containers and Layout of Field Measurement Devices. ....	19
Figure 5-1: Schematic Workflow of Gas Extraction, Separation/purification, Measurement and Back-calculation of Measured Signals to Gas Concentrations in Porewater. ....	36
Figure 5-2: Analytical Accuracy and Precision of He on Reference Gas Measured with the BDB-1 Samples. ....	41
Figure 5-3: Analytical Accuracy and Precision of Ne on Reference Gas Measured with the BDB-1 Samples. ....	41
Figure 5-4: Analytical Accuracy and Precision of Ar on Reference Gas Measured with the BDB-1 Samples. ....	42
Figure 5-5: Analytical Accuracy and Precision of <sup>20</sup> Ne/ <sup>22</sup> Ne and <sup>40</sup> Ar/ <sup>36</sup> Ar on Pure Air Measured with the BDB-1 Samples. ....	42
Figure 6-1: Lithologic Association According to Füchtbauer (1988) of the Porewater Chemistry Samples from Borehole BDB-1 at the Mont Terri URL. ....	46
Figure 6-2: Contents of Total Carbonate (top), Quartz (middle) and Total Clay Minerals (bottom) as a Function of Depth in Borehole BDB-1 at the Mont Terri URL. ....	48
Figure 6-3: Clay Mineralogy of Porewater Chemistry Samples from Borehole BDB-1 at the Mont Terri URL. ....	49
Figure 6-4: Individual Clay Mineral Contents (wt.% of whole rock) as a Function of Depth in Borehole BDB-1 at the Mont Terri URL. ....	50
Figure 6-5: Total Clay-Mineral Content Based on Gamma Logging (Willenberg-Spillmann, 2015) Compared to the Clay-mineral Contents Determined by XRD on Porewater Samples as a Function of Depth in Borehole BDB-1 at the Mont Terri URL. ....	51
Figure 6-6: Borehole Images of the Passwang Fm Between 97.9 and 99.4 m BHL with Open Fractures without Visible Wet Zones (left) and the Contact Passwang Fm – Opalinus Clay at 106.26 m BHL with a Weak, Bedding-parallel Moist Zone (right; from Fischer 2014). ....	53
Figure 6-7: Borehole Image of Shaly Facies 2 (167.6 – 169.0 m BHL, left) and Shaly facies 1 (197.0 – 198.4 m BHL, right) Showing its Typical Appearance without Any Wet Spots (from Fischer 2014). ....	53
Figure 6-8: Borehole Image of Sandy facies 2 (113.4 – 114.8 m BHL, left) and Sandy Facies 1 (181.5 – 190.0 m BHL, right) Showing the Typical Occurrences of Wet Spots along the Bedding Planes (dark) Indicating Water Inflow Areas (from Fischer 2014). ....	54

Figure 6-9: Borehole Imaging Log of the Non-fractured (189.20 – 190.7 m BHL, left) and Fractured (186.10 – 187.6 m BHL, right) Carbonate-rich Sandy Facies with Water Inflow Areas Around Open Fissures (from Fischer 2014). .....	54
Figure 6-10: Borehole Imaging Log Across the Main Fault in the Opalinus Clay from 226.10 – 227.4 m BHL with Water Inflow Areas Around Open Fissures (from Fischer 2014). .....	55
Figure 6-11: Borehole Imaging Log Showing the Opalinus Clay – Staffelegg Fm Interface at 236.80 m BHL and the Limestone Section at the Top of the Staffelegg Fm from 236.8 – 238.4 m BHL with Water Inflow Areas Along Bedding Planes and Open Fractures (from Fischer 2014). .....	55
Figure 6-12: Borehole Imaging Log of the Bituminous Claystone in the Staffelegg Fm from 243.4 – 244.9 m BHL with Clearly Visible Open Fractures and Pronounced Water Inflows (from Fischer 2014). .....	56
Figure 7-1: Grain Density (top) and Bulk Wet Density (bottom) as a Function of Depth in Borehole BDB-1 at the Mont Terri URL. ....	59
Figure 7-2: Pycnometer Porosity as a Function of Depth in Borehole BDB-1 at the Mont Terri URL. ....	60
Figure 7-3: Water Content Relative to the Wet Rock Weight Versus the Clay Content of the Different Lithologies in Borehole BDB-1. ....	62
Figure 7-4: Water Content Relative to the Wet Sample Weight ( $WC_{wet}$ ) Compared to the Clay Content Estimated from the Gamma Log as a Function of Depth in Borehole BDB-1 at the Mont Terri URL. ....	63
Figure 7-5: Water Content Obtained from $\delta^{18}O$ Versus that Obtained from $\delta^2H$ in the Isotope Diffusive Exchange Experiments. ....	65
Figure 7-6: Water Content Relative to the Wet Sample Weight Derived by Isotope Exchange Technique ( $WC_{IsoEx,wet}$ , average values) Versus that Derived by Drying at 105°C ( $WC_{Grav,wet}$ ). ....	65
Figure 7-7: Water Content Derived by Isotope Exchange Technique ( $WC_{IsoEx,wet}$ , open symbols) Compared to the Gravimetric Water Content ( $WC_{Grav,wet}$ , filled symbols) and the Clay Content Estimated from the Gamma Log as a Function of Depth in Borehole BDB-1 at the Mont Terri URL. ....	66
Figure 7-8: Water-loss Porosity, $\phi_{WL}$ , and the Clay Content Estimated from the Gamma Log as a Function of Depth in Borehole BDB-1 at the Mont Terri URL. ....	68
Figure 7-9: Water-loss Porosity, $\phi_{WL}$ , Versus the Pycnometer Porosity, $\phi_{Pyc}$ , of Rock Samples from Borehole BDB-1 at the Mont Terri URL. ....	69
Figure 7-10: Comparison of Gravimetric Dry Water Content (left) and Water-loss Porosity (right) of Noble Gas (NG) Samples with that of the Adjacent Porewater Chemistry (AQ) Samples. ....	70
Figure 7-11: Dry Water Content of the BDB-1 Noble Gas Samples and Adjacent Standard Porewater Samples as a Function of Clay Content. ....	71
Figure 7-12: Dry Water Content (top) and Water-loss Porosity (bottom) of the BDB-1 Noble Gas (NG) Samples and Adjacent Standard Porewater Samples as a Function of Depth. ....	71
Figure 7-13: BET Specific Surface Areas Versus Clay-mineral Content (left) and Pycnometer Porosity (right) of Rock Samples from Borehole BDB-1 at the Mont Terri URL. ....	72
Figure 7-14: Examples of $N_2$ Adsorption and Desorption Isotherms of Rock Samples from Borehole BDB-1 at the Mont Terri URL. ....	74
Figure 8-1: Schoeller-Diagram of Aqueous Extract Solutions from the Upper (43–70 m BHL, left) and Lower (70–105 m BHL, right) Part of the Passwang Fm. ....	82
Figure 8-2: Schoeller-Diagram of Aqueous Extract Solutions from the Sandy Facies 2 (left) and 1 (right) of the Opalinus Clay. ....	84

Figure 8-3: Schoeller-Diagram of Aqueous Extract Solutions from the Carbonate-rich Sandy Zone of the Opalinus Clay.....	85
Figure 8-4: Schoeller-Diagram of Aqueous Extract Solutions from the Shaly Facies 2 (left) and 1 (right) of the Opalinus Clay.....	85
Figure 8-5: Schoeller-Diagram of Aqueous Extract Solutions from the Staffelegg Fm. ....	87
Figure 8-6: Ion-ion Relationships in Aqueous Extract Solutions from Rocks of the Passwang Fm, Opalinus Clay and Staffelegg Fm. ....	90
Figure 8-7: Molar Br/Cl Ratio in Aqueous Extract Solutions and Squeezed Water Across the Sequence Passwang Fm – Opalinus Clay – Staffelegg Fm in Borehole BDB-1.....	91
Figure 8-8: Concentrations of SO <sub>4</sub> of Aqueous Extract Solutions Hypothetically Converted to the Water-loss Porosity Compared to SO <sub>4</sub> Concentrations in Squeezed Water Across the Sequence Passwang Fm – Opalinus Clay – Staffelegg Fm in Borehole BDB-1.....	97
Figure 8-9: Molar SO <sub>4</sub> /Cl Ratio in Aqueous Extract Solutions and Squeezed Water Across the Sequence Passwang Fm – Opalinus Clay – Staffelegg Fm in Borehole BDB- 1.....	98
Figure 8-10: Concentrations of Sr <sup>+2</sup> and SO <sub>4</sub> <sup>-2</sup> in Aqueous Extract Across the Sequence Passwang Fm – Opalinus Clay – Staffelegg Fm in Borehole BDB-1.....	99
Figure 8-11: Molar Sr/SO <sub>4</sub> Ratio vs Cl <sup>-</sup> Concentration in Aqueous Extract Solutions and Squeezed Water of Samples from the Opalinus Clay and Staffelegg Fm in Borehole BDB-1. ....	99
Figure 8-12: Molar Sr/SO <sub>4</sub> Ratio vs Cl <sup>-</sup> Concentration (closed symbols) and Saturation Index of Celestite (SI, open symbols) in Aqueous Extract Solutions and Squeezed Water of Samples from the Opalinus Clay and Staffelegg Fm in Borehole BDB-1.....	100
Figure 8-13: Behaviour of Mineral Saturation Indices During Removal of Water from Aqueous Extract Conditions (mass H <sub>2</sub> O = 1) to the Measured Water Content of Sample BDB1-221.28.....	103
Figure 8-14: Behaviour of Total Dissolved S and S-species During Removal of Water from Aqueous Extract Conditions (mass H <sub>2</sub> O = 1) to the Measured Water Content of Sample BDB1-221.28.....	104
Figure 8-15: Exchanged Cation Concentrations During Removal of Water from Aqueous Extract Conditions (mass H <sub>2</sub> O = 1) to the Measured Water Content of Sample BDB1-221.28.....	105
Figure 8-16: Molar Sr/SO <sub>4</sub> Ratio vs Br/Cl Ratios of Aqueous Extract Solutions of Rock Samples from Borehole BDB-1 and Compared to the Seawater Ratio and Ranges Given by Deep Groundwater in Triassic Lithologies. ....	108
Figure 9-1: Chloride Concentrations in Porewater Across the Passwang Fm, Opalinus Clay and Staffelegg Fm in Rock Samples from Borehole BDB-1 at the Mont Terri URL. ....	112
Figure 9-2: Cl Concentration and δ <sup>37</sup> Cl of Water Squeezed Under Increasing Pressure of Two Rock Samples from Shaly Facies 1 of the Opalinus Clay in Borehole BPC-C1.....	120
Figure 9-3: Chloride Stable Isotope Composition (δ <sup>37</sup> Cl) in Porewater Across the Passwang Fm, Opalinus Clay and Staffelegg Fm in Rock Samples from Borehole BDB-1 at the Mont Terri URL.....	121
Figure 9-4: Theoretical Profiles of Chloride and δ <sup>37</sup> Cl During Diffusion Across a Low-permeability Rock Formation (from Gimmi and Waber 2004).....	123
Figure 9-5: Bromide Concentrations in Porewater Across the Passwang Fm, Opalinus Clay and Staffelegg Fm in Rock Samples from Borehole BDB-1 at the Mont Terri URL. ....	124
Figure 9-6: Close-up of the Cl <sup>-</sup> (a) and Br <sup>-</sup> (b) Concentrations in Porewater Across the Passwang Fm – Opalinus Clay Interface in Borehole BDB-1 at the Mont Terri URL. ....	127

Figure 9-7: Close-up of Cl-isotope Ratios ( $\delta^{37}\text{Cl}$ ) in Porewater (a) and Molar Br/Cl (b) and Na/Cl (c) Ratios in Aqueous Extract Solutions Across the Passwang Fm – Opalinus Clay Interface in Borehole BDB-1 at the Mont Terri URL.....	128
Figure 10-1: $\delta^{18}\text{O}$ vs. $\delta^2\text{H}$ of Porewater, Groundwater and Recent Infiltration in Borehole BDB-1 at the Mont Terri URL.....	131
Figure 10-2: Distribution of Porewater $\delta^{18}\text{O}$ (a) and $\delta^2\text{H}$ (b) Across the Passwang Fm, Opalinus Clay and Staffelegg Fm in Borehole BDB-1 at the Mont Terri URL.....	133
Figure 10-3: Close-up of the $\delta^{18}\text{O}$ (a) and $\delta^2\text{H}$ (b) Values in Porewater Across the Passwang Fm – Opalinus Clay Interface in Borehole BDB-1 at the Mont Terri URL.....	136
Figure 11-1: Ar and He Amount in an Increasingly Contaminated Sample Gas as a Function of Relative Air Contamination.....	141
Figure 11-2: $^{40}\text{Ar}/^{36}\text{Ar}$ and $^3\text{He}/^4\text{He}$ Isotope Ratios in an Increasingly Contaminated Sample Gas as a Function of Relative Air Contamination.....	142
Figure 11-3: $^4\text{He}$ (left) and $^3\text{He}/^4\text{He}$ Isotope Ratios (right) in an Increasingly Contaminated Sample Gas as a Function of Relative Air Contamination.....	143
Figure 11-4: Comparison of Air Contamination Corrected and Uncorrected Concentration Values of Ar (left) and Ar-Isotope Ratio (right) for the BDB-1 Samples.....	143
Figure 11-5: The Problem of Unrealistic Upscaling of the Maximal Uncertainties on Air-contamination-corrected $^{40}\text{Ar}/^{36}\text{Ar}$ Values for High Degrees of Air-derived Ar.....	144
Figure 11-6: Fractions of He (left) and Absolute He Amounts (right) in the Sample Container Gas, Together with Sample Container Gas Concentrations in the Porewater as a Function of Borehole Depth.....	145
Figure 11-7: Fractions of Ne (left) and Absolute Ne Amounts (right) in the Sample Container Gas, Together with Sample Container Gas Concentrations in the Porewater as a Function of Borehole Depth.....	146
Figure 11-8: Fractions of Ne (left) and Absolute Ne Amounts (right) in the Sample Container Gas, Together with Sample Container Gas Concentrations in the Porewater as a Function of Borehole Depth.....	146
Figure 11-9: Ar/Ne, He/Ne and He/Ar Ratios of the BDB-1 Samples as Function of Sample Container Gas Concentration in Porewater.....	147
Figure 11-10: Ar/Ne, He/Ne and He/Ar Ratios of the BDB-1 Samples as Function of Borehole Depth.....	147
Figure 11-11: Ar Fraction as Function of the Ne Fraction in the Sample Container Gas of the BDB-1 Samples.....	149
Figure 11-12: $^4\text{He}$ Fraction as Function of the Ne Fraction in the Sample Container Gas of the BDB-1 Samples.....	150
Figure 11-13: $^4\text{He}$ Fraction as Function of the Ar Fraction in the Sample Container Gas of the BDB-1 Samples.....	150
Figure 11-14: Distribution $^4\text{He}$ Concentration in Porewater Across the Passwang Fm, Opalinus Clay and Staffelegg Fm in Borehole BDB-1 at the Mont Terri URL.....	153
Figure 11-15: Distribution of $^3\text{He}/^4\text{He}$ Isotope Ratio in Porewater Across the Passwang Fm, Opalinus Clay and Staffelegg Fm in Borehole BDB1 at the Mont Terri URL.....	153
Figure 11-16: Modelled Steady-state He Concentration Profiles from the Water-conducting Feature in the Passwang Fm Through the Opalinus Clay into the Staffelegg Fm... 160	
Figure 11-17: Simplified One-dimensional He Diffusion Profile for BDB-1 Resulting from Hypothetical Opening of the Water-conducting Fracture 70 ka Ago.....	162
Figure 11-18: Modern and Projected He Diffusion Profiles Along BDB-1 Modelled for Evolution with Open Boundary Conditions for the Last 70 ka (modern profile) and Assuming Continued Evolution Under Stagnant Boundary Conditions for the Next 30 ka (projected profile).....	164

Figure 11-19: Ar Concentration of Porewater from the BDB-1 Borehole as a Function of Depth..... 166

Figure 11-20:  $^{40}\text{Ar}/^{36}\text{Ar}$  Isotope Ratio of Porewater from the BDB-1 Borehole as a Function of Depth..... 166

Figure 12-1: Schoeller-Diagram of Groundwater from the Passwang Fm in Borehole BDB-1 and the Hauptrogenstein in Borehole BDS-2 at the Mont Terri URL..... 167

Figure 12-2:  $\delta^{18}\text{O}$  vs.  $\delta^2\text{H}$  of Groundwater from the Passwang Formation in Borehole BDB-1 and the Hauptrogenstein in Borehole BDS-2 at the Mont Terri URL..... 168



## 1. INTRODUCTION

The DB Experiment (Deep inclined borehole across the Opalinus Clay) at the Mont Terri URL focused on the long-term monitoring of hydraulic conditions and the characterisation of pore water geochemistry, petrophysical parameters, rock stratigraphy and structure along a continuous profile across the Opalinus Clay and its hanging wall and footwall in an undisturbed environment. The geochemical characterisation of porewater in the Opalinus Clay, and its interface to the overlying rocks of the Passwang Formation (Fm), took place within the DB-A Experiment, which was financed by an international consortium including IRSN in France, Nagra in Switzerland, NWMO in Canada, and swisstopo in Switzerland.

At the Mont Terri URL, borehole BDB-1 is the first borehole that crosscuts the Opalinus Clay in its entire thickness. Borehole BDB-1 cuts across the Jurassic sediment sequence of low-permeability from the Hauptrogenstein, through the Passwang Fm and Opalinus, and ending in the rocks of the Staffelegg Fm. The detailed stratigraphic profile encountered by borehole BDB-1 is given in Figure 1-1. Across the Hauptrogenstein and Passwang Fm, the borehole was water-drilled with low-mineralised, recent groundwater from the Hauptrogenstein as drilling fluid. Across the Opalinus Clay and into the Staffelegg Fm, the borehole was air-drilled. Groundwater could be collected from a water-conducting zone in the Passwang Fm at 58.6m BHL, but was not encountered in the lithologies in the footwall of the Opalinus Clay.

Borehole BDB-1 provided unique opportunities in several aspects for the characterisation of porewater in the low-permeability rocks at the Mont Terri URL. First, the borehole allowed collection of drill-core samples at a high spatial frequency within the Opalinus Clay and at the Passwang Fm – Opalinus Clay interface. Second, all samples experienced the same drilling conditions allowing a better comparison of obtained results and identification of possible artefacts induced by the drilling process. Third, all drill-core samples were subjected to the same strict sampling protocol, including time monitoring of the different steps and aiming to reduce exposure of the samples to air as much as possible, and thus reduce induced artefacts such sample desiccation and oxidation. Fourth, samples could be collected adjacent to each other for a laboratory comparison, allowing identification of pros and cons of different indirect porewater extraction techniques and artefacts induced in the laboratory treatment of the samples. And fifth, optimised porewater sampling and extraction techniques could be applied based on experience gained over the past 20 years.

The unique opportunities provided by borehole BDB-1 allowed improvement of our understanding of porewater evolution and the origin of porewater solutes, building on the work presented in Pearson et al. (2003), in addition to optimisation of indirect porewater extraction techniques and the identification of induced artefacts. Whereas some of the concepts and interpretations presented in Pearson et al. (2003) and other later work are supported by the findings made using rock material from borehole BDB-1, other interpretations have been revised to some degree, as described in this report.

The present report describes the results from RWI, University of Bern, of the porewater characterisation and distribution of natural tracers in Opalinus Clay and across the Opalinus Clay – Passwang Fm interface. For these investigations, more than 110 samples were collected across the entire profile and investigated at RWI, University of Bern. A similar number of samples was collected by the same field team and distributed to DB-A Experiment partner

laboratories for an inter-laboratory comparison, the results of which are reported in Mazurek et al. (2017).

The report has three main focuses, which include: 1) detailed description of the sampling strategies applied in the field and experimental and analytic techniques in the laboratory, 2) elaboration and interpretation of porewater characteristics and natural tracer profiles across the Opalinus Clay with special emphasis on the Opalinus Clay – Passwang Formation interface, and 3) deduction of evolutionary aspects of solute transport and porewater origin. Special emphasis was given to the spatial distribution of the data collected and their relationship to changes in rock mineralogy and structure (i.e., the different sedimentary facies of the Opalinus Clay). In order to facilitate understanding of these complexities, the data are colour-grouped according to their sedimentary occurrence along the depth profile in most of the graphical representations.

The report is structured in the following way:

Chapters 2 to 4 give detailed description of the drilling operations, drill-core sampling and conditioning, and the groundwater sampling in the Passwang Fm, all of them supported by field and lab protocols given in the Appendix.

Chapter 5 describes the experimental and analytical techniques applied to the core sections, and to the solutions and gases obtained from different extraction techniques in the laboratory. Special emphasis is given to the challenges associated with the determination of porewater noble gas concentrations, with respect to contamination by air, etc.

Chapters 6 and 7 present the results of the mineralogical and petrophysical parameters of rocks encountered along the profile from the Hauptrogenstein to the Staffelegg Fm. The number of samples investigated for petrophysical parameters (71) is more than twice as high compared to that investigated for the mineralogical composition (28). Derivation and interpretation of porewater tracer concentrations and composition, however, relies to a large degree on knowledge about the mineralogy of the sample investigated (e.g., clay content, minerals with rapid reaction kinetics, etc.). Where available, alternative information was used to infer this information (e.g., such as the clay content estimated from geophysical logging).

Chapters 8 to 11 describe in detail the concentrations of the natural tracers  $\text{Cl}^-$ ,  $\text{Br}^-$ ,  $\delta^{37}\text{Cl}$ ,  $\delta^{18}\text{O}$ ,  $\delta^2\text{H}$ , noble gases and other solutes (e.g.  $\text{SO}_4^{2-}$ ) in experimental solutions and gas, and their conversion to porewater concentrations. Special emphasis is given to the meaning of the tracer concentrations, with respect to in-situ porewater concentrations and the origin of porewater solutes obtained in solutions derived using different extraction techniques, such as aqueous extraction and high-pressure squeezing. With respect to  $\text{SO}_4^{2-}$ , which is (at least) the second most abundant anion in porewater of the Opalinus Clay, geochemical modelling strategies are applied to explain the differences obtained by aqueous extraction and high-pressure squeezing. In Chapter 11, the noble gas data are also assessed in a quantitative way by transport modelling.

Chapter 12 gives a description of the groundwater collected from a water-conducting zone in the Passwang Fm and its interpretation in terms of origin and residence time.

Finally, Chapter 13 gives a summary and some conclusions drawn from the presented data and their interpretation.



-Page left intentionally blank-

## 2. DRILLING OPERATIONS

The wellhead of BDB-1 is situated in the “parking niche” in the Hauptrogenstein Fm and the borehole has a mean azimuth and dip of  $330^{\circ}/44^{\circ}$ , which is roughly perpendicular to the local bedding. The borehole has a total length of 247.5 m and was drilled in two phases between 05-18 December, 2013, and 15-30 January, 2014. The first section (0 – 97.3 m BHL<sup>1</sup>) was wet drilled with a borehole diameter of 156 mm, using water as flushing media, and terminated approximately 9 m above the top of the Opalinus Clay. In order to seal off the encountered water conducting features and switch to dry drilling, the borehole was cemented and the second section (97.3 – 247.5 m) was drilled with air as flushing media, at a smaller borehole diameter of 122 mm, and terminated in the Stafflegg Fm after encountering increasing problems with wet-spots at 243.5 m and at terminal depth. The entirety of the borehole was cored using a wireline coring system, with core diameters of 101 mm for the first section and 85 mm for the second section. Further technical details of the drilling are given in Jaeggi et al. (2016).

During the two drilling phases, drilling operations continued from Monday to Friday between approximately 05:00 to 20:00 with the borehole being left waterlogged (during drilling phase 1) or actively ventilated (during phase 2) in the intervening periods. An additional standstill occurred at the beginning of phase 2, after approximately 8 m of dry drilling, when downhole humidity prevented further drilling. Installation of a desiccator into the downhole airstream was only partially successful and the borehole was cemented again between 90 and 105 m BHL to seal off potential water seepage. While finally successful, this resulted in a standstill of 5 days, during 2 of which the base of the borehole at 105.35 was exposed to actively ventilated air.

Two borehole logging campaigns with geophysical logs and borehole imaging were undertaken at the end of each drilling phase by Terratec Geophysical Services GmbH.

The obtained core quality was generally very good, with only minimal core loss. The bulk of the core loss occurred between 156.85 – 158.85 m BHL when a 2.2 m long piece of core had to be overcored.

Below 51 m BHL (Passwang-Fm), artesian water inflow was detected with an estimated rate of 5-10 L/min. For groundwater sampling, a single packer system was installed, sealing off a test interval between 51.0 and 59.65 m BHL. Visual examination of the retrieved cores from that section suggests that the water inflow is through open fractures between 58.5 and 58.8 m BHL (Jaeggi et al. 2016).

---

<sup>1</sup> m BHL = meter along borehole

### 3. DRILL-CORE SAMPLING FOR POREWATER INVESTIGATIONS

#### 3.1 CORE SAMPLING STRATEGY AND SAMPLE TYPES

Due to the multi-participant nature of the project, a total of 9 different sample types for 6 different parties had to be taken (Table 3-1), all with specific criteria regarding sample dimensions, location, lithology, treatment, etc. This required setting up a sampling plan, which strived to ensure that all parties obtained their requested samples, while at the same time allowing enough flexibility to deal with the potential restrictions presented by core quality and encountered lithology. It also required that sample designations for all sample types be clearly defined. The adopted naming scheme for BDB-1 samples was "BDB1 – (*avg. depth [m BHL]*) – (*sample type*)".

**Table 3-1: Sample Type Designations, Participating Research Groups and Analyses for BDB-1 Samples**

<b>Sample type</b>	<b>Participating Research Group</b>	<b>Analyses</b>
-AQ	RWI <sup>2</sup> , University of Bern	porewater chemistry
-SQ	RWI, University of Bern	porewater chemistry (squeezing)
-NG	RWI, University of Bern	noble gases in porewater
<i>-UNB</i>	<i>University of New Brunswick</i>	<i>porewater chemistry</i>
<i>-He</i>	<i>University of Ottawa</i>	<i>noble gases in porewater</i>
<i>-VD</i>	<i>University of Ottawa</i>	<i>porewater chemistry</i>
<i>-IRSN</i>	<i>Institut de Radioprotection et de Sûreté Nucléaire</i>	<i>porewater chemistry</i>
<i>-BGR</i>	<i>Bundesanstalt für Geowissenschaften und Rohstoffe</i>	<i>geomechanical testing</i>
<i>-Nagra</i>	<i>Nagra</i>	<i>mineralogy, petrophysics</i>

Notes: in italic font are sample types that are not covered in this report. A summary of these results can be found in Mazurek et al. (2017).

One of the aims of the DB-A experiment – to establish a continuous geochemical record between an encountered aquifer and the Opalinus Clay – required continuous sampling, with increased sampling frequency closer to the aquifer. The other aim – the benchmarking and inter-laboratory comparison study – necessitated that potential heterogeneities between these comparative samples were kept as minimal as possible by taking them directly adjacent to each other. For this purpose, a strict relative sequence for such samples was decided upon (Figure 3-1).

The request for obtaining a complete and detailed stratigraphic profile of the drilled sequence stood in competition to the copious demand for core samples, as these samples are usually only available for a cursory geologic survey during sampling and not for a detailed stratigraphic analysis. At the BDB-1 drill location, this issue was – for the first time – solved by removing a thin slice of the outer part of the drill core parallel to the core axis from all except the

<sup>2</sup> Rock-Water-Interaction group, Institute of Geological Sciences, University of Bern

geomechanical samples. This slice (colloquially termed the “stratigraphy slab”) allowed, together with the remaining parts of the core, to obtain a detailed, near-continuous stratigraphic profile over the entire borehole length.

At completion of the BDB-1 drilling, 250 drill-core samples, with a total length of over 54 m, had been sampled by the sampling team consisting of members from RWI / University of Bern, Swisstopo and a researcher from the University of Ottawa. A full sample inventory is given in Appendix A1.

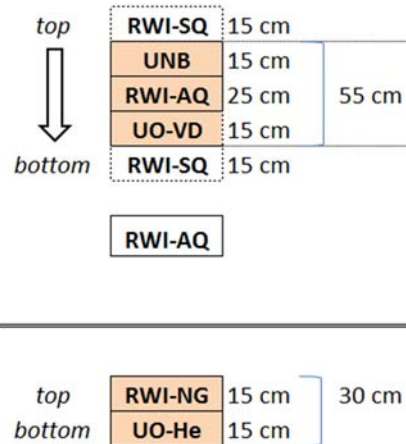


**Figure 3-1: Adjacency Criteria for Comparative Samples.**

### 3.2 Core Handling, Sampling Procedures and Laboratory Analyses

Preconditioning for the quantification of the chemical, isotope and dissolved gas composition of porewater in low-permeability rocks, as well as their geomechanical properties, is the preservation of the in-situ water saturated state of the rock material after drill-core extraction and during subsequent sampling. Any extended exposure to extrinsic fluids (such as drilling fluid, water used for core cleaning) or gases (primarily air) will result in changes of the original state and cause potential contamination or experimental problems related to sample desiccation.

During both drilling campaigns (05-18 December, 2013 and 15-30 January, 2014) samples planned for porewater and geomechanical characterisation were collected and conditioned on site immediately after recovery of the drill core from the borehole. To fulfill all requirements with respect to the sample descriptions and sample conditioning, three persons were fully occupied with these tasks during the drilling operations (Table 3-2).

**Table 3-2: Teams and Persons Involved in On-site Sampling**

<b>Team</b>	<b>On-site Sampling</b>	<b>Persons Involved</b>
	planning and coordination	D. Rufer
Swisstopo	geological description, porewater chemistry sampling	D. Jaeggi & Team
RWI, Uni Bern	porewater chemistry & noble gas sampling	D. Rufer, H.N. Waber
Uni Ottawa	porewater noble gas sampling	S. Qui
RWI, Uni Bern, swisstopo	groundwater sampling	H.N. Waber, D. Rufer, D. Jaeggi

The procedure for samples designated for porewater chemistry investigation was the same for all research groups (*cf.* Table 3-1). Differences existed, however, in the sampling for noble gas analyses for the University of Ottawa and the sampling for geomechanical testing by BGR. Details of the gas-sampling procedure for the University of Ottawa are provided in Mazurek et al. (2017).

The first section of the borehole, down to a depth of 97.30 m BHL, was wet-drilled using surface water available on site as drilling fluid. As a consequence, cores retrieved from this section had to be cleaned using groundwater available on site and subsequently wiped dry. As soon as the core was given a centreline marking and was metered, suitable sections up to a maximum of ca. 1 m length were photographed from one side using a high-resolution core scanner and immediately sealed into an evacuated, transparent plastic tube at the drill site to protect it from contamination with air. After transport to the roughly 300 m distant sample processing site, the core pieces were geologically surveyed by the on-site geologist from Swisstopo, and the positions of the different samples to be taken were agreed upon by the sampling team, all while the core section was sealed under vacuum. After cutting the sealed plastic tube and re-exposing the core section to air, the various samples were immediately processed in their appropriate way in such a sequence as to minimise exposure times to air, with priority given to samples for porewater gas analyses (Figure 3-2).

With exception of the “BGR” type samples for rock mechanical experiments, which required a preservation of the cylindrical shape of the rock, all samples had the “stratigraphy slab” cut off. On one side of the core section, approximately 1/3 of the circumference was taped parallel to the core axis using a strong industrial adhesive tape (SIGA Rissan<sup>3</sup>, normally used for vapour barriers in construction) and the metering information was copied over onto the duct tape in order to have it preserved on both the actual sample and the “stratigraphy slab”. After the core section to be sampled was cut out perpendicular to the core axis, an approximately 1 – 2 cm thick slice was pared off parallel to the core axis from the taped section, with the duct tape fixing this “stratigraphy slab” in its proper internal stratigraphic order in case of accidental dinking during sawing (Figure 3-3). All sawing was performed without water in order not to contaminate the samples.

For each retrieved core section, a standardised log was kept detailing the core section depth interval, the date and time of the drill-core recovery from the core barrel, the time of sealing of

<sup>3</sup> The tape is sold by SIGA, Switzerland ([www.siga.ch](http://www.siga.ch)). The 60 mm wide variant was used for easier application.

the individual core pieces into the plastic tube, and the time of their subsequent removal from the sealed plastic (Figure 3-2). It further records, for each sample taken from the core section, its owner, sample type, sample depth interval as well as the timestamps for the sample processing steps (sawing, temporary sealing, final sealing).

For the RWI, Uni Bern porewater noble gas samples, an additional log and an audiolog was recorded during sample preparation, noting the time of start and end of sawing and time, duration and attained pressures of all pumping steps (Appendix A2; Appendix A3). With these logs, exposure times to air can be deduced for each sample, allowing for quality control of the ensuing analyses.

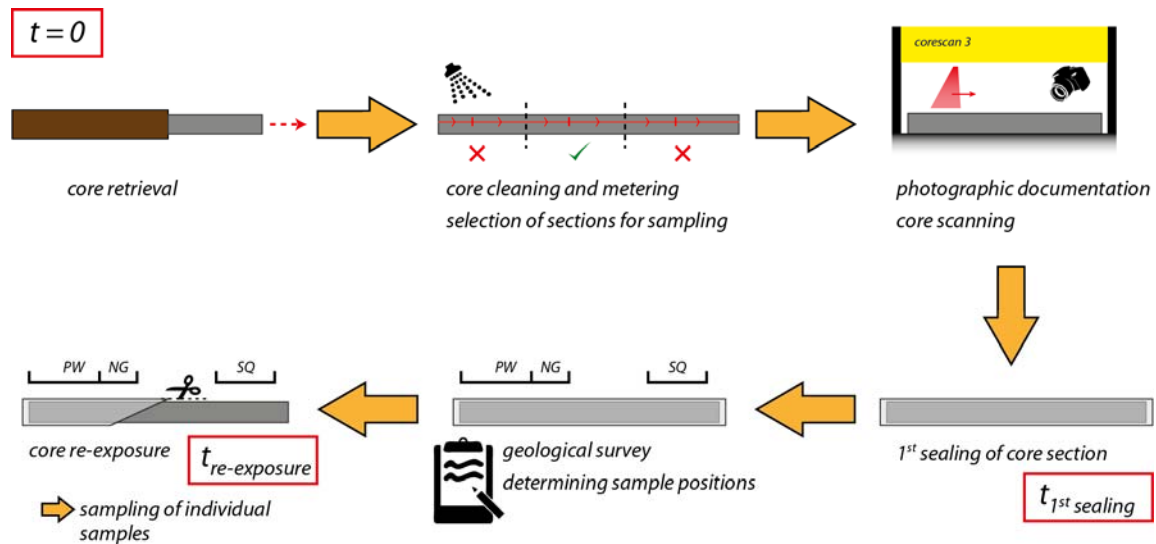


**Figure 3-2: Schematic Workflow of Core Processing Prior to Individual Sampling.**

The *total exposure duration* for a sample is given by the length of time between recovery of the core from the core barrel and its first sealing in the plastic tube, plus the duration between cutting of the plastic tube and either the preliminary or final sealing of the sample piece (after which the contamination potential with air is drastically reduced or completely inhibited, respectively).

Of the 250 drill-core samples collected and conditioned from BDB-1, a total of 116 samples were procured for further investigation at RWI, Uni Bern. These consisted of 63 AQ samples for porewater chemistry by conventional techniques, 22 SQ sample for porewater chemistry by high-pressure squeezing, 25 NG samples for porewater noble gas concentrations, and one additional sample for documentary purposes.

The results of the RWI, Uni Bern high-pressure squeezing samples (SQ-samples) as well as those of the other participation research groups are described in separate reports (*cf.* compilation by Mazurek et al. 2017).



**Figure 3-3: Removal of the “Stratigraphy-slab” by Dry Cutting on Site Immediately after Core Recovery.**

### 3.2.1 Porewater Chemistry Samples

Porewater chemistry samples further investigated at RWI, Uni Bern were denoted with the suffixes "-RWI-AQ" and "-RWI-SQ". For these samples, lithologically homogeneous sections of roughly 20 to 25 cm length were selected from the 1 m long plastic-sealed core section, cut dry and immediately placed in a plastic-coated thick Al-bag that was evacuated and heat-sealed. In case of several samples being taken at the same time, some of the samples were intermediately sealed into evacuated plastic bags using a household vacuum appliance as this provides a very rapid but less durable way of protecting samples from desiccation and air-contamination. At the end of a sampling day, all Al-bag sealed samples were additionally vacuum-sealed into a more robust, transparent plastic tube in order to protect the Al-bag from physical damage.

For the AQ- and SQ-type samples the *exposure duration after removal of the stratigraphy slab* is a part of the total exposure duration and corresponds to the length of time between the start of sawing to removal of the stratigraphy-slab and the preliminary or final sealing of the sample.

*Total exposure durations* range from 33 down to 8 minutes for the "-AQ" and "-SQ" type, with roughly 80% of all samples lying below 20 minutes (Figure 3-4). In terms of contamination or desiccation potential, the *exposure duration after removal of the stratigraphy slab* is much more critical. There, exposure durations range from 15 down to 1 minute (median<sup>4</sup>: 4 minutes), with over 80% of the samples lying below 5 minutes (Figure 3-5).

<sup>4</sup> The median is used for the AQ and SQ samples because the distribution of exposure durations is skewed, with a few high value outliers disproportionately influencing the arithmetic mean.

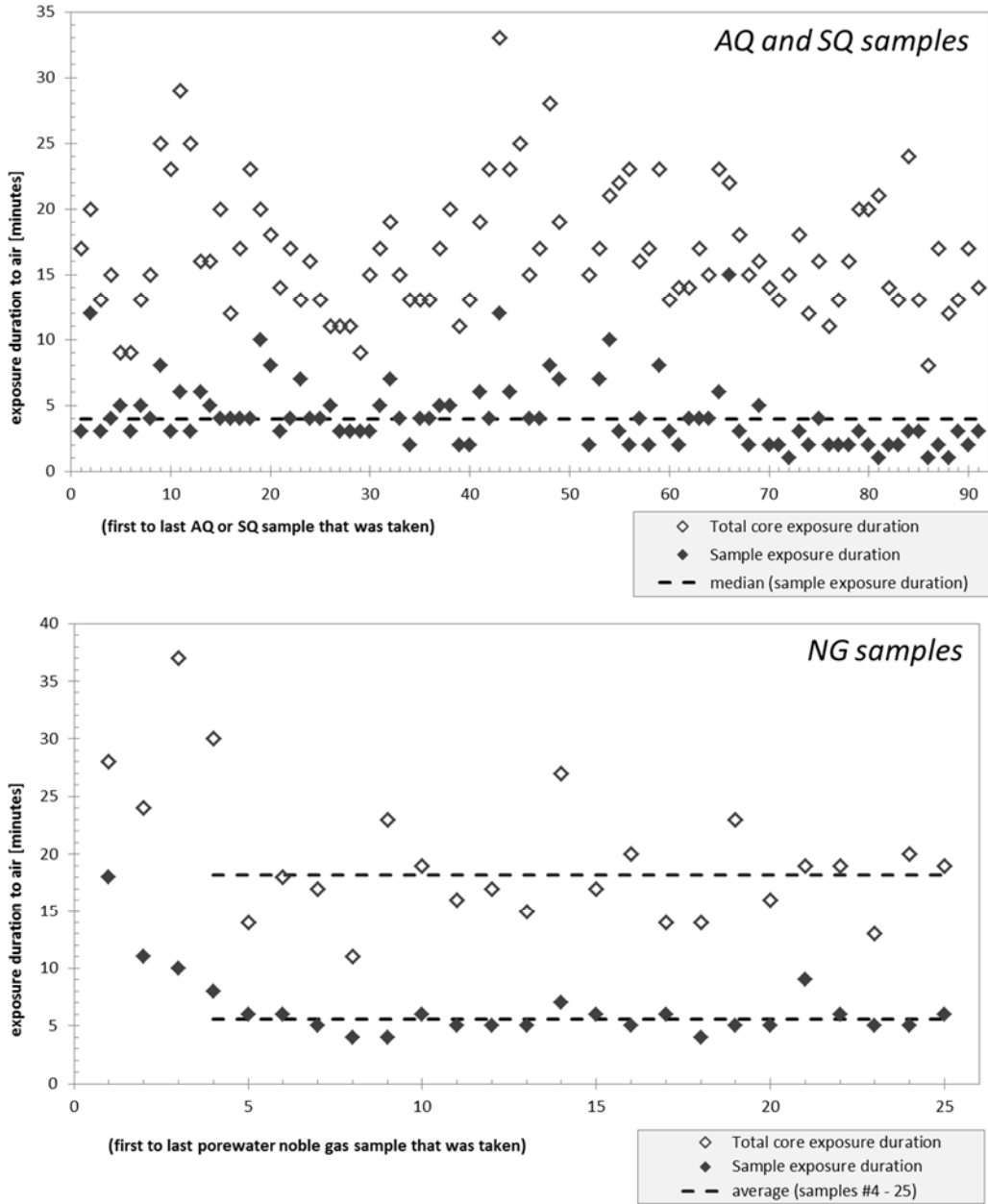


**Figure 3-4: Exposure Durations to Air for the AQ and SQ Samples (top) and for the NG Samples (bottom) Over the Course of the Sampling Campaign.**

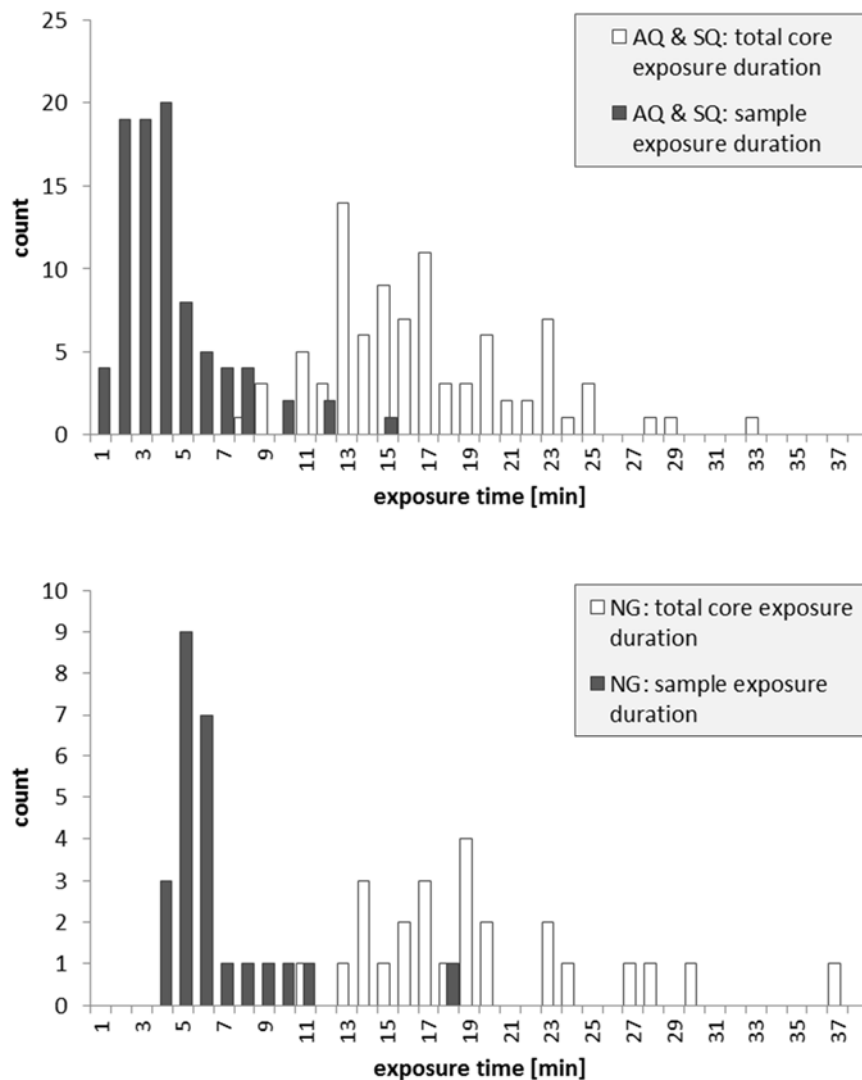


**Figure 3-5: Distribution of Exposure Durations to Air for the AQ and SQ Samples (top) and for the NG Samples (bottom).**

Of the porewater chemistry RWI-AQ-samples, 19 were investigated within the inter-laboratory comparison for their mineralogy, water content, density, porosity and total surface area (BET), and were subjected to aqueous extraction and isotope diffusive exchange experiments (Table 3-3). Another 44 samples were investigated in the so-called "Opalinus Clay – Passwang Formation interface" programme for their water content, density and porosity, and were subjected to aqueous extraction and isotope diffusive exchange experiments (Table 3-3).

Sample preparation and analyses in the lab occurred in two batches corresponding to the two drilling campaigns. Samples drilled in December, 2013 were prepared in early January, 2014 and samples drilled in January, 2014 were prepared in early February, 2014 (Table 3-3).

Of the total 22 RWI-SQ samples collected for squeezing under high pressure, 10 were actually subjected to squeezing. The squeezed water was later analysed for its chemical and isotope composition at RWI, Uni Bern. The results of that study are reported in Mazurek et al. (2017).

### 3.2.2 Porewater Noble Gas Samples

Porewater noble gas samples further investigated at RWI, Uni Bern were denoted with the suffix "-RWI-NG". For these samples lithologically homogeneous sections (see Figure 3-6) of roughly 10 to 15 cm length were selected from the 1 m long plastic-sealed core section, either utilizing existing bedding-parallel breaks in the core caused by diskings or by dry cutting on a rock saw. These sampled core sections were then trimmed by dry cutting to a square shaped central block in order to remove the partly degassed and contaminated rim of the core. The dimensions of the central block are, on average, 40 to 45 mm along the side and 85 mm in height (parallel to the core axis). Accordingly, the corresponding thickness of the removed rim is between about 20 to 30 mm, with the larger value pertaining to the thickness perpendicular to the side face of the central block and the smaller one measured along the latter's angle bisector. All cut surfaces were brushed off to remove rock powder created by the sawing process, the wet weight of the sample was then recorded, and the sample was photographed from one side for documentary purposes. The sample was then immediately sealed in a stainless steel container. The lids of these vacuum containers are fitted with a 30 cm copper tube and are connected to the containers by a ConFlat (CF) flange (soft metal gasket and knife edge) with a copper seal. As soon as the container was screwed shut finger tight, the air contained within the container was evacuated using a pump connected to the copper tube, simultaneous to final tightening of the CF seal in order to minimise porewater gas contamination by air. Upon sealing of the CF flange, and once rates of pressure drop began to level off (indicating conditions approaching a state where concurrent sample degassing begins), the container containing the sample was subjected to three flushing/evacuation cycles using commercially available N<sub>2</sub> (99.99% purity) as a means to dilute and pump off any residual air. The container was then vacuum-sealed by crimping the copper tube with screw-driven steel clamps during final pumping. Two clamps were used in order to provide redundancy in case of a leakage through the clamped part of the tube, which has been identified in former studies as the prevalent potential leaking point.

As for the AQ- and SQ- type samples, the *total exposure duration* for the NG samples is given by the length of time between core recovery from the core barrel and its final sealing of the sample piece in the stainless steel container. This total exposure duration includes the *exposure duration of the central block*, which is calculated as the length of time between the start of trimming the rim of the sample and the first flushing step (after which contamination by air is severely reduced).

*Total exposure durations* of NG samples range from 37 down to 11 minutes, with roughly 80% of all samples lying below 20 minutes. In terms of contamination or desiccation potential, however, the *exposure duration of the central block* is much more critical. There, exposure durations are between 18 and 4 minutes and a clear drop in exposure durations over the first four porewater noble gas samples is observable. This is attributable to a growing familiarisation of the sampling crew to the procedures and, hence, an increased efficiency. Following the first four samples, the *exposure durations of the central block* are narrowly confined, with an average of less than 6 minutes.

**Table 3-3: List of Porewater Chemistry (-RWI-AQ) Samples and Analysed Parameters**

Sample	Depth Interval (m BHL)	Date Sampled	Date Prepared	Geology	Mineralogy	WC, Density, Porosity	BET	Aqueous Extract	Isotope Exchange
BDB1-36.19-AQ	36.08 – 36.30	13.12.13	07.01.14	Hauptrogenstein		x		x	x
BDB1-43.78-AQ	43.65 – 43.90	13.12.13	07.01.14	Passwang Fm		x		x	x
BDB1-59.75-AQ	59.67 – 59.83	17.12.13	07.01.14	Passwang Fm		x		x	x
BDB1-60.79-AQ	60.70 – 60.87	17.12.13	07.01.14	Passwang Fm		x		x	x
BDB1-61.00-AQ	60.87 – 61.13	17.12.13	07.01.14	Passwang Fm		x		x	x
BDB1-61.52-AQ	61.42 – 61.62	17.12.13	08.01.14	Passwang Fm		x		x	x
BDB1-62.39-AQ	62.32 – 62.46	17.12.13	08.01.14	Passwang Fm		x		x	x
BDB1-62.80-AQ	62.70 – 62.90	17.12.13	08.01.14	Passwang Fm		x		x	x
BDB1-63.15-AQ	63.06 – 63.24	17.12.13	08.01.14	Passwang Fm		x		x	x
BDB1-63.80-AQ	63.71 – 63.89	17.12.13	08.01.14	Passwang Fm		x		x	x
BDB1-64.11-AQ	64.00 – 64.22	17.12.13	08.01.14	Passwang Fm		x		x	x
BDB1-64.88-AQ	64.76 – 65.00	17.12.13	08.01.14	Passwang Fm		x		x	x
BDB1-65.34-AQ	65.20 – 65.48	17.12.13	08.01.14	Passwang Fm		x		x	x
BDB1-65.70-AQ	65.60 – 65.80	17.12.13	08.01.14	Passwang Fm		x		x	x
BDB1-66.15-AQ	66.05 – 66.25	17.12.13	08.01.14	Passwang Fm		x		x	x
BDB1-66.70-AQ	66.60 – 66.80	17.12.13	08.01.14	Passwang Fm		x		x	x
BDB1-67.30-AQ	67.20 – 67.40	17.12.13	08.01.14	Passwang Fm		x		x	x
BDB1-67.80-AQ	67.70 – 67.90	17.12.13	08.01.14	Passwang Fm		x		x	x
BDB1-68.90-AQ	68.80 – 69.00	17.12.13	08.01.14	Passwang Fm		x		x	x
BDB1-70.30-AQ	70.20 – 70.40	17.12.13	not prep.	Passwang Fm					
BDB1-72.20-AQ	72.10 – 72.30	17.12.13	08.01.14	Passwang Fm		x		x	x
BDB1-74.30-AQ	74.20 – 74.40	18.12.13	not prep.	Passwang Fm					
BDB1-76.30-AQ	76.20 – 76.40	18.12.13	08.01.14	Passwang Fm		x		x	x
BDB1-79.30-AQ	79.20 – 79.40	18.12.13	not prep.	Passwang Fm					
BDB1-82.30-AQ	82.20 – 82.40	18.12.13	08.01.14	Passwang Fm		x		x	x
BDB1-83.95-AQ	83.85 – 84.05	18.12.13	not prep.	Passwang Fm					
BDB1-86.90-AQ	86.80 – 87.00	18.12.13	not prep.	Passwang Fm					
BDB1-89.45-AQ	89.35 – 89.55	18.12.13	08.01.14	Passwang Fm	x	x	x	x	x
BDB1-90.85-AQ	90.75 – 90.95	19.12.13	not prep.	Passwang Fm					
BDB1-93.24-AQ	93.15 – 93.33	19.12.13	08.01.14	Passwang Fm		x		x	x
BDB1-93.65-AQ	93.55 – 93.75	19.12.13	08.01.14	Passwang Fm	x	x	x	x	x
BDB1-97.10-AQ	97.00 – 97.20	19.12.13	08.01.14	Passwang Fm		x		x	x
BDB1-98.68-AQ	98.55 – 98.80	16.01.14	03.02.14	Passwang Fm		x		x	x

Notes: Shaded samples were used for inter-laboratory comparison; WC = water content, BET= total surface area.

Table 3-3 (cont.)

Sample	Depth Interval (m BHL)	Date Sampled	Date Prepared	Geology	Mineralogy	WC, Density, Porosity	BET	Aqueous Extract	Isotope Exchange
BDB1-100.63-AQ	100.50 – 100.75	16.01.14	03.02.14	Passwang Fm	x	x	x	x	x
BDB1-101.80-AQ	101.70 – 101.90	16.01.14	03.02.14	Passwang Fm		x		x	x
BDB1-102.93-AQ	102.80 – 103.05	16.01.14	03.02.14	Passwang Fm		x		x	x
BDB1-104.78-AQ	104.65 – 104.90	23.01.14	03.02.14	Passwang Fm		x		x	x
BDB1-108.24-AQ	108.1 – 108.38	23.01.14	03.02.14	Opalinus Clay		x		x	x
BDB1-113.88-AQ	113.75 – 114.00	23.01.14	03.02.14	Opalinus Clay		x		x	x
BDB1-114.80-AQ	114.70 – 114.90	23.01.14	04.02.14	Opalinus Clay	x	x	x	x	x
BDB1-119.86-AQ	119.75 – 119.97	23.01.14	04.02.14	Opalinus Clay	x	x	x	x	x
BDB1-120.68-AQ	120.55 – 120.80	23.01.14	04.02.14	Opalinus Clay		x		x	x
BDB1-128.24-AQ	128.10 – 128.38	23.01.14	04.02.14	Opalinus Clay	x	x	x	x	x
BDB1-132.63-AQ	132.50 – 132.75	24.01.14	04.02.14	Opalinus Clay	x	x	x	x	x
BDB1-144.17-AQ	144.06 – 144.27	25.01.14	04.02.14	Opalinus Clay	x	x	x	x	x
BDB1-161.18-AQ	161.05 – 161.30	28.01.14	04.02.14	Opalinus Clay	x	x	x	x	x
BDB1-166.08-AQ	165.95 – 166.20	28.01.14	04.02.14	Opalinus Clay	x	x	x	x	x
BDB1-172.70-AQ	172.60 – 172.80	28.01.14	04.02.14	Opalinus Clay	x	x	x	x	x
BDB1-175.33-AQ	175.20 – 175.45	28.01.14	04.02.14	Opalinus Clay	x	x	x	x	x
BDB1-178.73-AQ	178.60 – 178.85	29.01.14	04.02.14	Opalinus Clay	x	x	x	x	x
BDB1-189.71-AQ	189.58 – 189.83	29.01.14	04.02.14	Opalinus Clay	x	x	x	x	x
BDB1-192.68-AQ	192.55 – 192.80	29.01.14	04.02.14	Opalinus Clay	x	x	x	x	x
BDB1-198.13-AQ	198.00 – 198.25	29.01.14	04.02.14	Opalinus Clay		x		x	x
BDB1-203.68-AQ	203.55 – 203.80	29.01.14	04.02.14	Opalinus Clay	x	x	x	x	x
BDB1-209.00-AQ	208.88 – 209.12	30.01.14	04.02.14	Opalinus Clay	x	x	x	x	x
BDB1-213.85-AQ	213.75 – 213.95	30.01.14	04.02.14	Opalinus Clay		x		x	x
BDB1-217.98-AQ	217.85 – 218.10	30.01.14	05.02.14	Opalinus Clay		x		x	x
BDB1-219.49-AQ	219.38 – 219.60	30.01.14	05.02.14	Opalinus Clay		x		x	x
BDB1-221.28-AQ	221.15 – 221.40	30.01.14	05.02.14	Opalinus Clay	x	x	x	x	x
BDB1-225.18-AQ	225.05 – 225.30	30.01.14	05.02.14	Opalinus Clay		x		x	x
BDB1-227.43-AQ	227.30 – 227.55	30.01.14	05.02.14	Opalinus Clay		x		x	x
BDB1-229.68-AQ	229.54 – 229.82	30.01.14	05.02.14	Opalinus Clay		x		x	x
BDB1-231.18-AQ	231.05 – 231.30	30.01.14	05.02.14	Opalinus Clay		x		x	x
BDB1-233.63-AQ	233.50 – 233.75	30.01.14	05.02.14	Opalinus Clay		x		x	x
BDB1-235.14-AQ	235.00 – 235.28	30.01.14	05.02.14	Opalinus Clay		x		x	x
BDB1-237.88-AQ	237.78 – 237.98	31.01.14	05.02.14	Opalinus Clay		x		x	x
BDB1-243.37-AQ	243.28 – 243.45	31.01.14	05.02.14	Staffelegg Fm		x		x	x
BDB1-245.54-AQ	245.43 – 245.64	31.01.14	05.02.14	Staffelegg Fm		x		x	x

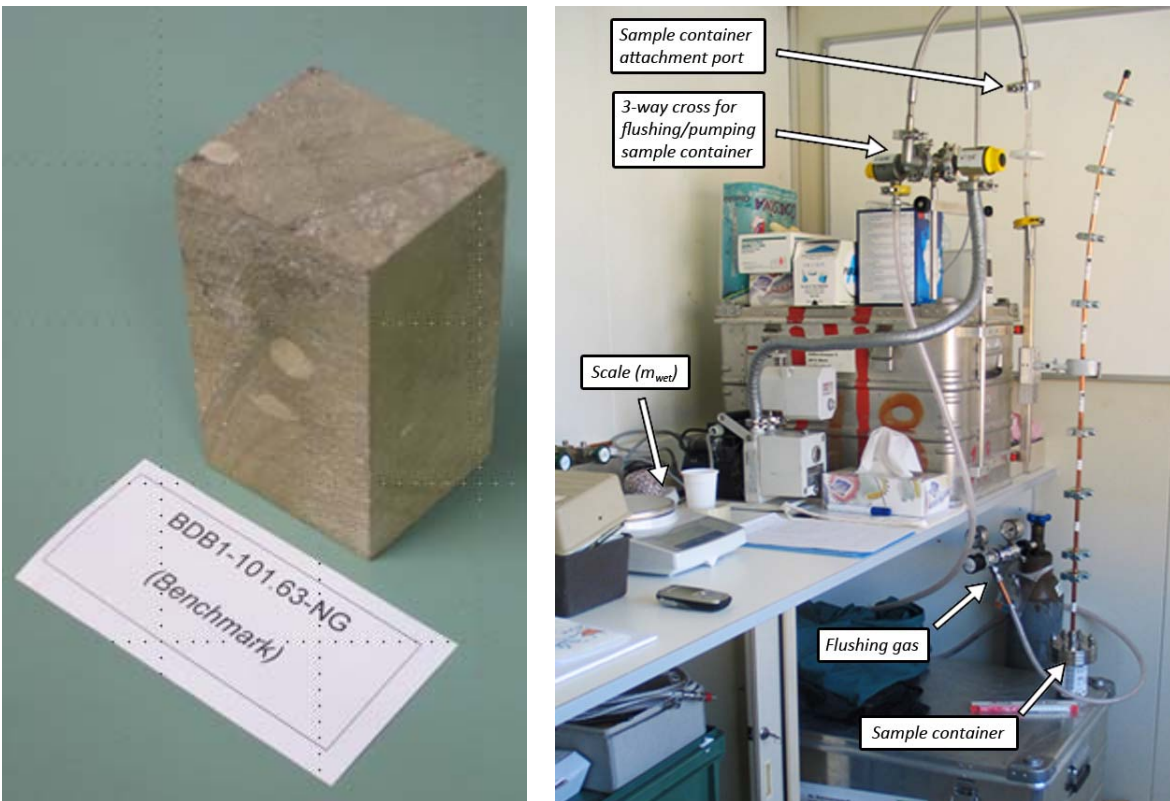


**Figure 3-6: Central Core Section Used for Porewater Noble Gas Extraction (left) and the Assembled Porewater Noble Gas Sampling Apparatus at RWI, Uni Bern (right).**

In order to minimize disturbance, due to sampling, of the dissolved gas inventory of the porewater, the durations of the N<sub>2</sub> flushing and pumping cycles were kept short and as uniform as possible. While flushing lasted approximately 3 to 4 seconds per cycle, the accumulated total pumping times of the initial pumping and the three pumping cycles average about 2.5 minutes, with average pressures after each pumping step between 6 to 7 mbar and individual final pressures in the sample containers ranging from 4.1 to 7 mbar (Appendix A3).

All of the 25 NG samples were analysed for petrophysical parameters (dry and wet bulk density, dry and wet water content) and dissolved He, Ne and Ar concentrations in the porewater. Isotope ratio analyses of <sup>20</sup>Ne/<sup>22</sup>Ne and <sup>40</sup>Ar/<sup>36</sup>Ar were performed on all 25 samples, while <sup>3</sup>He/<sup>4</sup>He analyses were performed on 18 samples.

Analyses of the NG samples were conducted in two batches between April 7<sup>th</sup> – August 8<sup>th</sup>, 2014 (18 samples) and between April 18<sup>th</sup> – April 28<sup>th</sup>, 2015 (7 samples). The first batch consisted of samples BDB1-101.63-NG to BDB1-246.99-NG, which were taken as part of the DB-A inter-laboratory comparison study. In addition, sample BDB1-66.40-NG was analysed as an analytical trial, as it was expected to have much lower He concentrations, being proximal to the water-conducting feature encountered between 50-59 m BHL. The analysis confirmed that these proximal samples can be expected to have lower He concentrations, by 1.5 orders of magnitude or more, requiring adaptations to the analytical protocol for such low concentration

samples and necessitating a time-consuming extension of the analytical calibration to lower values. The second batch, consisting of the remaining 7 samples, was then successfully analysed using the new protocol.

**Table 3-4: List of Porewater Noble Gas (-RWI-NG) Samples and Analysed Parameters**

Sample	Geology	Petrophys. Parameters	$^4\text{He}_{\text{H}_2\text{O}}$	$^4\text{He}_{\text{pw}}$	$(^3\text{He}/^4\text{He})_{\text{H}_2\text{O}}$	$(^3\text{He}/^4\text{He})_{\text{pw}}$	$\text{Ne}_{\text{H}_2\text{O}}$	$(^{20}\text{Ne}/^{22}\text{Ne})_{\text{H}_2\text{O}}$	$\text{Ar}_{\text{H}_2\text{O}}$	$\text{Ar}_{\text{pw}}$	$(^{40}\text{Ar}/^{36}\text{Ar})_{\text{H}_2\text{O}}$	$(^{40}\text{Ar}/^{36}\text{Ar})_{\text{pw}}$
BDB1-60.59-NG	Passwang Fm	x	b.c.	-	n.a.	n.a.	b.c.	-	x	-	x	-
BDB1-61.23-NG	Passwang Fm	x	b.c.	-	n.a.	n.a.	b.c.	-	x	-	x	-
BDB1-63.53-NG	Passwang Fm	x	x	-	n.a.	n.a.	b.c.	b.c.	x	-	x	-
BDB1-66.40-NG	Passwang Fm	x	x	-	-	-	-	-	x	-	x	-
BDB1-72.05-NG	Passwang Fm	x	x	-	n.a.	n.a.	b.c.	b.c.	x	-	x	-
BDB1-83.78-NG	Passwang Fm	x	x	-	n.a.	n.a.	b.c.	b.c.	x	-	x	-
BDB1-90.68-NG	Passwang Fm	x	x	-	n.a.	n.a.	-	-	x	-	x	-
BDB1-93.40-NG	Passwang Fm	x	x	x	x	x	x	x	x	x	x	x
BDB1-101.63-NG	Passwang Fm	x	x	-	x	-	-	-	x	-	x	-
BDB1-114.08-NG	Opalinus Clay	x	x	x	x	x	x	x	x	x	x	x
BDB1-120.86-NG	Opalinus Clay	x	x	-	x	-	-	-	x	-	x	-
BDB1-127.33-NG	Opalinus Clay	x	x	x	x	x	x	x	x	x	x	x
BDB1-133.46-NG	Opalinus Clay	x	x	x	x	x	x	x	x	x	x	x
BDB1-144.49-NG	Opalinus Clay	x	x	x	x	x	x	x	x	x	x	x
BDB1-160.25-NG	Opalinus Clay	x	x	x	x	x	x	x	x	x	x	x
BDB1-167.38-NG	Opalinus Clay	x	x	x	x	x	x	x	x	x	x	x
BDB1-173.47-NG	Opalinus Clay	x	x	x	-	-	x	x	x	x	x	x
BDB1-175.53-NG	Opalinus Clay	x	x	x	x	x	x	x	x	x	x	x
BDB1-178.53-NG	Opalinus Clay	x	x	x	x	x	x	x	x	x	x	x
BDB1-189.52-NG	Opalinus Clay	x	x	x	x	x	x	x	x	x	x	x
BDB1-193.13-NG	Opalinus Clay	x	x	x	x	x	x	x	x	x	x	x
BDB1-204.09-NG	Opalinus Clay	x	x	x	x	x	x	x	x	x	x	x
BDB1-209.37-NG	Opalinus Clay	x	x	x	x	x	x	x	x	x	x	x
BDB1-219.66-NG	Opalinus Clay	x	x	x	x	x	x	x	x	x	x	x
BDB1-246.99-NG	Staffelegg Fm	x	x	x	n.a.	n.a.	x	x	x	x	x	x

**Notes:**

Shaded = samples used for inter-laboratory comparison. X = analysed and data used for interpretation; "b.c.": analysed, data below calibration limit; "-": analysed, but data rejected due to sample contamination or analytical problems; "n.a.": not analysed.

#### 4. GROUNDWATER SAMPLING

From December 5<sup>th</sup> to 13<sup>th</sup>, 2013, the drilling encountered essentially non-fractured limestone and marlstone of the Hauptrogenstein (early Bajocian) with no recognisable water inflow. Drilling of this section was performed using water from a nearby water-conducting zone in the Hauptrogenstein as drilling fluid.

On Friday, December 13<sup>th</sup>, a water inflow was observed during drilling of the last core section, of 3 m length, down to 59.69 m BHL (borehole length). Several mm-wide open fractures were identified in this last core section and measurement of artesian outflow from the borehole suggested an inflow of about 5-10 L/min. Within one hour, the outflow and the electric conductivity of the flowing water stabilised, indicating that there was, indeed, a natural water inflow from the rock into the borehole.

Based on these observations, drilling was stopped and an inflatable single packer was installed by the authors and D. Jaeggi (swisstopo) to collect the inflowing groundwater from the packed-off interval extending from 51 m to 59.65 m BHL. The packer was equipped with two sampling lines: one for water sampling, and another for potential injection of N<sub>2</sub> gas, in case the water pressure was too low for artesian outflow and gas pumping was required. The water sampling line reached down to about 52.3 m and the gas pressure line ended at the bottom of the inflatable packer at 51 m BHL.

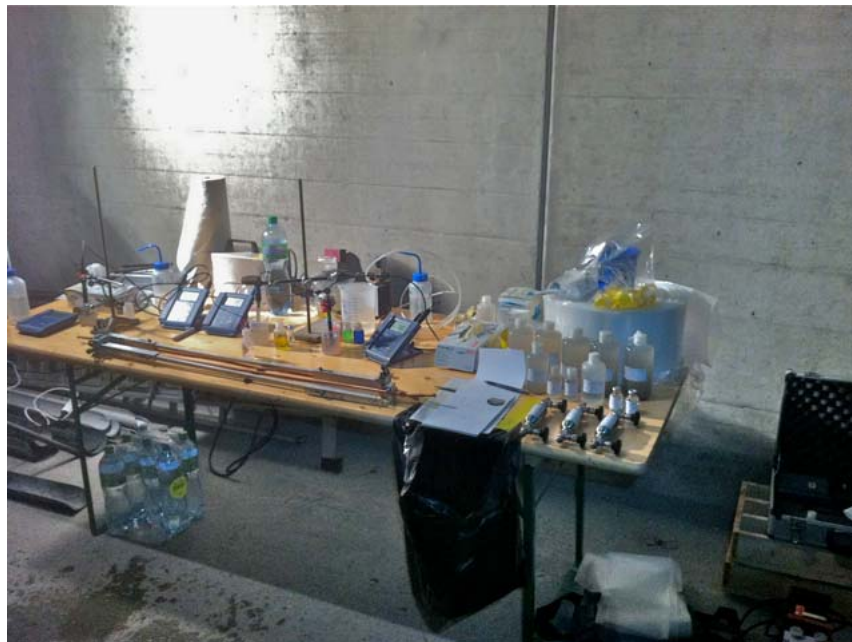
After insertion of the packer, but before its inflation, the electric conductivity of the water started to increase, by about a factor of two, indicating that the formation water was more highly mineralised than the mixture of drilling fluid and groundwater. After stabilisation of the packer at 30 bars, the interval pressure quickly stabilised at 7 bars and artesian outflow of the groundwater occurred through both the water sampling and the N<sub>2</sub>-gas line. The total flow rate was about 2 L/min and was limited by the diameter of the sampling lines (ca. 6 mm). After installation, the outflow was collected in a 580 L barrel, corresponding to about 3.5 interval volumes.

After a flushing time of about 18 hours, the first set of groundwater samples was collected on Saturday, December 14<sup>th</sup>. Based on the constant flow rate, this corresponds to about 2100 L of water that was discharged from the packer interval (or about 13 times the volume of the packer interval). A second set of groundwater samples was collected on Sunday, December 15<sup>th</sup>, and a third set on Monday, December 16<sup>th</sup>, in the early morning. From Saturday to Sunday, the interval pressure increased to about 8.7 bars, whereas the outflow remained constant (continuously controlled by the tube diameter) and essentially stable at 1 L/min per line (*cf.* detailed sampling protocol in Appendix A4).

After the third sampling early Monday morning, the packer was removed and drilling activities continued, without having been interrupted by the groundwater sampling activities over the weekend.

All three sampling campaigns included field measurements of T, pH, Eh, O<sub>2</sub> and electric conductivity (EC). Field measurements were conducted immediately after collecting the groundwater in various open plastic beakers. Field measurements were, therefore, not performed using a sophisticated flow-through sampling line, which would be required to obtain consistent results for dissolved oxygen and redox potential measurements (*cf.* Chapter 12).

Groundwater samples were collected in HDPE bottles for chemical, isotope and noble gas analyses. Samples for the analyses of anion concentrations,  $\delta^{18}\text{O}$ ,  $\delta^2\text{H}$ , and  $^3\text{H}$  were collected unfiltered and with no additives. Samples for the analyses of cation concentrations and  $\delta^{13}\text{C}$  were filtered on site using 0.45 $\mu\text{m}$  Millipore filters and the cation samples were subsequently acidified to pH of about 2 using  $\text{HNO}_3$ . The samples for  $^{14}\text{C}$  analyses were collected in-line into stainless steel cylinders (75 mL) to avoid any air contact. The noble gas samples were similarly collected in-line into copper tubes. Stainless steel cylinders and copper tubes were filled from bottom to top to ensure complete removal of all air from the containers.



Notes: The sample containers include copper tubes for noble gases (front), stainless steel cylinders for  $^{14}\text{C}$  (right, front), glass bottles for  $\delta^{13}\text{C}$  (right, middle) and HDPE bottles of various sizes for chemical and stable water isotopes (right, back).

**Figure 4-1: Groundwater Samples Collected in Appropriate Sample Containers and Layout of Field Measurement Devices.**

## 5. ANALYTICAL METHODS

### 5.1 MINERALOGICAL ANALYSES

Mineralogical analyses were performed on rim material of the cores from borehole BDB-1. This rim material was removed by hand from the core sections during the preparation of the saturated central core material, which was subsequently used for chemical and isotopic porewater investigation. This rim material might have undergone partial desaturation and possibly also contamination by the drilling fluid (i.e., groundwater in Passwang Fm and air in the Opalinus Clay). For mineralogical analyses, such effects are relatively unimportant, whereas the handling would inhibit any chemical and isotope porewater analyses. From the core sections, about 1 kg of rim material extending across the entire section was homogenised and split into smaller aliquots. Finally, about 300–400 g of homogenised crushed rock were ground in a ring mill to the grain size required for whole rock and clay mineralogical analyses.

#### 5.1.1 Whole Rock Mineralogy

The whole-rock mineralogy of the samples was determined by X-ray diffraction using a Philips PW3710 diffractometer. Homogenised rock material of a grain size of less than 2  $\mu\text{m}$  was mounted on a sample holder, disordered with a textured stamp (to minimize potential for artificial orientation of mineral grains associated with transfer of the rock powder to the sample holder), and scanned with Cu K $\alpha$  radiation from 2° to 70° 2 $\theta$  angle. Quantification of the contents of quartz, feldspars and carbonates (calcite, dolomite, siderite) was performed by an internal standardisation utilising the diffraction peak-intensity ratio of the mineral to that of an internal LiF-standard. The relative error of such determinations is about  $\pm$  5%.

The standardisation used is valid for individual mineral contents up to approximately 50 wt.%. In limestones the contents of calcite or dolomite often exceed 50 wt.% and the apparent concentrations obtained by XRD have to be corrected. The correction uses the total inorganic carbon content measured by IR-spectroscopy (cf. Section 5.1.2) from which the carbonate mineral contents are calculated according to their stoichiometry and XRD peak intensity. As a first approximation, the total sulphur concentration measured by IR-spectroscopy was converted to pyrite, thus neglecting the possible occurrence of trace contents of other sulphide and sulphate minerals.

Sheet silicates in the rocks of the Passwang Fm and Opalinus Clay consist mainly of clay minerals. The sum of the sheet silicates or the total clay-mineral content, respectively, was calculated by the difference of 100% minus the sum of non-sheet silicates.

#### 5.1.2 Inorganic Carbon, Organic Carbon and Total Sulphur of Whole Rock

The concentrations of total (TC) and inorganic (TIC) carbon and total sulphur ( $S_{\text{tot}}$ ) were analysed by infrared (IR) spectroscopy on a G4 ICARUS CS HF combustion analyser (former Ströhlein GmbH & Co, Germany, now Bruker).

For the analyses of TC, TIC and  $S_{\text{tot}}$  a few grams of rock powder are combusted at 1300°C in a ceramic crucible within a sealed high-frequency furnace to convert the carbon and sulphur present in the rock into CO<sub>2</sub> and SO<sub>2</sub> gas, respectively. After cleaning of water vapour and halogens by magnesium-perchlorate and halogen traps, respectively, these reaction gases are

subsequently measured by a solid-state IR detector. Using oxygen as a carrier gas during combustion, all carbon and sulphur in the rock is oxidised, resulting in the measurement of TC and  $S_{\text{tot}}$ . In turn, the analysis of TIC is conducted using nitrogen as a carrier gas to prevent oxidation of organic carbon in the rock. The content of organic carbon ( $C_{\text{org}}$ ) is then calculated by difference from TC and TIC. The uncertainty attached to this method is around 0.2 wt.% for TC, TIC and  $S_{\text{tot}}$ .

### 5.1.3 Clay Mineralogy

The clay mineralogy of the rock samples was determined by X-ray diffraction using a Philips PW1810 diffractometer. Homogenised rock material from the rim of the drill cores was first ground in a ring mill to a grain size of about 60  $\mu\text{m}$ . The clay fraction ( $< 2 \mu\text{m}$ ) was then separated by sedimentation in a column filled with a 0.01N  $\text{NH}_4\text{OH}$  solution. The clay fraction was removed from the supernatant suspension by centrifugation.

The separated clay material was mounted by sedimentation on three sample holders in order to obtain orientated samples. Each sample holder was subjected to different treatments: a) dried under air, b) saturated with ethylene glycol for the identification of expandable clay minerals, and c) heated at 550°C for 1 hour to allow the distinction between kaolinite and chlorite. The orientated samples were then scanned with  $\text{Cu K}\alpha$  radiation from 2° to 40°  $2\theta$  angle, at a scanning velocity of 2°/min.

The relative ratios of the individual clay-mineral contents were derived manually from the obtained diffractometer patterns. After manual peak deconvolution, the peak intensities of individual clay minerals are compared amongst each other, between the differently treated samples, and finally corrected for the mass attenuation of the individual clays. Comparison of a two-person evaluation and quantification reveals an average relative uncertainty of  $\pm 5\%$  for the individual clay mineral contents.

## 5.2 PETROPHYSICAL PARAMETERS

The way petrophysical parameters were determined depends on porewater sample type and their processing. For porewater chemistry samples (RWI-AQ samples), work included the determination of the water content, bulk wet density and grain density, from which the water-loss porosity and pycnometer porosity (also called total porosity) were calculated. For these samples, all density and water content measurements were performed at least in duplicate to minimise the analytical uncertainty. For porewater noble gas samples (RWI-NG samples), this included the mass of porewater, water content and the calculated water-loss porosity.

### 5.2.1 Water Loss, Mass of Porewater and Gravimetric Water Content

The water content of porewater chemistry and porewater noble gas samples was obtained by the gravimetric determination of water loss by drying the samples to constant weight conditions. In addition, the water content of porewater chemistry samples was also obtained by isotope mass balance of the diffusive isotope exchange technique (*cf.* Section 5.4.1).

For the RWI-AQ samples, about 160–250 g of saturated rock from the core centre was used for water-loss measurements to account for rock heterogeneity. The saturated rock was weighed

immediately after unpacking and removing the rim material from the drill core samples and then placed in a ventilated oven for drying at 105°C. The criterion used for attainment of constant mass during gravimetric measurements was a mass change of less than 0.005 g over a 14-day drying interval.

In addition to the water loss measurements performed on designated sample aliquots, the water loss was also determined on the two sample aliquots used for the isotope diffusive exchange technique. For the water-loss calculation of these samples, care was taken to accurately determine the small, but common, amount of transfer of test water to the rock sample during the experiment (*cf.* Section 5.4).

From previous studies, it is well known that the porewater in the Opalinus Clay at Mont Terri has an ionic strength well below that of seawater (Pearson et al. 2003). Therefore, the gravimetric water content,  $WC$ , can be taken to be identical to the porewater content,  $WC_{pw}$ , and no salinity correction has to be applied.

The calculation of the noble gas concentration in the porewater uses directly the mass of porewater contained in the rock cylinder used for outgassing. The mass of porewater,  $m_{pw}$ , obtained by drying the saturated rock cylinders is calculated from the water loss upon drying as:

$$m_{pw} = m_{rock, wet} - m_{rock, dry} \quad (1)$$

where  $m_{rock, wet}$  = mass of the wet rock sample at the time of sampling on site and  $m_{rock, dry}$  = mass of dry rock sample after reaching constant weight at 105°C in the lab.

The gravimetric water content,  $WC_{wet}$ , is calculated from the change in weight upon drying ( $m_{rock, wet} - m_{rock, dry}$ ) and is expressed relative to the wet mass  $m_{rock, wet}$  of the rock according to:

$$WC_{wet} = \frac{m_{rock, wet} - m_{rock, dry}}{m_{rock, wet}} \bullet 100\% . \quad (2)$$

Alternatively, and for the calculation of the bulk dry density (equation 8), the water content relative to the dry weight,  $WC_{dry}$ , is:

$$WC_{dry} = \frac{m_{rock, wet} - m_{rock, dry}}{m_{rock, dry}} \bullet 100\% . \quad (3)$$

The absolute error of the weight determinations in the laboratory and that for the porewater noble gas samples measured on the drill site is  $\pm 0.002$  g and  $\pm 0.05$  g, respectively. Applying the rules of uncertainty propagation, the uncertainty on the mass of porewater,  $m_{pw}$ , becomes:

$$\sigma_{m_{pw}} = \sqrt{\left(\sigma_{m_{rock, wet}}\right)^2 + \left(\sigma_{m_{rock, dry}}\right)^2} \quad (4)$$

and for  $WC_{wet}$ :

$$\sigma_{WC_{wet}} = \sqrt{\left(\left(\frac{\sigma_{m_{PW}}}{m_{PW}}\right)^2 + \left(\frac{\sigma_{m_{rock\ wet}}}{m_{rock\ wet}}\right)^2\right) \times (WC_{wet})^2} \quad (5)$$

and for  $WC_{dry}$ :

$$\sigma_{WC_{dry}} = \sqrt{\left(\left(\frac{\sigma_{m_{PW}}}{m_{PW}}\right)^2 + \left(\frac{\sigma_{m_{rock\ dry}}}{m_{rock\ dry}}\right)^2\right) \times (WC_{dry})^2}. \quad (6)$$

## 5.2.2 Bulk and Grain Density

The bulk wet density,  $\rho_{b, wet}$ , was measured on saturated rock material within 1 minute after unpacking and removing the rim material from the drill-core sample. The paraffin displacement method was applied, making use of Archimedes' principle. Homogeneous rock samples of a volume of approximately 1.5-2 cm<sup>3</sup> were taken from the saturated centre of the drill core. The sample volume was determined by weighing the rock sample in air and during immersion into paraffin using the density accessory kit of Mettler Toledo™. On average, after every third sample, the paraffin was replaced and its density newly determined. The paraffin density,  $\rho_p$ , was 0.8644 ± 0.005 g/cm<sup>3</sup> at 22°C during the first sample preparation campaign in early January, 2014, and 0.8644 ± 0.007 g/cm<sup>3</sup> at 22°C during the second sample preparation campaign in early February, 2014. The bulk wet density,  $\rho_{b, wet}$ , is calculated according to:

$$\rho_{b, wet} = \frac{\rho_p \bullet m_{rock, wet}}{m_{rock, wet} - m_{(rock, wet)_p}} \quad (7)$$

where  $\rho_p$  is the density of paraffin,  $m_{rock, wet}$  is the mass of the saturated rock sample (i.e., including the porewater) in air and  $m_{(rock, wet)_p}$  is the mass of the saturated rock sample immersed in paraffin.

Measurements of the bulk dry density of clay-rich rock material is commonly unreliable due to the effects of shrinking associated with the drying of swelling clay minerals. Therefore, the bulk dry density,  $\rho_{b, dry}$ , was calculated from the water content relative to the dry mass of the rock,  $WC_{dry}$ , and the bulk wet density,  $\rho_{b, wet}$ , according to:

$$\rho_{b, dry} = \frac{\rho_{b, wet}}{1 + WC_{(dry)}}. \quad (8)$$

Grain density measurements were determined with the He-gas displacement technique using a Micrometric AccuPyc II 1340 gas-pycnometer. In this technique, the difference of gas pressure is measured in a sample cell of constant volume in its empty state as well as when containing the solid sample, and the results converted to the grain (or material) density of the solid sample. For the present samples, about 7 g of dried powdered rock material (< 2µm) used for whole rock

mineralogical analyses were used. The grain density is determined as the average of 5 measuring cycles, of which the standard deviation (s.d.) has to be  $\leq 0.005 \text{ g/cm}^3$ .

Applying the rules of uncertainty propagation and the known uncertainty of mass determinations ( $\pm 0.002 \text{ g}$ ) and/or standard deviation of multiple measurements (paraffin density, He-pycnometry), the uncertainty on the bulk wet density,  $\rho_{b, wet}$ , determination becomes:

$$\sigma_{\rho_{b, wet}} = \rho_{b, wet} \cdot \sqrt{\left(\frac{\sigma_{m_{rock, wet}}}{m_{rock, wet}}\right)^2 + \left(\frac{\sigma_{\Delta m_P}}{\Delta m_P}\right)^2 + \left(\frac{\sigma_{\rho_P}}{\rho_P}\right)^2} \approx \sqrt{\frac{\sigma_{\rho_P}}{\rho_P}} \quad (9)$$

and for the calculated bulk dry density,  $\rho_{b, dry}$ :

$$\sigma_{\rho_{b, dry}} = \rho_{b, dry} \cdot \sqrt{\left(\frac{\sigma_{\rho_{b, wet}}}{\rho_{b, wet}}\right)^2 + \left(\frac{\sigma_{WC_{dry}}}{1 - WC_{dry}}\right)^2} \quad (10)$$

where  $\Delta m_P$  is the mass of the displaced paraffin and  $\rho_P$  is the density of paraffin.

For the grain density, the absolute uncertainty is taken to be the standard deviation of the 5 measurement cycles performed with the He-pycnometer.

### 5.2.3 Pycnometer Porosity and Water-Loss Porosity

The pycnometer (or total) porosity,  $\phi_{Pyc}$ , of a rock sample is the ratio of the total pore volume to the total volume of the sample ( $V_{pores}/V_{tot}$ ), where the total volume is the sum of the pore volume and the volume occupied by mineral grains (Norton & Knapp, 1977). The pycnometer porosity ( $\phi_{Pyc}$ ) is determined from the values of the calculated bulk dry density and the measured grain density according to:

$$\phi_{Pyc} = 1 - \left(\frac{\rho_{b, dry}}{\rho_g}\right) \quad (11)$$

where  $\rho_{b, dry}$  is the calculated bulk dry density and  $\rho_g$  is the measured grain density. The uncertainty associated to the pycnometer porosity can be expressed as:

$$\sigma_{\phi_{Pyc}} = \sqrt{\left(\frac{\sigma_{\rho_{b, dry}}}{\rho_g}\right)^2 + \left(\frac{\sigma_{\rho_g} \times \rho_{b, dry}}{\rho_g^2}\right)^2} \quad (12)$$

As can be seen from equation (12), the uncertainty of the pycnometer porosity depends primarily on the density of the paraffin used in the bulk density and He-pycnometric grain density measurements, respectively. The density of kerosene is strongly temperature dependent, and thus might differ from the producer's label, and has to be determined for each

batch of rock samples analysed. In the He-pycnometric measurement, the temperature dependence of the He pressure is corrected automatically and the uncertainty is given by the standard deviation of multiple measurement cycles.

The water-loss porosity or volumetric moisture content of a rock sample,  $\phi_{WL}$ , expressed as a fraction of one, is the ratio of the water-filled, connected pore volume to the total volume ( $V_{wat}/V_{tot}$ ) and is obtained according to:

$$\phi_{WL} = \frac{WC_{wet} \cdot \rho_g}{WC_{wet} \cdot \rho_g + (1 - WC_{wet}) \cdot \rho_{pw}} \quad (13)$$

where  $\rho_{PW}$  is the density of the pore water,  $\rho_g$  is the grain density of the rock, and  $WC_{wet}$  is water content of the rock relative to its wet weight (cf. equation 2).

As mentioned above the porewater in the Opalinus Clay at Mont Terri has an ionic strength below that of seawater (Pearson et al. 2003). For the rocks at the Mont Terri URL, the assumption of the porewater density being 1.00 g/cm<sup>3</sup>, and ignoring a salinity correction for the porosity calculations is justified and does not affect the calculations outside the analytical error.

The uncertainty on the water-loss porosity ( $\sigma_{\phi_{WL}}$ , here given as  $\sigma_{\phi_{WL}}^2$  for layout reasons) is calculated as:

$$\begin{aligned} (\sigma_{\phi_{WL}})^2 = & \left( \frac{WC_{wet} \cdot (1 - WC_{wet}) \cdot \rho_{pw}}{(WC_{wet} \cdot \rho_g + (1 - WC_{wet}) \cdot \rho_{pw})^2} \cdot \sigma_{\rho_g} \right)^2 \\ & + \left( \frac{WC_{wet} \cdot (1 - WC_{wet}) \cdot \rho_g}{(WC_{wet} \cdot \rho_g + (1 - WC_{wet}) \cdot \rho_{pw})^2} \cdot \sigma_{\rho_{pw}} \right)^2 \\ & + \left( \frac{\rho_g \cdot \rho_{pw}}{(WC_{wet} \cdot \rho_g + (1 - WC_{wet}) \cdot \rho_{pw})^2} \cdot \sigma_{WC_{wet}} \right)^2. \end{aligned} \quad (14)$$

Alternatively, water-loss porosity,  $\phi_{WL}$ , can also be derived from the measured bulk wet density,  $\rho_{b,wet}$ , and the gravimetric water content,  $WC_{wet}$ , for each sample according to:

$$\phi_{WL} = \frac{m_{pw} \cdot \rho_{b,wet}}{(m_{rock,dry} + m_{pw}) \cdot \rho_{pw}} = WC_{wet} \cdot \frac{\rho_{b,wet}}{\rho_{pw}}. \quad (15)$$

The uncertainty of the derived water-loss porosity becomes:

$$\sigma_{\phi_{WL}} = \sqrt{\left(\frac{\sigma_{WC_{wet}} \cdot \rho_{b,wet}}{\rho_{pw}}\right)^2 + \left(\frac{\sigma_{\rho_{b,wet}} \cdot WC_{wet}}{\rho_{pw}}\right)^2 + \left(\frac{\sigma_{\rho_{pw}} \cdot WC_{wet} \cdot \sigma_{\rho_{b,wet}}}{\rho_{pw}^2}\right)^2}. \quad (16)$$

#### 5.2.4 Specific Surface Area (BET)

The specific surface area of the rock samples was derived from N<sub>2</sub> adsorption isotherms that were measured with a Coulter SA 3100 surface analyser. Powdered rock material of a grain size ≤ 2 mm was weighed to an accuracy of ±0.001 grams and thoroughly desorbed of primary adsorbed gases by heating under vacuum at 150 °C for 1 hour. Subsequently, nitrogen adsorption isotherms of the powdered samples were measured in equilibrium with liquid nitrogen. The N<sub>2</sub>-surface area was calculated using the so-called BET method (Brunauer, Emmet and Teller method; Brunauer et al. 1938) for a pressure range of P/P<sub>0</sub> from 0 to 1. The specific surface area of the rock sample is then obtained from the N<sub>2</sub>-surface area and the sample weight, and expressed in m<sup>2</sup>/g<sub>rock</sub>.

### 5.3 AQUEOUS EXTRACTION

For aqueous extraction tests, saturated rock material from the central part of the on-site conditioned drill cores was selected in order to exclude any contamination from the drilling process. Such material was obtained by removing about 2 cm of the outer core rim using a chisel and hammer immediately after unpacking drill cores in the laboratory. Rock chips of about 10 cm<sup>3</sup> from the central part of the core were further disintegrated by hand along grain boundaries to pieces of a few mm<sup>3</sup> to avoid opening of mineral fluid inclusions. About 30 g of the disintegrated, saturated rock was immediately immersed in pre-prepared polypropylene tubes containing 30 mL of degassed oxygen- and CO<sub>2</sub>-free ultra-pure water. The preparation time, from the large chips until immersion of the small pieces into the water and closure of the polypropylene tube, was minimised to <5 minutes to suppress sulphide mineral oxidation and pore-water evaporation as much as possible. Subsequently, the closed tubes were quickly transferred into a glovebox where they were shaken, end-over-end, under a continuous N<sub>2</sub>-gas stream in an oxygen-free atmosphere. All sample handling was conducted using surgical rubber gloves in order to minimise Cl<sup>-</sup> contamination from the skin. For each preparation campaign a blank extraction was also performed.

Extraction conditions were chosen to 1) attain equilibrium with calcite by extracting over 48 hours, and 2) to suppress sulphide mineral oxidation. Aqueous extraction tests were performed for 69 samples, of which 6 were run in duplicate. Such duplicate extraction allows quality control with respect to the homogeneity of the extracted rock material. This is crucial in the case of the possible occurrence of solid sulphate and chloride minerals in the rock, but also in the case of sulphides (e.g., pyrite), where it helps to identify possible oxidation during the rock preparation and extraction process.

The solid:liquid (S:L) ratio relative to the saturated (wet) weight of rock was chosen to be about 1:1 (*cf.* Appendix B.1). For conversion of the solid:liquid ratio relative to the dry weight of rock in

the extraction tests, the wet weight of extracted rock was converted to dry weight using the water content measured on each sample.

After extraction, phase separation was conducted by centrifugation of the polypropylene tubes. The supernatant leach solutions were quickly removed using a syringe. From the syringe, the clear extract solution was transferred into PPE bottles, after filtration using 0.2 µm Millipore filters, and stored for analysis.

### 5.3.1 Chemical Analyses of extract solutions

After filtration, the supernatant solutions were immediately analysed for pH and titrated for their total alkalinity with a Metrohm Titrino DMP 785 system. Major anions ( $\text{Cl}^-$ ,  $\text{Br}^-$ ,  $\text{NO}_3^-$ ,  $\text{F}^-$ ,  $\text{SO}_4^{2-}$ ) and cations ( $\text{Na}^+$ ,  $\text{K}^+$ ,  $\text{Ca}^{2+}$ ,  $\text{Mg}^{2+}$ ,  $\text{NH}_4^+$ , and  $\text{Sr}^{2+}$ ) were later analysed in the remaining solutions by ion chromatography utilising a Metrohm ProfIC AnCat MCS IC system with automated 5 µL and 50 µL injection loops. The detection limit of this technique is 0.016 mg/L for anions and 0.1 mg/L for cations. The analytical error is  $\pm 5\%$  based on multiple measurements of high-grade, commercial check standard solutions (Sigma-Aldrich, Merck). To account for the highly-variable concentrations of individual anions and cations in the extract solutions, the analyses were conducted on the undiluted solution, on manually prepared dilution of 1:10 and, for some samples, on 1:100 dilution, in addition to the additional automated dilution of the instrument.

Concentrations of K, Mg and Sr that were close to, or below, the detection limit for the ion chromatographic method, were re-analysed using a Varian 710 ES ICP-OES system with a detection limit of 0.01 mg/L. The analytical error of the ICP-OES analyses is also  $\pm 5\%$  for these elements based on multiple measurements of high-grade, commercial check standard solutions (Sigma-Aldrich, Merck).

In the ultra-pure water used for extraction, as well as in all blank extraction tests, the concentrations of all analysed elements were below detection limit.

### 5.3.2 Chloride Isotope Analyses of Extract Solutions and Groundwater

Chloride stable isotope analyses ( $\delta^{35}\text{Cl}$ ) were performed by Hydroisotop GmbH, Schweitenkirchen, Germany, on extract solutions produced from 22 samples across the entire profile encountered by borehole BDB-1, and on one groundwater sample from the Passwang Fm.

At Hydroisotop GmbH, a specified volume of aqueous extract solution and groundwater, respectively, corresponding to a Cl concentration of 100 µg, was pipetted into a 20 mL headspace vial and heated at 130°C until complete evaporation. After cooling to room temperature, 0.4 mL of  $\text{H}_3\text{PO}_4$  (99% pure, liquid) and 10 µL ethanol were added, followed by heating the immediately- and tightly-closed vial for 20 hours at 130°C. After cooling to room temperature, the tightness of the headspace vial was checked. From the headspace vial, 6.0 µL of gas were transferred to another headspace vial, which was, again, immediately and tightly closed. The so-synthesised chloroethane was analysed by P&T-GC-IRMS at  $m/z$  64 and 66. Calculation of the  $\delta^{37}\text{Cl}$ -values was done against the IAEA reference standard for sodium chloride (ISL-354;  $^{37}\text{Cl}/^{35}\text{Cl}=0.31964\pm 0.00092$ ), which was processed in the same manner. Each sample was analysed in triplicate (Hydroisotop GmbH, 2016).

### 5.3.3 Conversion of Aqueous Extract Data to Porewater Concentrations

The solutes in an aqueous extract solution originate from different potential sources that have to be identified before ion concentrations can be converted to porewater ion concentrations. These sources are: 1) original solutes in porewater, 2) solutes in mineral fluid inclusions, and 3) induced mineral dissolution, precipitation, and ion exchange and sorption reactions during the extraction test.

In clay-dominated argillaceous rock samples of the Opalinus Clay, the volumes of fluid inclusions in the matrix are usually low relative to the volume of porewater, rendering this source of solutes as negligible (Waber et al. 2003a). In contrast, this source may become important in the more carbonate-rich and quartz-rich rocks of these stratigraphic units. A possible impact of the fluid inclusion solutes on the ion concentration in aqueous extract data was circumvented by disintegrating the rock material along its grain boundaries (see above), thus inhibiting (or at least greatly reducing) the opening of fluid inclusions in quartz and carbonate minerals (as will occur when grinding the rock).

Mineral reactions will inevitably take place during aqueous extraction and will modify the porewater solute concentrations. Therefore, conversion of solute concentrations measured in aqueous extract solution to porewater solute concentrations is only applicable for ions that are not involved in any reactions (i.e., that behave conservatively) and for which the only source is the porewater. In the Jurassic sedimentary rocks at Mont Terri, these conditions are met by the anions  $\text{Cl}^-$  and  $\text{Br}^-$ , whereas all cations and other anions are, to variable degrees, involved in mineral reactions (Waber et al. 2003a; cf. Chapters 8 and 9).

In addition to the chemical behaviour of an element, the porosity that is accessible to this element in its dissolved state has to be known to allow conversion of solute concentrations measured in aqueous extract solution to porewater solute concentrations. This accessible porosity is species-specific, depends on the rock mineralogy and texture, and has to be derived from comparison of different extraction techniques and/or theoretical approaches based on the petrophysical properties and mineralogy of the rock (cf. Chapters 7 and 9).

Once the chemical conservative behaviour of an element during aqueous extraction is proven, and the species-specific accessible porosity is known, the solute concentration measured in the aqueous extract solution can be converted to the porewater solute concentrations according to:

$$C_{pw} = C_{aqex} \cdot \frac{m_{w,aqex}}{m_{pw}} \cdot \frac{S_{wet}}{f_a} = C_{aqex} \cdot \frac{1}{\left(\frac{S^*}{L^*}\right) \cdot WC_{wet}} \cdot \frac{S_{wet}}{f_a} \quad (17)$$

where  $C_{pw}$  is the apparent solute concentration in pore water ( $\text{mg}/\text{kg}_{\text{H}_2\text{O}}$ ),  $C_{aqex}$  is the concentration of chemically conservative solutes in the aqueous extract solution ( $\text{mg}/\text{kg}_{\text{H}_2\text{O}}$ ),  $m_{w,aqex}$  is the mass of extraction water added,  $m_{pw}$  is the mass of porewater in the sample used for aqueous extraction,  $S_{wet}$  is the water saturation of the sample relative to in-situ conditions,  $f_a$  is the fraction of solute accessible pore volume per water-accessible (water-loss) porosity,  $S^*:L^*$  is the ratio of wet solid added to the mass of extraction water (wet solid:liquid ratio), and  $WC_{wet}$  is the gravimetric water content of the rock sample relative to dry mass ( $\text{kg}_{\text{H}_2\text{O}}/\text{kg}_{\text{rock}}$ ).

As mentioned above, the porewater in the Opalinus Clay at Mont Terri has an ionic strength well below that of seawater and the (ab initio unknown) density of porewater can be assumed to be 1

g/cm<sup>3</sup> without introducing significant uncertainty. Similarly, the saturation state,  $S_{wet}$ , is taken to be 1.00 based on the applied sampling and sample preparation protocols (see above).

The uncertainty of so-derived porewater compositions can be assessed by:

$$\sigma_{C_{pw}} = \sqrt{\left(\frac{\sigma_{C_{aqex}}}{C_{aqex}}\right)^2 + \left(\frac{\sigma_{S^*/L^*}}{\frac{S^*}{L^*}}\right)^2 + \left(\frac{\sigma_{WC_{wet}}}{WC_{wet}}\right)^2 + \left(\frac{\sigma_{f_a}}{f_a}\right)^2}. \quad (18)$$

From equations (17) and (18) it can be seen that the uncertainties of  $C_{aqex}$ , of  $f_a$  and  $S_{wet}$  are the main contributors to the overall uncertainty of  $C_{pw}$ . Whereas the relative uncertainties for  $C_{aqex}$  is well-defined to be  $\pm 5\%$ , those of  $S_{wet}$  and  $f_a$  are more difficult to assess. Assuming for  $S_{wet}$  a relative error of  $\pm 5\%$ , based on the applied sampling and sample preparation protocols, and for  $f_a$  a relative error of  $\pm 10\%$  for the Opalinus Clay at Mont Terri based comparison of aqueous extraction data to borehole water, squeezed water and long-term diffusion data (Pearson et al. 2003; Gimmi et al. 2014; cf. also Chapter 9), the propagated relative uncertainties for porewater concentrations of the chemically conservative  $Cl^-$  and  $Br^-$  become about 10-15%. A larger uncertainty has to be considered for the samples of the Passwang Fm, where  $f_a$  is not known and has to be assumed (cf. Chapter 9).

Note that the preparation of the aqueous extracts occurred using the saturated rock material, including the mass of porewater as indicated by wet solid:liquid ratio  $S^*:L^*$ . The conversion of the wet solid:liquid ratio to the dry solid liquid ratio  $S:L$  for extraction of previously dried rock can be formulated as:

$$\frac{Solid_{dry}}{m_{w, aqex}} = \frac{Solid_{wet} - m_{pw}}{m_{w, aqex}} = \frac{Solid_{wet} - (WC_{dry} \bullet m_{rock, dry})}{m_{w, aqex}}. \quad (19)$$

## 5.4 ISOTOPE DIFFUSIVE EXCHANGE TECHNIQUE

The porewater isotope composition,  $\delta^{18}O$  and  $\delta^2H$ , was determined by the diffusive exchange technique on the porewater chemistry (-AQ) samples. In this technique, the known water isotope composition of test water is equilibrated with the unknown porewater isotope composition using the gas phase as a diaphragm in a vapour-tight container. The mass and isotope composition of porewater and test water are related by mass balance relationships (Rogge 1997; R ubel 2000) according to:

$$m_{PW} \bullet c_{PW(t=0)} + m_{TW} \bullet c_{TW(t=0)} = (m_{PW} + m_{TW}) \bullet c_{TW(t=\infty)} \quad (20)$$

where  $m_{PW}$  and  $m_{TW}$  are the masses of porewater and test water,  $c_{PW}$  is the original (*in situ*) isotope composition of porewater, and  $c_{TW}$  is the isotope composition of the test water. Concentration,  $C$ , on the left side of the equation are prior to equilibration ( $t = 0$ ), while the concentration on the right side refers to the time after equilibration is achieved ( $t = \infty$ ) in the experiment.

The mass ( $m_{TW}$ ) and isotope composition ( $\delta^{18}O_{TW}$ ,  $\delta^2H_{TW}$ ) of test water before and at the end of the experiment are known. Solving equation (20) for the three unknowns of the porewater (i.e.,  $m_{PW}$ ,  $\delta^{18}O_{PW}$  and  $\delta^2H_{PW}$ ) requires two experiments with test water of different isotope composition. Each equilibration experiment reveals then two independent equations of type (20) for  $\delta^{18}O$  and  $\delta^2H$ . It should be noted that at complete equilibration, the mass balances remain correct even if a small amount of test water is transferred to the sample during the experiment.

The two test waters used in the preparation campaigns comprised laboratory tap water (LAB) and melt water of the N-GRIP ice core drilled in Greenland (TEW). The isotope composition of the LAB test water used in first preparation campaign (samples BDB1-36.10 to BBD1-97.10; January, 2014) was  $\delta^{18}O = -10.94\text{‰}$  and  $\delta^2H = -79.0\text{‰}$  and that of the TEW test water was  $\delta^{18}O = -26.96\text{‰}$  and  $\delta^2H = -208.6\text{‰}$ . In the second preparation campaign (samples BDB1-98.68 to BBD1-246.34; February, 2014), the LAB test water had  $\delta^{18}O = -10.97\text{‰}$  and  $\delta^2H = -79.2\text{‰}$  and the TEW test water had  $\delta^{18}O = -26.98\text{‰}$  and  $\delta^2H = -208.4\text{‰}$ .

For the equilibration experiments, originally saturated rock pieces of 3–4 cm<sup>3</sup> in size and from the centre of the drill core were placed in a vapour-tight container along with a small crystallisation dish containing the known mass of test water of known isotopic composition. Air exposure of the originally-saturated rock material during preparation was minimised to less than 2 minutes. The equilibration time of the three-reservoir system (porewater, test water, air inside the container) depends essentially on the size of the rock pieces, the rock permeability, and the distance of the rock pieces from the test water. Typical equilibration times for the Opalinus Clay range between about 2.5 and 20 days (Rogge 1997; Rübél 2000; Hobbs & Waber 2002). The present experiments had a minimum of 25 days duration to ensure that equilibration was achieved. It should be noted that during such isotope exchange experiments, the rock material is never in direct contact with the test water, in contrast to otherwise applied diffusion (radial and flow-through) and re-saturation techniques.

The uncertainty in the calculated porewater isotope composition depends mainly on the mass ratio of porewater to test water in the experiments (see below). This ratio was optimised by using about 200-250 g of rock material and test water volumes of 3–5 mL for the individual experiments and rock types, and based on previous experience with rock from the Mont Terri URL (Rübél et al. 2002; Hobbs & Waber 2002; Pearson et al. 2003). Before and after the experiments, weight records of the empty and filled vapour-tight glass container and crystallisation dish, the mass of the rock and of the test water were collected, allowing detection of possible evaporation of test water or porewater, and calculation of the propagated uncertainty.

After equilibration, the test water was removed from the crystallisation dish and stored in vapour-tight 3 mL and 5 mL PE-flasks, depending on the volume of test water used in the experiment. Analyses of the oxygen and hydrogen isotope compositions on the small-sized samples was conducted by isotope ratio infrared spectroscopy (IRIS) utilising a Picarro L2120-i cavity ring down spectrometer (CRDS) with vaporization module V1102-i and coupled to a HTC PAL autosampler (CTC Analytics). Post-run correction of oxygen and hydrogen stable isotope measurements followed the method of van Geldern and Barth (2012). All values are expressed in the standard delta notation ( $\delta^{18}O$ ,  $\delta^2H$ ) in per mil (‰) relative to the Vienna Standard Mean Ocean Water (VSMOW). For the present samples, the analytical error was 0.1‰ for  $\delta^{18}O$  and 1.0‰ for  $\delta^2H$  based on multiple measurements of internal and IAEA standards. Finally, the

gravimetric water content of the rock material used in the experiments was obtained by drying the material in an oven at 105 °C to constant mass.

The isotope diffusive exchange technique is sensitive to possible condensation of test water on the glass container walls and on the rock fragments, as well as to large differences between the salinity of the test water and porewater. Condensation and very large differences in salinity may result in uncontrollable desiccation-condensation processes with related isotope fractionation effects during the diffusive exchange experiments. Whereas condensation of test water can be inhibited by lowering the water-vapour pressure above the test-water surface through the addition of NaCl salt, the amount of NaCl added should be optimised with respect to the expected porewater salinity. Salinity-induced liquid-vapour fractionation is minimal for the oxygen isotopes of the water molecule, but may become significant for the hydrogen isotopes. According to Horita et al. (1993), the systematic effect on the  $\delta^2\text{H}$  value at room temperature is about  $2.7\text{‰} \cdot \Delta\text{M}$ , where  $\Delta\text{M}$  denotes the difference in salinity in mol/kg<sub>H<sub>2</sub>O</sub> between solutions.

From previous investigations it is known that the porewater Cl content of Opalinus Clay at the Mont Terri URL varies between about 0.2 to 0.4 M and around 0.1 M in the stratigraphically overlying limestones of the Passwang Fm (Pearson et al. 2003). Therefore, the salinity of the test waters was adjusted to 0.3 M NaCl in order to suppress condensation and to minimise the difference in salinity between test water and porewater. The difference in salinity is therefore <0.1 mol/kg<sub>H<sub>2</sub>O</sub> for most samples of the Opalinus Clay and <0.25 mol/kg<sub>H<sub>2</sub>O</sub> for samples from the Passwang Fm, and the absolute error due to salinity effects on the  $\delta^2\text{H}$  value of the test waters becomes <0.3‰ for Opalinus Clay and <1‰ for Passwang Fm samples, both being well within the analytical uncertainty.

#### 5.4.1 Water Content by the Isotope Diffusive Exchange Technique

Solving the mass-balance relations (equation 20) obtained for the measured  $\delta^{18}\text{O}$  and  $\delta^2\text{H}$  of the test waters, and relating it to the saturated mass of rock  $m_{R1}$  and  $m_{R2}$  used in the two experiments, yields the mass of porewater (and with that water content relative to the wet weight,  $WC_{IsoEx, wet}$ ) according to:

$$m_{PW} = \frac{m_{TW1} \cdot m_{R1} \cdot (C_{TW2}^0 - C_{TW2}^\infty) + m_{TW1} \cdot m_{R2} \cdot (C_{TW1}^\infty - C_{TW1}^0)}{m_{R1} \cdot m_{R2} \cdot (C_{TW2}^\infty - C_{TW1}^\infty)} \quad (21)$$

where  $m_{TW1}$  and  $m_{TW2}$  = mass of test waters 1 and 2,  $m_{R1}$  and  $m_{R2}$  = mass of saturated (wet) rock in experiment 1 and 2,  $C_{TW1}$  and  $C_{TW2}$  = isotope concentrations of test waters 1 and 2, and the superscripts 0 and  $\infty$  denote the tracer concentrations prior to and after equilibration of the test water with the pore water. Commonly, the average of the water contents obtained from mass balance calculations of the  $\delta^{18}\text{O}$  and  $\delta^2\text{H}$  values is used as  $WC_{IsoEx, wet}$ . Alternatively,  $WC_{IsoEx, dry}$  might be obtained by incorporating the rock mass used in the exchange experiments after drying to stable weight. This derivation of mass of porewater and water content differs from that originally established by Rogge (1997) and Rubel (2000) in that it includes, in each case, both experiments (i.e., one with a test water isotope composition close to the expected porewater and one with a test water isotope composition far from to the expected porewater).

### 5.4.1.1 Uncertainty

The uncertainty in the water content derived by the isotope diffusive exchange technique depends mainly on the mass ratio of porewater to test water in the experiments and is minimised when this ratio comes close to unity. By applying Gauss's law of error propagation, the uncertainty attached to the mass of porewater becomes:

$$\sigma(m_{PW}) = \sqrt{\left\{ dm_{PW} dm_{TW1} \cdot \sigma(m_{TW1}) \right\}^2 + \left\{ dm_{PW} dm_{TW2} \cdot \sigma(m_{TW2}) \right\}^2 + \left\{ dm_{PW} dC_{TW1}^0 \cdot \sigma(C_{TW1}^0) \right\}^2 + \left\{ dm_{PW} dC_{TW2}^0 \cdot \sigma(C_{TW2}^0) \right\}^2 + \left\{ dm_{PW} dC_{TW1}^\infty \cdot \sigma(C_{TW1}^\infty) \right\}^2 + \left\{ dm_{PW} dC_{TW2}^\infty \cdot \sigma(C_{TW2}^\infty) \right\}^2} \quad (22)$$

where  $\sigma(m) = 0.002$  g and  $\sigma(C) = 0.1\text{‰}$  for  $\delta^{18}\text{O}$  and  $1.0\text{‰}$  for  $\delta^2\text{H}$ , and  $d$  = sensitivity of parameter a to parameter b (e.g.  $dm_{PW} dm_{TW1} = \{(C_{TW1}^0 - C_{TW1}^\infty) / (C_{TW1}^\infty - C_{TW2}^\infty)\}$ , etc.).

The uncertainty of the water content,  $WC_{IsoEx}$ , relative to the wet and dry rock weight can then be calculated from  $\sigma(m_{PW})$  by applying equations (5) and (6), respectively.

## 5.4.2 Derivation of Porewater Isotope Composition

Rearranging the mass balance relationship given in equation (20), and solving it for  $C_{PW}$  (following insertion of the  $\delta^{18}\text{O}$  and  $\delta^2\text{H}$  values measured on the test waters before and after equilibration, and the different masses of rock and test water used in the two experiments) delivers the isotope composition,  $\delta^{18}\text{O}$  and  $\delta^2\text{H}$ , of the porewater according to:

$$C_{PW} = \frac{C_{TW1}^\infty \cdot m_{TW2} \cdot m_{R1} \cdot (C_{TW2}^\infty - C_{TW2}^0) - C_{TW2}^\infty \cdot m_{TW1} \cdot m_{R2} \cdot (C_{TW1}^\infty - C_{TW1}^0)}{m_{TW2} \cdot m_{R1} \cdot (C_{TW2}^\infty - C_{TW2}^0) - m_{TW1} \cdot m_{R2} \cdot (C_{TW1}^\infty - C_{TW1}^0)} \quad (21)$$

with the same variables as in equation (21).

### 5.4.2.1 Uncertainty

Similar to the mass of porewater, the uncertainty in the porewater isotope composition derived by the isotope diffusive exchange technique depends mainly on the mass ratio of porewater to test water and the different mass of rock used in the experiments. It is minimised when this ratio becomes close to unity. By applying Gauss's law of error propagation, the uncertainty attached to the mass of porewater becomes:

$$\sigma(C_{PW}) = \sqrt{\begin{aligned} & \{dC_{PW} dm_{TW1} \cdot \sigma(m_{TW1})\}^2 + \{dC_{PW} dm_{TW2} \cdot \sigma(m_{TW2})\}^2 + \\ & \{dC_{PW} dC_{TW1} \cdot \sigma(C_{TW1})\}^2 + \{dC_{PW} dC_{TW2} \cdot \sigma(C_{TW2})\}^2 + \\ & \{dC_{PW} dC_{TW1} \cdot \sigma(C_{TW1})\}^2 + \{dC_{PW} dC_{TW2} \cdot \sigma(C_{TW2})\}^2 \end{aligned}} \quad (22)$$

where  $\sigma(m) = 0.002$  g and  $\sigma(C) = 0.1\text{‰}$  for  $\delta^{18}\text{O}$  and  $1.0\text{‰}$  for  $\delta^2\text{H}$ , and  $d$  = sensitivity of parameter a to parameter b. The error on the porewater isotope calculation was calculated individually for each sample and given in the raw data tables in Appendix C1.

## 5.5 NOBLE GAS ANALYSES

The determination of porewater noble gas concentrations is based on the quantitative release of (dissolved) gases in the porewater of a rock sample under conditions different from those prevailing in situ (e.g., Osenbrück et al. 1998; Rübél and Sonntag 2000; Rübél et al. 2002). Due to their low solubility in water under ambient conditions (Weiss 1971, 1970), noble gases are quantitatively released from the porewater of the rock sample. The chemical inertness of noble gases inhibits any reaction during out-gassing, so that the released amounts of noble gases can be calculated into concentrations in porewater using the mass of porewater of the rock sample.

After sealing the evacuated sample container, the dissolved gases are quantitatively released from the porewater by molecular diffusion into the void volume of the container. The time required to reach equilibrium conditions depends on the transport properties of the rock material, as well as the sample size and geometry. It has been demonstrated that, for sedimentary rocks, equilibration times of up to two months suffice to attain steady state with regards to He and, that under these conditions, significantly less than 1% of the  $^4\text{He}$  stays dissolved in the porewater (Bigler 2003; Osenbrück et al. 1998). For the samples in this study, dissolved gases in the porewater were allowed to outgas into the evacuated void of the gas-tight sample container over a time span of 2-6 months (samples measured in 2014) and 16 months (samples measured in 2015) at a constant temperature of  $20.5 \pm 0.5^\circ\text{C}$ .

Noble gas analyses were conducted at the Institute of Geological Sciences, University of Bern, to determine  $^4\text{He}$ ,  $^{20}\text{Ne}$ ,  $^{22}\text{Ne}$  and  $^{40}\text{Ar}$  concentrations, and  $^{40}\text{Ar}/^{36}\text{Ar}$  isotope ratios, as well as at the Institute of Environmental Physics, University of Bremen, Germany, for  $^3\text{He}/^4\text{He}$  isotope ratio measurements.

Extraction of the gas from the sample container was done by rapid expansion into 3 identical, well-defined volumes (termed “*splits*”), with a total volume approximately five times larger than the gas volume in the sample container, before the latter was again closed off (Figure 5-1). This ensured the extraction of a large fraction (> 80%) of gas from the sample container, while at the same time splitting the gas into equal fractions for duplicate or triplicate analysis (gas separation/purification and measurement). The rapid expansion also minimises pressure-change-induced alteration of the equilibrated gas composition in the sample container by renewed diffusion or evaporation of  $\text{H}_2\text{O}$ .

Separation and purification of the different noble gas species of interest was achieved by running the gas from one of the three equal-volume splits through a sequential combination of a

Ti-sponge getter operated at 650°C and a N<sub>2</sub>(liq.)-cooled cold trap filled with activated charcoal. This results in two purified gas fractions: one containing He plus Ne, and the other containing Ar. The gas of each of these purified fractions is again split into 3 equal volumes (termed “aliquots”), primarily to provide fail-safe redundancy for the following measurement step. On one aliquot of the He plus Ne gas fraction, <sup>3</sup>He/<sup>4</sup>He ratios were determined in Bremen according to the procedure given in Sültenfuss et al. (2009). The measurements in Bern were performed by introducing the gas from one aliquot into a calibrated reference volume, from which it is sequentially measured three times using a Pfeiffer QMS200 quadrupole mass spectrometer equipped with an in-line faraday cup detector. Gas ionisation was by a tungsten filament using an emission current of 0.7 mA and a cathode potential of 50 V. The low cathode potential is used to reduce the isobaric interference of doubly ionised <sup>40</sup>Ar<sup>++</sup> on the <sup>20</sup>Ne<sup>+</sup> signal to below 0.1% of the <sup>40</sup>Ar<sup>+</sup> signal, which is necessary if <sup>20</sup>Ne/<sup>22</sup>Ne ratios are to be determined. In consideration of the reduced amounts of gas available per measurement, the mass spectrometer was operated in static mode (Poole et al. 1997).

As the gas passes through the separation and purification line, certain volumes of the line are closed off and the corresponding fractions of gas are removed from that which is leftover for analysis. This applies to: 1) the original gas in its unprocessed form due to, e.g., the closing-off and removal of the sample container and the inlet part of the line after the initial expansion of the gas from the sample container into the 3 equal-volume splits; as well as 2) various fractions of He, Ne and Ar at later stages in the purification process. As a result, the gas amounts of the different noble gas species have to be back-calculated from their measured amount in the reference volume to their respective amount in the sample container. This is done using species-specific factors to account for their specific loss during separation and purification – in order to obtain the amount of that species in one of the splits after the initial expansion – and a common factor to account for the loss of gas during the initial expansion from the sample container into the 3 splits. While the former factors are determined using multiple analyses of known amounts of reference gases, the latter varies solely with the gas volume in the sample container. In the end, the noble gas amount in the sample container (determined as the average from the analyses of all measured splits) is expressed as concentration per mass of porewater in the sample and given as ccSTP<sup>5</sup>/g. The terminology distinguishes between values that are uncorrected for air contamination, indicated by the index “H<sub>2</sub>O” (e.g., ccSTP/g<sub>H<sub>2</sub>O</sub>) and contamination corrected values, indicated by the index “pw” (e.g., ccSTP/g<sub>pw</sub>). For details concerning air contamination, see Section 3.2.2; cited data is given without suffix unless its type is clearly specified by the literature.

In generalised form, the (uncorrected) total amount of a specific noble gas species, *i*, in one split ( $n_{i\_split}$ ) and in the sample container ( $n_{i\_sample}$ ) is calculated as:

$$n_{i\_split} = n_{i\_Vref} \times f_i \quad [\text{ccSTP}] \quad (23)$$

and

$$n_{i\_sample} = (3 \times n_{i\_split}) \times f_{exp} \quad [\text{ccSTP}] \quad (24)$$

and the corresponding (uncorrected) concentration  $C_{i\_H_2O}$  in the in the sample porewater as:

---

<sup>5</sup> STP as defined by IUPAC (0°C, 100 kPa) (McNaught and Wilkinson 1997)

$$C_{i_{H_2O}} = \frac{n_{i_{sample}}}{m_{PW}} \quad [\text{ccSTP}] \quad (25)$$

where  $n_{i_{Vref}}$  is the measured amount of the noble gas species in the reference volume (in ccSTP);  $f_i$  is the empirically determined species-dependent factor accounting for the partial loss of the species during separation and purification (which is to some extent dependent on the amount of gas of a given species being treated, particularly at lower gas amounts); and  $m_{PW}$  is the mass of porewater in the sample. The common factor,  $f_{exp.}$ , accounts for the loss of sample gas during the expansion from the sample container into 3 splits and is calculated as:

$$f_{exp.} = \left( \frac{(3 \times V_{split}) + V_{exp.line} + V_{sample\ gas}}{V_{sample\ gas}} \right) \quad (26)$$

with  $V_{sample\ gas}$  being the volume of gas in the sample container,  $V_{exp.line}$  the volume of the extraction line between the sample container and the 3 splits, and  $V_{split}$  the volume of one of the 3 splits into which the sample gas is expanded during the initial expansion. While the latter two are constant volumes,  $V_{sample\ gas}$  is calculated geometrically as the sum of the constant volume of the sample container plus the variable volume of the crimped-off interface copper tube minus the volume of the rock material as:

$$V_{sample\ gas} = V_{sample\ cont.} + (\pi \times r_{tube}^2 \times h_{tube}) - V_{rock} \quad [cm^3] \quad (27)$$

with  $V_{sample\ cont.} = 350\ cm^3$ ;  $r_{tube} = 0.4\ cm$  (radius of the copper tube) and  $h_{tube}$  = length of the copper tube in cm. As the shape of the rock material closely resembles a cuboid,  $V_{rock}$  is calculated geometrically using the average length and width measured along the small axis on top and bottom of the cuboid and the central height along the long axis.

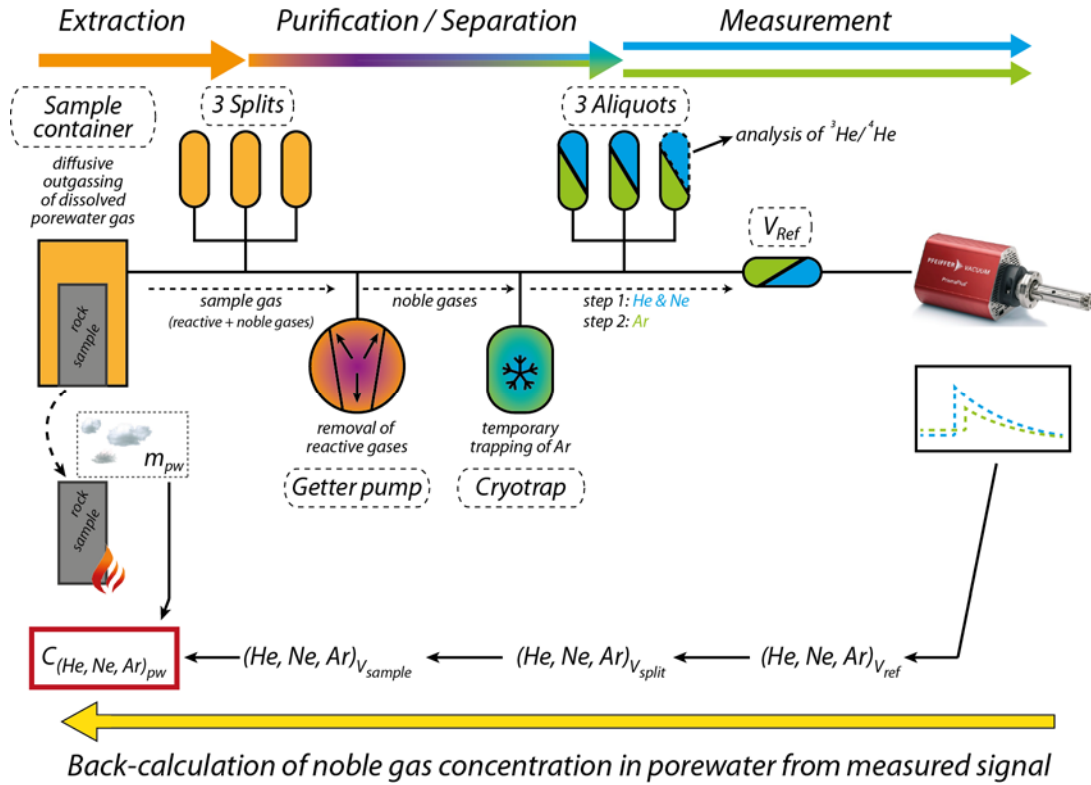


**Figure 5-1: Schematic Workflow of Gas Extraction, Separation/purification, Measurement and Back-calculation of Measured Signals to Gas Concentrations in Porewater.**

### 5.5.1 Uncertainty on Noble Gas Measurements

The overall *uncertainty for the entire analytical procedure* (consisting of extraction, purification and measurement of a specific noble gas species of a sample) is dependent on the uncertainties of the measured gas amount in the reference volume and each parameter involved in back-calculating it into a concentration of gas in porewater in the sample container.

Corresponding to equations (15), (16) for the water-loss porosity and to (23), (24) for the noble gas measurement, the uncertainty  $\sigma_{C_{iH_2O}}$  on the concentrations of a given noble gas species  $i$  in the porewater based on the analysis of one split is calculated as:

$$\sigma_{C_{iH_2O}} = C_{iH_2O} \times \sqrt{\left(\frac{\sigma_{n_{iVref}}}{n_{iVref}}\right)^2 + \left(\frac{\sigma_{f_i}}{f_i}\right)^2 + \left(\frac{\sigma_{f_{exp}}}{f_{exp}}\right)^2 + \left(\frac{\sigma_{m_{pw}}}{m_{pw}}\right)^2}. \quad (28)$$

This total uncertainty is composed of:

$\sigma_{n_{iVref}}$  : The *uncertainty on the amount of gas species  $i$  in the reference volume,  $V_{ref}$ .*

This is calculated by propagating the uncertainties on the measured signal intensities and the uncertainties on this gas species' calibration curve relating these signal intensities to  $n_{iVref}$ .

If multiple aliquots are measured, weighted means of the individual  $n_{iVref}$  and  $\sigma_{n_{iVref}}$  are calculated and used for further calculation.

$\sigma_{f_i}$  : The *uncertainty on the fraction of gas in  $V_{ref}$  relative to  $V_{split}$  after purification.*

The values of  $f_i$  were determined for the different species,  $i$ , on multiple analyses of reference gas mixture. They empirically show a slight dependence on the amount of gas, which becomes more pronounced for very low gas amounts, most likely due to an increasing effect of adsorption/desorption phenomena on the low gas concentrations in the getter and cryotrap. The uncertainty  $\sigma_{f_i}$  is determined by the parametrical uncertainty on the regressed empirical relation.

$\sigma_{f_{exp}}$  : The *uncertainty on the fraction of sample gas available for purification in  $V_{split}$  after the initial expansion from the sample container.*

This is propagated from the volumetric uncertainties on  $V_{split}$ ,  $V_{exp. line}$  and  $V_{sample gas}$  (Eq. 23). While the fixed volumes  $V_{split}$  and  $V_{exp. line}$  are determined to  $\pm <1.0\%$ , the principal contribution to the uncertainty on  $V_{sample gas}$  is  $V_{rock}$  (Eq. 24).

$\sigma_{m_{PW}}$  : The uncertainty on the gravimetric determination of the mass of porewater (Eq. 4).

If multiple splits of a sample have been analysed, the resulting uncertainty on the average value is the larger of either: a) 1 standard deviation of the multiple results, or b) the propagated uncertainty on the average value.

In the case of the BDB-1 samples, the relative uncertainty on  $m_{pw}$  is  $< 0.8\%$  for all samples, with only 4 samples above  $0.5\%$ . The relative uncertainties on the noble gas contents in the sample container are - particularly for Ne and Ar - higher for samples that have been measured using the adjusted analytical protocol for low-concentration, primarily due to a large increase in  $\sigma_{f_i}$  at low concentrations of gas during purification. The resulting average relative uncertainties on the air-contamination uncorrected values are  $2.2\%$  and  $3.4\%$  for He;  $1.7\%$  and  $19.5\%$  for Ne, and  $2.5\%$  and  $30.5\%$  for Ar concentrations in the porewater, and  $4.4\%$  and  $43.5\%$  for  $^{40}\text{Ar}/^{36}\text{Ar}$  isotope ratios, measured using the normal analytical protocol and the one adjusted for low gas concentrations, respectively.

## 5.5.2 Analytical Uncertainty versus Total Uncertainty

The *analytical uncertainty* is the net result of uncertainties arising during the handling and measurement of a sample *after it has been stored for diffusive equilibration*, and is quantifiable as shown in the previous section. It does, however, *not comprise uncertainties that arise prior to the sample being processed in the lab*. As such, the *total uncertainty* on noble gas data also consists of uncertainties due to various effects, which may occur during:

1. The drilling of the core section, such as variable degree of degassing of the core due to variations in drilling time or drilling media composition and pressure, as well as leaving the core downhole for extended periods of time because of mechanical problems.

2. The retrieval of the core, such as variable influence of pressure relief due to textural differences of the core material. This could lead to an increase in diffusivity and variable loss of noble gases (particularly of He, due to its high concentration in the porewater).
3. The handling of the core after retrieval and during on-site sampling of the noble gas samples. This concerns aspects such as variations in exposure time of the sample to air (in particular of the central piece before it is sealed in the sample container) and variations in pumping duration during flushing of the sample container.

It should be noted that these effects are equally valid for noble gas samples, porewater samples and samples for squeezing.

While it is almost impossible to assess the influences of such aspects in a quantitative manner, it is evident that keeping detailed logs on all of these parameters of interest can help to qualitatively identify or refute potential causes for seemingly aberrant noble gas data.

During sampling of BDB-1, detailed logs were kept containing the necessary information to determine exposure time of a core section to air between its retrieval and the processing of noble gas samples. They also contain exposure time of the dry-cut rock sample to air during noble gas sampling, as well as detailed pumping durations and attained pressures for each flushing/pumping step (*cf.* Appendix A2). This allows comparison of these parameters between different samples in order to assess whether an observed discrepancy in, e.g., He concentration, could be attributed to sampling problems.

Nonetheless, the total uncertainty that must be attributed to noble gas data is almost certainly larger than the analytical uncertainty, and this has to be considered during data interpretation.

### 5.5.3 Analytical Limits and Accuracy

Immediately prior to each sample or standard measurement, static backgrounds were measured identical to sample and standard measurements but without the admission of an analyte gas. Lower limits of detection (LOD) for the QMS measurement were then calculated for each isotope as the lowest amount of gas with that mass in the reference volume,  $V_{\text{Ref.}}$ , for which the recorded signal is higher than the average of the corresponding static background signals, plus 3 standard deviations, over the entire measurement campaign.

As the relationship between the noble gas amounts in  $V_{\text{Ref}}$  and in the splits (into which the sample container gas is initially extracted) depends on the empirical factor,  $f_i$  (after Eq. 23), the lower limit of calibration (LOC) is given as the lowest amount of each gas species in 1 split for which the calculated  $f_i$  has been empirically determined. For lower gas amounts, the calculated  $f_i$  is extrapolated from its calibrated range, with the consequence of decreasing accuracy and precision the further away the calculated  $f_i$  value is from the calibrated range.

For He and Ar, the LOD on the more abundant isotope ( $^{20}\text{Ne}$ ,  $^{40}\text{Ar}$ ) is roughly one order of magnitude lower than the LOC on the corresponding gas species, while for He LOD and LOC are similar.

**Table 5-1: Limits of Detection (LOD) and Limits of Calibration (LOC) Valid for the BDB-1 Analyses**

	<i>Limit of Detection (LOD)</i>				<i>Limit of Calibration (LOC)</i>			
	$V_{Ref}$ [ccSTP]	1 split [ccSTP]	sample [ccSTP]	porewater [ccSTP/g <sub>H2O</sub> ] o]	1 split [ccSTP]	sample [ccSTP]	porewater [ccSTP/g <sub>H2O</sub> ]	
<sup>4</sup> He	2.1E-09	5.1E-07	3.4E-06	1.7E-07	He	2.0E-06	1.3E-05	6.7E-07
<sup>20</sup> Ne	5.7E-11	1.4E-07	9.3E-07	4.7E-08	Ne	4.5E-07	3.0E-06	1.7E-07
<sup>22</sup> Ne	1.4E-11	1.5E-08	1.0E-07	5.0E-09				
<sup>40</sup> Ar	2.1E-08	7.4E-06	4.9E-05	2.5E-06	Ar	1.5E-04	1.0E-03	5.0E-05
<sup>36</sup> Ar	1.1E-10	3.3E-08	2.2E-07	1.1E-08				

Notes: The LOD and LOC values for the abundance in the sample container and the concentration in porewater base on  $f_{exp.} = 0.15$  (Eq. 24) and  $m_{pw} = 20$  g (representative for the bulk of BDB-1 noble gas samples). As such, they only serve as a rough illustration of approximate lower analytical limits on these parameters and are therefore given in italics. The sample specific LOD and LOC for these depend on the actual  $f_{exp.}$  and  $m_{pw}$  of the sample and can vary from the value given in the table.

#### 5.5.4 Monitoring Analytical Accuracy and Precision Using Reference Gases

Together with the BDB-1 samples, a reference gas of known composition has repeatedly been analysed to verify the analytical accuracy and precision of the measurements. In order to be roughly similar to the sample compositions, air doped with commercially-available pressurised He (99.99 % purity) to obtain a He/Ar ratio of  $0.12 \pm 0.01$  was used as reference gas and measured at concentrations on the same order of magnitude as those of the samples analysed during the same period. In 2015, the second reference gas measurement was performed using the analytical protocol for low-concentration gases. Pure air<sup>6</sup> has additionally been measured to verify the fidelity of the <sup>20</sup>Ne/<sup>22</sup>Ne and <sup>40</sup>Ar/<sup>36</sup>Ar measurements. A summary of the obtained data is given in Table 5-2 and illustrated in Figures 5-2 to 5-5.

For He concentrations, all analysed He-doped reference gases reproduce the expected values within a relative analytical uncertainty of 2% (relative standard deviation) of the measured values, which is well within the long-term reproducibility determined over the last ~2 years using this analytical setup.

For Ne concentrations, all analysed He-doped reference gases reproduce the expected values within a relative analytical uncertainty of 3% (relative standard deviation) of the measured values, which is again within the long-term reproducibility.

Measurements of the <sup>20</sup>Ne/<sup>22</sup>Ne signatures for all but one analysis fall within the long-term reproducibility. He-doped reference gases analysed in 2015 show higher analytical uncertainties due to lower gas concentrations when compared to the 2014 gases (over an order of magnitude lower). The mean of the measured <sup>20</sup>Ne/<sup>22</sup>Ne ratios is  $9.90 \pm 1.63$  (1 s.d.), which is within uncertainty equal to the air reference value of 9.78 (de Laeter 2003). Measurements of pure air reproduce with a mean value of  $9.06 \pm 0.63$  (1 s.d.), which is slightly lower than the air

<sup>6</sup> The gas has been collected on 10.12.2014 in the Bremgarten Forest near Bern, Switzerland; T = 3.5°C; RH = 70%

reference value but overlaps, within uncertainty, with the range of long-term reproducibility on pure air.

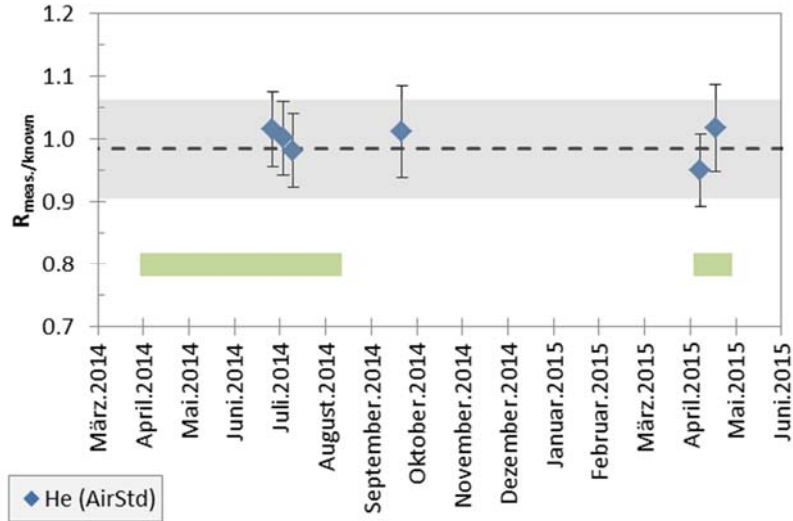
**Table 5-2: Analytical Accuracy and Precision of Reference Gases Measured with BDB-1 Samples**

	He	1 s.d.	Ne	1 s.d.	Ar	1 s.d.	$^{20}\text{Ne}/^{22}\text{Ne}$	1 s.d.	$^{40}\text{Ar}/^{36}\text{Ar}$	1 s.d.	
	<i>(average ratio<sub>measured/known</sub>)</i>						<i>(average measured values)</i>				
He-doped air:	1.00	0.02	0.99	0.03	0.99	0.05	9.90	1.63	303.00	5.85	
pure air:							9.06	0.63	298.81	2.29	
<i>long-term reproducibility:</i>											
He-doped air:	0.98	0.08	0.98	0.06	1.00	0.11	10.71	2.76	298.96	11.52	
pure air:							9.87	0.64	296.75	3.23	

Notes: The official air reference values for  $^{20}\text{Ne}/^{22}\text{Ne}$  and  $^{40}\text{Ar}/^{36}\text{Ar}$  are 9.78 and 298.56 (de Laeter 2003; Lee et al. 2006). The long-term reproducibility refers to all performed measurements of the respective gas types using this analytical setup. For He-doped air, He/Ar ratios range from 0.12 to 5.06, over two orders of magnitude in concentration; pure air has been measured over 1.5 orders of magnitude in concentration.

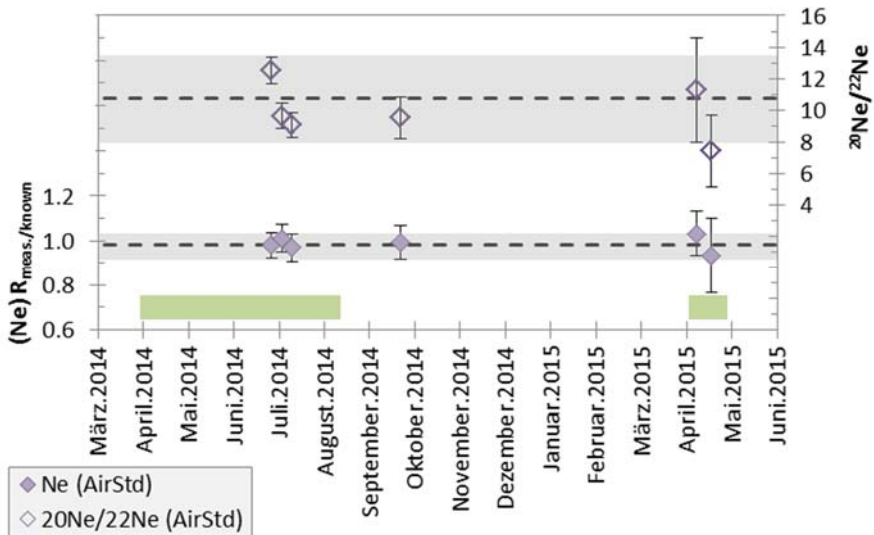
For Ar concentrations, all but one of the analysed He-doped reference gases reproduce the expected values within a relative analytical uncertainty of 5% (relative standard deviation) of the measured values, which is within the long-term reproducibility.

Measurements of the  $^{40}\text{Ar}/^{36}\text{Ar}$  signatures also range within the long-term reproducibility for all but one analysis. Similar to  $^{20}\text{Ne}/^{22}\text{Ne}$ , there is an increase in uncertainty on the  $^{40}\text{Ar}/^{36}\text{Ar}$  ratios, particularly for the second of the 2015 measurements, due to low gas concentrations (particularly for  $^{36}\text{Ar}$ ). The mean of the measured  $^{40}\text{Ar}/^{36}\text{Ar}$  ratios is  $303.00 \pm 5.85$  (1 s.d.), which is within uncertainty equal to the air reference value of 298.56 (Lee et al. 2006). Measurements of pure air reproduce with a mean value of  $298.81 \pm 2.29$  (1 s.d.), identical to the air reference value.



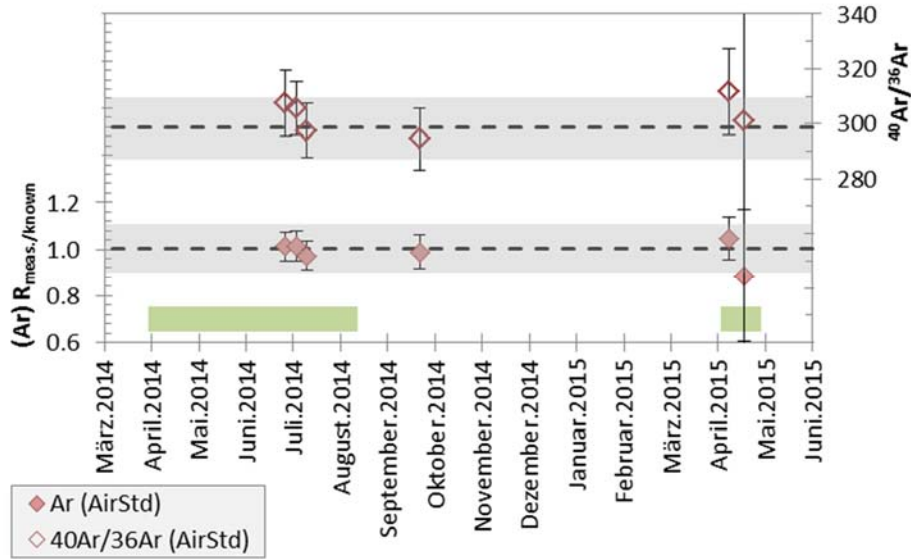
Notes: The dotted line and shaded area represent the long-term reproducibility on reference gases (Table 5-2); the two blocks indicate the time range over which the BDB-1 samples were analysed.

**Figure 5-2: Analytical Accuracy and Precision of He on Reference Gas Measured with the BDB-1 Samples.**



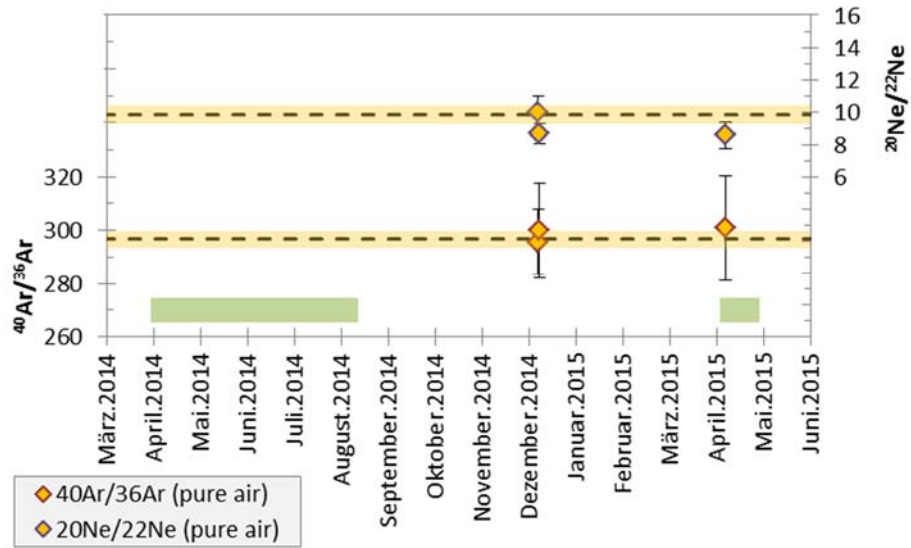
Notes: The dotted line and shaded area represent the long-term reproducibility on reference gases (Table 5-2); the two blocks indicate the time range over which the BDB-1 samples were analysed.

**Figure 5-3: Analytical Accuracy and Precision of Ne on Reference Gas Measured with the BDB-1 Samples.**



Notes: The dotted line and shaded area represent the long-term reproducibility on reference gases (Table 5-2); the two blocks indicate the time range over which the BDB-1 samples were analysed.

**Figure 5-4: Analytical Accuracy and Precision of Ar on Reference Gas Measured with the BDB-1 Samples.**



Notes: The dotted line and shaded area represent the long-term reproducibility on reference gases (Table 5-2); the two blocks indicate the time range over which the BDB-1 samples were analysed.

**Figure 5-5: Analytical Accuracy and Precision of <sup>20</sup>Ne/<sup>22</sup>Ne and <sup>40</sup>Ar/<sup>36</sup>Ar on Pure Air Measured with the BDB-1 Samples.**

### 5.5.5 A Note Concerning the $^{40}\text{Ar}/^{36}\text{Ar}$ Reference Value for Air

It should be noted that, in the past, the commonly used value for the  $^{40}\text{Ar}/^{36}\text{Ar}$  isotope ratio of air was  $295.5 \pm 0.5$  as given by Steiger and Jäger (1977). This value is based on empirical data by Nier (1950), who used a volumetrically prepared  $^{40}\text{Ar}/^{36}\text{Ar}$  mixture at a ratio of approximately 100:1 as a calibration gas. The volumetric nature of this approach, however, coupled with the compositional dissimilarity to Ar in air, and the use of two-way valves with vacuum grease stopcocks in Nier's experimental design, make the evaluation of systematic errors difficult. In consequence, Lee et al. (2006) have reanalysed the atmospheric  $^{40}\text{Ar}/^{36}\text{Ar}$  ratio by isotope-ratio mass spectrometry (IRMS) using two independent, gravimetrically-prepared calibration gases, one of which has a near-air  $^{40}\text{Ar}/^{36}\text{Ar}$  ratio. They determined the atmospheric  $^{40}\text{Ar}/^{36}\text{Ar}$  ratio to a value of  $298.56 \pm 0.31$  and this value has been adopted as the official reference value by the Commission on Isotopic Abundance and Atomic Weights (CIAAW) of the International Union of Pure and Applied Chemistry (IUPAC) in 2009 (Berglund and Wieser 2011). The present report therefore adopts the updated value of 298.56 by Lee et al. (2006), and all  $^{40}\text{Ar}/^{36}\text{Ar}$  measurements on the BDB-1 noble gas samples are calibrated against this reference value.

In order to compare literature data, which uses the old value of 295.5 as the air reference value, with data based on the new 298.56 value, it is easiest to express both datasets as relative to the particular air reference value used. For this, the ratios of the measured  $^{40}\text{Ar}/^{36}\text{Ar}$  values of the analyte relative to the air reference value of 298.56 ( $R/R_{\text{air}}$ ) is additionally indicated throughout this report.

## 5.6 NOBLE GAS AND PARENT RADIONUCLIDE ANALYSES ON ROCK SAMPLES

For the calculation of in situ He production rates in the rock and release coefficients from the rock into the porewater, U, Th, Li and K contents, as well as  $^4\text{He}$ , were determined in the rock matrix. For  $^3\text{He}/^4\text{He}$  ratios, only upper limits could be determined, as  $^3\text{He}$  was at or below the limit of measurement.

Element concentrations have been measured by X-ray spectrometry on bulk samples for U and Th, and by flame spectroscopy on completely digested rock material for K and Li. The analyses were performed at the Kola Scientific Centre in Apatity and by Neva Geological Expedition in St. Petersburg, Russia. Isotopic abundances and ratios were determined by fusion of the dried bulk rock samples at  $1600^\circ\text{C}$ , purification and separation of the released gas with Ti-Zr getter and  $\text{N}_2(\text{liq.})$  cooled cold traps, and measurement by mass spectrometry as described in Tolstikhin et al. (2010). In these samples,  $^4\text{He}$  originally dissolved in the porewater has been lost by out-gassing prior to the determination of  $^4\text{He}$  in the rock.

The analytical uncertainties ( $1\sigma$ ) for these measurements are given by the labs as follows:  $[\text{K}] = \pm 3\%$ ;  $[\text{Li}] = \pm 20\%$ ;  $[\text{U}]$ ,  $[\text{Th}]$  and  $[\text{He}] = \pm 10\%$ . The  $^4\text{He}$  blanks were  $1 \times 10^{-6} \text{ NmL } ^4\text{He}/\text{g}_{\text{rock}}$  (I. Tolstikhin, *pers. comm.* 2016).

## 5.7 GROUNDWATER ANALYSES

### 5.7.1 On-site Measurements

Groundwater samples were analysed on site for T, pH, Eh,  $\text{O}_2$  and electric conductivity (EC). Measurements were conducted immediately after collecting the groundwater using: Knick

Portamess instruments equipped with a Knick SE 101N electrode for pH and T, a Hamilton Oxytrode Platinum electrode for Eh, a Knick Oxygen Sensor SE 302 for O<sub>2</sub>, and a Knick SE 204 electrode for EC.

## 5.7.2 Chemical and Isotope Analyses

The on-site filtered groundwater samples were analysed in the RWI Geochemistry Laboratories of the Institute of Geological Sciences, University of Bern, for their major dissolved cations and anions (Na<sup>+</sup>, K<sup>+</sup>, Ca<sup>2+</sup>, Mg<sup>2+</sup>, NH<sub>4</sub><sup>+</sup>, Sr<sup>2+</sup>, F<sup>-</sup>, Cl<sup>-</sup>, Br<sup>-</sup>, NO<sub>3</sub><sup>-</sup>, SO<sub>4</sub><sup>2-</sup>) by ion chromatography utilising a Metrohm ProfIC AnCat MCS IC system with automated 5µL and 50µL injection loops. The analytical error of this method is ± 5% based on multiple measurements of high-grade, commercial, check standard solutions (Sigma-Aldrich, Merck). Total alkalinity and the lab pH were obtained by end-point titration using a Metrohm Titrino DMP 785 system. Concentrations of Ba, Al, Fe<sub>tot</sub> and Mn<sub>tot</sub> were analysed by optical emission inductively coupled plasma spectrometry using a Varian 710 ES ICP-OES system with a detection limit of 0.01 mg/L. The analytical error of the ICP-OES analysis is ± 5% for these elements based on multiple measurements of high-grade, commercial, check standard solutions (Sigma-Aldrich, Merck). Finally, dissolved silicon was obtained by colorimetric techniques to avoid possible amounts of colloidal Si using a Varian Cary 50 spectro-photometer.

The stable isotope of water, expressed as δ<sup>18</sup>O and δ<sup>2</sup>H in per mil (‰) relative to VSMOW, were analysed in parallel at the RWI Geochemistry Laboratories, University of Bern, and at Hydroisotop GmbH, Schweitenkirchen, Germany. In both labs δ<sup>18</sup>O and δ<sup>2</sup>H were analysed by isotope ratio infrared spectroscopy (IRIS) utilising a Picarro L2120-i cavity ring down spectrometer (CRDS) with vaporization module V1102-i and coupled to a HTC PAL auto-sampler (CTC Analytics). Post-run correction of oxygen and hydrogen stable isotope measurements was done according to van Geldern and Barth (2012). In both laboratories the analytical error (1σ) was ±0.1‰ for δ<sup>18</sup>O and ±1.0‰ for δ<sup>2</sup>H based on multiple measurements of internal and IAEA standards, and duplicate analyses agreed well within this error.

Tritium (<sup>3</sup>H) was analysed at Hydroisotop GmbH by fluid scintillation spectrometry, LSC, after electrolytic enrichment. Results are given in Tritium Units (TU) with double standard deviation and with 1 TU corresponding to 0.119 Bq/L. The <sup>3</sup>H results relate to the date of measurement and no half-life correction was applied.

The stable carbon isotope composition of dissolved carbon, δ<sup>13</sup>CDIC, was analysed by conventional isotope ratio mass spectrometry (IRMS) at Hydroisotop GmbH and is expressed in per mil (‰) relative to the VPDB standard. The analytical error (1σ) on these measurements is ±0.3 ‰.

The activity of the radiogenic <sup>14</sup>C in the dissolved carbon was analysed by accelerator mass-spectrometry (AMS) at ETH Zürich, Switzerland, via Hydroisotop GmbH. Results are given in %-modern carbon with double standard deviation.

Concentrations of He, Ne, Ar, Kr und Xe and the isotope ratios of <sup>3</sup>He/<sup>4</sup>He, <sup>20</sup>Ne/<sup>22</sup>Ne and <sup>40</sup>Ar/<sup>36</sup>Ar were analysed at EAWAG, Dübendorf, Switzerland, on the groundwater samples collected in-line into copper tubes. The analyses were performed according the procedure given in Beyerle et al. (2000) and the results are given with their respective double standard deviations.

## 6. ROCK COMPOSITION AND WATER-CONDUCTING FEATURES

Quantitative analyses of the rock mineralogical composition were performed on the 19 samples that constitute the "*porewater method comparison program*". Three of these samples come from the bottom of the Passwang Fm, 15 samples come from the Opalinus Clay, and 1 sample comes from the Stafflegg Fm. Additionally included are 9 samples from the Opalinus Clay that were collected for Nagra for comparison with geophysical and geochemical logs, and that are originally reported in Becker (2014). The mineralogical data of the porewater chemistry samples are compiled in Table 6-1.

Information about lithostratigraphy, as well as occurrence and location of water-conducting and major tectonic features, is important in the context of the interpretation of porewater data. Such information was obtained from drill-core logging and borehole imaging and compiled from the reports by Fischer (2014), Jaeggi et al. (2016), Reisdorf et al. (2016) and Hostettler et al. (2017).

### 6.1 WHOLE ROCK MINERALOGY

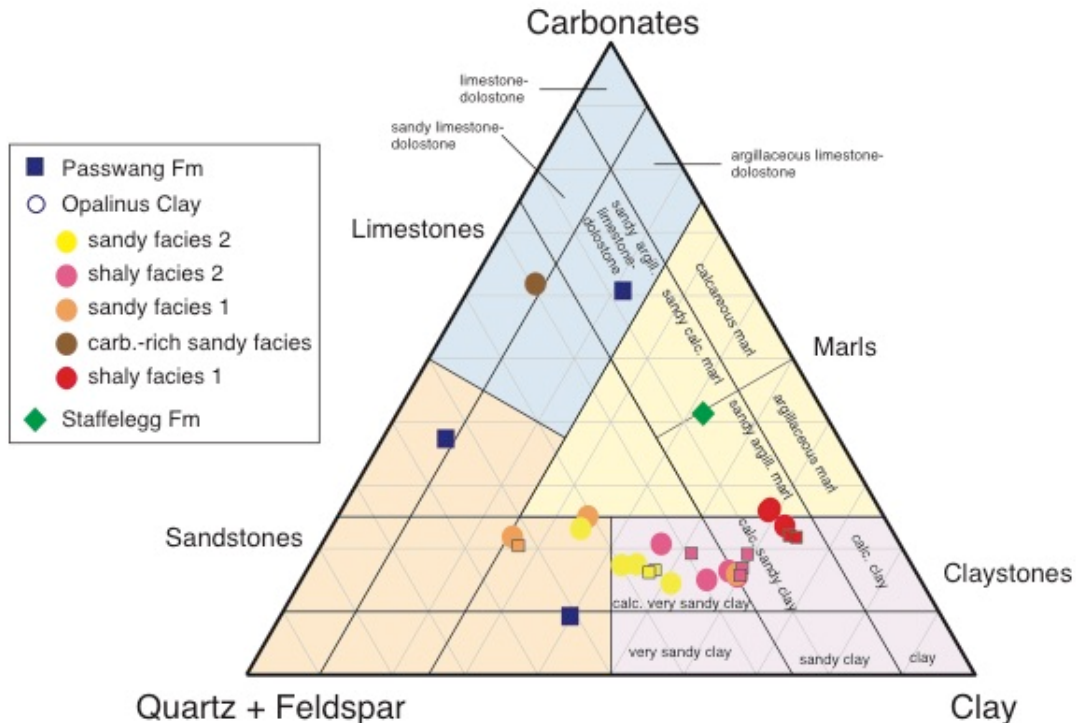
Extending from about 37 m to 106 m BHL, the rock sequence of the Passwang Fm constitutes a highly variable alternation of limestone, sandy limestone, sandy-argillaceous limestone, argillaceous limestone, sandy marl, and marlstone to sandstone (Hostettler et al. 2017; *cf.* Figure 1-1). This variability of the Passwang Fm rocks is also reflected in the mineralogy of the three samples investigated here. These cover the range from sandy-argillaceous limestone to calcareous sandstone and argillaceous sandstone (Figure 6-1). The clay-mineral content of these samples varies from 9–39 wt.%, the total carbonate from 9–61 wt.%, and the quartz and feldspar from 17–53 wt.%, with K-feldspar content reaching as high as 8 wt.% (Table 6-1). Total carbonate is mainly made of calcite, but dolomite/ankerite might be present in as much as 11 wt.%, whereas siderite is absent (Table 6-1). Pyrite as a major sulphur-bearing phase is present in small amounts of 0.3–1.3 wt.% and organic carbon from 0.5–1.0 wt.%

The Opalinus Clay displays a more homogeneous mineralogical composition. From its top at 106.2 m BHL to its bottom at 236.8 m BHL, it generally evolves towards more clay-rich rocks, except for carbonate-rich sandy facies between 186.3 m and 190.3 m BHL, which consist of argillaceous limestone and limestone (Figure 6-1).

In the two sections of Opalinus Clay sandy facies, the clay-mineral content varies between 25–50 wt.% (average of  $39 \pm 9$  wt.%;  $n=9$ ), total carbonate from 15–25 wt.% (average of  $19 \pm 4$  wt.%;  $n=9$ ), and that of quartz and feldspar from 34–52 wt.% (average of  $41 \pm 7$  wt.%;  $n=9$ ). Calcite is the dominant carbonate mineral, but substantial amounts of dolomite/ankerite (up to 6 wt.%) and siderite (up to 3 wt.%) are also present. Quartz is significantly more abundant than the feldspars, and K-feldspar (up to 5 wt.%) dominates over plagioclase. Pyrite is heterogeneously distributed and varies between 0.6 wt.% and 2.6 wt.%. In turn, organic carbon contents are rather homogeneous and vary between 0.3 wt.% and 0.9 wt.% (Table 6-1).

The two sections of Opalinus Clay shaly facies are more clay-rich, with a clay-mineral content between 45 wt.% and 63 wt.% (average of  $57 \pm 5$  wt.%,  $n=14$ ). Here the total carbonate content varies between 15 wt.% and 26 wt.% (average of  $20 \pm 4$  wt.%;  $n=14$ ) and that of quartz and feldspar from 14–32 wt.% (average of  $22 \pm 6$  wt.%;  $n=14$ ). Calcite is the dominant carbonate mineral and contents of dolomite/ankerite are generally below 1 wt.%, thus lower than in the

sandy facies (Table 6-1). In contrast, the contents of siderite are higher than in the sandy facies and there exists a distinction between the more siderite-rich upper shaly facies 2 (2.4–7 wt.%) and the lower siderite-poor shaly facies 1 (1.3–3.8 wt.%). As in the sandy facies, quartz is significantly more abundant than the feldspars, the contents of which are lower than in the sandy facies (Table 6-1). Pyrite and organic carbon are heterogeneously distributed and vary between 0.7 wt.% and 1.8 wt.%, and between 0.4 wt.% and 1.2 wt.%, respectively (Table 6-1).



**Notes:** The legend is given in the stratigraphic sequence from top to bottom (*cf.* Fig. 1-1). The small squares represent additional samples collected for Nagra and are given for comparison.

**Figure 6-1: Lithologic Association According to Füchtbauer (1988) of the Porewater Chemistry Samples from Borehole BDB-1 at the Mont Terri URL.**

The ~4 m thick carbonate-rich sandy facies in the Opalinus Clay, between 186.3 m and 190.3 m BHL, is exceptional and consists of dark-gray, calcareous, silt-sandy claystone layers that alternate silty to sandy calcareous lenses and decimeter-size layers. The porewater sample collected from this layer is characterised by its very high carbonate content of 62 wt.%, mainly consisting of calcite, and its low clay-mineral content of only 8 wt.% (Figure 6-1, Table 6-1). As shown in Chapter 6, the limestone is also exceptional in its very low water content and water-loss porosity.

The only sample analysed from the Staffelegg Fm at 246 m BHL towards the bottom of the borehole consists of sandy argillaceous marl (Figure 6-1). It differs from the Opalinus Clay by its higher calcite content and by the almost complete absence of dolomite/ankerite and siderite.

Characteristic of the rocks of the upper Staffelegg Fm, which were previously called *Posidonia shale*, are the very high contents in pyrite (5.3 wt.%, including other sulphides) and especially organic carbon (8.46 wt.%; Table 6-1), the latter defining these rocks as bituminous marls and claystones.

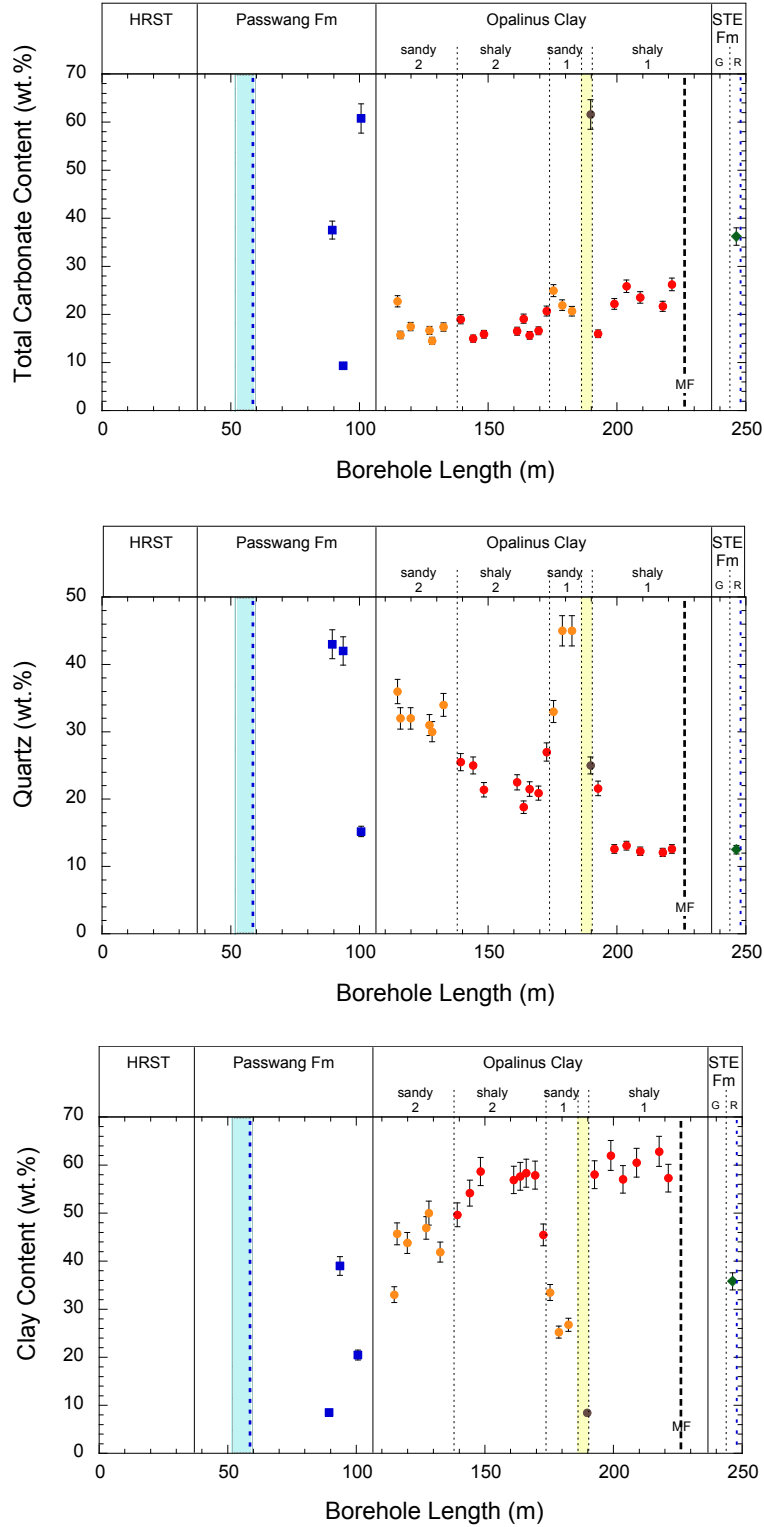
From stratigraphic top to bottom, and as a function of borehole length, the most striking feature is the large variability in mineralogical composition in the Passwang Fm and the differences observed between the different facies of the Opalinus Clay.

Although only represented by three samples, the large variation of total carbonate, quartz and clay-mineral contents in the Passwang Fm (Figure 6-2) reflects the macroscopic aspect of the alternation from limestone to sandstone to marlstone on the decimetre scale, as shown in Figure 1-1. The large variation in mineralogical composition also has an impact on the total porosity and species-specific transport porosity, which renders the derivation of such porosity more difficult when mineralogical data for each sample is not available. Some support, however, might be obtained from the gamma log conducted in the borehole, which can be used to estimate clay mineral content (*cf.* Section 6.2 and Chapter 9).

In the Opalinus Clay there is a general tendency toward higher clay-mineral contents with depth, with increased clay-mineral content primarily compensated by a decrease in quartz content. The total carbonate content remains fairly constant (Figure 6-2). The general tendency is, however, interrupted by the sandy facies 1 and the adjacent carbonate-rich sandy facies, where the total clay-mineral content decreases below 30 wt.% over a distance of about 20 m due to increases in quartz and total carbonate contents, respectively (Figure 6-2). Such distinct differences in mineralogical composition of the Opalinus Clay have not been encountered previously in porewater investigations at the Mont Terri URL, where only short boreholes drilled from the URL tunnels were investigated (Pearson et al. 2003). As for the rock of the Passwang Fm, this may pose some difficulties in using a single value for the species-specific transport porosity across the entire Opalinus Clay.

The most prominent tectonic feature in the Opalinus Clay at the Mont Terri URL, the so-called Main Fault, was encountered by the BDB-1 borehole at a depth of about 226.10 – 227.4 m BHL within shaly facies 1. No mineralogy data are available from the Main Fault, but the petrophysical and porewater chemical data of a sample collected towards the lower end of the Main Fault reveal no significant differences to over- and underlying samples (*cf.* Chapters 7–10), suggesting that the mineralogy might be similar to the surrounding shaly facies.

For the Staffelegg Fm it should be mentioned that macroscopic core inspection (Jaeggi et al. 2016; Hostettler et al. 2017) and geophysical borehole logging (Fischer 2014) revealed an ~2 m thick argillaceous limestone layer in the Opalinus Clay – Staffelegg Fm interface between 236.8 m BHL and 238.4 m BHL (indicated in pale yellow in Figure 6-2).

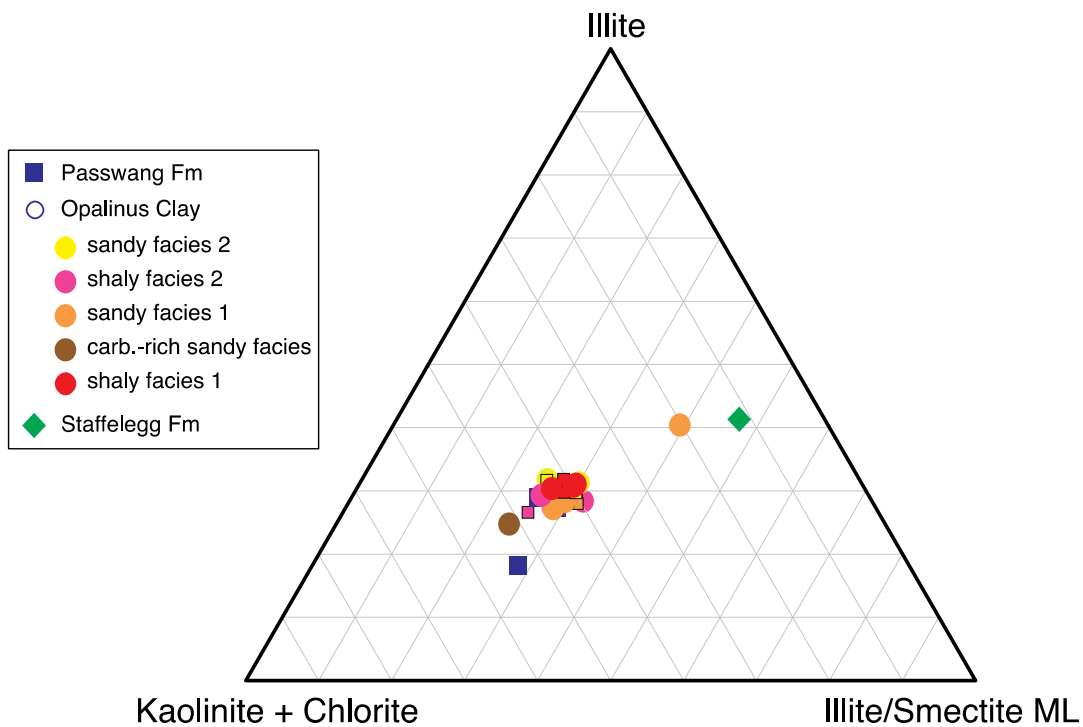


Notes: MF: main fault; yellow area: carbonate-rich sandy facies; bright bluish area: packer interval; blue dotted lines: water inflows

**Figure 6-2: Contents of Total Carbonate (top), Quartz (middle) and Total Clay Minerals (bottom) as a Function of Depth in Borehole BDB-1 at the Mont Terri URL.**

## 6.2 CLAY MINERALOGY

The clay fraction of most the porewater samples from borehole BDB-1 is rather homogeneously composed (Table 6-1) and clusters in the triangular illite–illite/smectite ML – kaolinite+chlorite diagram around about 30% illite, 30% illite/smectite mixed layers and 40% of kaolinite and chlorite (Figure 6-3). Exceptions from this general behaviour are one sample in the Passwang Fm at 100.63 m BHL and the sample from the carbonate-rich sandy facies in the Opalinus Clay (189.71 m BHL), both of which have a low total clay-mineral content (20 and 8 wt.%, respectively) and a higher proportion of kaolinite compared to the majority of the samples (Figure 6-6). In turn, the sample collected at the top of sandy facies 1 (175.33 m BHL) and that of the Staffelegg Fm are dominated by illite and illite/smectite mixed layers, and have significantly lower contents in kaolinite and chlorite (Figure 6-3).

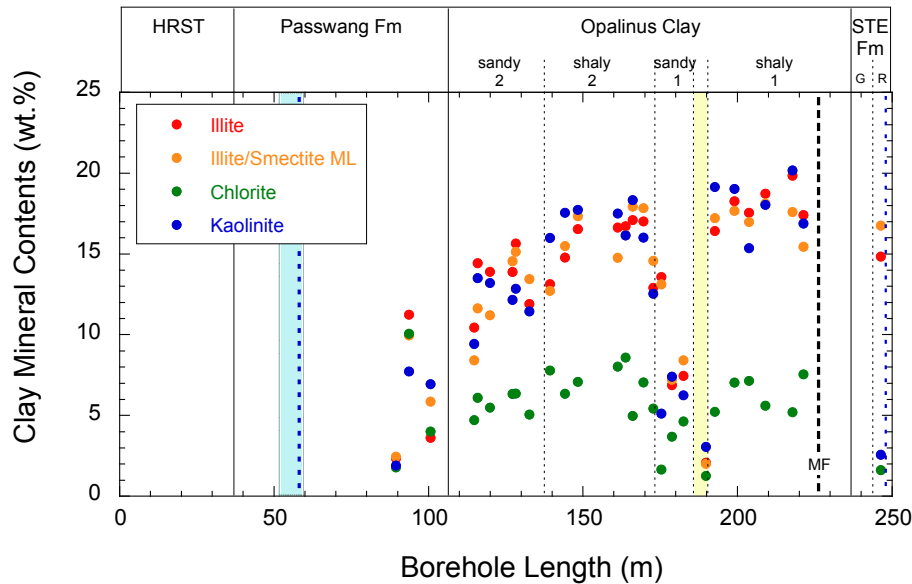


Notes: The legend is given as stratigraphic sequence from top to bottom (cf. Fig. 1-1). The small squares represent additional samples collected for Nagra and are given for comparison.

**Figure 6-3: Clay Mineralogy of Porewater Chemistry Samples from Borehole BDB-1 at the Mont Terri URL.**

As a function of their stratigraphic level or borehole depth, respectively, the contents of the illite, illite/smectite and kaolinite increase in similar proportions from about 10 wt.% in the whole rock to about 18 wt.% toward greater depth (Figure 6-4). Chlorite is more evenly distributed between about 5 wt.% and 8 wt.% in the whole rock. The clay mineral compositions of sandy facies 1 and the adjacent carbonate-rich sandy facies (sample BDB1-189.71) in the Opalinus Clay differ from this general pattern by their distinctly low individual clay mineral contents, as already observed in the total clay content (cf. Figure 6-2c).

Across the entire Opalinus Clay and its different facies, the ratios of illite to illite/smectite mixed-layers, and illite to kaolinite, remain constant, except for the shallowest sample in sandy facies 1 at 175.33 m BHL. Due to the rather constant chlorite content, a slight tendency toward increasing illite to chlorite, and kaolinite to chlorite, ratios is observed from top to bottom of the Opalinus Clay (though not statistically significant).

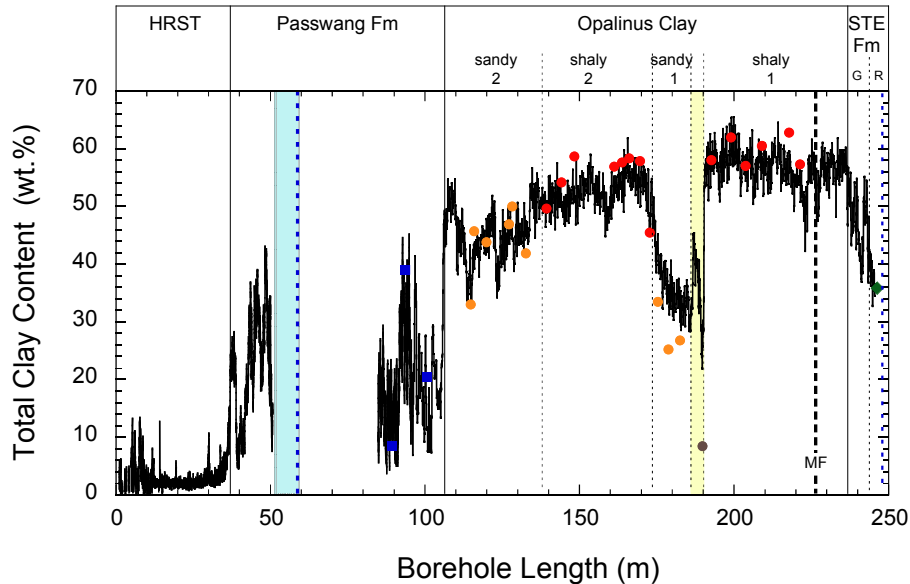


Notes: MF: main fault; yellow area: carbonate-rich sandy facies; bright bluish area: packer interval; blue dotted lines: water inflows

**Figure 6-4: Individual Clay Mineral Contents (wt.% of whole rock) as a Function of Depth in Borehole BDB-1 at the Mont Terri URL.**

The homogeneous clay-mineral distribution in the Opalinus Clay indicates similar diagenetic alteration of the original clay mineral association across the entire clay, independent of sedimentary facies. It also facilitates comparison of experimental data that might be influenced by individual clay minerals (e.g., isotope diffusive exchange, squeezing, etc.; see below). Furthermore, the homogeneous clay-mineral distribution, especially in the Opalinus Clay, might be advantageous for the conversion of geophysical logs to total clay-mineral content (Willenberg-Spillmann 2015) and, thus, allow extrapolation of a continuous distribution across the entire sedimentary sequence. Figure 6-5 shows such a distribution of the clay-mineral content, as derived from geophysical logging data and using the present samples for calibration. The conversion of the geophysical data to total clay-mineral content should, however, still be treated carefully, as it considers only the measured clay-mineral content and neglects, e.g., that the contents of K-feldspar and refractory U-Th-bearing minerals also contribute to the gamma-ray inventory and may vary greatly between limey, sandy and marly lithologies (e.g., for K-Feldspar by a factor of 2 between sandy and shaly facies). It appears that such variability may account for overestimation of the clay content based on the geophysical log when compared to the measured data in sandy facies 1 of the Opalinus Clay (Figure 6-5). Nevertheless, such an

approach helps – as a first assumption – to fill in gaps for intervals where no other information is available for the estimation of the species-specific transport porosity (*cf.* Chapter 9).



Notes: MF: main fault; yellow area: carbonate-rich sandy facies; bright bluish area: packer interval; blue dotted lines: water inflows

**Figure 6-5: Total Clay-Mineral Content Based on Gamma Logging (Willenberg-Spillmann, 2015) Compared to the Clay-mineral Contents Determined by XRD on Porewater Samples as a Function of Depth in Borehole BDB-1 at the Mont Terri URL.**

### 6.3 OPEN FRACTURES, WATER-CONDUCTING FEATURES AND WET SPOTS

Structural features, possible water-inflow points and wet spots were assessed by macroscopic core mapping (Jaeggi et al. 2014) and by various borehole logs (Fischer 2014).

In the rocks of the Hauptrogenstein, small open fractures are abundant and distributed across the entire depth interval. Accumulations of open fractures were observed from 11–12 m and 30–34 m. Increases in temperature and electric conductivity in the borehole logs at about 11.5 m and 30.5 m BHL suggest inflow of groundwater in these intervals (Fischer 2014).

In the rocks of the Passwang Fm accumulations of open fractures were encountered across the interface to the Hauptrogenstein from 35–40 m BHL and from 48–50 m. Pronounced increases in temperature and electric conductivity in the borehole logs at about 37.3 m, 46.0 and 48.5 m BHL indicate inflow of groundwater at these locations (Fischer 2014). No borehole logs are available from 50–97 m BHL in the Passwang Fm. Here, the localisation of the water inflow into the packed-off interval from 51–59.65 m must rely on the macroscopic drill-core description. The visual examination suggests that the inflow of groundwater collected from this interval is through open fractures in the Passwang Fm rocks between 58.5 and 58.8 m BHL (Jaeggi et al. 2014). Other accumulations of open fractures are described from 62–65 m, 72.9–73.8 m and

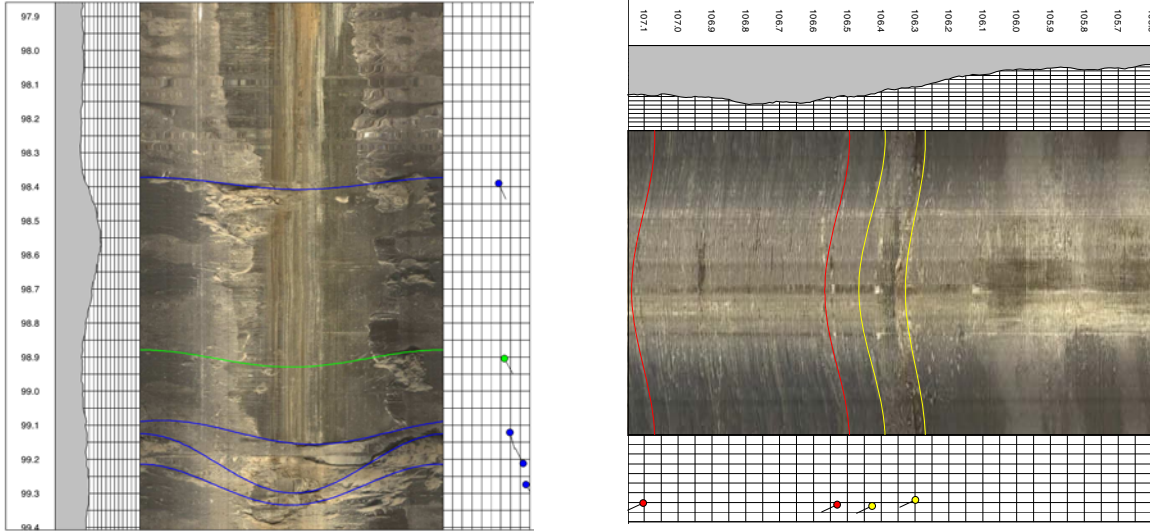
77.6 m BHL. In the lower part of the Passwang Fm, where again geophysical logs are available, a set of four open fractures occurs between 98.4 and 99.4 m BHL, although without significant excursion in the conductivity log or visible wet areas in the borehole image (Figure 6-6, left). No additional 'visibly open' fractures were identified further down to the bottom of the Passwang Fm at 106.25 m BHL.

The interface of the Passwang Fm and Opalinus Clay (106.25 m BHL) has a rather tight appearance. Only a few moist zones are visible along the bedding planes (Figure 6-6, right), which is commonly observed in the sandy facies of the Opalinus Clay (see below).

The sediments of the Opalinus Clay commonly display only scarce tectonic features, such as fissures, fractures and shear zones. Nevertheless, differences in the transport of water are observed in the different lithologies and facies. Both sections of shaly facies 1 and 2 have a homogenous appearance and very few moist zones are visible in the borehole image log (Figure 6-7). In turn, occurrences of moist zones (wet spots) are frequently observed in the coarser-grained sandy facies (Figure 6-8) and the carbonate-rich sandy facies along the bedding planes (Figure 6-9, left). This indicates that in the rocks of the sandy facies, the porewater is more easily squeezed from the rock along the pressure gradient induced by the borehole.

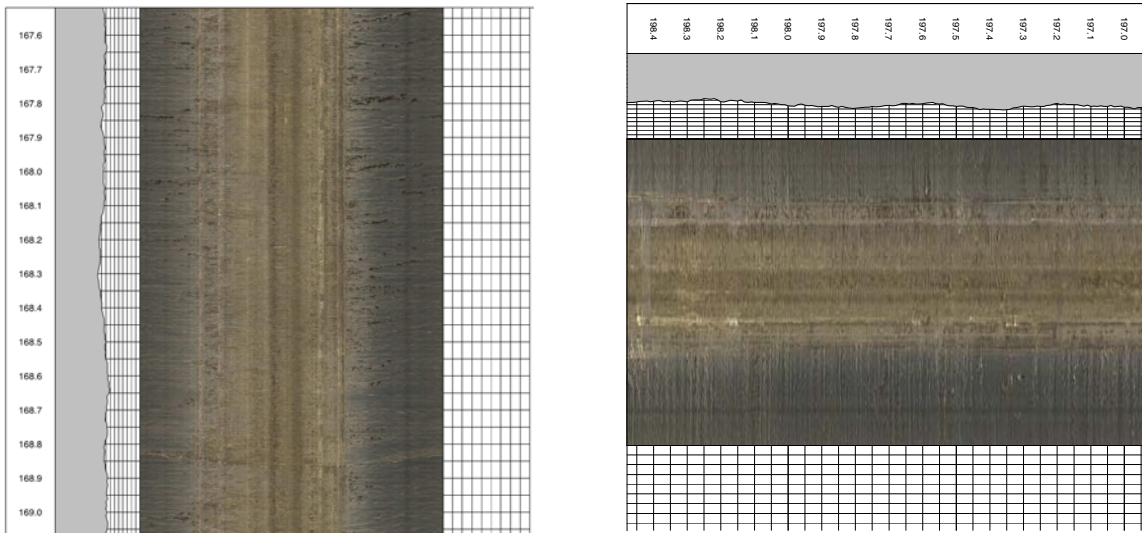
In the Opalinus Clay, open structures identified by macroscopic drill-core inspection and geophysical logging are limited to two depth zones in the carbonate-rich sandy facies and shaly facies 1. An individual open fracture occurs at 186.6 m BHL (Fig. 6-9, right) within the carbonate-rich sandy facies. The pronounced wetting of the borehole wall suggests significant movement of porewater along this feature and borehole-induced pressure gradients. Within shaly facies 1, a series of open fissures occurs at a depth of about 226.10 – 227.4 m BHL, constituting the most prominent tectonic feature of the Opalinus Clay at Mont Terri, the so-called Main Fault. Also in this zone, wetting of the borehole wall is observed when compared to the undisturbed rock above the Main Fault (Figure 6-10), although this is somewhat less pronounced than in the open fracture of the carbonate-rich sandy facies. Nevertheless, it appears that the movement of porewater is facilitated in the Main Fault compared to the undisturbed shaly facies.

At the interface Opalinus Clay – Staffelegg Fm, several bedding- and fracture-related wet spots are observed at the interface and in the underlying limestone layer of the Staffelegg Fm, just below the interface (Figure 6-11). Open fractures are observed at the interface (236.80 m BHL) itself and at 237.3 m BHL in the limestone of the Staffelegg Fm. Between 243.5 m BHL and 234.8 m BHL, in the bituminous marl of the Staffelegg Fm, several open fractures are observed by borehole imaging and in the drill core. The pronounced water inflows observed in this zone caused termination of air drilling to greater depth (Figure 6-12).



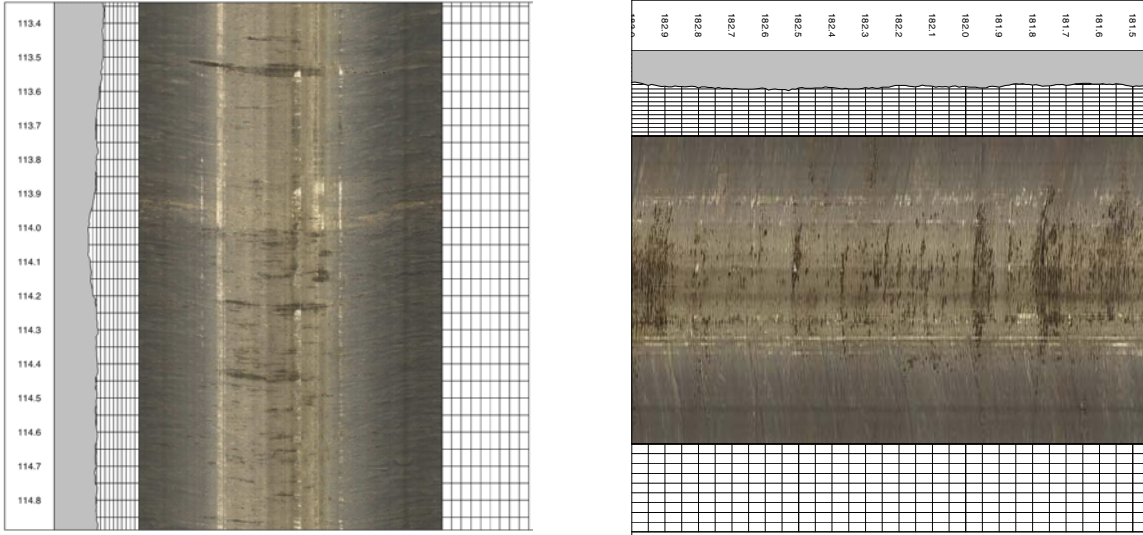
Notes: Note that the borehole was dry-drilled with air. Line colour coding: blue = open fracture, bright green = induced fracture, red = bedding plane, yellow = lithology change.

**Figure 6-6: Borehole Images of the Passwang Fm Between 97.9 and 99.4 m BHL with Open Fractures without Visible Wet Zones (left) and the Contact Passwang Fm – Opalinus Clay at 106.26 m BHL with a Weak, Bedding-parallel Moist Zone (right; from Fischer 2014).**



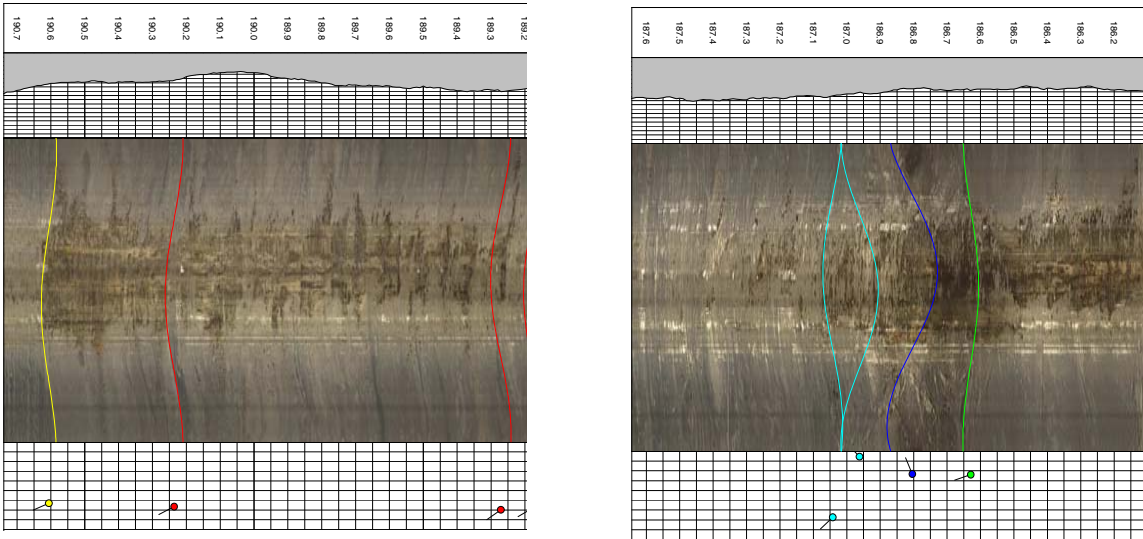
Notes: Note that the borehole was dry-drilled with air.

**Figure 6-7: Borehole Image of Shaly Facies 2 (167.6 – 169.0 m BHL, left) and Shaly facies 1 (197.0 – 198.4 m BHL, right) Showing its Typical Appearance without Any Wet Spots (from Fischer 2014).**



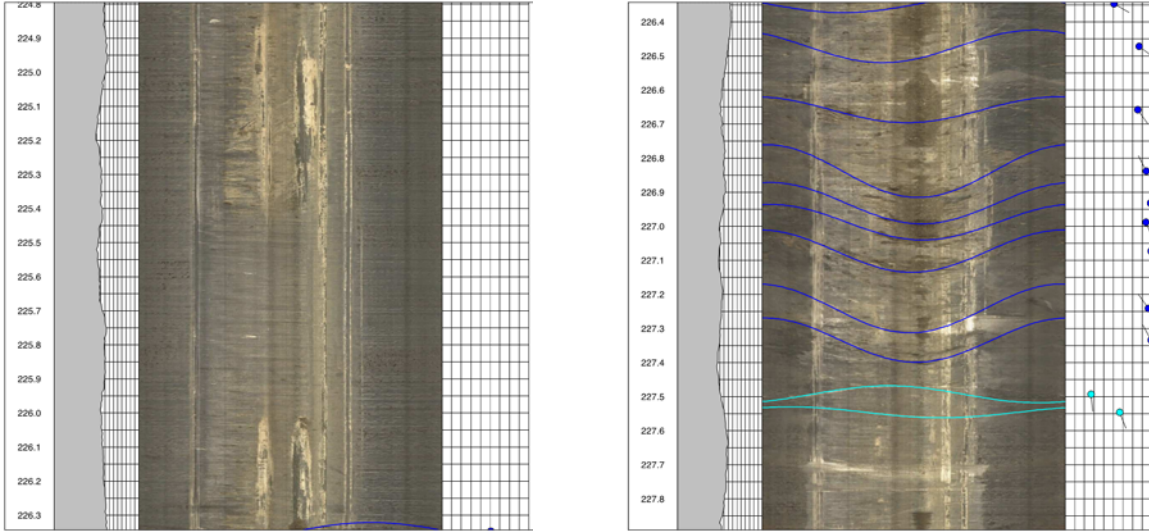
Notes: Note that the borehole was dry-drilled with air.

**Figure 6-8: Borehole Image of Sandy facies 2 (113.4 – 114.8 m BHL, left) and Sandy Facies 1 (181.5 – 190.0 m BHL, right) Showing the Typical Occurrences of Wet Spots along the Bedding Planes (dark) Indicating Water Inflow Areas (from Fischer 2014).**



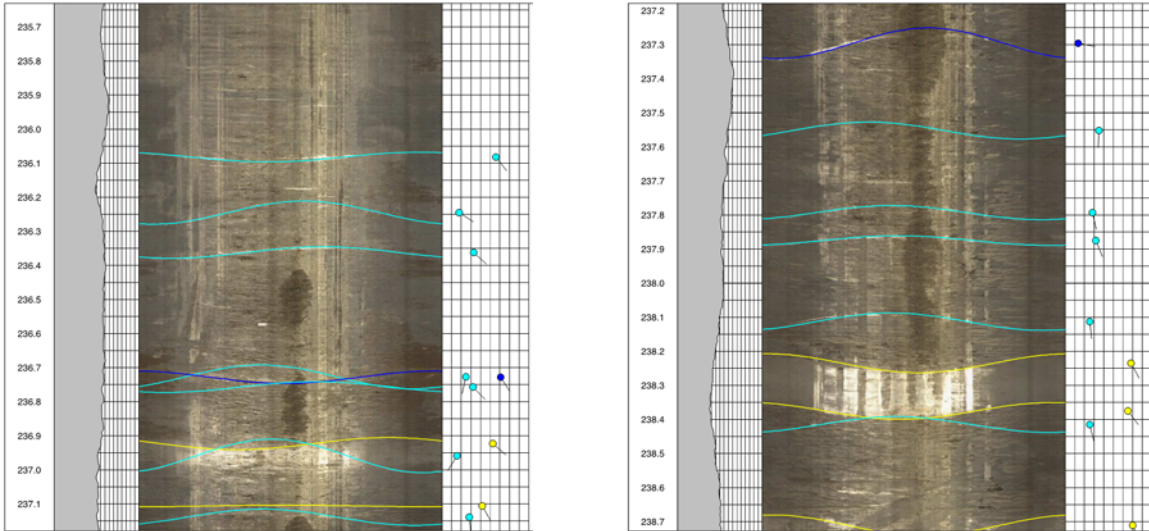
Notes: Note that the borehole was dry-drilled with air. Line colour coding: red = bedding plane, yellow = lithology change, turquoise = sealed fractures, bright green = induced fracture.

**Figure 6-9: Borehole Imaging Log of the Non-fractured (189.20 – 190.7 m BHL, left) and Fractured (186.10 – 187.6 m BHL, right) Carbonate-rich Sandy Facies with Water Inflow Areas Around Open Fissures (from Fischer 2014).**



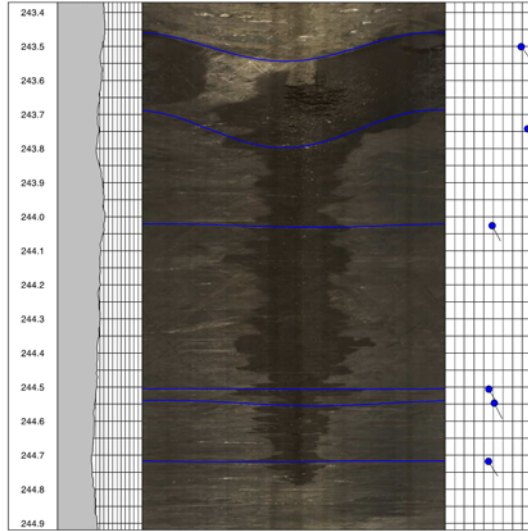
Notes: Note that the borehole was dry-drilled with air. Line colour coding: blue = open fracture, turquoise = sealed fractures.

**Figure 6-10: Borehole Imaging Log Across the Main Fault in the Opalinus Clay from 226.10 – 227.4 m BHL with Water Inflow Areas Around Open Fissures (from Fischer 2014).**



Notes: Note that the borehole was dry-drilled with air. Line colour coding: blue = open fracture, turquoise = sealed fractures, yellow = lithology change.

**Figure 6-11: Borehole Imaging Log Showing the Opalinus Clay – Stafflegg Fm Interface at 236.80 m BHL and the Limestone Section at the Top of the Stafflegg Fm from 236.8 – 238.4 m BHL with Water Inflow Areas Along Bedding Planes and Open Fractures (from Fischer 2014).**



Notes: Note that the borehole was dry-drilled with air; blue lines = open fracture.

**Figure 6-12: Borehole Imaging Log of the Bituminous Claystone in the Staffelegg Fm from 243.4 – 244.9 m BHL with Clearly Visible Open Fractures and Pronounced Water Inflows (from Fischer 2014).**

Table 6-1: Mineralogical Composition of Porewater Chemistry Samples

Sample	Depth m BHL	Strati- graphie	Member / Facies	Lithology (field)	Calcite wt. %	Dolomite / Ankerite wt. %	Siderit wt. %	Quartz wt. %	Plagio- clase wt. %	K- Feldspar wt. %	Pyrite wt. %	S tot wt. %	C org. wt. %	C anorg. wt. %	Total Clay Content wt. %	Illite wt. %	Ill-Sm ML wt. %	Chlorite wt. %	Kaolinite wt. %
BDB1-89.45	89.45	PAF	Himichopf - Mb.	li sst	29	8.9	0.0	43	1.9	8.0	0.5	0.28	0.53	4.58	9	2	2	2	2
BDB1-93.65	93.65	PAF	Himichopf - Mb.	sa ma	9	0.6	0.0	42	1.9	6.0	1.3	0.68	0.48	1.13	39	11	10	10	8
BDB1-100.63	100.63	PAF	Sissach - Mb.	sa lst	50	11.2	0.0	15	0.1	2.0	0.5	0.28	0.97	7.39	20	4	6	4	7
BDB1-114.80	114.80	OPA	sandy facies 2	clst & lst la	22	1.1	0.0	36	1.0	4.0	2.6	1.37	0.65	2.75	33	10	8	5	9
BDB1-115.88*	115.88	OPA	sandy facies 2	clst & lst la	14	0.8	0.8	32	0.9	3.0	2.1	1.12	0.59	1.89	46	14	12	6	14
BDB1-119.86	119.86	OPA	sandy facies 2	clst & lst la	15	0.6	1.5	32	1.0	4.0	1.0	0.52	0.70	2.09	44	14	11	5	13
BDB1-127.15*	127.15	OPA	sandy facies 2	clst & lst la	13	0.9	2.9	31	1.0	3.0	0.7	0.39	0.63	1.97	47	14	15	6	12
BDB1-128.24	128.24	OPA	sandy facies 2	clst & lst la	10	1.1	3.1	30	1.0	3.0	0.8	0.40	0.68	1.71	50	16	15	6	13
BDB1-132.63	132.63	OPA	sandy facies 2	clst & lst la	14	0.8	2.5	34	1.1	4.0	0.8	0.44	0.78	2.06	42	12	13	5	11
BDB1-139.31*	139.31	OPA	shaly facies 2	silt clst	16	0.0	3.1	26	1.0	2.0	1.8	0.98	0.99	2.24	50	13	13	8	16
BDB1-144.17	144.17	OPA	shaly facies 2	silt clst	9	1.1	4.5	25	0.8	3.0	0.9	0.48	1.16	1.74	54	15	15	6	18
BDB1-148.31*	148.31	OPA	shaly facies 2	silt clst	9	1.1	5.6	21	0.6	2.0	0.7	0.39	0.66	1.83	59	17	17	7	18
BDB1-161.18	161.18	OPA	shaly facies 2	silt clst	11	0.3	5.0	23	0.9	2.0	0.7	0.36	0.52	1.91	57	17	15	8	18
BDB1-163.75*	163.75	OPA	shaly facies 2	silt clst	12	0.0	6.8	19	0.6	2.0	1.1	0.60	0.67	2.19	58	17	16	9	16
BDB1-166.08	166.08	OPA	shaly facies 2	silt clst	9	1.8	4.7	22	1.1	2.0	0.7	0.40	0.67	1.82	58	17	18	5	18
BDB1-169.48*	169.48	OPA	shaly facies 2	silt clst	12	0.1	4.4	21	0.7	2.0	1.1	0.57	0.79	1.93	58	17	18	7	16
BDB1-172.70	172.70	OPA	shaly facies 2	silt clst	18	0.5	2.4	27	1.1	4.0	1.0	0.53	0.71	2.46	45	13	15	5	13
BDB1-175.33	175.33	OPA	sandy facies 1	clst & sst la	16	6.4	2.4	33	1.7	5.0	1.0	0.53	0.88	3.01	33	14	13	2	5
BDB1-178.73	178.73	OPA	sandy facies 1	clst & sst la	19	1.1	1.8	45	1.6	5.0	0.6	0.33	0.61	2.62	25	7	7	4	7
BDB1-182.48*	182.48	OPA	sandy facies 1	clst & sst la	17	1.9	2.1	45	1.7	5.0	0.6	0.30	0.31	2.47	27	7	8	5	6
BDB1-189.71	189.71	OPA	carb.-rich sandy f.	lst	59	0.7	2.1	25	0.9	3.0	0.2	0.11	0.90	7.39	8	2	2	1	3
BDB1-192.68	192.68	OPA	shaly facies 1	clst	12	0.6	3.8	22	0.9	2.0	1.1	0.58	0.42	1.87	58	16	17	5	19
BDB1-198.93*	198.93	OPA	shaly facies 1	clst	19	0.0	2.7	13	0.5	1.0	1.0	0.55	0.65	2.63	62	18	18	7	19
BDB1-203.68	203.68	OPA	shaly facies 1	clst	24	0.5	1.3	13	0.6	1.5	1.4	0.74	0.49	3.10	57	18	17	7	15
BDB1-209.00	209.00	OPA	shaly facies 1	clst	21	0.1	2.3	12	0.5	1.5	1.3	0.70	0.45	2.80	60	19	18	6	18
BDB1-217.73*	217.73	OPA	shaly facies 1	clst	18	1.0	3.1	12	0.6	1.0	1.3	0.67	0.53	2.57	63	20	18	5	20
BDB1-221.28	221.28	OPA	shaly facies 1	clst	24	0.4	1.6	13	0.7	1.5	1.0	0.53	0.64	3.14	57	17	15	8	17
BDB1-246.34	246.34	STF	Rietheim Mb.	bit ma	36	0.7	0.0	13	0.8	1.0	5.3	2.81	8.46	4.37	36	15	17	2	3

**Notes:**

Clay mineral contents as wt.% per whole rock; cf. Section 5.1 for derivation of individual mineral contents. PAF = Passwang Formation, OPA = Opalinus Clay, STF = Staffelegg Formation. Field lithology after Hostettler et al. (2017): li sst = limy sandstone, sa ma = sandy marl, lst = limestone; sa lst = sandy limestone, clst = claystone, silt clst = silty claystone, clst & lst la = claystone with limestone layers, clst & sst la = claystone with sandstone layers, arg ma = argillaceous marl, bit ma = bituminous marl. Shaded samples were used for inter-laboratory comparison, \* samples from Becker (2014).

## 7. PETROPHYSICAL PARAMETERS

Quantitative analyses of the rock petrophysical parameters were performed on the 19 samples that constitute the "*porewater method comparison program*" and 50 samples mainly devoted to the "*Passwang Fm – Opalinus Clay interface programme*". Whereas gravimetric bulk density, gravimetric water-loss and water content from isotope exchange data are available for all of these samples, grain density and BET data are only available for a smaller subset of samples.

Petrophysical parameters were produced using the same methods for 9 samples from the Opalinus Clay that were collected for Nagra for comparison with geophysical and geochemical logs and that are originally reported in Becker (2014). These samples are also discussed here. The complete petrophysical data of the porewater chemistry samples are compiled in Table 7-1.

### 7.1 GRAIN AND BULK DENSITY

In the rocks of the Passwang Fm grain density values range from 2.711 g/cm<sup>3</sup> to 2.816 g/cm<sup>3</sup> (Figure 7-1). The large variation reflects the alternation between clay-rich marl layers and almost pure limestone layers. Additional variation is induced by highly-variable contents of dolomite/ankerite in the carbonate-rich layers and of feldspars in the more sandy layers.

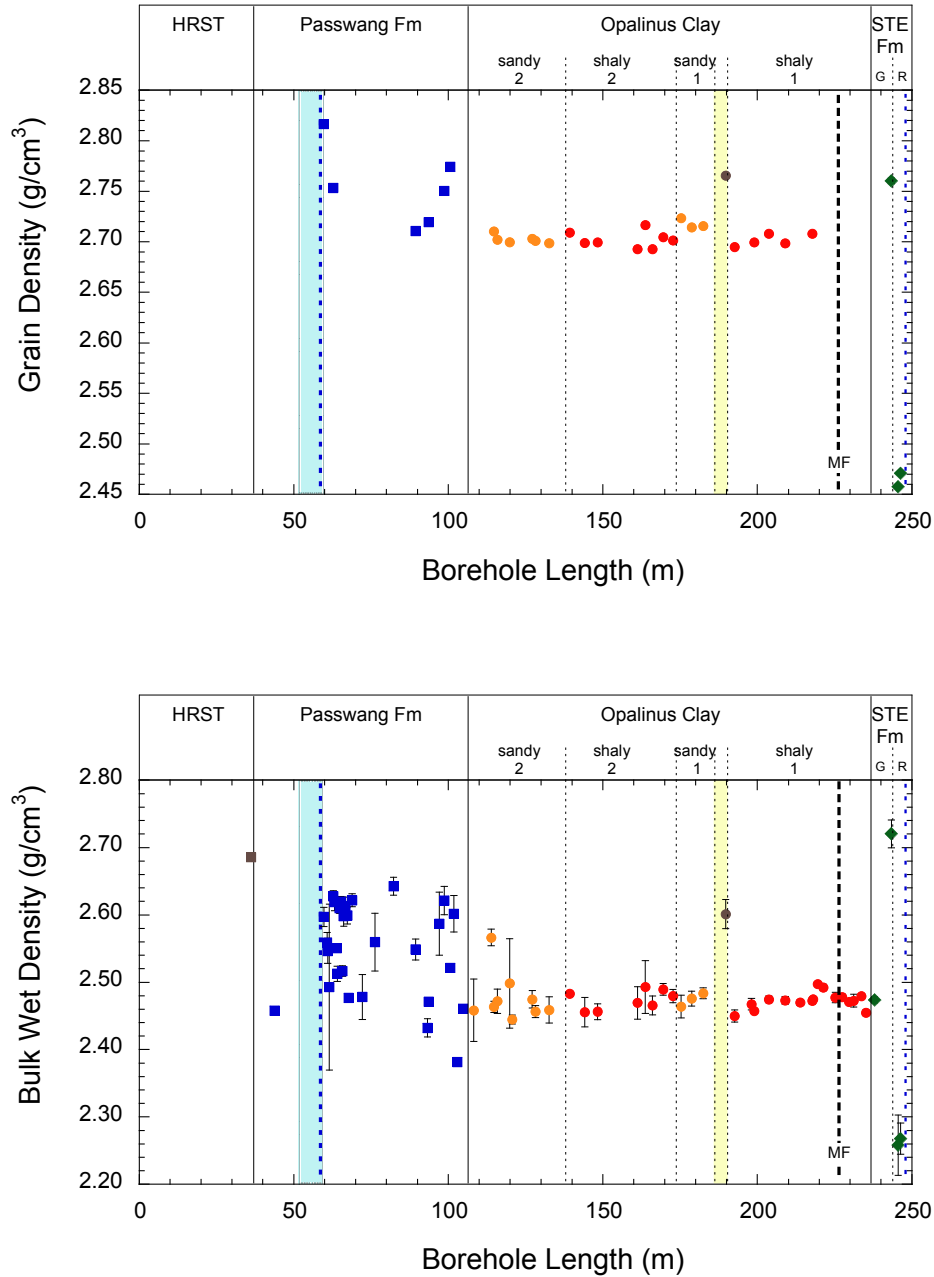
The larger data set available of bulk wet density measurements shows a similar high variability across the entire Passwang Fm, ranging from 2.382 g/cm<sup>3</sup> to 2.643 g/cm<sup>3</sup> (n=29). The pronounced variability is attributed to differences in mineralogy and porosity in the sediment layers.

In the Opalinus Clay rocks, the grain density shows only minimal variation, although some differences are observed between the individual facies (Figure 7-1). Sandy facies 2 and both shaly facies have almost identical grain density values of 2.702 ± 0.003 g/cm<sup>3</sup> (n=9) and 2.703 ± 0.005 g/cm<sup>3</sup> (n=24), respectively, in spite of the lower clay content in sandy facies 2 (*cf.* Chapter 6). In contrast, sandy facies 1 has a higher grain density of 2.718 ± 0.005 g/cm<sup>3</sup> (n=3), corresponding to its significantly lower clay content. An even higher grain density of 2.766 g/cm<sup>3</sup> is displayed by the rock of the carbonate-rich sandy facies, which has less than 10 % total clay content (*cf.* Chapter 6).

Little variation is also observed in the bulk wet density of most of the Opalinus Clay rocks (Figure 7-1). In contrast to the grain density, however, bulk wet density values are very similar in both the shaly facies (2.472 ± 0.012 g/cm<sup>3</sup>, n=24) and sandy facies 1 (2.474 ± 0.010 g/cm<sup>3</sup>, n=3), whereas the rocks of sandy facies 2 display large variation (2.432 – 2.566 g/cm<sup>3</sup>, n=9), especially in closer proximity to the Passwang Fm at the top (Figure 7-1). A uniquely high bulk wet density of 2.601 g/cm<sup>3</sup> is recorded for the rock of the carbonate-rich sandy facies.

In the Staffelegg Fm, differences in grain and bulk density are similarly related to lithological differences. The uppermost sample in the Staffelegg Fm is similar to shaly facies 1 of the Opalinus Clay and has similar density values. The sample of the sandy limestone layer rich in belemnites adjacent to the Rietheim Mb. (BDB1-243.37) has elevated grain and bulk density values when compared to the Opalinus Clay and is more similar to limestone samples of the Passwang Fm (Figure 7-1). The bituminous clay rock of the Rietheim Mb. has the overall

lowest grain density ( $2.464 \pm 0.010 \text{ g/cm}^3$ ,  $n=2$ ) and bulk wet density ( $2.257 \pm 0.034 \text{ g/cm}^3$ ) values in the entire profile (Figure 7-1, Table 7-1).



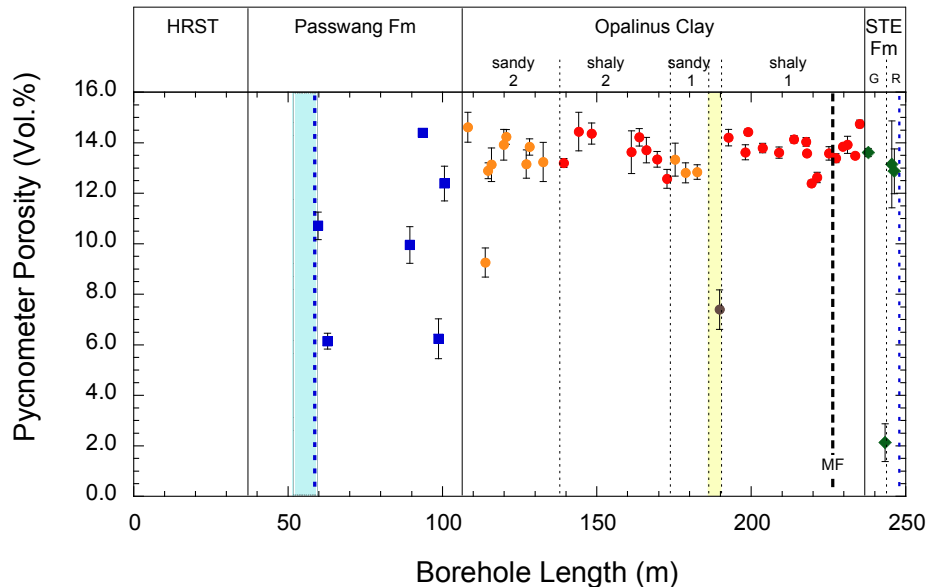
Notes: Error bars indicate the standard deviation of triplicate measurements (for grain density inside the symbol size). MF: main fault; yellow area: carbonate-rich sandy facies; bright bluish area: packer interval; blue dotted lines: water inflows

**Figure 7-1: Grain Density (top) and Bulk Wet Density (bottom) as a Function of Depth in Borehole BDB-1 at the Mont Terri URL.**

## 7.2 PYCNOMETER POROSITY

The porosity obtained from the measured grain density and the calculated bulk dry density, as per equation (11), i.e., the so-called pycnometer porosity, shows generally the same dependence on the rock mineralogy and texture as the density values. For the rock samples of the Opalinus Clay, the very homogenous grain density values allow extrapolation of the pycnometer porosity (using the average values of the individual facies) for samples for which no grain density values were analysed (Table 7-1).

In the rocks of the Passwang Fm, the pycnometer porosity varies by more than a factor of 2 (6.1 – 14.4 vol.%, n=6) for samples for which grain density values are available. Along the profile, the variation of the pycnometer porosity appears to correlate with the total clay content, with higher values in clay-rich layers compared to limestone layers (*cf.* Figures 7-3 and 6-5).



**Notes:** Error bars indicate the propagated error of the density measurements. MF: main fault; yellow area: carbonate-rich sandy facies; bright bluish area: packer interval; blue dotted lines: water inflows

**Figure 7-2: Pycnometer Porosity as a Function of Depth in Borehole BDB-1 at the Mont Terri URL.**

The rocks of the Opalinus Clay display little variation in the pycnometer porosity between 12.4 vol.% and 14.8 vol.% (average:  $13.6 \pm 0.6$  vol.%, n=35), except for one sample in sandy facies 2 and the sample from the carbonate-rich sandy facies (Figure 7-2). These latter samples, with porosity values of 9.3 vol.% and 7.4 vol.%, respectively, are both characterised by low total clay contents and elevated total carbonate contents, especially the sample from the carbonate-rich sandy facies (*cf.* Figure 6-2). Rocks of sandy facies 1 have similar (high) pycnometer porosity values ( $13.0 \pm 0.3$  vol.%, n=3) to the surrounding rock of the shaly facies in spite of their low clay content of ~30 wt.%, and have similar total carbonate contents as well. These sandy rocks are, however, characterised by elevated quartz contents (Figure 6-2). The pycnometer porosity, therefore, depends on differences in the primary, detrital mineralogy as

well as the degree and type of diagenetic cementation (e.g., as indicated by the carbonate-rich sandy facies).

In the rocks of the Stafflegg Fm the large variation in pycnometer porosity is established, as expected, from the large differences in the density values. The sample of the sandy limestone layer rich in belemnites (BDB1-243.37) has the overall lowest pycnometer porosity (2.1 vol.%) across the entire profile. In turn, the bituminous clay rock of the Rietheim Mb. has a similar porosity to the shaly facies of the Opalinus Clay, in accordance with its high clay content.

### 7.3 WATER CONTENT

The water content was determined by two different methods: a) by the gravimetric water loss of the originally saturated samples during drying at 105°C to constant weight conditions, and b) by mass balance of the isotope data gathered in the isotope diffusive exchange experiments.

#### 7.3.1 Water Content from Water Loss

The gravimetric water loss and water content is identical to the absolute and relative mass of porewater present in the connected pore space of an originally saturated rock sample. It therefore corresponds to the porewater where solute transport takes place in low-permeability rocks.

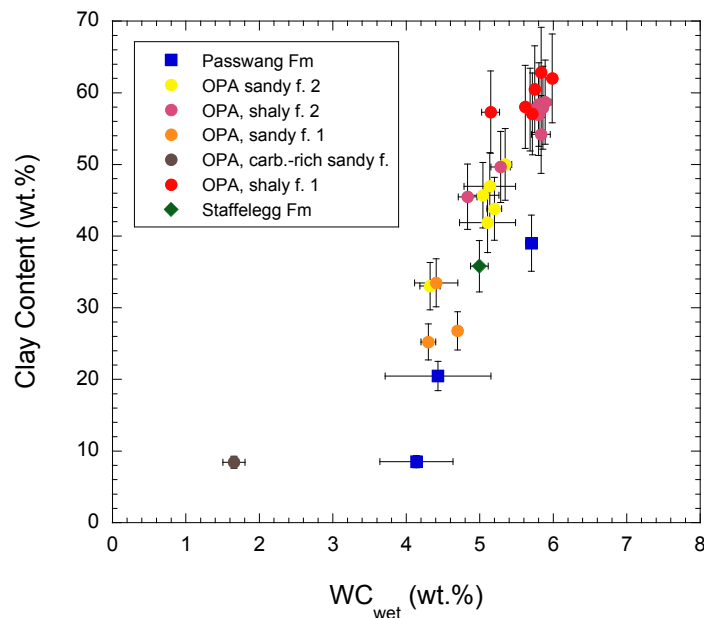
For the porewater chemistry samples, the gravimetric water content was analysed in triplicate using aliquots of originally saturated rock material, with sub-sample masses of about 160 – 250 g. For the porewater noble gas samples, the water content was analysed on the single rock cylinders used for gas equilibration, with sample masses of about 310 – 435 g (*cf.* Section 7.5).

The water content relative to the wet weight of the rocks encountered in borehole BDB-1 display a similar variability and dependency on the lithology, as is observed for bulk and grain density and the pycnometer porosity.

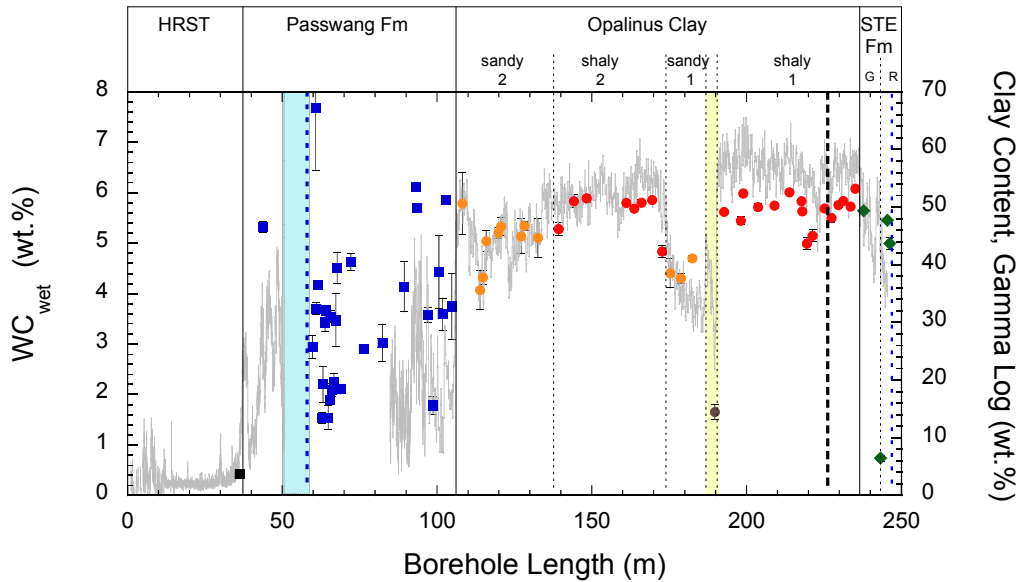
The only limestone sample of the Hauptrogenstein displays the lowest water content of the entire rock sequence, at only 0.42 wt.%.

Water contents of the rocks of the Passwang Fm cover a large range from 1.53 – 7.68 wt.%. There are too few mineralogical analyses available to deduce a reliable relationship between water content and mineralogy in these rocks (Figure 7-3). However, by comparing the water content with the total clay content derived from the gamma log (where available), there appears a rather well developed trend toward a positive correlation between water content and clay content (Figure 7-4). As expected, this indicates that in clay-poor lithologies, such as limey, sandy marl and limestone, most of the porewater (as determined by the water content) is present in the clay portion and not along grain boundaries of carbonate and non-sheet silicate minerals. This is further reflected in the large variability of the standard deviation of triplicate water content measurements, highlighting the heterogeneity of the rock material from the Passwang Fm on a cm-scale, and the inherent difficulty in attempting to prepare three identical samples (*cf.* Figures 7-3 and 7-4, and Table 7-1).

The rocks of the Opalinus Clay show a similar general trend between water content and clay content (Figures 7-3 and 7-4). Based on the larger variability of the clay content (and the larger number of samples), the water content of sandy facies 2 is higher and has a larger spread ( $4.07 - 5.79$  wt.%, average  $5.04 \pm 0.53$  wt.%,  $n=9$ ) compared to that of sandy facies 1 ( $4.30 - 4.70$  wt.%,  $4.47 \pm 0.21$  wt.%,  $n=3$ ). Similar observations exist for shaly facies 2 ( $4.83 - 5.89$  wt.%, average  $5.62 \pm 0.37$  wt.%,  $n=8$ ) and shaly facies 1 ( $4.99 - 56.08$  wt.%, average  $5.67 \pm 0.30$  wt.%,  $n=16$ ). The suggested larger spread in shaly facies 2 is, however, essentially caused by two samples at the interface of sandy facies 2 and 1, at the top and bottom, respectively (Figure 7-4). The carbonate-rich sandy facies displays a much lower water content of only 1.66 wt.%. This value falls off the trend line between water content and clay content given by the sandy and shaly facies, which would indicate a water content for samples with such clay contents of about 3.4 wt.% (Figure 7-3).



clay contents and when compared to the Opalinus Clay rocks (*cf.* Figures 7-3 and 7-4). This further highlights how restricted straight correlation can be between water content and clay content.



Notes: Error bars indicate the standard deviation of triplicate measurements. MF: main fault; yellow area: carbonate-rich sandy facies; bright bluish area: packer interval; blue dotted lines: water inflows

**Figure 7-4: Water Content Relative to the Wet Sample Weight ( $WC_{wet}$ ) Compared to the Clay Content Estimated from the Gamma Log as a Function of Depth in Borehole BDB-1 at the Mont Terri URL.**

### 7.3.2 Water Content from Isotope Mass Balance

From the isotope diffusive exchange technique, the mass of porewater and water content of the rock samples used in the experiments can be derived by mass balance of the  $\delta^{18}\text{O}$ - and  $\delta^2\text{H}$ -values measured before and after equilibration, according to equation (21). Commonly, the water content of the wet rock mass ( $WC_{IsoEx, wet}$ ) is derived and reported as average value of the two isotope experiments. The calculation of the water content relative to dry weight includes additional measurement and calculation steps and, thus, uncertainty can exist (e.g., due to possible loss of rock material during the transfer from the experimental device to a device suitable for drying the rock material after the experiment).

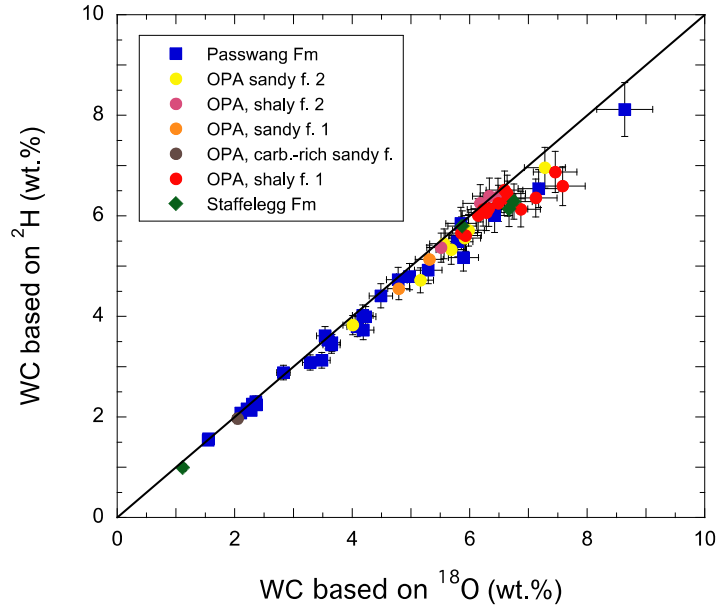
In theory, if no perturbation during preparation and equilibration occurred, the water content calculated by mass balance of the  $\delta^{18}\text{O}$  and  $\delta^2\text{H}$  values should be identical within error. As seen in Figure 7-5, this is the case for most samples. The good correspondence between the two values gives confidence in the reliability of the experimentally-derived porewater isotope composition (*cf.* Chapter 10).

However, toward higher water contents of more than  $\approx 5$  wt.%, there seems a tendency that  $WC_{IsoEx, wet}$  calculated from the  $\delta^{18}O$ -values yields somewhat higher values ( $\leq 10$  %) compared to those calculated from the  $\delta^2H$ -values (Figure 7-5). For the sample from the Passwang Fm with the highest  $WC_{IsoEx, wet}$  neither mineralogical nor gamma log data exist. The other samples with such high water contents have elevated clay contents, independent of the formation, as shown above. This suggests that the isotope composition may, indeed, be affected to a certain degree by isotope exchange reactions with bound water on the clay surface or clay interlayers, as suggested previously (e.g., Pearson et al. 2003). Experimental and theoretical confirmation of these qualitative arguments is, however, still pending.

In this context, it is worth mentioning that the water content derived from the  $\delta^{18}O$  mass balance is more sensitive to the uncertainty in the isotope measurement than that from the  $\delta^2H$  mass balance, and also more sensitive than the derived porewater signature. Thus, the uncertainty in the measured  $\delta^{18}O$ -values of 0.1 ‰ may change the water content by almost 10 %, whereas the porewater isotope signature is only affected on the second decimal place. In turn, the uncertainty in the measured  $\delta^2H$ -values of 1.0 ‰ changes the water content by less than 10 % and the porewater isotope signature is affected at the first decimal place.

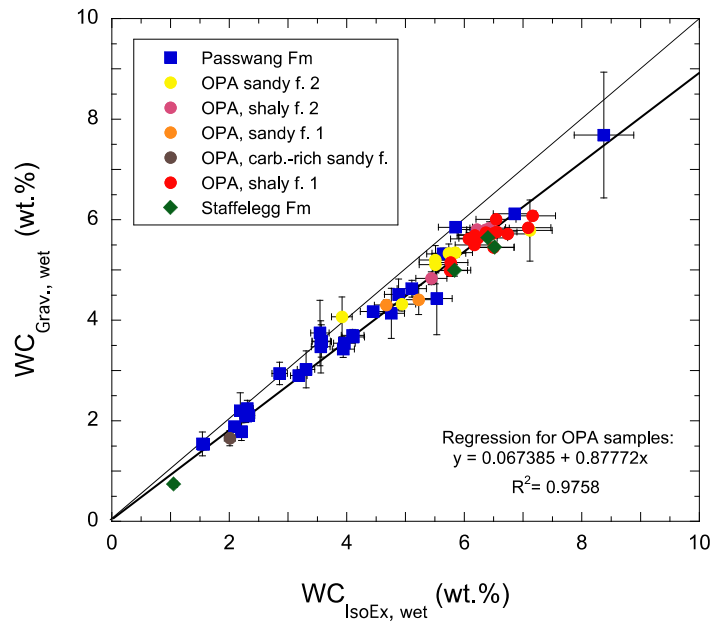
A similar trend for the water content derived by mass balance of measured  $\delta^{18}O$ - and  $\delta^2H$ -values is observed when comparing the average  $WC_{IsoEx, wet}$  derived by the isotope diffusive exchange technique to that derived by drying to constant weight at 105 °C (Figure 7-6). The two differently derived water contents correlate well ( $R^2 = 0.974$ ), but the regression line has an intercept (0.22) suggesting some processes that affect the water content derived by from the isotope experiments. Similar to what is observed for water content calculated from the  $\delta^{18}O$ - and  $\delta^2H$ -values, the average of  $WC_{IsoEx, wet}$  is higher by about 10 % compared to the gravimetric water content,  $WC_{Grav, wet}$ .

The differences in water contents derived by isotope exchange and gravimetric techniques seem primarily related to the clay content of the individual samples, as shown in Figure 7-7. Independent of the stratigraphic formation, the most pronounced difference of around 10 % between the two water contents is observed for samples with clay contents of more than 35 wt.%, corresponding to water contents of more than 5 wt.%. As shown in Chapter 9, the porewater Cl concentrations drop from about 12 g/L at the bottom of the Opalinus Clay to less than 0.1 g/L in the Passwang Fm. This could suggest that if, during the experiment, an exchange with bound water would occur, such exchange would be independent of the porewater salinity in the present range. As mentioned above, however, experimental and theoretical confirmation of these qualitative arguments is still pending and no final conclusion can be drawn at this stage.



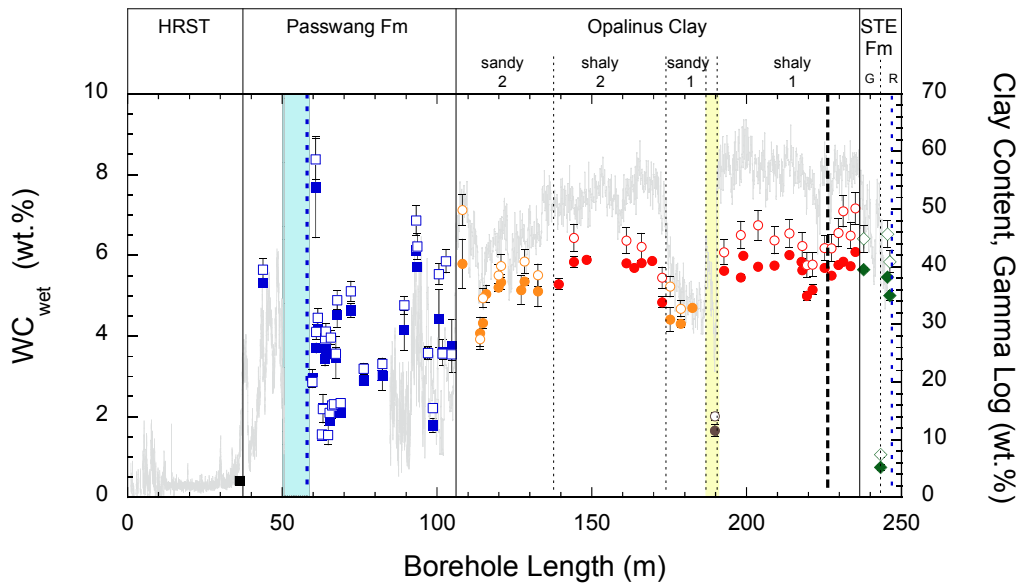
Notes: Error bars indicate the propagated error of the water contents.

**Figure 7-5: Water Content Obtained from  $\delta^{18}\text{O}$  Versus that Obtained from  $\delta^2\text{H}$  in the Isotope Diffusive Exchange Experiments.**



Notes: Error bars indicate the propagated error for  $WC_{\text{IsoEx, wet}}$  and the standard deviation of triplicate measurements for  $WC_{\text{Grav., wet}}$ .

**Figure 7-6: Water Content Relative to the Wet Sample Weight Derived by Isotope Exchange Technique ( $WC_{\text{IsoEx, wet}}$ , average values) Versus that Derived by Drying at 105°C ( $WC_{\text{Grav., wet}}$ ).**



**Notes:** Error bars indicate the propagated error for  $WC_{IsoEx,wet}$  and the standard deviation of triplicate measurements for  $WC_{Grav,wet}$ . MF: main fault; yellow area: carbonate-rich sandy facies; bright bluish area: packer interval; blue dotted lines: water inflows

**Figure 7-7: Water Content Derived by Isotope Exchange Technique ( $WC_{IsoEx,wet}$ , open symbols) Compared to the Gravimetric Water Content ( $WC_{Grav,wet}$ , filled symbols) and the Clay Content Estimated from the Gamma Log as a Function of Depth in Borehole BDB-1 at the Mont Terri URL.**

## 7.4 WATER-LOSS POROSITY

The ratio of the water-filled, connected pore volume to the total volume ( $V_{wat}/V_{tot}$ ), the so-called water-loss porosity,  $\phi_{WL}$ , is obtained from the water-loss and the grain density according to equation (13). This porosity describes the total volume of water present in the pore space of a rock. Depending on the clay content, a significant proportion of this water is bound on clay surfaces and interlayers, whereas the porewater, i.e., the free water where solute transport occurs, comprises only a fraction of this total water.

In contrast to the pycnometer porosity, the water-loss porosity is less dependent on the grain density of the rock. For example, a change in grain density from  $2.70 \text{ g/cm}^3$  to  $2.75 \text{ g/cm}^3$  alters the water-loss porosity in the range of 1 – 19 vol.% by less than 2 % relative, and that from  $2.70 \text{ g/cm}^3$  to  $2.78 \text{ g/cm}^3$  by less than 4 % relative. This latter value corresponds to the highest grain density measured in the Passwang Fm. In the Opalinus Clay, the small variation in grain density modifies the water-loss porosity only within the uncertainty band, except for the carbonate-rich sandy facies with its substantially higher grain density (*cf.* Section 7-1).

In a first assumption, these relatively small modifications of the water-loss porosity by changes in grain density allow estimation of the water-loss porosity based on average values for the rocks of the different formations, without inducing unacceptable uncertainty. For the

heterogeneously composed Passwang Fm, however, a better accuracy of water-loss porosity and porewater concentrations (*cf.* Chapter 9) would be obtained if grain density values were available for all samples.

The water-loss porosity shows the same dependence on the rock mineralogy as the water content (*cf.* Figures 7-7 and 7-8). In the heterogeneously composed Passwang Fm, the spread in water-loss porosity is large compared to the more homogeneous Opalinus Clay, although differences occur in the latter between the sandy facies and shaly facies.

The only sample of the Hauptrogenstein consists of limestone and displays, along with its very low clay content, the lowest water-loss porosity of the entire rock sequence at  $1.14 \pm 0.23$  vol.%.

In the rocks of the Passwang Fm, the water-loss porosity varies by more than a factor of 4 (4.1 – 18.6 vol.%,  $n=29$ ) for all samples. Note that this range also includes samples for which the water-loss porosity has been calculated with an assumed average grain density. The minimum and maximum might therefore deviate by about  $\pm 2 - 4$  % relative. At clay contents of more than 30 wt.%, the water-loss porosity appears to correlate fairly well with the total clay content (Figure 7-8), as already observed for the water content (*cf.* Figures 7-7 and 7-8). At lower clay contents, such correlation is no longer established, which is partly due to the lack of data about the clay content. The variability of the water-loss porosity reflects the heterogeneity of the rocks of the Passwang Fm and the often rather large uncertainty for individual samples given by the standard deviation of triplicate measurements, suggesting that this heterogeneity occurs on the cm-scale.

In lithologies of the Passwang Fm, with water-loss porosity values of less than 10 vol.%, the difference between water-loss porosity and pycnometer porosity may exceed 10 %, trending toward lower water-loss porosity values (Figure 7-9). This indicates that, in these rocks, a significant portion of the total pore space is not accessible for solute transport. Most likely, this pore space is not accessible for water and consists instead of mineral fluid inclusions. As most of the lithologies of the Passwang Fm are sand-rich, the largest part of such fluid inclusions might be contained in detrital quartz, which can reach, and exceed, 40 wt.% in the few samples for which mineralogy data are available (*cf.* Figure 6-2). An important consequence of this observation is that rock samples of the Passwang Fm (and other similarly composed rocks) have to be gently disintegrated along the grain boundaries and not pulped for aqueous extraction tests in order to avoid contamination by the fluid inclusions.

The large variability in water-loss porosity and clay content indicate that, for the rocks of the Passwang Fm, the assumption of a unique factor for the ratio of water-loss porosity to species-specific porosity (or *geochemical porosity* according to Pearson 1999) is no longer applicable, as this is commonly done for the more homogeneously composed Opalinus Clay (*cf.* Chapter 9). For the rocks of the Passwang Fm, alternative concepts for the derivation of the species-specific porosity have to be applied.

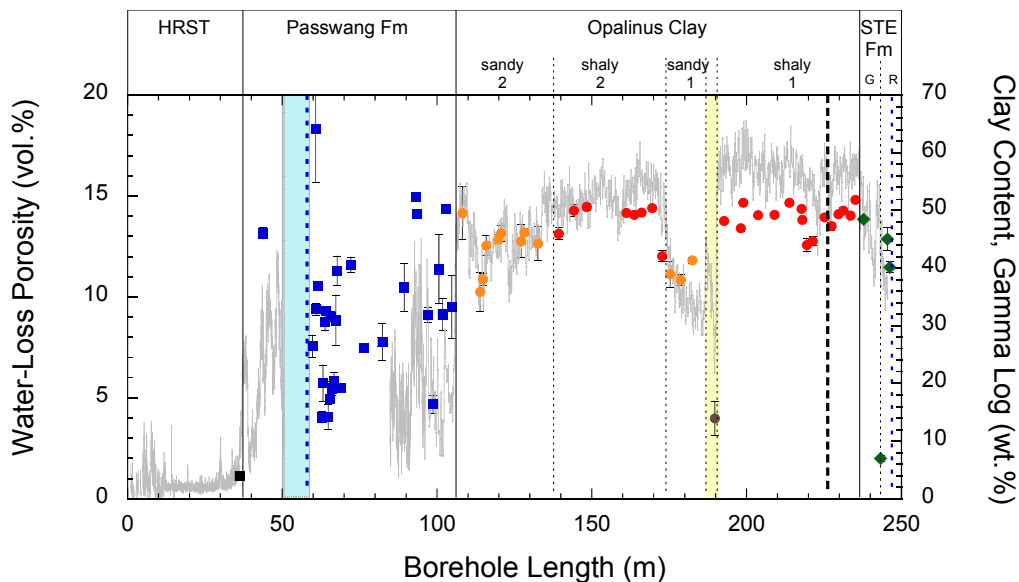
The rocks of the Opalinus Clay display much less variation in water-loss porosity compared to those of the Passwang Fm, covering a range from 10.3 – 14.5 vol.% ( $n=24$ ). The uncertainty for individual samples, and given by the standard deviation of triplicate measurements, is lower when compared to the more heterogeneously composed rock of the Passwang Fm.

There exist, however, differences between the individual facies. Rocks of sandy facies 2 display the largest spread in water-loss porosity from 10.3 – 14.2 vol.% ( $n=9$ ), coinciding with its variable clay content (Figure 7-8). Rocks of sandy facies 1 have low, but rather similar, water-

loss porosity between 10.9 vol.% and 11.8 vol.%. In contrast, rocks of the two shaly facies have similarly high water-loss porosity between 13.1 vol.% and 14.8 vol.% (n=23), except for one sample adjacent to sandy facies 1. The water-loss porosity of this sample is 12.0 vol.%, in agreement with its lower clay content (Figure 7-8). The overall lowest water-loss porosity in the Opalinus Clay of only 4.4 vol.% is recorded for the rock from the carbonate-rich sandy facies.

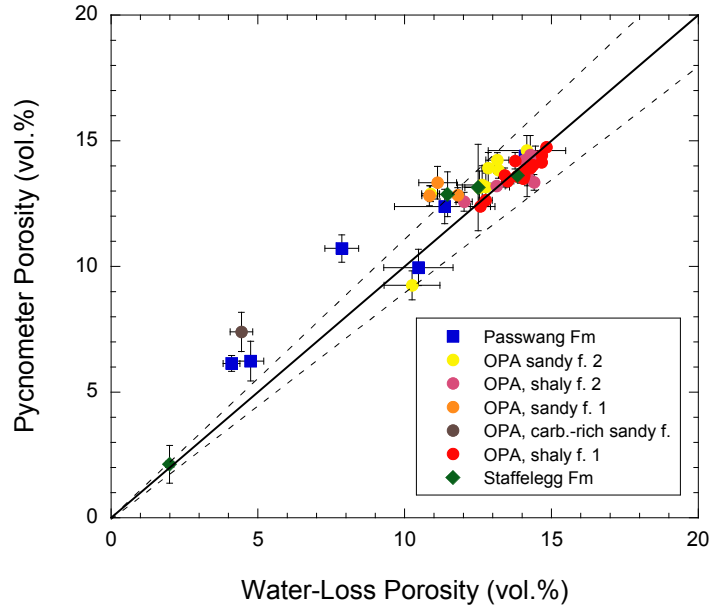
The comparison of water-loss porosity and pycnometer porosity reveals that the two values are identical within the uncertainty band for most of the rocks of shaly facies 1 and 2 of the Opalinus Clay (Figure 7-9). The only exception is the sample with the lowest water-loss porosity adjacent to sandy facies 1. In contrast, most of the rocks of sandy facies 1 and 2 have larger pycnometer porosity compared to the water-loss porosity (Figure 7-9). For sandy facies 1 this difference exceeds 10 %. The difference is most pronounced for the rock from the carbonate-rich sandy facies. This coincides with the higher quartz ( $\pm$  carbonate) contents and the lower clay contents in the rocks of the different sandy facies. As for the rocks of the Passwang Fm, the difference between the two porosity values is attributed to mineral fluid inclusions in the detrital quartz.

The clay-rich rocks of the Staffelegg Fm have water-loss porosity values (11.5 – 13.9 vol.%, n=3) in the range of those of the Opalinus Clay, except for the sandy limestone layer rich in belemnites (BDB1-243.37), which has a very low water-loss porosity of 2 vol.%, in agreement with the mineralogy.



Notes: Error bars indicate the propagated error of  $\phi_{WL}$ . MF: main fault; yellow area: carbonate-rich sandy facies; bright bluish area: packer interval; blue dotted lines: water inflows

**Figure 7-8: Water-loss Porosity,  $\phi_{WL}$ , and the Clay Content Estimated from the Gamma Log as a Function of Depth in Borehole BDB-1 at the Mont Terri URL.**



Notes: Error bars indicate the propagated error of the porosity values; solid line = 1:1 ratio, stippled lines = 10% deviation from 1:1 ratio.

**Figure 7-9: Water-loss Porosity,  $\phi_{WL}$ , Versus the Pycnometer Porosity,  $\phi_{Pyc}$ , of Rock Samples from Borehole BDB-1 at the Mont Terri URL.**

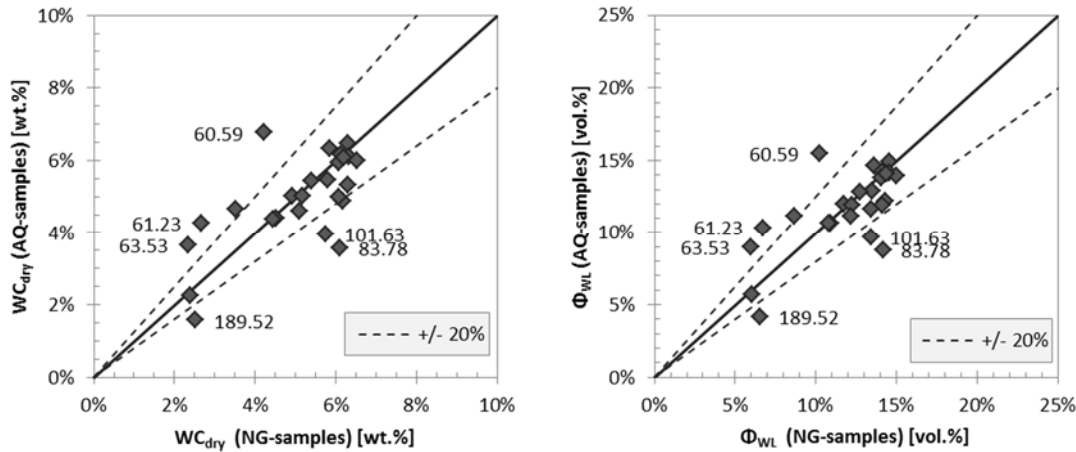
## 7.5 WATER CONTENT AND POROSITY OF POREWATER NOBLE GAS SAMPLES

The gravimetric dry water content ( $WC_{dry}$ ) measured on the noble gas samples varies within a range of 2.3 – 6.5 wt.% (Table 7-2), which corresponds to porewater masses ( $m_{pw}$ ) of 6.85 – 26.18 g per sample.

The dry water content of the noble gas samples was determined as a single measurement on the entire volume of the rock cuboid used for out-gassing and not on multiple, smaller-sized rock pieces, as was done for the AQ porewater samples. Nonetheless, most of the values correlate within about  $\pm 20\%$  with the data from the nearest corresponding standard porewater sample (Figure 7-10).

Samples BDB1-60.59-NG, BDB1-61.23-NG and BDB1-63.53-NG show lower dry water contents than the nearest (distance  $\leq 30$  cm) porewater chemistry (AQ) sample of comparable lithology. It is noted that these NG samples suffered from prolonged exposure times of the central core piece to air, on account of having been the first to be sampled during this campaign (*cf.* Figure 3-4, Appendix A3). Nonetheless, this probably cannot fully explain the observed offset in  $WC_{dry}$ , for which the absolute loss of porewater in the NG samples would have to be between 5 to 8 g, which is far too much to solely have been lost by the additional exposure to air without actively pumping the sample (pumping times are within the normal range, Appendix A3). For sample BDB1-101.63-NG, the corresponding AQ porewater sample's Al-bag had to be resealed after approximately 50 minutes due to leakage. This could potentially have led to a partial desaturation of the AQ sample. Samples BDB1-83.78-NG and BDB1-189.52-NG show no

indication of sampling anomalies for either the NG or AQ sample. For both, however, lithological differences between the two sample types might be a potential reason for the observed differences in  $WC_{dry}$ , with BDB1-189.52-NG being slightly sandier in its lower half and BDB1-83.78-NG being more bio-detritus-rich and over 1 m away from its corresponding AQ sample.

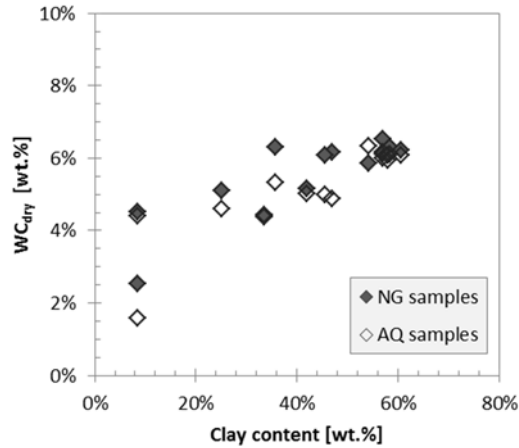


Notes: See text for labelled sample; no error bars given for legibility reasons.

**Figure 7-10: Comparison of Gravimetric Dry Water Content (left) and Water-loss Porosity (right) of Noble Gas (NG) Samples with that of the Adjacent Porewater Chemistry (AQ) Samples.**

As for the porewater chemistry samples, a tentative positive correlation between clay content and water content is observed for the porewater noble gas samples (Figure 7-11; *cf.* Figure 7-3). As a function of depth, the dry water contents show less variance in the shaly sections of the Opalinus clay when compared to the sandy and bioclast-rich sections of the formation, as well as when compared to the lithologically more heterogeneous Passwang Fm (Figure 7-12). The samples from the Opalinus Clay show fairly constant dry water contents between 3.5 to 6.5 wt.-% with distinctly lower values (1.6 and 2.5 wt.-%) in the lower sandy carbonate-rich facies. Similarly low values are observed for the samples at 66.15 and 66.40 m BHL, which are derived from limestone layers.

Grain densities determined on the AQ porewater samples for the Opalinus Clay lie in a narrow range between 2.693 g/cm<sup>3</sup> and 2.724 g/cm<sup>3</sup>, except for the sample from the carbonate-rich sandy facies with 2.766 g/cm<sup>3</sup> (*cf.* Section 7-1). The rocks of the Stafflegg Fm show a larger variability, and the AQ sample next to the NG sample has a comparably low grain density of 2.471 g/cm<sup>3</sup>. For samples where no grain density measurement are available, an average value of 2.70 g/cm<sup>3</sup> is used (*cf.* Table 7-1). As a result of this almost uniform grain density, the water-loss porosity values calculated according to Equation (15) show equal behaviour to the dry water contents in terms of comparability between AQ and NG samples (Figure. 7-10), as well as in terms of their distribution with depth (Figure 7-12). The water-loss porosity of the noble gas samples range from 6.0 to 15.0 wt.-% (Table 7-2).



**Notes:** The clay content for both NG and AQ samples is derived from the AQ sample material. The error in the clay content is  $\pm 10\%$ .

**Figure 7-11: Dry Water Content of the BDB-1 Noble Gas Samples and Adjacent Standard Porewater Samples as a Function of Clay Content.**

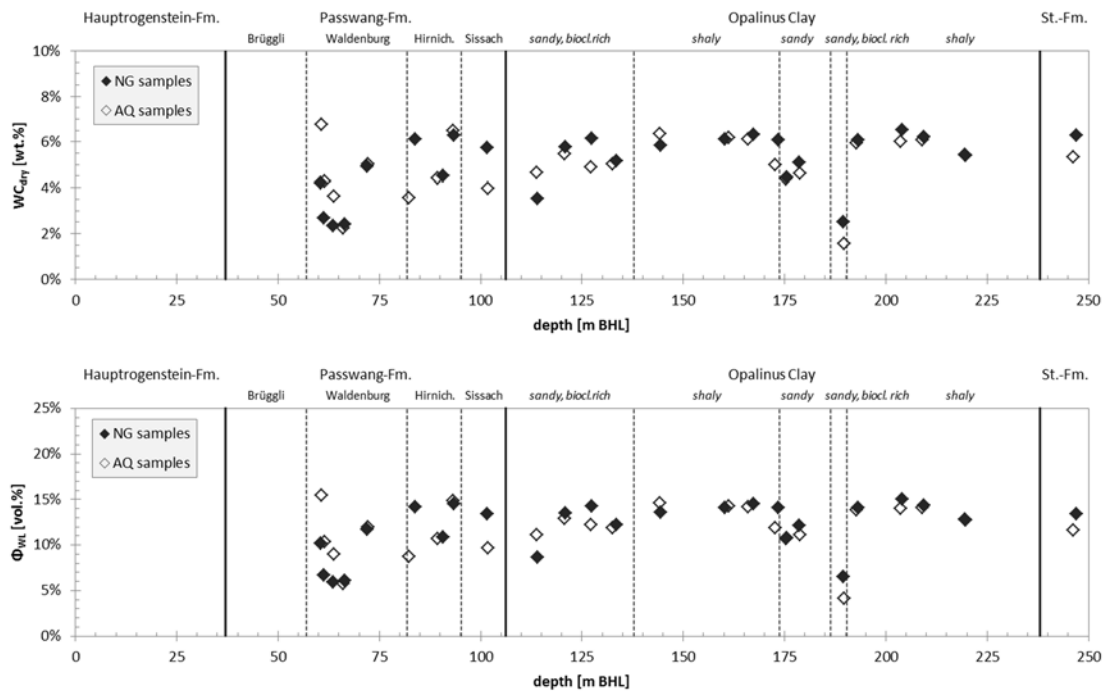


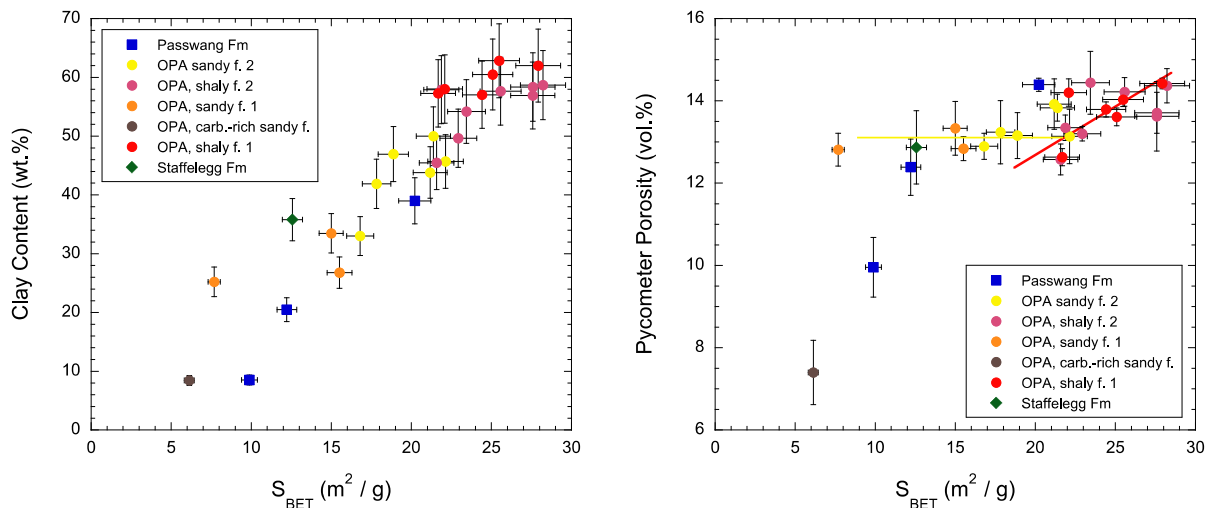
**Figure 7-12: Dry Water Content (top) and Water-loss Porosity (bottom) of the BDB-1 Noble Gas (NG) Samples and Adjacent Standard Porewater Samples as a Function of Depth.**

## 7.6 SPECIFIC SURFACE AREA (N<sub>2</sub>-BET)

The N<sub>2</sub>-BET adsorption technique delivers the specific surface area, which is generally considered as the external surface area between mineral grains – not including the internal (interlayer) surface area of smectite clay minerals.

The N<sub>2</sub>-BET specific surface areas of the rocks encountered in borehole BDB-1 vary between 6.1 m<sup>2</sup>/g and 28.2 m<sup>2</sup>/g (Table 7-1). The lowest value corresponds to the sample BDB1-189.71 of the carbonate-rich facies, whereas the highest values is recorded for sample BDB1-148.31 in shaly facies 2 of the Opalinus Clay.

A positive correlation between N<sub>2</sub>-BET specific surface area and the clay content is established, with the exception of a few samples (Figure 7-13). The correlation is best developed for samples from the Opalinus Clay and the Passwang Fm, for which the proportion of illite plus illite/smectite mixed layers to kaolinite plus chlorite – i.e., the ratio of swelling to non-swelling clay minerals – is very similar and varies only slightly between 1.1 and 1.6 (*cf.* Section 6.2, Figure 6-3). For one sample from the Opalinus Clay sandy facies 1 (BDB1-175.73) and the Staffelegg Fm (BDB1-246.34), this proportion is larger than 4 and for the sample from the Opalinus Clay carbonate-rich facies (BDB1-189.71) it is smaller than 1. These three samples do not align with the positive N<sub>2</sub>-BET specific surface area and the clay content given by the other samples (Figure 7-13). This indicates that the N<sub>2</sub>-BET specific surface area depends not only on the total clay content, but also on the ratio of swelling to non-swelling clay minerals.



Notes: Error bars indicate  $\pm 5\%$  for BET and the propagated error of the porosity values.

**Figure 7-13: BET Specific Surface Areas Versus Clay-mineral Content (left) and Pycnometer Porosity (right) of Rock Samples from Borehole BDB-1 at the Mont Terri URL.**

The correlation between N<sub>2</sub>-BET specific surface area and the clay content appears to level off above total clay contents of more than about 55 wt%. Such high clay contents are only reached

in the shaly facies of the Opalinus Clay. The weak positive correlation observed for these samples between the  $N_2$ -BET specific surface area and the pycnometer porosity (Figure 7-13) suggests that the  $N_2$ -BET surface area of these rocks has an additional contribution from the (very) small-sized non-clay matrix. In contrast, such contribution seems absent in samples of both sandy facies, as indicated by the lack of a correlation between  $N_2$ -BET specific surface area and the pycnometer porosity (Figure 7-13). This might be associated with a larger average grain size and/or stronger degree of diagenetic cementation in the sandy facies.

Figure 7-14 displays examples of  $N_2$  isotherms for the different lithologies of the various formations. Where possible, the sample with the lowest, intermediate and highest  $N_2$ -BET surface area was chosen for display. Corresponding to the differences in  $N_2$ -BET surface area, the  $N_2$  isotherms also show differences in the total volume of  $N_2$  adsorbed and the shape of the typical hysteresis between adsorption and desorption. It can be seen that the degree of hysteresis mainly depends on the total clay content and is smaller at lower clay contents. Below about 25 wt.% total clay content the hysteresis is only weakly pronounced, as shown by samples of the Passwang Fm and the sandy and carbonate-rich sandy facies of the Opalinus Clay. Furthermore, the break in the desorption curve, which in clay-rich rocks typically occurs at  $P_s/P_0$  of about 0.5, seems to disappear. In contrast, the ratio of swelling to non-swelling clay seems to have less influence on the shape of  $N_2$  isotherms than on the total  $N_2$ -BET surface area (see above), as can be seen by comparing the isotherms of the samples from the carbonate-rich sandy facies of the Opalinus Clay and the Staffelegg Fm with those of the sandy and shaly facies of the Opalinus Clay (Figure 7-14).

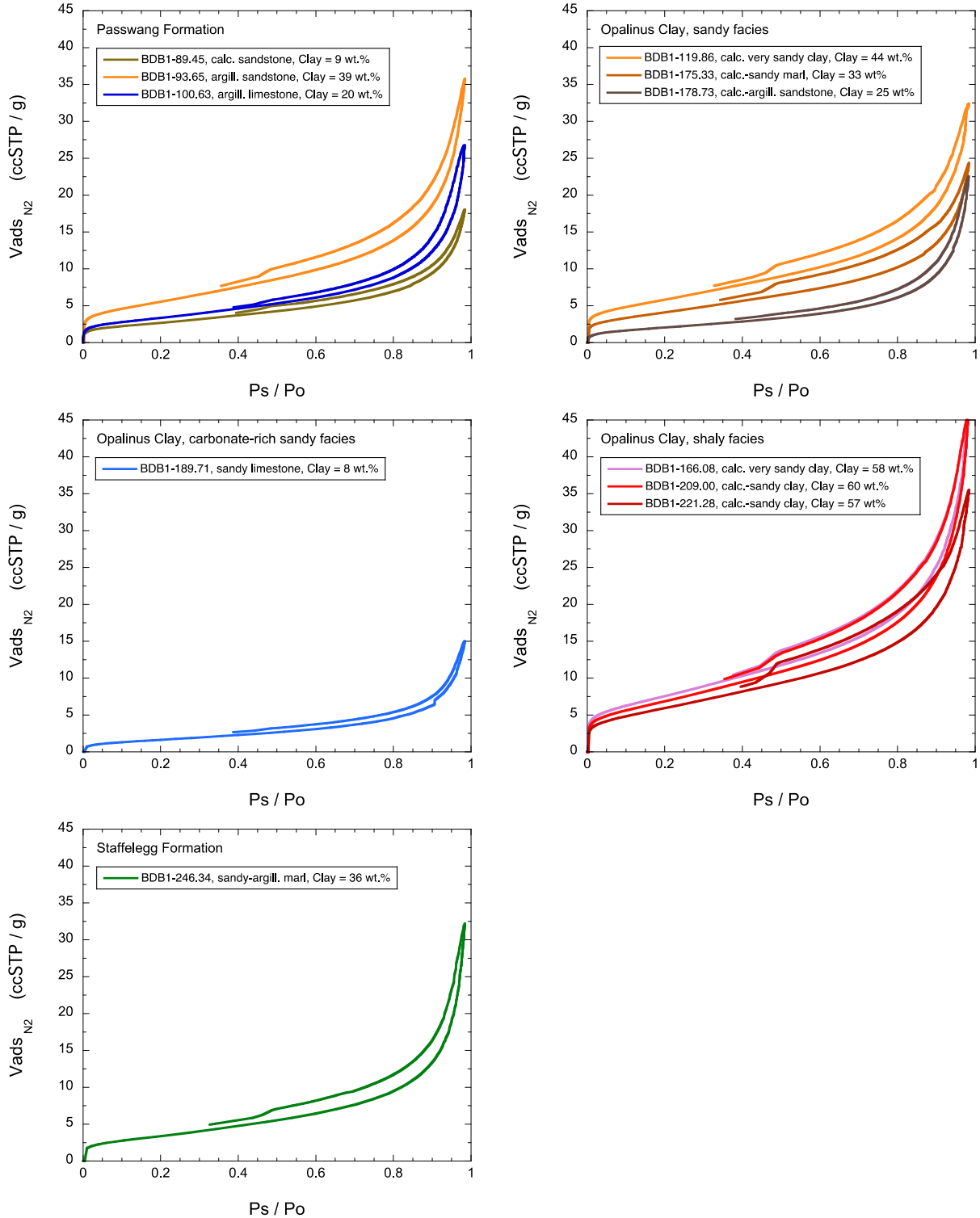


**Figure 7-14: Examples of  $N_2$  Adsorption and Desorption Isotherms of Rock Samples from Borehole BDB-1 at the Mont Terri URL.**

Table 7-1: Petrophysical Data of Porewater Chemistry Samples

Sample	Depth	Stratigraphie	Member / Facies	Lithology	Grain Density (average, n=3) g/cm3	Stdev g/cm3	Bulk Dry Density (calc.) g/cm3	prop. error g/cm3	Bulk Wet Density (average, n=3) g/cm3	Stdev g/cm3	Pycnom. Porosity vol. %	prop. error vol. %	BET (m2/g) m2/g	Total Clay Content wt. %
	m BHL													
BDB1-36.19	36.19	HRST	Brüggli - Mb.	sa lst			2.672	0.0035	2.686	0.0027				
BDB1-43.78	43.78	PAF	Waldenburg - Mb.	sa lst			2.324	0.0058	2.458	0.0054				
BDB1-59.75	59.75	PAF	Waldenburg - Mb.	sa lst	2.816	0.0031	2.515	0.0150	2.597	0.0143	10.72	0.54		
BDB1-60.79	60.79	PAF	Waldenburg - Mb.	sa lst			2.397	0.0354	2.559	0.0152				
BDB1-61.00	61.00	PAF	Waldenburg - Mb.	sa lst			2.452	0.0181	2.547	0.0186				
BDB1-61.52	61.52	PAF	Waldenburg - Mb.	sa lst			2.342	0.0811	2.442	0.0845				
BDB1-62.80	62.80	PAF	Waldenburg - Mb.	lst	2.753	0.0017	2.584	0.0086	2.628	0.0082	6.14	0.32		
BDB1-63.15	63.15	PAF	Waldenburg - Mb.	lst			2.551	0.0155	2.619	0.0128				
BDB1-63.80	63.80	PAF	Waldenburg - Mb.	sa lst			2.461	0.0054	2.550	0.0035				
BDB1-64.11	64.11	PAF	Waldenburg - Mb.	sa lst			2.420	0.0110	2.513	0.0113				
BDB1-64.88	64.88	PAF	Waldenburg - Mb.	lst			2.563	0.0100	2.610	0.0080				
BDB1-65.34	65.34	PAF	Waldenburg - Mb.	lst			2.568	0.0079	2.620	0.0078				
BDB1-65.70	65.70	PAF	Waldenburg - Mb.	sa lst			2.424	0.0081	2.517	0.0079				
BDB1-66.15	66.15	PAF	Waldenburg - Mb.	sa lst			2.541	0.0149	2.598	0.0149				
BDB1-66.70	66.70	PAF	Waldenburg - Mb.	sa lst			2.549	0.0138	2.613	0.0135				
BDB1-67.30	67.30	PAF	Waldenburg - Mb.	sa lst			2.493	0.0181	2.599	0.0126				
BDB1-67.80	67.80	PAF	Waldenburg - Mb.	sa lst			2.356	0.0082	2.477	0.0034				
BDB1-68.90	68.90	PAF	Waldenburg - Mb.	sa lst			2.566	0.0097	2.622	0.0096				
BDB1-72.20	72.20	PAF	Waldenburg - Mb.	sa lst			2.359	0.0319	2.478	0.0332				
BDB1-76.30	76.30	PAF	Himichopf - Mb.	sa lst			2.485	0.0416	2.560	0.0429				
BDB1-82.30	82.30	PAF	Himichopf - Mb.	lst			2.552	0.0161	2.643	0.0133				
BDB1-89.45	89.45	PAF	Himichopf - Mb.	li sst	2.711	0.0011	2.441	0.0196	2.549	0.0156	9.96	0.72	9.9	9
BDB1-93.24	93.24	PAF	Himichopf - Mb.	sa ma			2.284	0.0129	2.432	0.0137				
BDB1-93.65	93.65	PAF	Himichopf - Mb.	sa ma	2.719	0.0008	2.328	0.0043	2.471	0.0041	14.39	0.16	20.2	39
BDB1-97.10	97.10	PAF	Sissach - Mb.	lst			2.498	0.0453	2.587	0.0468				
BDB1-98.68	98.68	PAF	Sissach - Mb.	sa lst	2.750	0.0042	2.579	0.0214	2.621	0.0212	6.24	0.79		
BDB1-100.63	100.63	PAF	Sissach - Mb.	sa ma	2.774	0.0003	2.430	0.0190	2.521	0.0053	12.39	0.68	12.2	20
BDB1-101.80	101.80	PAF	Sissach - Mb.	sa ma			2.502	0.0274	2.602	0.0271				
BDB1-102.93	102.93	PAF	Sissach - Mb.	sa ma			2.242	0.0040	2.382	0.0042				
BDB1-104.78	104.78	PAF	Sissach - Mb.	sa ma			2.357	0.0167	2.461	0.0052				

**Notes:**

Pycnom.Poro = porosity from bulk and grain density; cf. Section 5.2 for derivation of individual values. HRST = Hauptrogenstein, PAF = Passwang Formation, OPA = Opalinus Clay, STF = Stafflegg Formation. Field lithology after Hostettler et al. (2017): li sst = limy sandstone, sa ma = sandy marl, lst = limestone; sa lst = sandy limestone, clst = claystone, silt clst = silty claystone, clst & lst la = claystone with limestone layers, clst & sst la = claystone with sandstone layers, arg ma = argillaceous marl, bit ma = bituminous marl. Shaded samples were used for inter-laboratory comparison, \* samples from Becker (2014).

Table 7-1 (cont.)

Sample	Depth	Stratigraphie	Member / Facies	Lithology	Grain Density (average, n=3) (g/cm <sup>3</sup> )	Stdev (g/cm <sup>3</sup> )	Bulk Dry Density (calc.) (g/cm <sup>3</sup> )	prop. error (g/cm <sup>3</sup> )	Bulk Wet Density (average, n=3) (g/cm <sup>3</sup> )	Stdev (g/cm <sup>3</sup> )	Pycnom. Porosity (vol.%)	prop. error (vol.%)	BET (m <sup>2</sup> /g)  (m <sup>2</sup> /g)	Total Clay Content  (wt.%)
BDB1-108.24	108.24	OPA	sandy facies 2	clst & lst la	2.702	0.0003	2.308	0.0160	2.432	0.0061	14.61	0.59		
BDB1-113.88	113.88	OPA	sandy facies 2	clst & lst la	2.702	0.0003	2.452	0.0155	2.566	0.0123	9.26	0.57		
BDB1-114.80	114.80	OPA	sandy facies 2	clst & lst la	2.710	0.0009	2.361	0.0085	2.463	0.0081	12.90	0.31	16.8	33
BDB1-115.88*	115.88	OPA	sandy facies 2	clst & lst la	2.702	0.0013	2.347	0.0179	2.472	0.0180	13.14	0.66	22.1	46
BDB1-119.86	119.86	OPA	sandy facies 2	clst & lst la	2.700	0.0008	2.324	0.0165	2.450	0.0172	13.92	0.61	21.2	44
BDB1-120.68	120.68	OPA	sandy facies 2	clst & lst la	2.702	0.0003	2.318	0.0079	2.445	0.0068	14.23	0.29		
BDB1-127.15*	127.15	OPA	sandy facies 2	clst & lst la	2.703	0.0013	2.347	0.0150	2.475	0.0130	13.16	0.56	18.9	47
BDB1-128.24	128.24	OPA	sandy facies 2	clst & lst la	2.701	0.0016	2.327	0.0087	2.456	0.0089	13.84	0.33	21.4	50
BDB1-132.63	132.63	OPA	sandy facies 2	clst & lst la	2.699	0.0011	2.341	0.0208	2.459	0.0194	13.24	0.77	17.8	42
BDB1-139.31*	139.31	OPA	shaly facies 2	silt clst	2.709	0.0008	2.352	0.0048	2.483	0.0037	13.20	0.18	22.9	50
BDB1-144.17	144.17	OPA	shaly facies 2	silt clst	2.699	0.0013	2.309	0.0206	2.456	0.0217	14.44	0.77	23.4	54
BDB1-148.31*	148.31	OPA	shaly facies 2	silt clst	2.700	0.0015	2.312	0.0112	2.456	0.0117	14.37	0.42	28.2	59
BDB1-161.18	161.18	OPA	shaly facies 2	silt clst	2.693	0.0027	2.326	0.0226	2.469	0.0240	13.63	0.84	27.6	57
BDB1-163.75*	163.75	OPA	shaly facies 2	silt clst	2.717	0.0010	2.330	0.0094	2.471	0.0098	14.22	0.35	25.6	58
BDB1-166.08	166.08	OPA	shaly facies 2	silt clst	2.693	0.0018	2.323	0.0133	2.466	0.0141	13.71	0.50	27.6	58
BDB1-169.48*	169.48	OPA	shaly facies 2	silt clst	2.705	0.0014	2.344	0.0083	2.489	0.0087	13.35	0.31	21.9	58
BDB1-172.70	172.70	OPA	shaly facies 2	silt clst	2.701	0.0015	2.361	0.0100	2.480	0.0099	12.58	0.37	21.6	45
BDB1-175.33	175.33	OPA	sandy facies 1	clst & sst la	2.724	0.0011	2.360	0.0178	2.464	0.0169	13.33	0.65	15.0	33
BDB1-178.73	178.73	OPA	sandy facies 1	clst & sst la	2.714	0.0005	2.367	0.0108	2.476	0.0110	12.81	0.40	7.7	25
BDB1-182.48*	182.48	Opalinus	sandy facies 1	clst & sst la	2.716	0.0008	2.367	0.0079	2.484	0.0081	12.84	0.29	15.5	27
BDB1-189.71	189.71	OPA	carb.-rich sandy f.	limestone	2.766	0.0008	2.561	0.0216	2.601	0.0215	7.40	0.78	6.1	8
BDB1-192.68	192.68	OPA	shaly facies 1	clst	2.695	0.0025	2.312	0.0086	2.450	0.0091	14.20	0.33	22.1	58
BDB1-198.13	198.13	OPA	shaly facies 1	clst	2.703	0.0007	2.335	0.0080	2.467	0.0082	13.63	0.30		
BDB1-198.93*	198.93	OPA	shaly facies 1	clst	2.700	0.0007	2.310	0.0034	2.457	0.0036	14.43	0.13	27.9	62
BDB1-203.68	203.68	OPA	shaly facies 1	clst	2.708	0.0007	2.334	0.0050	2.475	0.0050	13.79	0.18	24.4	57
BDB1-209.00	209.00	OPA	shaly facies 1	clst	2.699	0.0020	2.331	0.0055	2.473	0.0058	13.61	0.21	25.1	60
BDB1-213.85	213.85	OPA	shaly facies 1	clst	2.703	0.0007	2.321	0.0040	2.470	0.0042	14.14	0.15		
BDB1-217.73*	217.73	OPA	shaly facies 1	clst	2.708	0.0012	2.328	0.0045	2.472	0.0047	14.03	0.17	25.5	63
BDB1-217.98	217.98	OPA	shaly facies 1	clst	2.703	0.0007	2.336	0.0027	2.475	0.0028	13.58	0.10		
BDB1-219.49	219.49	OPA	shaly facies 1	clst	2.703	0.0007	2.368	0.0033	2.497	0.0015	12.39	0.12		
BDB1-221.28	221.28	OPA	shaly facies 1	clst	2.709	0.0018	2.367	0.0054	2.492	0.0047	12.63	0.21	21.7	57
BDB1-225.18	225.18	OPA	shaly facies 1	clst	2.703	0.0007	2.336	0.0072	2.477	0.0076	13.58	0.27		
BDB1-227.43	227.43	OPA	shaly facies 1	clst	2.703	0.0007	2.341	0.0047	2.478	0.0045	13.39	0.18		
BDB1-229.68	229.68	OPA	shaly facies 1	clst	2.703	0.0007	2.329	0.0008	2.471	0.0006	13.84	0.04		
BDB1-231.18	231.18	OPA	shaly facies 1	clst	2.703	0.0007	2.327	0.0091	2.473	0.0096	13.92	0.34		
BDB1-233.63	233.63	OPA	shaly facies 1	clst	2.703	0.0007	2.338	0.0019	2.479	0.0018	13.49	0.08		
BDB1-235.14	235.14	OPA	shaly facies 1	clst	2.703	0.0007	2.304	0.0040	2.455	0.0042	14.75	0.15		
BDB1-237.88	237.88	STF	Gross Wolf Mb.	arg ma	2.703	0.0007	2.335	0.0044	2.474	0.0045	13.61	0.16		
BDB1-243.37	243.37	STF	Gross Wolf Mb.	lst	2.760	0.0028	2.701	0.0205	2.720	0.0206	2.13	0.75		
BDB1-245.54	245.54	STF	Rietheim Mb.	bit ma	2.457	0.0011	2.134	0.0423	2.258	0.0447	13.14	1.72		
BDB1-246.34	246.34	STF	Rietheim Mb.	bit ma	2.471	0.0009	2.153	0.0220	2.268	0.0230	12.87	0.89	12.6	36

Table 7-1 (cont.)

Sample	Depth	Stratigraphie	Member / Facies	Lithology	WC grav,dry (AqEx-S)	prop. error	WC grav,wet (AqEx-S)	prop. error	WL-P (AqEx-S, rel. wet w.)	prop. error	WC grav,dry (average, n=3)	Stdev	WC grav,wet (average, n=3)	Stdev	WC from 18O MassB.	prop. error	WC from 2H MassB.	prop. error	WC IsoEx MassB (average)	prop. error	WL-P (average, n=3)	Stdev
	m BHL				wt.%	wt.%	wt.%	wt.%	vol.%	vol.%	wt.%	wt.%	wt.%	wt.%	wt.%	wt.%	wt.%	wt.%	wt.%	wt.%	vol.%	vol.%
BDB1-36.19	36.19	HRST	Brüggli - Mb.	sa lst	0.516	0.0013	0.514	0.0013	1.40	0.46	0.421	0.086	0.419	0.085							1.14	0.23
BDB1-43.78	43.78	PAF	Waldenburg - Mb.	sa lst	5.765	0.0014	5.451	0.0013	13.68	1.01	5.618	0.127	5.319	0.114	5.797	0.260	5.485	0.298	5.64	0.28	13.36	0.28
BDB1-59.75	59.75	PAF	Waldenburg - Mb.	sa lst	3.264	0.0015	3.161	0.0014	8.42	1.08	3.032	0.238	2.943	0.225	2.831	0.115	2.886	0.145	2.86	0.13	7.86	0.57
BDB1-60.79	60.79	PAF	Waldenburg - Mb.	sa lst	6.768	0.0016	6.339	0.0014	15.69	1.13	8.336	1.462	7.683	1.250	8.638	0.477	8.117	0.536	8.38	0.51	18.59	2.69
BDB1-61.00	61.00	PAF	Waldenburg - Mb.	sa lst	3.881	0.0016	3.736	0.0015	9.64	0.80	3.841	0.130	3.699	0.121	4.180	0.177	4.022	0.208	4.10	0.19	9.55	0.29
BDB1-61.52	61.52	PAF	Waldenburg - Mb.	sa lst	4.275	0.0017	4.099	0.0015	10.52	0.85	4.357	0.077	4.175	0.071	4.489	0.199	4.412	0.240	4.45	0.22	10.70	0.17
BDB1-62.80	62.80	PAF	Waldenburg - Mb.	lst	1.677	0.0016	1.650	0.0015	4.41	0.52	1.556	0.112	1.532	0.109	1.556	0.066	1.569	0.082	1.56	0.07	4.11	0.28
BDB1-63.15	63.15	PAF	Waldenburg - Mb.	lst	2.679	0.0016	2.609	0.0015	6.86	0.65	2.253	0.370	2.203	0.354	2.212	0.088	2.165	0.107	2.19	0.10	5.83	0.90
BDB1-63.80	63.80	PAF	Waldenburg - Mb.	sa lst	3.646	0.0020	3.518	0.0018	9.11	0.82	3.550	0.178	3.428	0.166	4.087	0.176	3.798	0.199	3.94	0.19	8.88	0.42
BDB1-64.11	64.11	PAF	Waldenburg - Mb.	sa lst	3.845	0.0017	3.703	0.0016	9.56	0.81	3.806	0.066	3.667	0.061	4.228	0.177	3.996	0.204	4.11	0.19	9.47	0.15
BDB1-64.88	64.88	PAF	Waldenburg - Mb.	lst	1.835	0.0016	1.802	0.0016	4.80	0.57	1.566	0.245	1.541	0.237	1.550	0.065	1.540	0.080	1.54	0.07	4.12	0.62
BDB1-65.34	65.34	PAF	Waldenburg - Mb.	lst	1.991	0.0016	1.953	0.0016	5.19	0.59	1.923	0.070	1.886	0.068	2.103	0.084	2.080	0.103	2.09	0.09	5.02	0.18
BDB1-65.70	65.70	PAF	Waldenburg - Mb.	sa lst	3.817	0.0016	3.676	0.0015	9.50	0.79	3.676	0.122	3.545	0.113	4.190	0.178	3.731	0.191	3.96	0.18	9.18	0.28
BDB1-66.15	66.15	PAF	Waldenburg - Mb.	sa lst	2.247	0.0015	2.198	0.0014	5.82	0.60	2.141	0.137	2.096	0.131	2.302	0.090	2.259	0.110	2.28	0.10	5.56	0.34
BDB1-66.70	66.70	PAF	Waldenburg - Mb.	sa lst	2.494	0.0015	2.434	0.0014	6.42	0.62	2.297	0.172	2.245	0.164	2.372	0.094	2.243	0.111	2.31	0.10	5.94	0.42
BDB1-67.30	67.30	PAF	Waldenburg - Mb.	sa lst	4.246	0.0015	4.073	0.0014	10.46	0.84	3.599	0.561	3.472	0.521	3.590	0.144	3.527	0.174	3.56	0.16	8.99	1.27
BDB1-67.80	67.80	PAF	Waldenburg - Mb.	sa lst	5.111	0.0018	4.863	0.0016	12.32	0.96	4.728	0.337	4.514	0.307	4.976	0.222	4.794	0.261	4.88	0.24	11.49	0.73
BDB1-68.90	68.90	PAF	Waldenburg - Mb.	sa lst	2.190	0.0016	2.143	0.0015	5.68	0.60	2.153	0.095	2.107	0.091	2.358	0.093	2.307	0.113	2.33	0.10	5.59	0.23
BDB1-72.20	72.20	PAF	Waldenburg - Mb.	sa lst	5.030	0.0016	4.789	0.0014	12.15	0.93	4.854	0.185	4.629	0.169	5.294	0.235	4.922	0.264	5.11	0.25	11.77	0.40
BDB1-76.30	76.30	PAF	Himichopf - Mb.	sa lst	3.001	0.0015	2.913	0.0014	7.62	0.68	2.987	0.061	2.900	0.057	3.285	0.131	3.087	0.152	3.19	0.14	7.59	0.14
BDB1-82.30	82.30	PAF	Himichopf - Mb.	lst	3.564	0.0016	3.441	0.0015	8.93	0.76	3.119	0.395	3.023	0.371	3.485	0.141	3.130	0.155	3.31	0.15	7.89	0.92
BDB1-89.45	89.45	PAF	Himichopf - Mb.	li sst	4.416	0.0016	4.229	0.0014	10.69	0.58	4.320	0.540	4.140	0.497	4.784	0.201	4.733	0.245	4.76	0.22	10.47	1.18
BDB1-93.24	93.24	PAF	Himichopf - Mb.	sa ma	6.479	0.0016	6.085	0.0014	15.12	1.10	6.519	0.051	6.120	0.045	7.173	0.349	6.543	0.378	6.86	0.36	15.18	0.09
BDB1-93.65	93.65	PAF	Himichopf - Mb.	sa ma	6.140	0.0017	5.785	0.0015	14.31	0.57	6.047	0.086	5.702	0.077	6.424	0.303	6.011	0.341	6.22	0.32	14.10	0.19
BDB1-97.10	97.10	PAF	Sissach - Mb.	lst	3.576	0.0015	3.453	0.0014	8.95	0.75	3.707	0.156	3.574	0.145	3.539	0.145	3.615	0.184	3.58	0.16	9.25	0.36
BDB1-98.68	98.68	PAF	Sissach - Mb.	sa lst	1.652	0.0015	1.625	0.0014	4.35	0.88	1.818	0.181	1.785	0.174	2.281	0.087	2.134	0.102	2.21	0.09	4.76	0.45
BDB1-100.63	100.63	PAF	Sissach - Mb.	sa ma	3.738	0.0013	3.604	0.0012	9.40	0.33	4.643	0.784	4.433	0.719	5.895	0.256	5.170	0.268	5.53	0.26	11.37	1.71
BDB1-101.80	101.80	PAF	Sissach - Mb.	sa ma	3.967	0.0015	3.816	0.0014	9.84	0.80	3.723	0.346	3.589	0.321	3.655	0.144	3.477	0.168	3.57	0.16	9.28	0.78
BDB1-102.93	102.93	PAF	Sissach - Mb.	sa ma	6.243	0.0014	5.876	0.0013	14.65	1.07	6.217	0.042	5.853	0.037	5.851	0.258	5.851	0.319	5.85	0.29	14.59	0.09
BDB1-104.78	104.78	PAF	Sissach - Mb.	sa ma	4.394	0.0014	4.209	0.0013	10.78	0.84	3.898	0.702	3.749	0.651	3.649	0.145	3.438	0.168	3.54	0.16	9.66	1.58

**Notes:**

WC = water content; MassB. = mass balance; WC<sub>isoEx</sub> = average of water content derived by isotope mass balance: cf. Section 5.2 for derivation of individual values. HRST = Hauptrogenstein, PAF = Passwang Formation, OPA = Opalinus Clay, STF = Staffelegg Formation. Field lithology after Hostettler et al. (2017): li sst = limy sandstone, sa ma = sandy marl, lst = limestone; sa lst = sandy limestone, clst = claystone, silt clst = silty claystone, clst & lst la = claystone with limestone layers, clst & sst la = claystone with sandstone layers, arg ma = argillaceous marl, bit ma = bituminous marl. Shaded samples were used for inter-laboratory comparison, \* samples from Becker (2014).

Table 7-1 (cont.)

Sample	Depth	Stratigraphie	Member / Facies	Lithology	WC	prop.	WC	prop.	WL-P	prop.	WC	Stdev	WC	Stdev	WC from	prop.	WC from	prop.	WC IsoEx	prop.	WL-P	Stdev
					grav,dry (AqEx-S)	error	grav,wet (AqEx-S)	error	(AqEx-S, rel. wet w.)	error	grav,dry (average, n=3)	wt.%	grav,wet (average, n=3)	wt.%	18O MassB.	error	2H MassB.	error	MassB (average)	error	(average, n=3)	error
BDB1-108.24	108.24	OPA	sandy facies 2	clst & lst la	5.377	0.0013	5.102	0.0011	12.69	0.33	6.145	0.686	5.787	0.611	7.280	0.348	6.959	0.404	7.12	0.38	14.16	1.32
BDB1-113.88	113.88	OPA	sandy facies 2	clst & lst la	4.645	0.0015	4.439	0.0014	11.15	0.37	4.244	0.429	4.070	0.395	4.008	0.162	3.830	0.190	3.92	0.18	10.26	0.95
BDB1-114.80	114.80	OPA	sandy facies 2	clst & lst la	4.348	0.0014	4.167	0.0013	10.54	0.49	4.519	0.151	4.324	0.138	5.160	0.223	4.720	0.247	4.94	0.23	10.88	0.30
BDB1-115.88*	115.88	OPA	sandy facies 2	clst & lst la							5.311	0.240	5.043	0.216							12.55	0.50
BDB1-119.86	119.86	OPA	sandy facies 2	clst & lst la	5.430	0.0014	5.150	0.0013	12.79	0.51	5.484	0.113	5.199	0.101	5.563	0.245	5.447	0.296	5.51	0.27	12.85	0.22
BDB1-120.68	120.68	OPA	sandy facies 2	clst & lst la	5.473	0.0021	5.189	0.0018	12.89	0.48	5.632	0.207	5.332	0.186	5.916	0.270	5.560	0.308	5.74	0.29	13.16	0.39
BDB1-127.15*	127.15	OPA	sandy facies 2	clst & lst la							5.138	0.390	5.138	0.351							12.77	0.80
BDB1-128.24	128.24	OPA	sandy facies 2	clst & lst la	5.556	0.0014	5.263	0.0012	13.05	0.85	5.650	0.097	5.348	0.087	5.980	0.272	5.715	0.317	5.85	0.29	13.20	0.17
BDB1-132.63	132.63	OPA	sandy facies 2	clst & lst la	5.014	0.0015	4.774	0.0013	11.92	0.60	5.382	0.423	5.106	0.380	5.686	0.257	5.329	0.292	5.51	0.27	12.64	0.84
BDB1-139.31*	139.31	OPA	shaly facies 2	silt clst							5.284	0.146	5.284	0.131							13.13	0.30
BDB1-144.17	144.17	OPA	shaly facies 2	silt clst	6.340	0.0015	5.962	0.0013	14.61	0.78	6.196	0.143	5.834	0.127	6.482	0.303	6.382	0.368	6.43	0.34	14.28	0.31
BDB1-148.31*	148.31	OPA	shaly facies 2	silt clst							5.891	0.086	5.891	0.076							14.46	0.17
BDB1-161.18	161.18	OPA	shaly facies 2	silt clst	6.175	0.0015	5.815	0.0013	14.26	1.47	6.159	0.059	5.801	0.052	6.337	0.287	6.393	0.360	6.36	0.32	14.17	0.14
BDB1-163.75*	163.75	OPA	shaly facies 2	silt clst							5.686	0.069	5.686	0.061							14.07	0.14
BDB1-166.08	166.08	OPA	shaly facies 2	silt clst	6.120	0.0014	5.767	0.0012	14.15	1.00	6.162	0.067	5.804	0.059	6.180	0.294	6.250	0.370	6.21	0.33	14.18	0.11
BDB1-169.48*	169.48	OPA	shaly facies 2	silt clst							5.860	0.063	5.860	0.056							14.41	0.12
BDB1-172.70	172.70	OPA	shaly facies 2	silt clst	5.000	0.0015	4.762	0.0013	11.90	0.76	5.080	0.141	4.835	0.128	5.513	0.242	5.371	0.289	5.44	0.27	12.03	0.28
BDB1-175.33	175.33	OPA	sandy facies 1	clst & sst la	4.384	0.0013	4.200	0.0012	10.67	0.54	4.611	0.321	4.407	0.293	5.313	0.238	5.137	0.282	5.22	0.26	11.12	0.65
BDB1-178.73	178.73	OPA	sandy facies 1	clst & sst la	4.613	0.0015	4.410	0.0014	11.13	0.41	4.495	0.109	4.302	0.100	4.794	0.188	4.554	0.219	4.67	0.20	10.85	0.26
BDB1-182.48*	182.48	Opalinus	sandy facies 1	clst & sst la							4.700	0.069	4.700	0.063							11.81	0.15
BDB1-189.71	189.71	OPA	carb.-rich sandy f.	limestone	1.573	0.0012	1.548	0.0012	4.17	0.35	1.683	0.156	1.655	0.151	2.051	0.083	1.971	0.100	2.01	0.09	4.44	0.39
BDB1-192.68	192.68	OPA	shaly facies 1	clst	5.951	0.0014	5.617	0.0012	13.82	1.33	5.954	0.003	5.620	0.003	6.146	0.279	6.006	0.335	6.08	0.31	13.77	0.05
BDB1-198.13	198.13	OPA	shaly facies 1	clst	5.680	0.0015	5.375	0.0013	13.31	0.50	5.762	0.091	5.448	0.081	6.871	0.333	6.133	0.351	6.50	0.34	13.41	0.14
BDB1-198.93*	198.93	OPA	shaly facies 1	clst							5.987	0.012	5.987	0.011							14.67	0.02
BDB1-203.68	203.68	OPA	shaly facies 1	clst	6.000	0.0014	5.660	0.0013	13.98	0.49	6.065	0.073	5.718	0.065	7.126	0.360	6.359	0.378	6.74	0.37	14.05	0.11
BDB1-209.00	209.00	OPA	shaly facies 1	clst	6.085	0.0014	5.736	0.0012	14.10	1.09	6.099	0.023	5.748	0.020	6.489	0.307	6.250	0.361	6.37	0.33	14.07	0.05
BDB1-213.85	213.85	OPA	shaly facies 1	clst	6.415	0.0015	6.029	0.0013	14.78	0.52	6.395	0.032	6.010	0.029	6.639	0.311	6.442	0.369	6.54	0.34	14.67	0.11
BDB1-217.73*	217.73	OPA	shaly facies 1	clst							5.836	0.021	5.836	0.018							14.37	0.04
BDB1-217.98	217.98	OPA	shaly facies 1	clst	5.949	0.0014	5.615	0.0012	13.85	0.49	5.969	0.023	5.633	0.020	6.323	0.297	6.146	0.354	6.23	0.33	13.82	0.04
BDB1-219.49	219.49	OPA	shaly facies 1	clst	5.443	0.0014	5.162	0.0012	12.83	0.48	5.349	0.133	4.993	0.120	5.859	0.274	5.657	0.323	5.76	0.30	12.58	0.34
BDB1-221.28	221.28	OPA	shaly facies 1	clst	5.281	0.0014	5.016	0.0013	12.52	0.91	5.428	0.135	5.148	0.121	5.931	0.271	5.609	0.311	5.77	0.29	12.76	0.23
BDB1-225.18	225.18	OPA	shaly facies 1	clst	6.045	0.0014	5.700	0.0013	14.05	0.51	6.031	0.013	5.688	0.011	6.230	0.272	6.128	0.329	6.18	0.30	13.95	0.09
BDB1-227.43	227.43	OPA	shaly facies 1	clst	5.845	0.0015	5.523	0.0013	13.64	0.50	5.817	0.089	5.497	0.079	6.284	0.301	6.065	0.355	6.17	0.33	13.51	0.21
BDB1-229.68	229.68	OPA	shaly facies 1	clst	6.084	0.0013	5.735	0.0012	14.12	0.49	6.112	0.027	5.760	0.024	6.593	0.313	6.512	0.381	6.55	0.35	14.10	0.03
BDB1-231.18	231.18	OPA	shaly facies 1	clst	6.269	0.0014	5.899	0.0012	14.49	0.51	6.203	0.058	5.840	0.051	7.584	0.383	6.594	0.388	7.09	0.39	14.29	0.17
BDB1-233.63	233.63	OPA	shaly facies 1	clst	6.029	0.0013	5.686	0.0012	14.01	0.49	6.078	0.045	5.730	0.040	6.643	0.301	6.343	0.349	6.49	0.33	14.04	0.04
BDB1-235.14	235.14	OPA	shaly facies 1	clst	6.512	0.0014	6.113	0.0013	14.97	0.52	6.475	0.031	6.082	0.028	7.455	0.371	6.873	0.408	7.16	0.39	14.83	0.12
BDB1-237.88	237.88	STF	Gross Wolf Mb.	arg ma	5.941	0.0014	5.608	0.0013	13.84	0.50	5.978	0.055	5.641	0.049	6.670	0.319	6.140	0.352	6.40	0.34	13.85	0.09
BDB1-243.37	243.37	STF	Gross Wolf Mb.	lst	0.699	0.0016	0.694	0.0016	1.89	0.52	0.746	0.065	0.740	0.064	1.116	0.062	0.997	0.073	1.06	0.07	2.00	0.14
BDB1-245.54	245.54	STF	Rietheim Mb.	bit ma	5.795	0.0013	5.478	0.0012	12.47	0.64	5.768	0.024	5.453	0.022	6.754	0.313	6.284	0.351	6.52	0.33	12.51	0.04
BDB1-246.34	246.34	STF	Rietheim Mb.	bit ma	5.334	0.0014	5.064	0.0012	11.64	0.53	5.258	0.133	4.995	0.120	5.874	0.245	5.801	0.299	5.84	0.27	11.46	0.27

**Table 7-2: Petrophysical Data of Noble Gas Samples**

Sample	Depth	Stratigraphie	Member / Facies	Lithology	Grain Density (average, n=3) g/cm <sup>3</sup>	Stdev	m <sub>rock wet</sub> g	m <sub>pw</sub> g	WC dry wt. %	WL-P vol. %
					estimated uncertainty (1σ)	< 0.003	< 0.05	< 0.06	< 0.02	< 0.05
BDB1-60.59-NG	60.59	PAF	Waldenburg - Mb.	sa lst	2.7		321.36	12.98	4.21	10.21
BDB1-61.23-NG	61.23	PAF	Waldenburg - Mb.	sa lst	2.7		337.18	8.79	2.68	6.74
BDB1-63.53-NG	63.53	PAF	Waldenburg - Mb.	sa lst	2.7		395.82	9.08	2.35	5.96
BDB1-66.40-NG	66.4	PAF	Waldenburg - Mb.	sa lst	2.7		293.30	6.85	2.39	6.07
BDB1-72.05-NG	72.05	PAF	Waldenburg - Mb.	sa lst	2.7		328.98	15.42	4.92	11.72
BDB1-83.78-NG	83.78	PAF	Waldenburg - Mb.	mst	2.7		340.07	19.58	6.11	14.16
BDB1-90.68-NG	90.68	PAF	Himichopf - Mb.	li sst	2.711	0.0011	390.12	16.84	4.51	10.89
BDB1-93.40-NG	93.4	PAF	Himichopf - Mb.	sa ma	2.7		377.00	22.33	6.3	14.53
BDB1-101.63-NG	101.63	PAF	Sissach - Mb.	sa ma	2.7		428.52	23.32	5.76	13.45
BDB1-114.08-NG	114.08	OPA	sandy facies 2	clst & lst la	2.702	0.0003	355.27	12.06	3.51	8.66
BDB1-120.86-NG	120.86	OPA	sandy facies 2	clst & lst la	2.702	0.0003	375.89	20.56	5.79	13.51
BDB1-127.33-NG	127.33	OPA	sandy facies 2	clst & lst la	2.703	0.0013	353.46	20.52	6.16	14.28
BDB1-133.46-NG	133.46	OPA	sandy facies 2	clst & lst la	2.699	0.0011	317.75	15.59	5.16	12.22
BDB1-144.49-NG	144.49	OPA	shaly facies 2	silt clst	2.699	0.0013	341.22	18.85	5.85	13.63
BDB1-160.25-NG	160.25	OPA	shaly facies 2	silt clst	2.693	0.0027	317.00	18.27	6.11	14.14
BDB1-167.38-NG	167.38	OPA	shaly facies 2	silt clst	2.693	0.0018	374.92	22.26	6.31	14.53
BDB1-173.47-NG	173.47	OPA	shaly facies 2	silt clst	2.701	0.0015	337.37	19.30	6.07	14.08
BDB1-175.53-NG	175.53	OPA	sandy facies 1	clst & sst la	2.724	0.0011	388.11	16.51	4.44	10.79
BDB1-178.53-NG	178.53	OPA	sandy facies 1	clst & sst la	2.714	0.0005	411.46	19.95	5.1	12.15
BDB1-189.52-NG	189.52	OPA	carb.-rich sandy f.	lst	2.766	0.0008	434.86	10.70	2.52	6.52
BDB1-193.13-NG	193.13	OPA	shaly facies 1	clst	2.695	0.0025	407.65	23.36	6.08	14.08
BDB1-204.09-NG	204.09	OPA	shaly facies 1	clst	2.708	0.0007	427.60	26.18	6.52	15.01
BDB1-209.37-NG	209.37	OPA	shaly facies 1	clst	2.699	0.0020	351.33	20.54	6.21	14.35
BDB1-219.66-NG	219.66	OPA	shaly facies 1	clst	2.703	0.0007	416.38	21.36	5.41	12.74
BDB1-246.99-NG	246.99	STF	Rietheim Mb.	bit ma	2.471	0.0009	310.92	18.40	6.29	13.45

**Notes:**

Grain density from neighbouring porewater sample where available, otherwise assumed; cf. Section 5.2 for derivation of individual values. PAF = Passwang Formation, OPA = Opalinus Clay, STF = Staffelegg Formation. Field lithology after Hostettler et al. (2017): sa lst = sandy limestone, li sst = limy sandstone, sa ma = sandy marl, mst = marlstone, lst = limestone; clst = claystone, silt clst = silty claystone, clst & lst la = claystone with limestone layers, clst & sst la = claystone with sandstone layers, arg ma = argillaceous marl, bit ma = bituminous marl. Shaded samples were used for inter-laboratory comparison.

## 8. AQUEOUS EXTRACTION DATA

During aqueous extraction, a known mass of rock, including its porewater, is immersed in a known volume of ultra-pure water. The induced dilution of the porewater triggers mineral dissolution and cation exchange reactions – as the diluted porewater attempts to re-equilibrate with the new conditions. The type and degree of such reactions depends on the original porewater composition, mineral saturation states and reaction kinetics, and whether the extraction is performed under closed or open conditions with respect to the atmosphere. Thus, the type and degree of induced reactions depend on the rock mineralogy, experimental duration and solid:liquid (S:L) ratio of the extraction, in addition to the possibility of the rock and the suspension to exchange with atmospheric O<sub>2</sub> and CO<sub>2</sub> during extraction.

Conservative behaviour of a solute during extraction may be indicated by a linear correlation of solute concentrations with variable S:L ratios and will have a zero-concentration intercept at a S:L ratio of 0 (infinite dilution). Such linearity is a necessary, but not sufficient proof of conservative behaviour, as fast reaction kinetics with respect to extraction time will also result in such a linear behaviour. Minerals with such fast reaction kinetics will attain equilibrium with the extract solution. In turn, a linear behaviour may also be indicated if the solute inventory is much larger compared to the addition brought to the extract solution by mineral dissolution and/or exchange reactions. Non-linearity will become evident for slow dissolution reactions with respect to the duration of the extraction and will result in variable under-saturation with respect to the specific mineral phase.

In the rocks of the Passwang Fm, Opalinus Clay and Staffelegg Fm, the minerals involved in reactions during aqueous extraction are carbonates, sulphides and clays. Halides are not known to occur, so the Cl<sup>-</sup> and Br<sup>-</sup> in the aqueous extract solutions can be considered as conservative and originate exclusively from the original porewater, as shown previously (e.g., Pearson et al. 2003). Dissolution of carbonate and sulphide minerals, and cation exchange reactions, inevitably occur during aqueous extraction. The extract conditions for the experiments were chosen in order to assure certain controls over such reactions and to minimise others. This includes a reaction time sufficient to reach calcite equilibrium, and controlled atmospheric conditions to suppress oxidation of sulphides (*cf.* Section 5.3 and below). Cation exchange and sorption reactions cannot be suppressed and the dilution of the porewater results in a preference of divalent cations on the clay interlayers and surfaces, and displacement of the monovalent cations into the extract solution. As these reactions involve all major cations, they are strongly linked with mineral dissolution reactions.

Sulphate minerals, such as gypsum and celestite, are other candidates that would dissolve during aqueous extraction. If present in large enough amounts (i.e., on the order of one weight per cent), such minerals would potentially reach equilibrium during extraction at a S:L ratio of 1:1. In the rocks of the Passwang Fm, Opalinus Clay and Staffelegg Fm at Mont Terri, such sulphate minerals are known to occur in veins, nodules (e.g., Waber and Schürch 2000; Gaucher et al. 2003; de Haller et al. 2014) and the excavation disturbed zone (e.g., Gaucher et al. 2003; Nussbaum et al. 2011). In the undisturbed rock matrix, sulphate mineral phases have not been unequivocally confirmed, although Gaucher et al. (2003) claim to have observed a celestite-type mineral phase based on normative calculations from chemical analysis of a sample of the Opalinus Clay shaly facies. The same authors further indicate the presence of native sulphur in the shaly facies of the Opalinus Clay. The occurrence of native sulphur has not been confirmed by later studies. In turn, Lerouge et al. (2014) found traces of sulphate

phases with variable Ba-Sr ratios, including the pure end-member celestite in one out of fourteen samples from the BDB-1 borehole investigated in great detail for mineralogical composition. These sulphate phases were observed by optical and scanning electron microscopy in a sample of sandy facies 1 adjacent to the carbonate-rich sandy facies. The quantity of the phases was, however, too low to be detected by XRD. Lerouge et al. (2014) describe these Ba-Sr sulphates as having “precipitated later than sparite, and probably dolomite/ankerite, in some large residual porosity of the rock maintained in silty zones lately”. In all other samples it appears that Sr in the rock is almost entirely associated with the carbonate minerals and detrital feldspar as shown by Lerouge et al. (2010). Nevertheless, the presence or absence of diagenetic sulphate minerals in the Opalinus Clay at Mont Terri in large enough amounts to play a role in the control of the porewater composition is still a matter of debate (e.g., Pearson et al. 2003, 2011).

In the present study, aqueous extractions were only performed at S:L ratio of 1:1 and no evidence can be gained for the conservative or non-conservative behaviour of individual ions. From a detailed study about different sampling and preparation techniques, combined with different extraction conditions and conducted in five different laboratories, it is known that  $\text{Cl}^-$  and  $\text{Br}^-$  in the Opalinus Clay at Mont Terri behave conservative during aqueous extraction (Waber et al. 2003). A linear relationship with an intercept at zero was also obtained for  $\text{SO}_4^{2-}$  if the extraction was conducted on originally saturated rock material quickly after drilling and using degassed water. Based on differences in the  $\text{SO}_4/\text{Cl}$  ratio between aqueous extract solutions and borehole water collected over months from packer intervals in near-by boreholes, Waber et al. (2003a) did not attest  $\text{SO}_4^{2-}$  a fully conservative behaviour during aqueous extraction. However, these authors concluded that in the Opalinus Clay and underlying Staffelegg Fm (Liassic rocks) the largest proportion of  $\text{SO}_4^{2-}$  in the extract solution must have been derived from the original porewater based on the spatial distribution of  $\text{SO}_4^{2-}$  concentrations in equally prepared aqueous extract solutions.

Based on these findings the present aqueous extraction tests were performed on originally saturated core material within one to three weeks after recovery under controlled atmosphere in a glovebox and, using degassed water, thus minimising the exposure to atmospheric  $\text{O}_2$  and  $\text{CO}_2$  (cf. Section 5.3). Combined with the high spatial resolution of samples across the different lithologies, this allows a more detailed interpretation of aqueous extraction data.

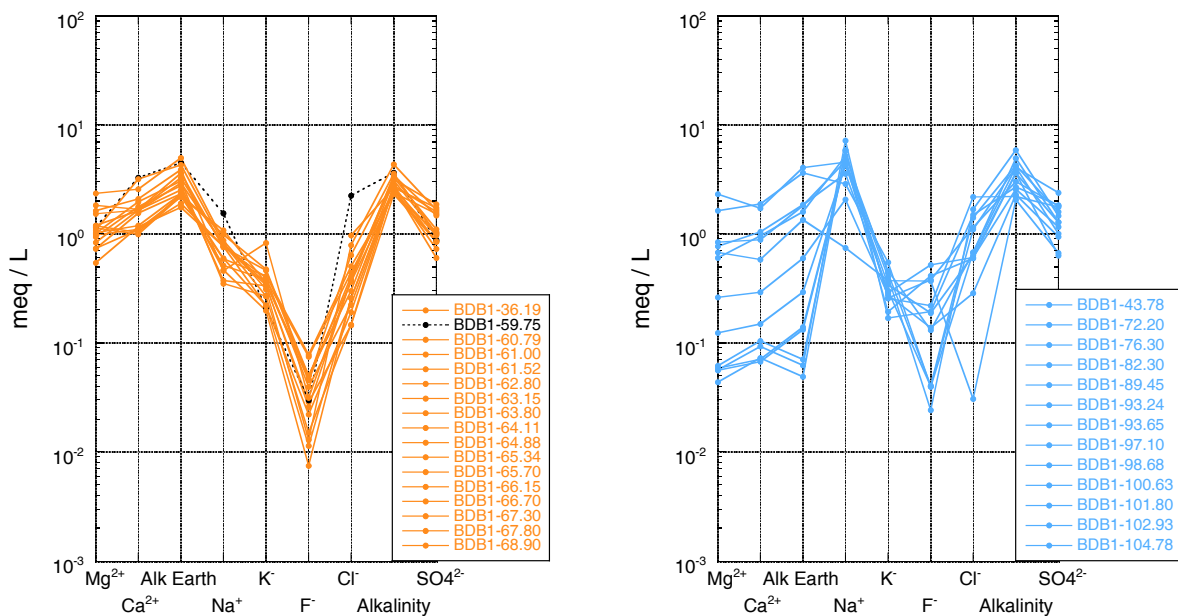
## 8.1 PASSWANG FORMATION ROCKS

Aqueous extract solutions of the Passwang Fm are generally of a Ca-Mg-HCO<sub>3</sub>-SO<sub>4</sub> chemical type, with total dissolved solids (TDS) of 221 – 487 mg/L (n = 17) from 43 – 70 m BHL and of a Na-HCO<sub>3</sub>-SO<sub>4</sub> type with TDS of 267 – 673 mg/L (n = 12) from 70 – 105 m BHL.

In the upper part of the Passwang Fm, dissolved ion concentrations in aqueous extract solutions are rather similar, and differ only within about a factor of five, except for  $\text{F}^-$  and  $\text{Cl}^-$  which vary by almost one order of magnitude (Figure 8-1, Appendix B2). Concentrations of the alkaline earth elements dominate over those of the alkaline elements, and  $\text{HCO}_3^-$  is the most abundant anion followed by  $\text{SO}_4^{2-}$  and  $\text{Cl}^-$ . At measured pH values of 7.74 – 8.39, the extract solutions are slightly under-saturated to over-saturated with respect to calcite ( $\text{SI}_{\text{calcite}} = -0.12$  to  $+0.60$ ) at corresponding log partial pressures of  $\text{CO}_2$  of  $-3.34$  to  $-2.46$ , i.e., above that of air (log  $\text{pCO}_2$  ca.  $-3.5$ ). This indicates that the extract solutions exchanged with air after separation from the rock material by centrifugation, during the transfer of the solutions to the pH and alkalinity measurement devices. Adjusted for calcite saturation, the extract solutions have pH values of

7.39 – 8.34 at corresponding log pCO<sub>2</sub> values of –3.29 to –2.06. At these conditions, the extract solution is under-saturated with respect to disordered dolomite, gypsum, celestite, strontianite and fluorite, except for a few samples that are close to, or at, equilibrium with strontianite and fluorite (Appendix B3).

In the absence of any mineralogy and geophysical log data, it is difficult to judge how the solute concentrations in the extract solutions may depend on the clay content of the samples. The dominant reactions during extraction are carbonate and possibly minor sulphide mineral dissolution, and less cation exchange reactions. This is supported by the large variation in molar Na/Cl and SO<sub>4</sub>/Cl ratios (0.7–24.2 and 0.2–10.9, respectively) compared to the small range in the ratios of (Ca+Mg)/alkalinity (0.5–1.5) and the independence of these ratios relative to the highly variable water content of the samples (cf. Figure 7-4).



**Notes:** Sample BDB1-59.75 (left, black) represents the first sample collected after the break between Phase 1 and 2 in the drilling and displays clear evaporation effects.

**Figure 8-1: Schoeller-Diagram of Aqueous Extract Solutions from the Upper (43–70 m BHL, left) and Lower (70–105 m BHL, right) Part of the Passwang Fm.**

In the lower part of the Passwang Fm dissolved ion concentrations display a large scatter (more than an order of magnitude differences), especially in the earth alkaline elements (Figure 8-1, Appendix B2). The most prominent difference from the extract solutions from the upper to the lower sections is the transition to Na<sup>+</sup> becoming the dominant cation; Cl<sup>-</sup> concentrations increase toward the Opalinus Clay. Bicarbonate remains the most abundant anion, followed by SO<sub>4</sub><sup>-2</sup>, which occurs in similar concentrations to the upper section. The extract solutions become more alkaline with depth in the formation, with measured pH values of 7.98 – 9.27. The fluids are at equilibrium or over-saturated with respect to calcite ( $SI_{\text{calcite}} = +0.04$  to  $+0.52$ ), with the exception of two carbonate-rich samples at around 93 m BHL and one sample at about 203 m BHL (Appendix B3). Corresponding log partial pressures of CO<sub>2</sub> vary between –4.28 and

–2.54 and are, thus, above and below the CO<sub>2</sub> partial pressure of air. Adjusted for calcite saturation, the extract solutions have pH values of 7.50 – 9.45 at corresponding log pCO<sub>2</sub> values of –4.50 to – 2.00. At these conditions, the extract solutions are under-saturated with respect to disordered dolomite, strontianite and fluorite, except for a few samples that are close to, or at, equilibrium with strontianite, and are strongly under-saturated with respect to gypsum and celestite (Appendix B3).

Whereas Na<sup>+</sup> and HCO<sub>3</sub><sup>-</sup> concentrations appear to mimic the clay content estimated from the gamma log, the concentrations of Cl<sup>-</sup> and SO<sub>4</sub><sup>-2</sup> seem to increase independently of the clay content in the lowest 20 m of the Passwang Fm (toward the Opalinus Clay). Molar ratios of Na/Cl and SO<sub>4</sub>/Cl become more similar between samples (2.7–7.8 and 0.4–1.8, respectively) and vary much less than in the upper part of the formation. The molar (Ca+Mg)/alkalinity ratio is similar, which displays little variation (0.04–0.51), with the exception of two limestone layers with ratios of 1.0 and 1.3. These differences indicate 1) the stronger influence of cation exchange reactions compared to carbonate (and sulphide) dissolution and, 2) the change from a Ca<sup>+2</sup> – Mg<sup>+2</sup>-dominated porewater composition to a Na<sup>+</sup>-dominated one, in which Cl<sup>-</sup> and SO<sub>4</sub><sup>-2</sup> become more and more significant with increasing proximity to the Opalinus Clay.

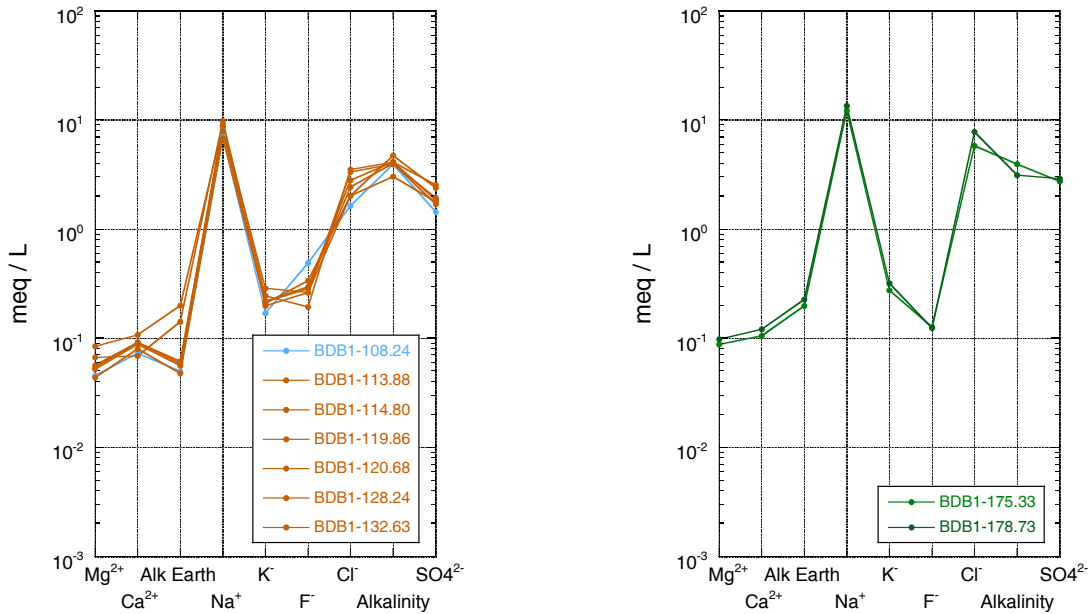
## 8.2 OPALINUS CLAY ROCKS

Aqueous extract solutions of the Opalinus Clay show a gradual change in chemical type and total dissolved solids (TDS) from sandy facies 2 at its top to shaly facies 1 at the bottom. Most striking are the very small variations in dissolved ion concentrations in the individual facies and across the entire formation (Figures 8-2 to 8-4, Appendix B2). The ionic strength of the extract solutions increases almost constantly from 0.8E-03 M to 2.1E-02 M. The constant increase is only interrupted by two samples with clay contents below 40 wt.% and corresponding lower water contents (samples BDB1-114.80, shaly facies 2 and BDB1-189.71, carbonate-rich sandy facies; *cf.* Chapters 6 and 7).

In sandy facies 2, aqueous extract solutions are of the Na-HCO<sub>3</sub>-Cl-SO<sub>4</sub> chemical type with TDS of 517 – 742 mg/L, except for sample BDB1-108.24 at the very top, which is still of Na-HCO<sub>3</sub>-SO<sub>4</sub>-Cl type and similar to the lowermost samples of the Passwang Fm (Figure 8-2, Appendix B2). Dissolved ion concentrations become very similar and vary only by a factor of 2 with increasing distance from the Passwang Fm. Toward the bottom of sandy facies 2, concentrations of Cl<sup>-</sup> in the extract solutions become almost identical to the alkalinity. The extract solutions are alkaline with very homogenous measured pH values between 8.70 and 8.98. At these conditions the solutions are essentially at equilibrium with calcite (SI<sub>calcite</sub> = –0.06 ± 0.07, n= 7) at corresponding log pCO<sub>2</sub> values of –3.73 ± 0.15 (i.e., below that of the atmosphere). At calcite equilibrium the extract solutions are under-saturated with respect to disordered dolomite (SI = –0.78 ± 0.11), strontianite (SI = –0.44 ± 0.07) and fluorite (SI = –1.14 ± 0.26), and strongly under-saturated with respect to gypsum (SI = –3.26 ± 0.11) and celestite (SI = –2.43 ± 0.15) (Appendix B.3).

In the underlying shaly facies 2, the chemical type of the aqueous extract solutions changes to Na-Cl-HCO<sub>3</sub>SO<sub>4</sub>, illustrating the most prominent increase in dissolved ion concentrations, which are those of Na<sup>+</sup> and Cl<sup>-</sup> (Appendix B2). This change is paralleled by an increase in TDS from 767 mg/L to 922 mg/L. The four samples have almost identical extract solution compositions, as shown in Figure 8-4. At the alkaline measured pH values of 8.50 to 8.95, the solutions are under-saturated with respect to calcite (SI<sub>calcite</sub> = –0.37 ± 0.13, n= 4) at corresponding log pCO<sub>2</sub> values around or below that of the atmosphere (values of –3.54 ± 0.20). The samples all

contain abundant calcite (9–18 wt.%, *cf.* Chapter 6) so that this under-saturation is geochemically not plausible and reflects exchange of the solutions with air ( $\text{CO}_2$  ingassing) after separation from the rock material by centrifugation during the transfer of the solutions to the pH and alkalinity measurement devices. Adjusted for calcite saturation, the extract solutions have even more alkaline pH values of  $9.25 \pm 0.11$  at corresponding  $\log p\text{CO}_2$  values far below that of air ( $-4.07 \pm 0.17$ ). They are under-saturated with respect to disordered dolomite ( $\text{SI} = -1.33 \pm 0.26$ ), stronitanite ( $\text{SI} = -0.82 \pm 0.16$ ) and fluorite ( $\text{SI} = -1.70 \pm 0.05$ ) and strongly under-saturated with respect to gypsum ( $\text{SI} = -3.21 \pm 0.09$ ) and celestite ( $\text{SI} = -2.43 \pm 0.05$ ) (Appendix B3).



Notes: Sample BDB1-108.24 (left, bright blue) at the Opalinus Clay – Passwang interface is of the chemical type as Passwang Fm extract solutions.

**Figure 8-2: Schoeller-Diagram of Aqueous Extract Solutions from the Sandy Facies 2 (left) and 1 (right) of the Opalinus Clay.**

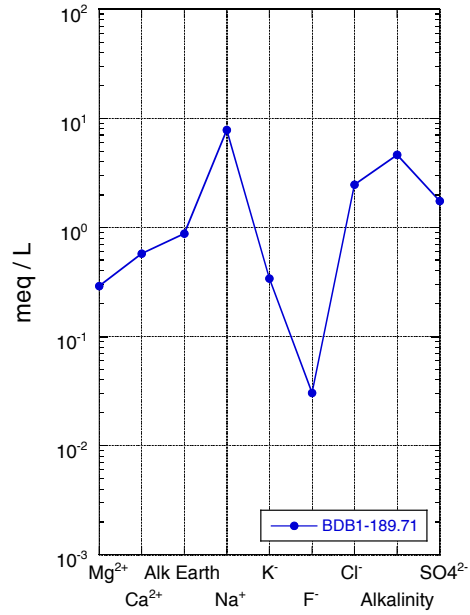


Figure 8-3: Schoeller-Diagram of Aqueous Extract Solutions from the Carbonate-rich Sandy Zone of the Opalinus Clay.

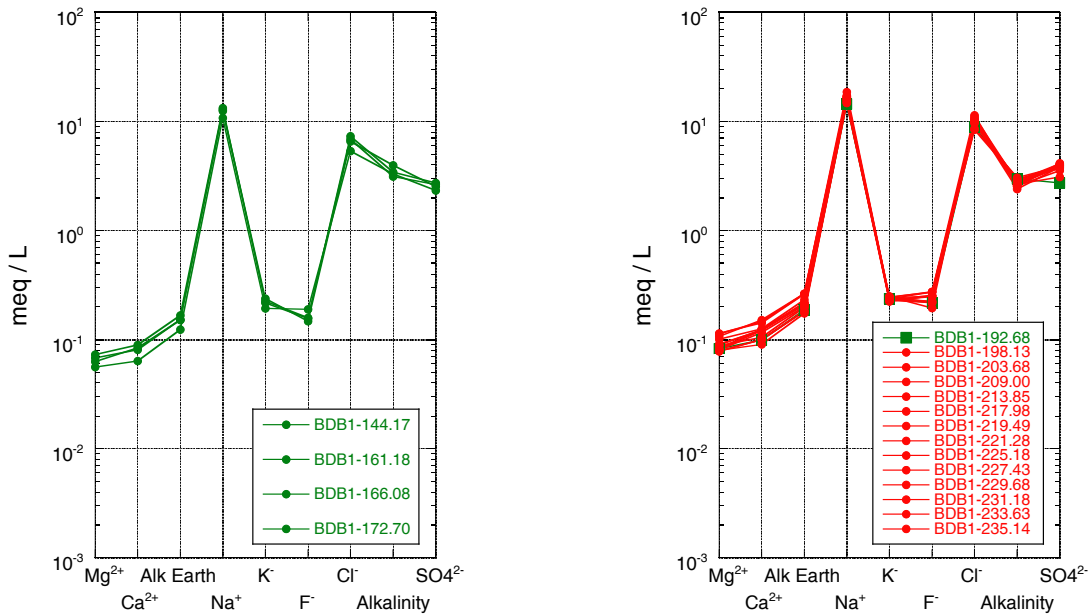


Figure 8-4: Schoeller-Diagram of Aqueous Extract Solutions from the Shaly Facies 2 (left) and 1 (right) of the Opalinus Clay.

In sandy facies 1 the same general trends continue: the extract solutions are of the same Na-Cl-HCO<sub>3</sub>-SO<sub>4</sub> chemical type as in the overlying shaly facies 2, though with increased TDS of 875 mg/L to 936 mg/L. The extract solutions of only two samples show very similar chemical compositions (Figure 8-2, Appendix B2). The solutions have measured pH values of 8.68 and 8.75, and corresponding log pCO<sub>2</sub> values of -3.70 and -3.62, and are slightly under-saturated with respect to calcite ( $SI_{\text{calcite}} = -0.15$  and  $-0.08$ ). At calcite saturation, the extract solutions have pH values of 9.01 and 9.07 at corresponding log pCO<sub>2</sub> values below that of air (-3.90 and -3.74) and are under-saturated with respect to disordered dolomite, strontianite and fluorite, and strongly under-saturated with respect to gypsum ( $SI = -3.07$  and  $-2.99$ ) and celestite ( $SI = -2.32$  and  $-2.12$ ) (Appendix B3).

A different picture emerges for the only sample of the carbonate-rich sandy facies between shaly facies 2 and sandy facies 1. Due to the exceptionally low clay content (8 wt.%) and corresponding low water content (1.55 wt.%) this sample behaves during extraction more like a limestone sample. This is illustrated by elevated concentrations of earth alkaline elements compared to the overlying shaly facies 2 and underlying sandy facies 1 (cf. Figure 8-3, along with Figures 8-2 and 8-4), indicating a significant proportion of carbonate dissolution. As a result of the small portion of porewater present in this sample, it has a lower TDS (666 mg/L), HCO<sub>3</sub><sup>-</sup> becomes again the dominant anion, and the extract solution is of the Na-HCO<sub>3</sub>-Cl-SO<sub>4</sub> chemical type, similar to those of sandy facies 2 above. The extract solution has a less alkaline measured pH value of 8.18 and is over-saturated with respect to calcite ( $SI_{\text{calcite}} = 0.20$ ) at a log pCO<sub>2</sub> value of -2.88 (above that of the atmosphere). This over-saturation with respect to calcite is geochemically not plausible and reflects outgassing of CO<sub>2</sub> after separation from the rock material by centrifugation. At calcite saturation, the extract solution has a pH values of 8.08 at corresponding log pCO<sub>2</sub> value above that of air (-2.68) and is under-saturated with respect to disordered dolomite ( $SI = -0.40$ ), strontianite ( $SI = -0.74$ ) and fluorite ( $SI = -2.24$ ) and strongly under-saturated with respect to gypsum ( $SI = -2.45$ ) and celestite ( $SI = -2.16$ ; Appendix B3).

Another major change in the chemical type of aqueous extract solutions occurs after the first sample of shaly facies 1. From here to the bottom of Opalinus Clay the solutions are of the Na-Cl-SO<sub>4</sub> type with TDS increasing from 979 mg/L to 1209 mg/L, illustrating the further increase in dissolved ion concentrations of Na<sup>+</sup>, Cl<sup>-</sup> and SO<sub>4</sub><sup>-2</sup> (Appendix B2). Extract solutions of the 14 samples show very similar compositions and the competition between SO<sub>4</sub><sup>-2</sup> and alkalinity (HCO<sub>3</sub><sup>-</sup> + CO<sub>3</sub><sup>-2</sup>), as second most abundant anion is clearly seen in Figure 8-3. Measured pH values ( $8.81 \pm 0.04$ ), corresponding log pCO<sub>2</sub> values ( $-3.82 \pm 0.07$ ) and under-saturation with respect to calcite ( $SI = -0.20 \pm 0.03$ ), are similar to those in the extract solution of shaly facies 2. Adjusted for calcite saturation, the extract solutions have even alkaline pH values ( $9.19 \pm 0.08$ ,  $n = 14$ ) at corresponding log pCO<sub>2</sub> values far below that of air ( $-4.11 \pm 0.10$ ). They are under-saturated with respect to disordered dolomite ( $SI = -1.01 \pm 0.05$ ), strontianite ( $SI = -0.77 \pm 0.04$ ) and fluorite ( $SI = -1.23 \pm 0.10$ ) and strongly under-saturated with respect to gypsum ( $SI = -2.93 \pm 0.09$ ) and celestite ( $SI = -2.28 \pm 0.08$ , Appendix B3).

### 8.3 STAFFELEGG FORMATION ROCKS

In the Staffelegg Fm, three of the four aqueous extract solutions are essentially identical in chemical type (Na-Cl-SO<sub>4</sub> type), TDS (1088 – 1161 mg/L) and composition (Figure 8-5, Appendix B2) to the deepest samples in shaly facies 1 of the Opalinus Clay. They also show the same behaviour in mineral saturation states, with log pCO<sub>2</sub> values of  $-4.06 \pm 0.25$  at calcite saturation, under-saturated with respect to dolomite, strontianite and fluorite, and strongly

under-saturated with respect to gypsum ( $SI = -2.86 \pm 0.02$ ) and celestite ( $SI = -2.19 \pm 0.05$ ; Appendix B3).

The fourth sample (BDB1-243.37) represents a limestone band with a very low water content (0.69 wt.%) and – according to the gamma log – a clay content of less than about 30 wt.%. The extract solution of this sample is comparable to that of the carbonate-rich facies of the Opalinus Clay (*cf.* Figures 8-3 and 8-5), with low TDS (402 mg/L) and is of  $\text{Na-HCO}_3\text{-Cl-SO}_4$  chemical type, with increased concentrations of earth alkaline elements and with  $\text{HCO}_3^-$  as the dominant anion. At calcite saturation, the extract solution of this sample has a pH of 8.45 at a log  $p\text{CO}_2$  of  $-3.38$  and is under-saturated with respect to dolomite, strontianite and fluorite (Appendix B3). As all other extract solutions, this sample is strongly under-saturated with respect to gypsum ( $SI = -2.57$ ) and celestite ( $SI = -2.18$ ).

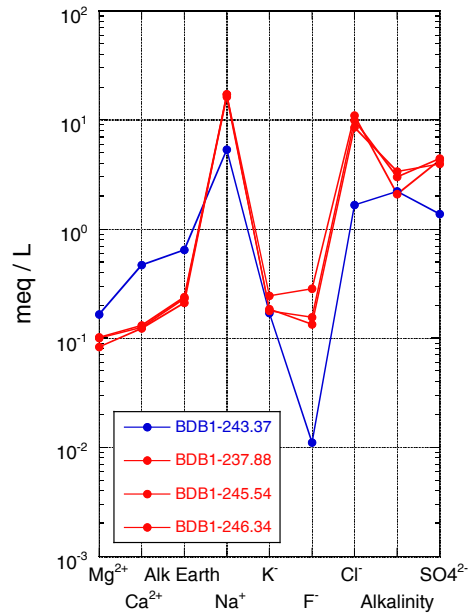


**Figure 8-5: Schoeller-Diagram of Aqueous Extract Solutions from the Staffelegg Fm.**

#### 8.4 GENERAL FEATURES OF AQUEOUS EXTRACT SOLUTIONS

In the Passwang Fm, the compositions of aqueous extract solutions vary in an irregular way, except for the deepest samples close to the Opalinus Clay. Based on the low concentrations of  $\text{Cl}^-$ , the porewater component in these extract solutions is minor, or of a similar Ca-Mg- $\text{HCO}_3^-$ -dominated type as the extract solutions themselves. The compositions of the extract solutions are variably influenced by mineral dissolution reactions (mainly carbonate minerals) and cation exchange. This is indicated by the absence of correlations between individual ions (Figure 8-6a to f) and ion-ion ratios, except for some trends in the Br/Cl ratio (*cf.* Section 8.5).

In contrast, aqueous extract solutions are consistently of similar chemical composition across the entire clay-rich section of the Opalinus Clay and Staffelegg Fm. Changes along this section

include increasing concentrations of  $\text{Na}^+$ ,  $\text{Cl}^-$  and  $\text{SO}_4^{2-}$  and a decrease in alkalinity with greater depth, and as a function of the exchange with groundwater in the overlying Passwang Fm. Between  $\text{Cl}^-$  and  $\text{Br}^-$  a well-defined linear correlation is established that increasingly deviates from seawater toward lower  $\text{Br}/\text{Cl}$  ratios with increasing  $\text{Cl}^-$  concentrations (Figure 8-6a). A correlation is also established between  $\text{Na}^+$  and  $\text{Cl}^-$ , which becomes linear from the base of sandy facies 2 down to the Staffelegg Fm. The  $\text{Na}-\text{Cl}$  ratios in this section are above the molar 1:1 ratio and the seawater dilution line (Figure 8-6b). Though less well-defined, linear trends are also established between  $\text{Cl}^-$  and  $\text{SO}_4^{2-}$  and  $\text{Na}^+$  and  $\text{SO}_4^{2-}$  (Figures 8-6c and d). At almost constant and very low  $\text{Ca}^{+2}$  concentrations, alkalinity decreases by a factor of  $\sim 2$  from the top of the Opalinus Clay down to the Staffelegg Fm, as a function of increasing  $\text{Cl}^-$  and  $\text{SO}_4^{2-}$  concentrations and ionic strengths of the solutions (Figure 8-6e). Exceptions from this behaviour are the two clay-poor samples from the carbonate-rich sandy facies and the limestone layer in the Staffelegg Fm. No trend is established between  $\text{Sr}^{+2}$  and  $\text{SO}_4^{2-}$  and the  $\text{Sr}^{+2}$  concentrations remain almost constant at remarkably low concentrations (Figure 8-6f).

As shown above, partial pressures of  $\text{CO}_2$ , calculated from measured values and adjusted for calcite saturation, are below that of the atmosphere across the entire clay-rich section of the Opalinus Clay and Staffelegg Fm. This indicates that exchange with atmospheric  $\text{CO}_2$  and, thus, with  $\text{O}_2$  was minimal during extraction. Therefore, oxidation reactions were successfully suppressed. Combined with the above ion-ion relationships, it can be concluded that the porewater portion in the aqueous extract solutions increases from the top of the Opalinus Clay and downward into the Staffelegg Fm. The contribution of dissolution reactions with carbonate (and other) minerals is small and the dominant reactions are related to cation exchange. In the clay-rich rocks, cation exchange reactions buffer the aqueous extract system, depending on the ionic strength of the porewater. During extraction, dilution of the porewater results in significant lowering of the ionic strength, which results in a preference for divalent cations on the exchange sites and, thus, the displacement of monovalent cations by divalent cations.

To what degree the observed low concentrations of  $\text{Ca}^{+2}$ ,  $\text{Mg}^{+2}$  and particularly  $\text{Sr}^{+2}$  (Figure 8-6f) can be explained by the induced exchange reactions cannot be defined from the extract solution data alone, and the results need to be explored by geochemical modelling. In this context, it is interesting to recall that all extract solutions are consistently under-saturated with respect to gypsum and celestite by two orders of magnitude or more. This might suggest that the observed increase in  $\text{SO}_4$  concentrations in the extract solutions is associated with an increase in porewater  $\text{SO}_4$  concentration rather than with artefacts induced during extraction, such as pyrite oxidation and/or mineral sulphate dissolution. This issue will be explored in more detail in Section 8.6.

## 8.5 MOBILE ELEMENTS (Cl, Br)

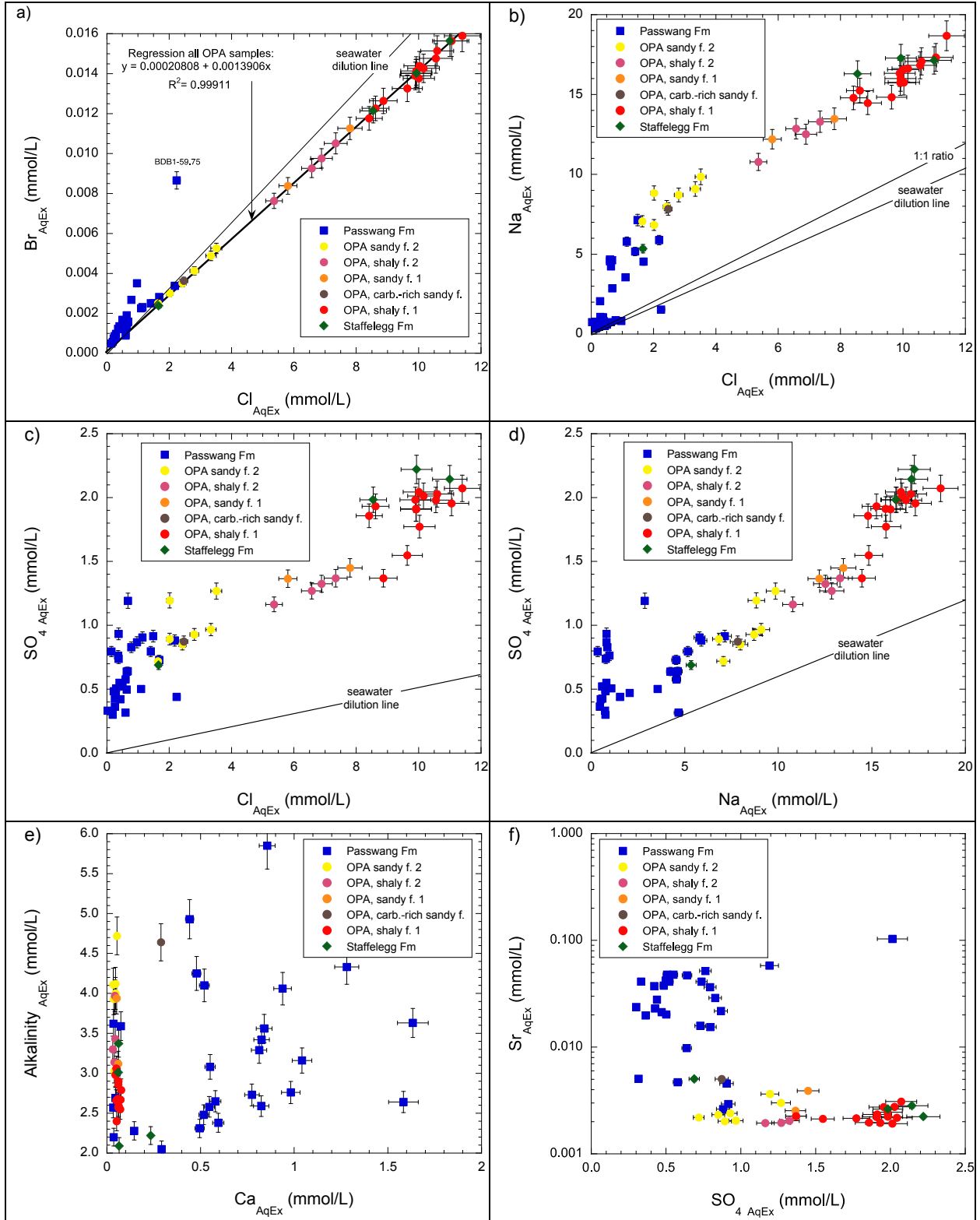
The rocks of the investigated stratigraphic units do not contain halide-bearing mineral phases that would be dissolved during aqueous extraction. For the clay-rich shaly facies rocks of the Opalinus Clay, the effect of sample preparation with respect to grain size was shown to be minimal (Waber et al. 2003a). Such effect can, however, not *a priori* be excluded for carbonate- and quartz-dominated samples, where fluid from fluid inclusions might possibly influence the extract solution composition. To minimize such contributions, all samples were only gently disintegrated along the grain boundaries instead of milling to a specific grain size (*cf.* Section 5.3). Dissolved  $\text{Cl}^-$  and  $\text{Br}^-$  in the aqueous extract solutions of all units investigated in this study can, thus, be considered chemically conservative or mobile elements, as previously shown for Opalinus Clay samples from Mont Terri (e.g., Pearson et al. 2003).

Back-calculation of  $\text{Cl}^-$  and  $\text{Br}^-$  concentrations from aqueous extract solutions to porewater concentrations requires knowledge about the anion-accessible porosity under in-situ conditions (*cf.* Chapter 9). In a homogenous, clay-rich argillaceous rock, aqueous extract  $\text{Cl}^-$  and  $\text{Br}^-$  concentrations can be normalised to the water-loss porosity and then scaled with an average fraction for the anion-accessible porosity, as has been done previously for the Opalinus Clay at Mont Terri (e.g., Pearson et al. 2003). Application of an average value is, however, inapplicable for the rocks of the Passwang Fm and the carbonate-rich sandy facies, which have significantly lower and more variable clay contents when compared to the majority of the Opalinus Clay.

So far, no difference in anion-accessible porosity is known for  $\text{Cl}^-$  and  $\text{Br}^-$ . Consequently the Br/Cl ratio obtained from aqueous extraction represents that of the in-situ porewater. As shown in Figure 8-6a, aqueous extract concentrations of  $\text{Cl}^-$  and  $\text{Br}^-$  correlate linearly from the bottom of the Passwang Fm across the Opalinus Clay to the Staffelegg Fm. In the middle and upper part, a different and less-defined correlation, with a steeper slope, is recognised (note that sample BDB1-59.57 seems to have been influenced by the 'break' in drilling activities between Phase 1 and Phase 2 and the flushing of the borehole during this time period).

The correlation indicated in Figure 8-6a becomes even more pronounced when looking at the spatial distribution of the Br/Cl ratios (Figure 8-7). In the Passwang Fm, close to the water-conducting zone at about 58 m BHL, the molar Br/Cl ratios scatter between values  $4\text{E-}03$  and  $3\text{E-}03$  before they gradually decrease to values of about  $1.6\text{E-}03$  at the junction with the Opalinus Clay. The gradual decrease is interrupted at two locations (67 m and 93 m BHL) with low values of around  $1.5\text{E-}03$ . At 93 m BHL, two samples were collected within 40 cm of one another, and both yield the same molar Br/Cl ratio, indicating that these low values are real. Comparison with water squeezed from samples adjacent to the aqueous extract samples is hindered by the fact that squeezed water could only be obtained at 500 MPa for a sample at 82.7 m BHL and at 300 MPa for a sample at 100.43 m BHL (Mazurek et al. 2017). At least for clay-rich rocks, it was shown that such high pressures induce ion-filtration effects and result in lowered  $\text{Cl}^-$  concentrations compared to the in-situ porewater (e.g., Waber & Oyama 2000; Fernández et al. 2003; Mazurek et al. 2015). It appears that at very high pressures such effects also influence the Br/Cl ratio, as indicated by the sample at 82.7 m BHL, which has a significantly lower ratio compared to that in the solution of the adjacent aqueous extract sample (Figure 8-7).

High molar Br/Cl ratios above  $3\text{E-}03$  are typical for low-Cl, fresh groundwater in Jurassic limestone environments, for which concentrations of Br are above detection limit (e.g., Waber et al. 2014). The high molar Br/Cl ratios in porewater at greater distance from the underlying Opalinus Clay indicate that this porewater consists primarily of a fresh water component. The decrease in the Br/Cl ratio in aqueous extract solutions of the Passwang Fm toward the Opalinus Clay can, thus, be explained by an increasing exchange of Cl and Br with the underlying Opalinus Clay porewater.

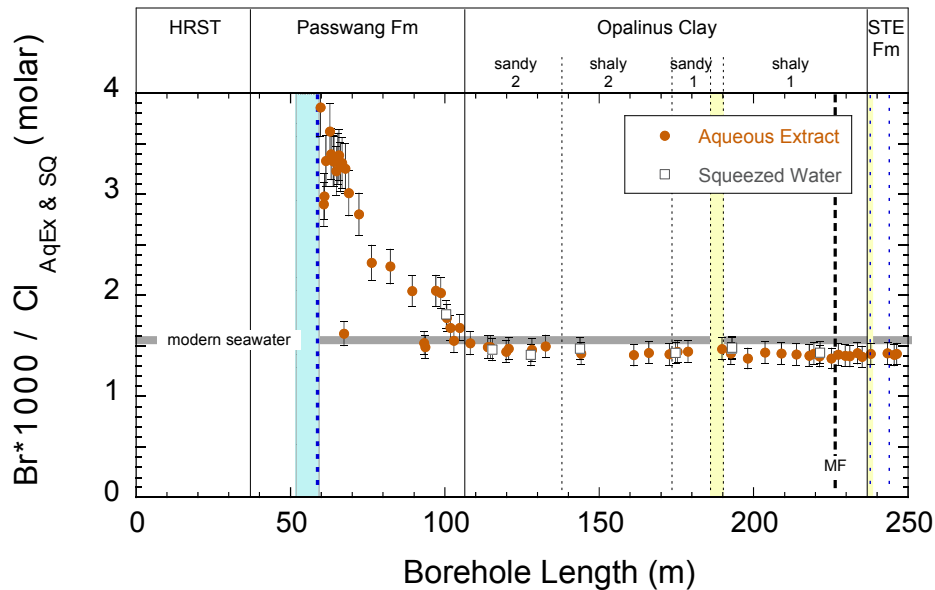


Notes: a) Br vs. Cl, b) Na vs. Cl, c) SO<sub>4</sub> vs. Cl, d) SO<sub>4</sub> vs Na, e) alkalinity vs Ca, f) Sr vs SO<sub>4</sub>

**Figure 8-6: Ion-ion Relationships in Aqueous Extract Solutions from Rocks of the Passwang Fm, Opalinus Clay and Staffelegg Fm.**

The Br/Cl ratio of modern seawater is not unique and depends on the mixing behaviour, climatic and other environmental conditions. Improvements in analytical techniques in the past decades further yield better precision in the determination of Br/Cl ratios in seawater and other solutions. The larger water bodies (Pacific, Atlantic and Indian Oceans) have Br/Cl ratios between  $1.520\text{E}-03$  and  $1.598\text{E}-03$ . More extreme values towards higher and lower values are observed for smaller, less well-mixed water bodies mainly in warmer climatic areas. Therefore, comparison of paleo-fluids should preferably be made to such a range of values instead of using a single value – as the size, mixing behaviour and climatic conditions of paleo-seawater bodies are often not known precisely.

Ratios of Br/Cl in aqueous extract solutions of the Opalinus Clay in borehole BDB-1 range from  $1.376\text{E}-03$  to  $1.527\text{E}-03$ , with an average of  $1.434\text{E}-03 \pm 0.037\text{E}-03$  ( $n=28$ ). Extract solutions of the Staffelegg Fm have an average Br/Cl ratio of  $1.418\text{E}-03 \pm 0.006\text{E}-03$ . For the Opalinus Clay, there is agreement between Br/Cl ratios of aqueous extract solutions and water squeezed at pressures below 200 MPa (Figure 8-7).



Notes: Error bars are propagated error. Squeezed water data from Mazurek et al. (2017); displayed is only the lowest pressure water.

**Figure 8-7: Molar Br/Cl Ratio in Aqueous Extract Solutions and Squeezed Water Across the Sequence Passwang Fm – Opalinus Clay – Staffelegg Fm in Borehole BDB-1.**

All Br/Cl ratios in the Opalinus Clay and the Staffelegg Fm are below the range of modern seawater and the deviation from the seawater dilution line increases with increasing depth (Figures 8-6a and 8-7). This indicates that a non-marine component is present in the porewater, in addition to a potential marine component. In combination with the total porewater  $\text{Cl}^-$  and  $\text{Br}^-$  concentrations (*cf.* Chapter 9), this non-marine component appears to comprise more than 50% of the present-day porewater.

This latter statement needs some clarification, as previously the porewater in Opalinus Clay has been interpreted as a residual water of purely marine origin. Thus, Pearson and Waber (2001) and Pearson et al. (2003) interpreted the Br/Cl ratios combined with the SO<sub>4</sub>/Cl ratio (*cf.* Section 8.6) of water collected from boreholes, squeezed water and aqueous extraction data from the Opalinus Clay as indicative of a seawater origin for the porewater. In these works, the scatter in the data was essentially ascribed to analytical problems. In addition, the Br/Cl ratios of the different water types were compared to a "general seawater" value of 1.5E-03, which is below the range of seawater analyses given in the literature. A closer look at this scatter of the solution data used by Pearson and Waber (2001) and Pearson et al. (2003) reveals that the Br/Cl ratios of aqueous extract solutions varied from 1.040–1.790E-03 (n=6), of squeezed water from 1.240–1.770E-03 (n=15), and in borehole waters from 1.240–1.980E-03 (n=20, 3 boreholes). Although averaging at "about 1.5E-03, the same as that of seawater" (Pearson and Waber 2001), the scatter seems too large to unequivocally assign the porewater in the Opalinus Clay to be of purely marine origin. Improvements have been made over many years, particularly in the analytics of bromide at low concentrations. Precision and accuracy have greatly increased and laboratory inter-comparisons using different types of analytical techniques support this conclusion (e.g., Mazurek et al. 2017).

The 1) consistent data set of more than 30 samples from borehole BDB-1 across the entire argillaceous sequence at the Mont Terri URL, 2) regular spatial distribution of the Br/Cl ratio, and 3) agreement between different methods and laboratories, suggest that the hypothesis postulated by Pearson and Waber (2001) and Pearson et al. (2003) should be revised. Based on the porewater Br/Cl ratios in rock samples of borehole BDB-1, there is a significant portion of non-marine water present in the porewater of the Opalinus Clay in addition to a marine residual component.

## 8.6 ORIGIN OF SULPHATE

Origin and concentration of dissolved sulphate in the porewater of the Opalinus Clay has been a matter of debate since the first attempts at porewater characterisation. It was readily observed that the behaviour of dissolved sulphate differs from that of mobile elements, especially during sampling of sulphate with different techniques (see discussions in Pearson et al. 2003). Based on the existing data about water collected over long time periods from boreholes, Pearson and Waber (2001) and Pearson et al. (2003) suggested that the SO<sub>4</sub> concentration in the porewater of the Opalinus Clay at Mont Terri might be controlled by the SO<sub>4</sub>/Cl ratio of seawater. These authors were, however, also aware that this working hypothesis was essentially based on very few samples from the depth zone in the Opalinus Clay with the highest Cl<sup>-</sup> concentration (borehole BWS-A1), whereas other borehole waters and squeezed waters display SO<sub>4</sub>/Cl ratios above that of seawater (*cf.* also Figure 4.3 in Pearson and Bath 2003). These authors further mentioned that "only sparingly soluble SO<sub>4</sub> minerals celestite and barite are present in the Opalinus Clay, and every attempt was made to exclude oxygen from the leaching process. Thus, the source of the high SO<sub>4</sub>/Cl ratios in aqueous leachates is unknown, and these ratios must be used with caution". In later modelling studies, Pearson et al. (2011) also evaluated, in more detail, potential solubility controls of SO<sub>4</sub><sup>-2</sup> and/or Sr<sup>+2</sup> by celestite, combined with selective diffusion of Cl and SO<sub>4</sub><sup>-2</sup>.

### 8.6.1 Sulphur Inventory in the Rock

So far, detailed mineralogical investigations do not confirm disseminated occurrence of sulphate mineral phases across the entire Opalinus Clay at Mont Terri. However, celestite, barite, and rarely gypsum, are described to occur in veins and concretions (Waber & Schürch 2000; Gaucher et al. 2003; de Haller et al. 2014). In the samples investigated for this study, none of these sulphate minerals were identified. If present, they would be below 0.5 wt.%, representing the detection limit of the applied XRD measurements. In turn, Lerouge et al. (2014) found traces of Sr-Ba solid solution phases in one out of fourteen samples. Mineral solid solutions of Sr-Ba phases were detected in late-developed pore space of a sample from sandy facies 1 adjacent to the carbonate-rich sandy facies.

In contrast, sulphide minerals (mainly pyrite) are present in all samples (*cf.* Chapter 6). Pyrite oxidation during sampling, sample preparation and aqueous extraction was attempted to be suppressed as much as possible by the applied procedures (*cf.* Section 5.3); success of that approach is indicated by the CO<sub>2</sub> partial pressures of the extract solutions, which are below that of the atmosphere in the clay-rich samples (*cf.* Sections 8.2 to 8.4).

Waber et al. (2003a) investigated the potential for pyrite oxidation during various steps, from the drilling process, to sample storage and preparation, and to the extraction procedure. Based on mass balance considerations, these authors concluded that oxidation is greatly minimised if drill-core samples are quickly processed (within days) after recovery, the central part of the drill core is immersed in ultra-pure water in its originally saturated state, and the extraction occurs under oxygen-free conditions in a glovebox. Wersin et al. (2013) applied geochemical modelling, including reaction kinetics, and concluded that pyrite oxidation is successfully suppressed if the above criteria are followed. In both of these studies, it was concluded that the contribution by pyrite oxidation to the sulphate concentration in aqueous extract solutions does not exceed about 10% and is, thus, close to the analytical uncertainty of the dissolved SO<sub>4</sub><sup>-2</sup> determination.

### 8.6.2 Sulphate in Borehole Water and Squeezed Water

During the WS-Experiments at the Mont Terri URL, four boreholes were dedicated to sampling borehole water that accumulated over long periods of time (months to years) in packer intervals (Griffault et al. 2003). The BWS-boreholes were core-drilled with flushing by compressed air and distributed across the Opalinus Clay at locations with variable porewater Cl<sup>-</sup> concentrations. One borehole (BWS-A6) did not deliver any water over the entire observation period from 1996 to 1999. Note that during each sampling campaign, an overpressure of N<sub>2</sub> was commonly applied to the packer intervals to force the small volumes of borehole water into the sampling lines (*cf.* Griffault et al. 2003 and references therein).

Minimum and maximum SO<sub>4</sub><sup>-2</sup> and Cl<sup>-</sup> concentrations, and SO<sub>4</sub>/Cl ratios, of borehole water are given in Table 8-1. In the individual boreholes, SO<sub>4</sub><sup>-2</sup> concentrations in the accumulated borehole water varied between 19 % and 45 %, while those of Cl<sup>-</sup> displayed somewhat less variation between 9 % and 36 %. Ratios of SO<sub>4</sub>/Cl were higher compared to that of seawater in the low-Cl borehole waters (BWS-A2 and BWS-A3) and varied around that of seawater in the borehole water richest in Cl<sup>-</sup> (BWS-A1; Table 8-1). The variability of the SO<sub>4</sub>/Cl ratios in borehole water was between 27 % and 45 %, highest in the borehole water richest in Cl<sup>-</sup>. Large variation was observed also for the Sr<sup>+2</sup> concentrations, ranging from 50 % to 65 % in the individual borehole waters (Table 8-1). In this context, it is worthwhile mentioning that the SO<sub>4</sub><sup>-2</sup>

concentration in modern seawater is about 30 % higher than those measured, and that of  $\text{Sr}^{+2}$  more than 10 times lower than that in the borehole water richest in  $\text{Cl}^-$  (Table 8-1). This suggests that, at least some of the Sr must have been derived from a source other than seawater.

The large spread in solute concentrations analysed in these borehole waters is also reflected in the calculated mineral saturations states. Using the measured data, calcite saturation indices range from  $-0.22$  to  $+0.45$  due to the changing conditions in the boreholes and the difficulty associated with pH, alkalinity and TIC measurements (see discussion in Pearson et al. 2003). However, all borehole waters, independent of their  $\text{Cl}^-$  concentration, and in spite of their large variability in  $\text{SO}_4^{-2}$  and  $\text{Sr}^{+2}$  concentrations, were essentially at saturation with celestite ( $\text{SI}_{\text{celestite}} = -0.02$  to  $+0.14$ ; Table 8.1). In addition, some of the collected borehole waters even reached saturation, or were over-saturated, with respect to gypsum (Table 8.1). From the in-situ porewater perspective, these observations are somehow contradictory. If the in-situ porewater  $\text{SO}_4^{-2}$  concentrations were mineral-solubility controlled, then constant concentrations as a function of time would be expected at a given location and  $\text{Cl}^-$  concentration. In the case of solubility control by celestite, this would mean constant  $\text{SO}_4^{-2}$  and  $\text{Sr}^{+2}$  concentrations. The observation of highly variable  $\text{SO}_4^{-2}$  and  $\text{Sr}^{+2}$  concentrations, but saturation with respect to celestite, in the borehole water indicates that this solubility control is induced and occurs in the packer intervals, but not the undisturbed rock matrix (i.e., not in the in-situ porewater).

Water squeezed under high pressure from samples of the BDB-1 borehole (Mazurek et al. 2017) cover a similar range in  $\text{Cl}^-$  concentrations as the BWS borehole waters, and display associated  $\text{SO}_4^{-2}$  concentrations in range of 8.0–29.3 mmol/L (771–2814 mg/L). This range is somewhat larger than that observed for the borehole waters (Table 8-1). Ratios of  $\text{SO}_4/\text{Cl}$  are all above that of seawater, except for one sample. For samples from similar location and  $\text{Cl}^-$  concentration, the squeezed water display similar large variation in  $\text{SO}_4^{-2}$  concentrations (20-45 %) and  $\text{Sr}^{+2}$  concentrations (41-43 %), similar to what is observed for the borehole waters (Table 8-1). The squeezed water samples also are at saturation with respect to celestite, except for one, and under-saturated with respect to gypsum (Table 8-1). These characteristics, which are similar to those of borehole waters, suggest that squeezed waters also are subject to induced solubility controls, altering the  $\text{SO}_4^{-2}$  and  $\text{Sr}^{+2}$  concentrations from those prevailing under in-situ conditions. Whereas there seem to be certain similarities in the Sr- $\text{SO}_4$  system of borehole water and squeezed water, the same squeezed waters constantly display  $\text{Br}/\text{Cl}$  lower than that of modern seawater, whereas the borehole waters show both lower and higher ratios.

To derive in-situ porewater composition using geochemical modelling strategies, Pearson et al. (2003, 2011) fixed the  $\text{SO}_4^{-2}$  concentration in borehole water to the seawater  $\text{SO}_4/\text{Cl}$  ratio, or fixed it to celestite saturation or redox potential. Later model approaches used  $\text{SO}_4/\text{Cl}$  ratios obtained from aqueous extraction, and assumed saturation with celestite to constrain  $\text{SO}_4^{-2}$  and  $\text{Sr}^{+2}$  concentrations in the modelled porewater (e.g., Mäder 2009). Saturation with celestite was based on the fact that borehole water and squeezed water with high  $\text{Cl}^-$  concentrations from the Opalinus Clay at Mont Terri are commonly close to, or at saturation with, celestite.

Fixation of the  $\text{SO}_4^{-2}$  concentration in the in-situ porewater to the seawater  $\text{SO}_4/\text{Cl}$  ratio means that dissolved  $\text{SO}_4^{-2}$  is treated as a mobile element. In such a case, it should theoretically be possible to convert the  $\text{SO}_4^{-2}$  concentrations of aqueous extract solutions in the same way as the  $\text{Cl}^-$  concentration, i.e., by back-calculation using the anion accessible porosity (cf. Chapter 9). However, such derived  $\text{SO}_4^{-2}$  concentrations from extract solutions are inconsistent with those obtained for squeezed water and borehole water from the BWS boreholes.

**Table 8-1: Chemical Data and Mineral Saturation Indices of Borehole Waters from BWS-A Boreholes and Squeezed Water from Borehole BDB-1**

Borehole	Water Type	Stratigraphie	Facies	Cl			Br			SO4			Sr			Br/Cl			SO4/Cl		
				Min mg/L	Max mg/L	n	Min molar	Max molar	n	Min molar	Max molar	n									
BWS-A3	Borehole Water	OPA	shaly f.2	3580	5551	7	12.0	17.0	6	610	1115	7	27.0	67.4	4	1.447E-03	1.983E-03	6	6.258E-02	8.972E-02	7
BWS-A2	Borehole Water	OPA	sandy f.1	5884	6460	7	16.7	47.0	7	1300	1610	7	21.5	42.7	5	1.235E-03	1.810E-03	7	6.758E-02	9.213E-02	7
BWS-A1	Borehole Water	OPA	shaly f.1	8500	10958	15	27.0	36.3	12	1175	1950	15	28.4	80.5	13	1.344E-03	1.664E-03	12	4.214E-02	7.597E-02	15
BDB-1	Squeezed Water	OPA	sandy f.2	3245	4777	2	10.7	15.2	2	771	958	2	10.7	18.2	2	1.411E+00	1.464E+00	2	5.957E-02	1.089E-01	2
BDB-1	Squeezed Water	OPA	shaly f.2		5486	1		18.2	1		1246	1		30.6	1		1.473E+00	1		8.385E-02	1
BDB-1	Squeezed Water	OPA	sandy f.1		8601	1		27.8	1		1156	1		47.9	1		1.432E+00	1		4.962E-02	1
BDB-1	Squeezed Water	OPA	shaly f.1	10086	11182	3	36.4	36.1	3	1540	2814	3	36.8	65.0	3	1.433E+00	1.483E+00	3	5.473E-02	9.475E-02	3
	Seawater Pacific (Nordstrom et al., 1979)				19353			69.7			2712						1.598E-03			5.172E-02	
	Seawater Arabian Sea (courtesy HNW, 2005)				21043			79.9			2940		7.2				1.609E-03			5.151E-02	

Mineral Saturation Indices (SI)

Borehole	Water Type	Stratigraphie	Facies	SI calcite			SI celestite			SI gypsum		
				Min	Max	n	Min	Max	n	Min	Max	n
BWS-A3	Borehole Water	OPA	shaly f.2	-0.22	0.24	7	-0.02	0.07	4	-0.81	0.06	7
BWS-A2	Borehole Water	OPA	sandy f.1	0.24	0.16	5	0.14	0.06	5	-0.60	0.17	5
BWS-A1	Borehole Water	OPA	shaly f.1	-0.05	0.45	14	0.09	0.10	13	-0.36	0.26	14
BDB-1	Squeezed Water	OPA	sandy f.2		1.25	1		-0.43	1		-1.78	1
BDB-1	Squeezed Water	OPA	shaly f.2		0.58	1		0.04	1		-0.61	1
BDB-1	Squeezed Water	OPA	sandy f.1		0.75	1		0.08	1		-0.52	1
BDB-1	Squeezed Water	OPA	shaly f.1		-0.31	1		0.08	1		-0.33	1
	Seawater Pacific (Nordstrom et al., 1979)				0.76						-0.63	
	Seawater Arabian Sea (courtesy HNW, 2005)				0.90			-0.65			-0.58	

**Notes:** Borehole water data from Griffault et al. (2003) and modelled mineral saturation states from Waber (1999, 2001); data of squeezed water at lowest pressure from Mazurek et al. (2017); n = number of samples

The possibility of  $\text{SO}_4^{-2}$  concentrations in the in-situ porewater being controlled by celestite means that such mineral phase would potentially modify the  $\text{SO}_4^{-2}$  concentrations in aqueous extract solution by dissolution of such mineral phase(s) during extraction. Therefore, the S-system has to be inspected in combination with the  $\text{Sr}^{+2}$  concentrations in aqueous extract solutions, squeezed water and borehole water, and in combination with cation exchange reactions, during the collection of such solutions.

### 8.6.3 Sulphate in Aqueous Extract Solutions

As outlined in Sections 8.1 to 8.4, dissolved  $\text{SO}_4^{-2}$  concentrations of aqueous extract solutions are highly variable in the Passwang Fm and become more homogenous in the Opalinus Clay and the Staffelegg Fm. In the argillaceous rocks,  $\text{SO}_4^{-2}$  concentrations are correlated with  $\text{Cl}^-$  and  $\text{Na}^+$ , whereas  $\text{Sr}^{+2}$  concentrations remain almost unchanged at increasing  $\text{SO}_4^{-2}$  concentrations (Figure 8-6).

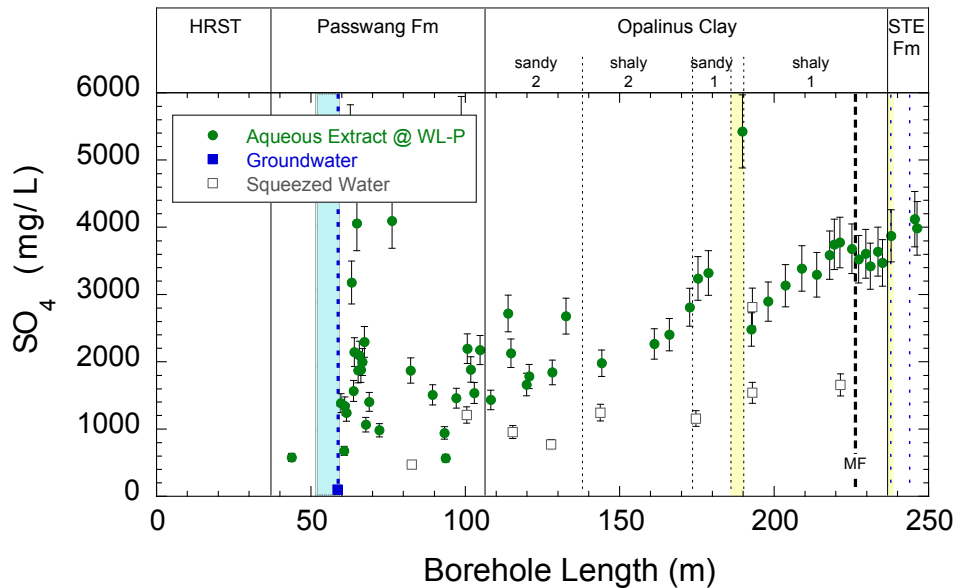
As far, unresolved problem, is that the conversion of  $\text{SO}_4^{-2}$  concentrations of aqueous extract solutions to the water-loss porosity results in apparent  $\text{SO}_4^{-2}$  concentrations that are generally higher than those of water squeezed from the adjacent samples (Figure 8-8) and also higher compared to borehole water collected from the BWS boreholes (cf. Table 8-1). Obviously this discrepancy would become more pronounced if the  $\text{SO}_4^{-2}$  concentrations of aqueous extract solutions were scaled (yet unknown) to  $\text{SO}_4^{-2}$ -accessible porosity under in-situ conditions. Nevertheless, this indicates that  $\text{SO}_4^{-2}$  concentrations are modified from that of the in-situ porewater in the aqueous extract solutions as well as in the waters squeezed under high pressure and collected from boreholes.

Inspection of ion-ion ratios, saturation states and geochemical modelling give further insight into this problem. The  $\text{SO}_4/\text{Cl}$  ratio of aqueous extract solutions decrease from the Passwang Fm into sandy facies 2 of the Opalinus Clay and remain rather constant from the bottom of shaly facies 2 down to the Staffelegg Fm, except for the carbonate-rich sandy facies and the limestone layer in the Staffelegg Fm (Figure 8-9). Over the entire cross-section, the  $\text{SO}_4/\text{Cl}$  ratio of aqueous extract solutions are higher than that of modern seawater and also higher than water squeezed from samples adjacent to the aqueous extract samples. Total  $\text{SO}_4^{-2}$  concentrations in the aqueous extract solution, however, increase along the section toward the Staffelegg Fm (or with increasing  $\text{Cl}^-$  concentrations), whereas  $\text{Sr}^{+2}$  concentrations remain rather stable (Figure 8-10). This contrast in the behaviour observed for the squeezed waters, where the concentrations of  $\text{SO}_4^{-2}$  remain stable within a factor of 2 (except one sample) and those of  $\text{Sr}^{+2}$  increase. As a consequence the  $\text{Sr}/\text{SO}_4$  ratios in aqueous extract solutions decrease with increasing  $\text{Cl}^-$  concentrations, whereas those of the squeezed waters increase (Figure 8-11). Exceptions from the general trend in the aqueous extract solutions are the clay-poor samples from the carbonate-rich sandy facies and the limestone layer in the Staffelegg Fm (Figure 8-11).

As mentioned above, all extract solutions in the Opalinus Clay and Staffelegg Fm are consistently strongly under-saturated with respect to gypsum and celestite, by two orders of magnitude or more (cf. Sections 8.2 and 8.3). In contrast, water squeezed from adjacent samples show variable slight under-saturation to over-saturation with respect to celestite. For the Opalinus Clay and the Staffelegg Fm, the saturation state of celestite in the different solution types is illustrated in Figure 8-12 as a function of borehole length and in relation to the  $\text{Sr}/\text{SO}_4$  ratio of the corresponding solution. The trends observed in Figure 8-11 are now visible as a function of distance from the interface of the Passwang Fm to the bottom of the borehole in the

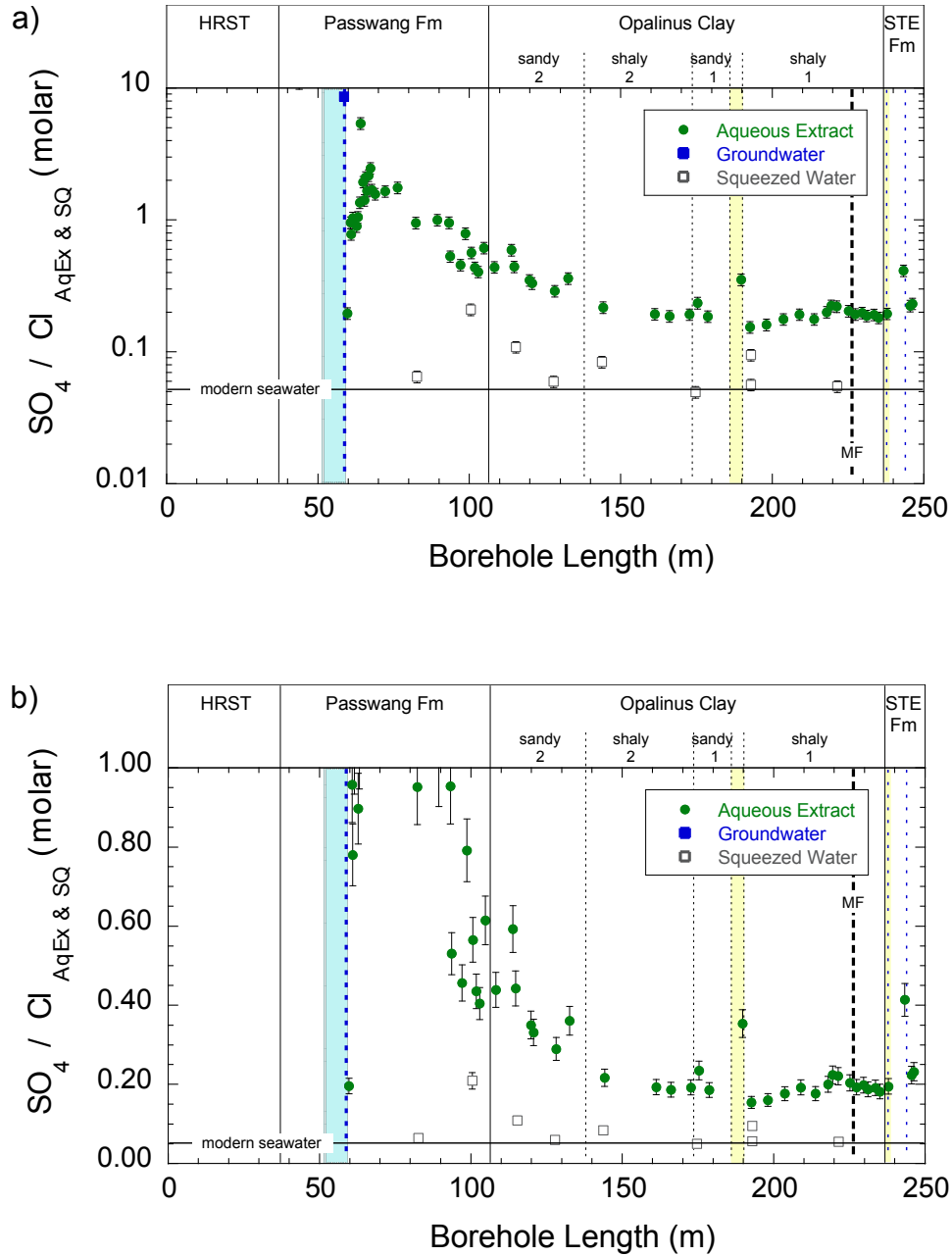
Staffelegg Fm. The Sr/SO<sub>4</sub> ratios in aqueous extract solutions decrease, whereas those of the squeezed waters increase with increasing distance from the Passwang Fm, and the aqueous extract solutions are greatly under-saturated with respect to celestite whereas the squeezed water are close to saturation.

Saturation with celestite does not depend on measured concentrations, but on the activity product of dissolved SO<sub>4</sub><sup>2-</sup> and Sr<sup>2+</sup>. At the low ionic strength of the aqueous extract solutions of less than 0.017 Mol (*cf.* Appendix B.2), total S<sup>VI</sup> and Sr occur mainly as free ions (*i.e.*, as SO<sub>4</sub><sup>2-</sup> and Sr<sup>2+</sup>). In contrast, with the more than one order of magnitude higher ionic strength of the squeezed waters, competition with SO<sub>4</sub><sup>2-</sup> and Sr<sup>2+</sup> aqueous complexes becomes important. For instance, in the high-Cl aqueous extract sample BDB1-221.28, more than 95 % and 85 % of the total S<sup>VI</sup> and total Sr occur as the free ion SO<sub>4</sub><sup>2-</sup> and Sr<sup>2+</sup>, respectively, with the remaining portion of Sr occurring as uncharged SrSO<sub>4</sub><sup>0</sup> complex. In contrast, in the squeezed water from the adjacent sample (BDB1-221.50) only 59 % of the total S<sup>VI</sup> occurs as free SO<sub>4</sub><sup>2-</sup> ion, whereas the remaining S<sup>VI</sup> occurs as NaSO<sub>4</sub><sup>-</sup> (18 %), CaSO<sub>4</sub><sup>0</sup> (12%) and MgSO<sub>4</sub><sup>0</sup> (10 %) complexes. Interestingly total Sr in this sample occurs to 90 % as free Sr<sup>2+</sup> and the SrSO<sub>4</sub><sup>0</sup> complex makes only about 10 %, *i.e.*, less than in the low-ionic strength aqueous extract.



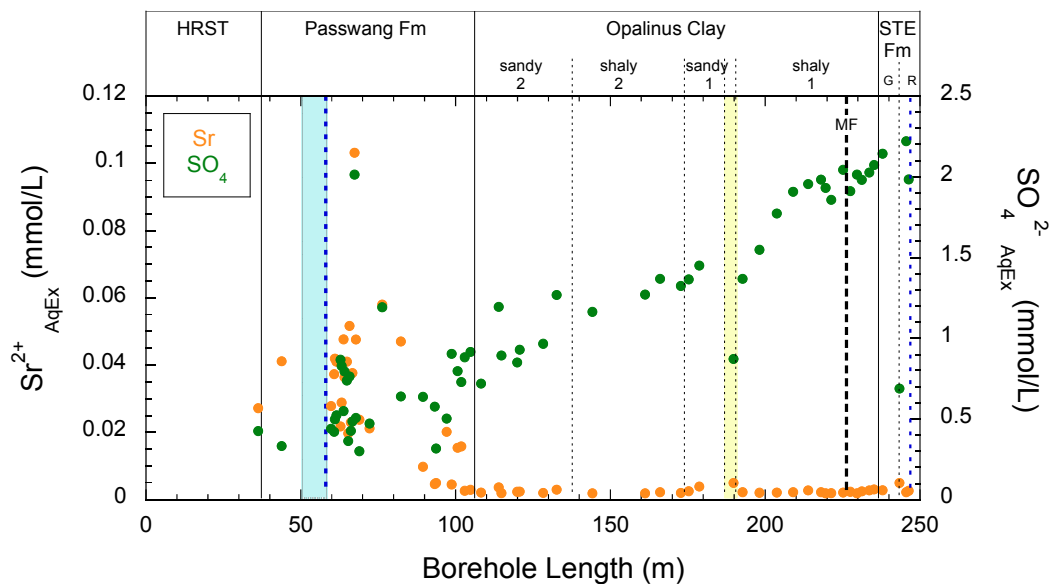
Notes: Error bars are  $\pm 10\%$ . Squeezed water data from Mazurek et al. (2016); displayed is only the lowest pressure water.

**Figure 8-8: Concentrations of SO<sub>4</sub> of Aqueous Extract Solutions Hypothetically Converted to the Water-loss Porosity Compared to SO<sub>4</sub> Concentrations in Squeezed Water Across the Sequence Passwang Fm – Opalinus Clay – Staffelegg Fm in Borehole BDB-1.**



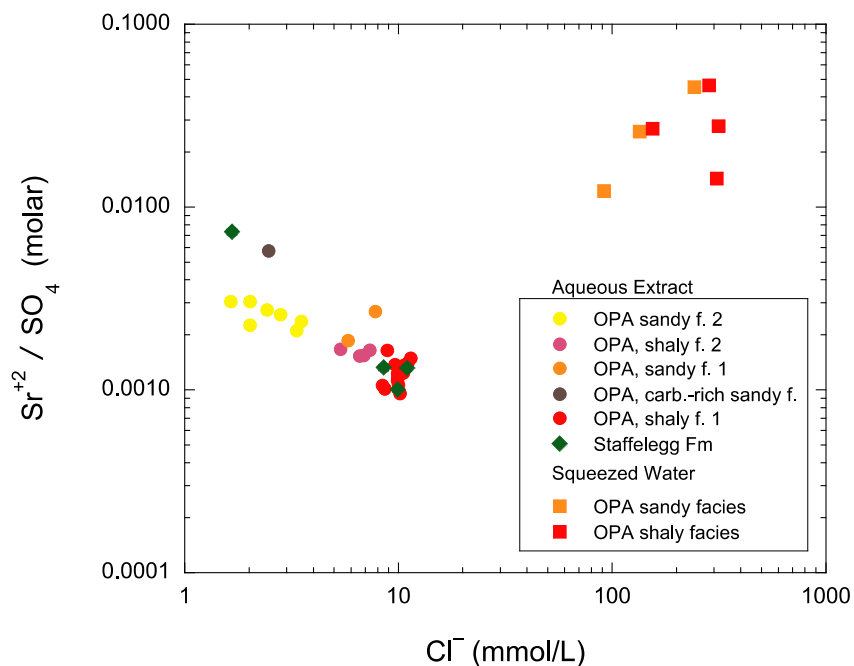
Notes: a) log scale, b) linear scale; error bars are conservative  $\pm 10\%$  (propagated error is smaller). Squeezed water data from Mazurek et al. (2016); displayed is only the lowest pressure water.

**Figure 8-9: Molar  $\text{SO}_4/\text{Cl}$  Ratio in Aqueous Extract Solutions and Squeezed Water Across the Sequence Passwang Fm – Opalinus Clay – Staffelegg Fm in Borehole BDB-1.**



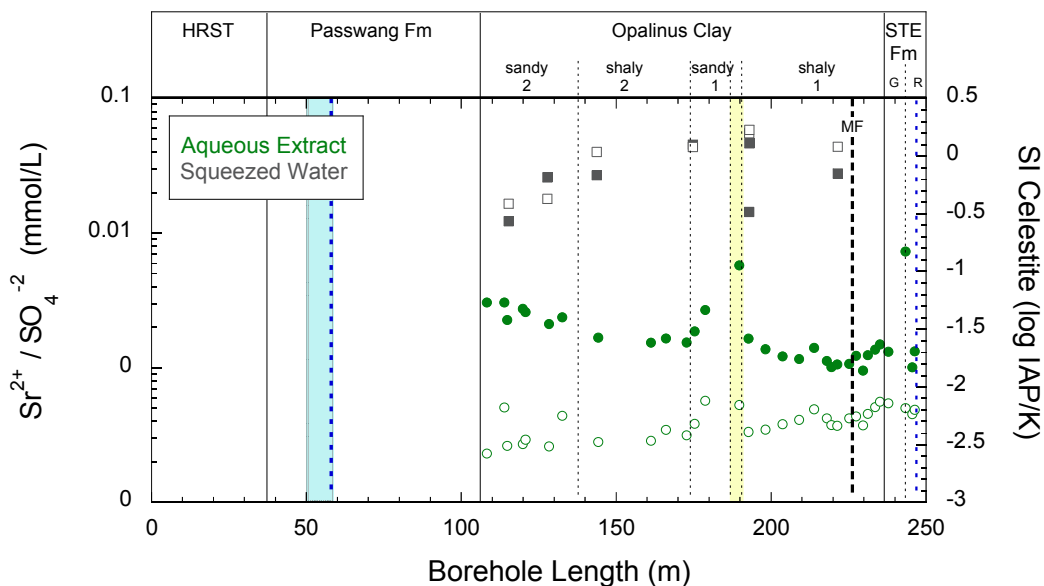
Notes: The analytical error is  $\pm 5\%$ .

**Figure 8-10: Concentrations of  $\text{Sr}^{2+}$  and  $\text{SO}_4^{2-}$  in Aqueous Extract Across the Sequence Passwang Fm – Opalinus Clay – Staffelegg Fm in Borehole BDB-1.**



Notes: Squeezed water data from Mazurek et al. (2016); displayed is only the lowest pressure water.

**Figure 8-11: Molar  $\text{Sr}/\text{SO}_4$  Ratio vs  $\text{Cl}^-$  Concentration in Aqueous Extract Solutions and Squeezed Water of Samples from the Opalinus Clay and Staffelegg Fm in Borehole BDB-1.**



Notes: Squeezed water data from Mazurek et al. (2016); displayed is only the lowest pressure water.

**Figure 8-12: Molar Sr/SO<sub>4</sub> Ratio vs Cl<sup>-</sup> Concentration (closed symbols) and Saturation Index of Celestite (SI, open symbols) in Aqueous Extract Solutions and Squeezed Water of Samples from the Opalinus Clay and Stafflegg Fm in Borehole BDB-1.**

Combining all of the above observations, two different hypotheses may be formulated. First, dissolved sulphate in the aqueous extract solutions stems, to a large degree, from celestite dissolution during extraction; Sr is removed from the low-ionic strength solution by ion exchange and the SO<sub>4</sub><sup>-2</sup> and Sr<sup>+2</sup> concentrations of squeezed water represent more or less porewater concentrations. Second, the observed increase in SO<sub>4</sub> concentrations in the aqueous extract solutions from 0.719 mmol/L (69.1 mg/L) to 2.221 mmol/L (213.3 mg/L) appears to be associated with an increase in porewater SO<sub>4</sub> concentration, whereas the SO<sub>4</sub><sup>-2</sup> and Sr<sup>+2</sup> concentrations of squeezed water are potentially affected, to unknown degrees, by reactions before and during the squeezing procedure.

Based on ion-ion ratios and saturation states alone, the complexity of the system cannot be resolved, mainly because of the involvement of Sr in cation exchange reactions. One argument, however, favours the second hypothesis, as the degree of celestite dissolution in aqueous extract solutions would have to be different in the upper part compared to the lower part of the Opalinus Clay to explain the observed increase in SO<sub>4</sub><sup>-2</sup> with depth. This means that celestite would have to be present in different amounts in the upper and lower Opalinus Clay in order to allow complete dissolution in samples from the upper part, but only partial dissolution in samples from the lower part. For such a scenario, no support from mineralogical data is available.

Further support for the first hypothesis can be obtained from geochemical model calculations. Two different types of model calculations were performed with aqueous extract solutions and the adjacent squeezed water, with one sample each from the sandy, the carbonate-rich (no squeezed water available) and the shaly facies. Model calculations were performed with the

geochemical code PhreeqC using the Wateq4F thermodynamic database (Parkhurst and Appelo 1999; v. 2.18, 2011).

First, simulations were done using the measured aqueous extract solutions:

- The dilution of the porewater during aqueous extraction was simulated backwards in that the ultra-pure water added was removed stepwise until the water content of the sample was reached.
- The only constraint applied was calcite saturation at each step, as calculated for the aqueous extract solutions (*cf.* Appendix B3).
- The cation exchange capacity was that tabulated by Waber et al. (2003a) for the Opalinus Clay, normalised to the clay content of the BDB-1 sample used in the simulation, and adjusted for the extract conditions (*i.e.*, to 30 g of rock).
- During each step, the calculated exchange composition was updated and equilibrated with the solution for the following step.
- Selective coefficients used for cation exchange reactions were those of Mäder (2009). Except for  $K^+$ , these coefficients correspond to the generic coefficients used by Pearson et al. (2003).
- Celestite, gypsum and fluorite were allowed to precipitate, after saturation is attained, to derive the mineral amount possibly dissolved during extraction.
- During the extraction steps, closed-system conditions with respect to  $CO_2$  were maintained to simulate the extraction in the glovebox.
- The final solution was adjusted to a “best-guess” partial pressure of  $CO_2$  in the porewater to explore the effects of the carbonate system on the sulphur system (a  $\log pCO_2$  of -2.5 was applied; *cf.* Pearson et al. 2003).

Additional simulations were done using the measured aqueous extract solutions, but now modified with the  $SO_4^{-2}$  and  $Sr^{+2}$  concentrations measured in the squeezed water:

- Measured concentrations of  $SO_4^{-2}$  and  $Sr^{+2}$  of squeezed water were calculated to match the dilution induced by the aqueous extraction.
- The other solute concentrations and pH were those of the aqueous extract solutions. The resulting larger charge imbalance (about 10 % compared to <2 %) of the constructed solution was kept constant throughout all simulations.
- All other steps were identical to those performed for the non-modified aqueous extract solutions.

In these models, the final calculated Cl concentration matches that calculated from the Cl<sup>-</sup> concentration of the aqueous extract solutions normalised to the water content and, if scaled with the Cl-accessible porosity, to that of the squeezed waters. Comparison of the calculated exchange population with measured ones and judgement of the calculated mineral phase transfer were used as pro and cons to assess the two hypotheses described above. The results of the simulations are given in Table 8-2, illustrated for sample BDB1-221.28 in Figures 8-13 to 8-15, and summarised below.

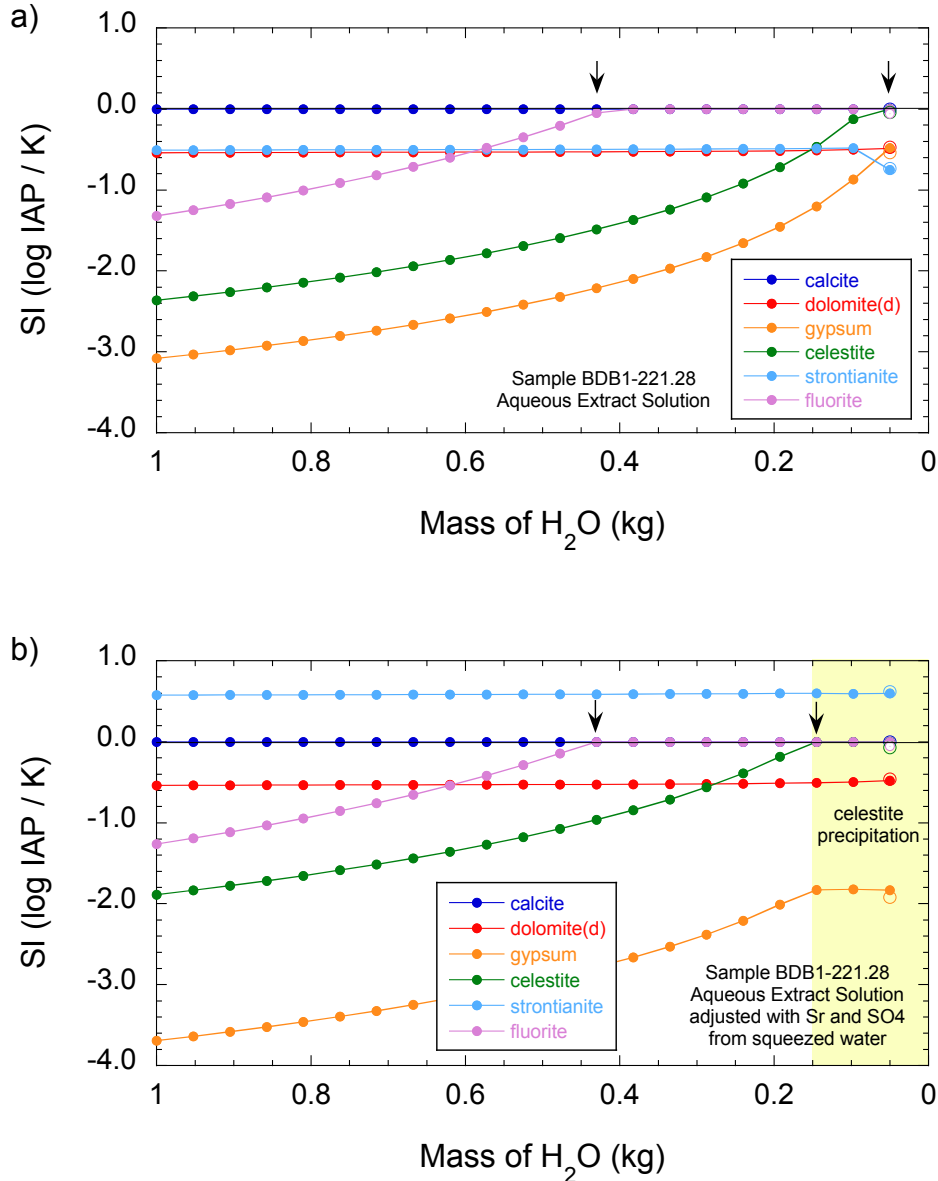
Using the aqueous extract data, the modelled exchangeable populations for Sr match those of measured Sr populations for the sandy and shaly facies of the Opalinus Clay. In contrast, modelled Sr populations overestimate the measured ones by a factor of 2 (sandy facies) to 23 (shaly facies) when using the  $\text{SO}_4^{-2}$  and  $\text{Sr}^{+2}$  of squeezed water. Aqueous extract solutions with the measured concentrations reach saturation with celestite just at or slightly before 100 % reduction of the water added in the extraction (i.e., essentially when back-calculated to their measured water content). In turn, aqueous extract solutions with  $\text{Sr}^{+2}$  and  $\text{SO}_4^{-2}$  concentrations adopted from the squeezed water reach saturation with celestite after 90–95 % reduction of the water added in the extraction (i.e., before their measured water content and in spite of the significantly lower  $\text{SO}_4^{-2}$  concentrations). The celestite mass transfer up to 100 % removal of water added is in the order of  $4\text{E-}05$  to  $8\text{E-}04$  mol/L, corresponding to about 0.01–0.25 wt.% of celestite per kg of rock. These amounts are too low to be detected by XRD techniques even if celestite is present at all in the rock matrix. Moreover, these amounts or molar  $\text{SO}_4$  contents, respectively, are orders of magnitude smaller than  $\text{SO}_4^{-2}$  concentrations measured in the aqueous extract solutions when converted to the same solid:liquid ratio at celestite saturation ( $1.4\text{E-}02$  –  $4.2\text{E-}02$  mol/L). Therefore, the effect of possible celestite dissolution during aqueous extraction is negligible. Note that the comprehensive occurrence of celestite in the rock matrix is still under debate and, more likely, Sr in the rock is associated with carbonate minerals and exchange sites, except for very localised occurrences of traces of Sr-Ba sulphate phases (e.g., Lerouge et al. 2010, 2014). For the aqueous extract solutions with  $\text{Sr}^{+2}$  and  $\text{SO}_4^{-2}$  concentrations adopted from the squeezed water, this indicates that a desiccation of only 5–10 % of the original porewater is sufficient to potentially precipitate celestite in the rock sample. None of the solutions attain saturation with gypsum, but all reach it with respect to fluorite. The mass transfers of fluorite are, however, even lower than those calculated for celestite.

The model results obtained for the measured aqueous extract solutions are more consistent with independent measured data than those using the  $\text{SO}_4^{-2}$  and  $\text{Sr}^{+2}$  concentrations of the squeezed water. This suggests that the  $\text{SO}_4^{-2}$  concentrations in the aqueous extract solutions are not substantially modified during extraction and represent a better proxy for the porewater concentration than those of the squeezed water. Consequently, the increase in  $\text{SO}_4^{-2}$  concentrations observed in the aqueous extract solutions from the top of the Opalinus Clay to the Stafflegg Fm also reflect an increase in the porewater  $\text{SO}_4^{-2}$  concentrations.

The above model calculations suggest that  $\text{SO}_4^{-2}$  and  $\text{Sr}^{+2}$  concentrations in squeezed water are affected by reactions before and/or during the squeezing procedure. Induced celestite saturation and precipitation is likely to occur in such samples given the fragility of the  $\text{SO}_4$ -Sr system and its connectivity with the carbonate system via reactions of calcite (by pressure solution and pH neutralisation reactions) and related cation exchange. Furthermore, squeezed samples are exposed for hours to days to the atmosphere, potentially leading to partial desiccation and, thus, passive enrichment of dissolved constituents. Enrichment of  $\text{SO}_4^{-2}$  by a factor of 7 (e.g., Traber 2004) was observed in aqueous extracts produced from Opalinus Clay samples collected along a profile from the tunnel wall into the undisturbed rock. The model calculations suggest that ~5 % evaporation is sufficient to reach celestite saturation. Such small desiccation is probably as difficult to suppress during the conditioning and squeezing of samples as is the suppression of induced mineral reactions and related cation exchange.

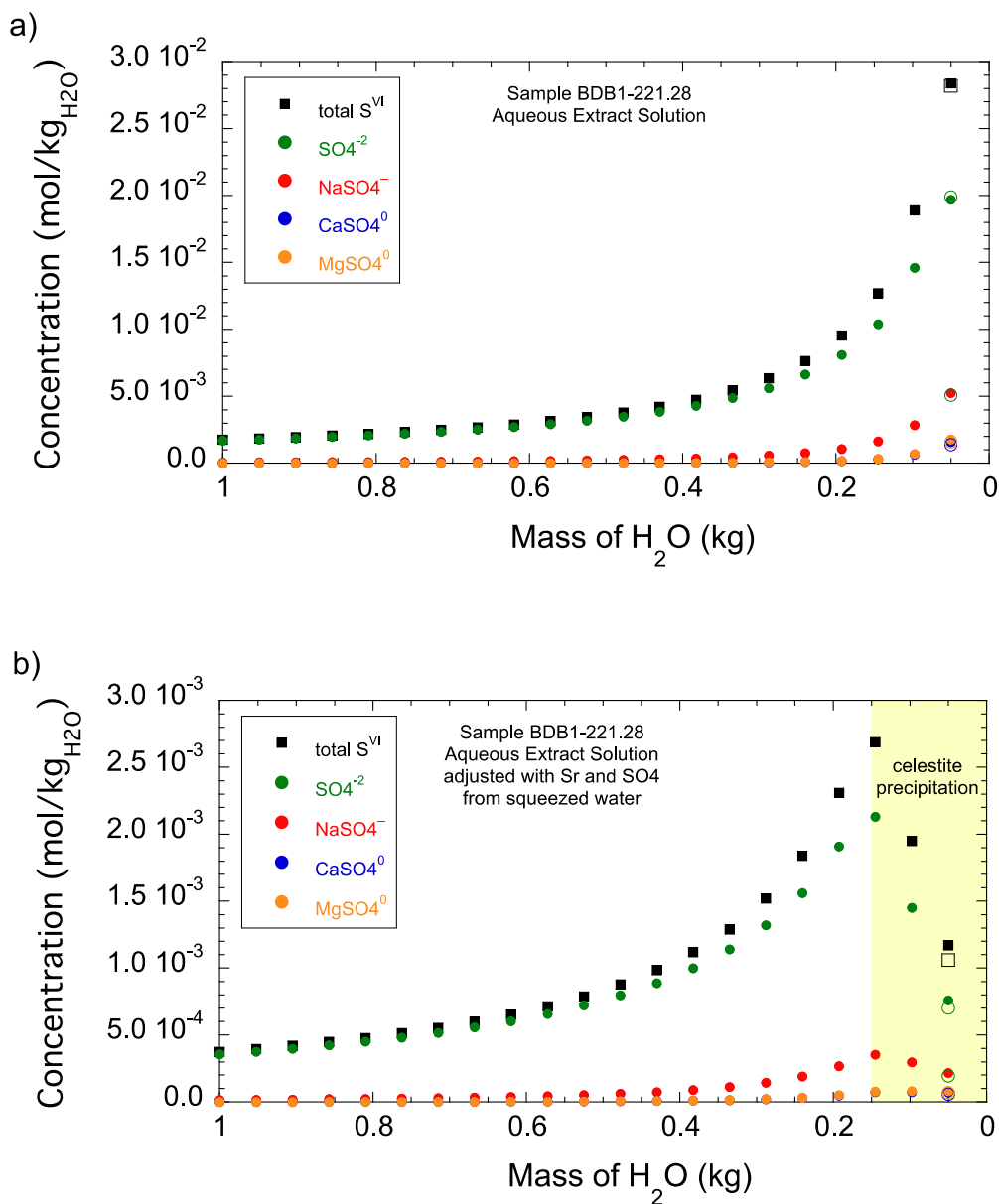
It remains a question why borehole waters of the BWS boreholes have  $\text{SO}_4^{-2}$  and  $\text{Sr}^{+2}$  concentrations similar to those of squeezed water. Again, the small amount of desiccation might be the answer. The BWS boreholes were drilled with pressurised air and the packer interval has remained gas-filled since. It is thus likely that in these boreholes celestite

precipitation controls the water finally accumulating in the intervals. Investigations of the borehole walls by aqueous extraction could shed more light on this issue.



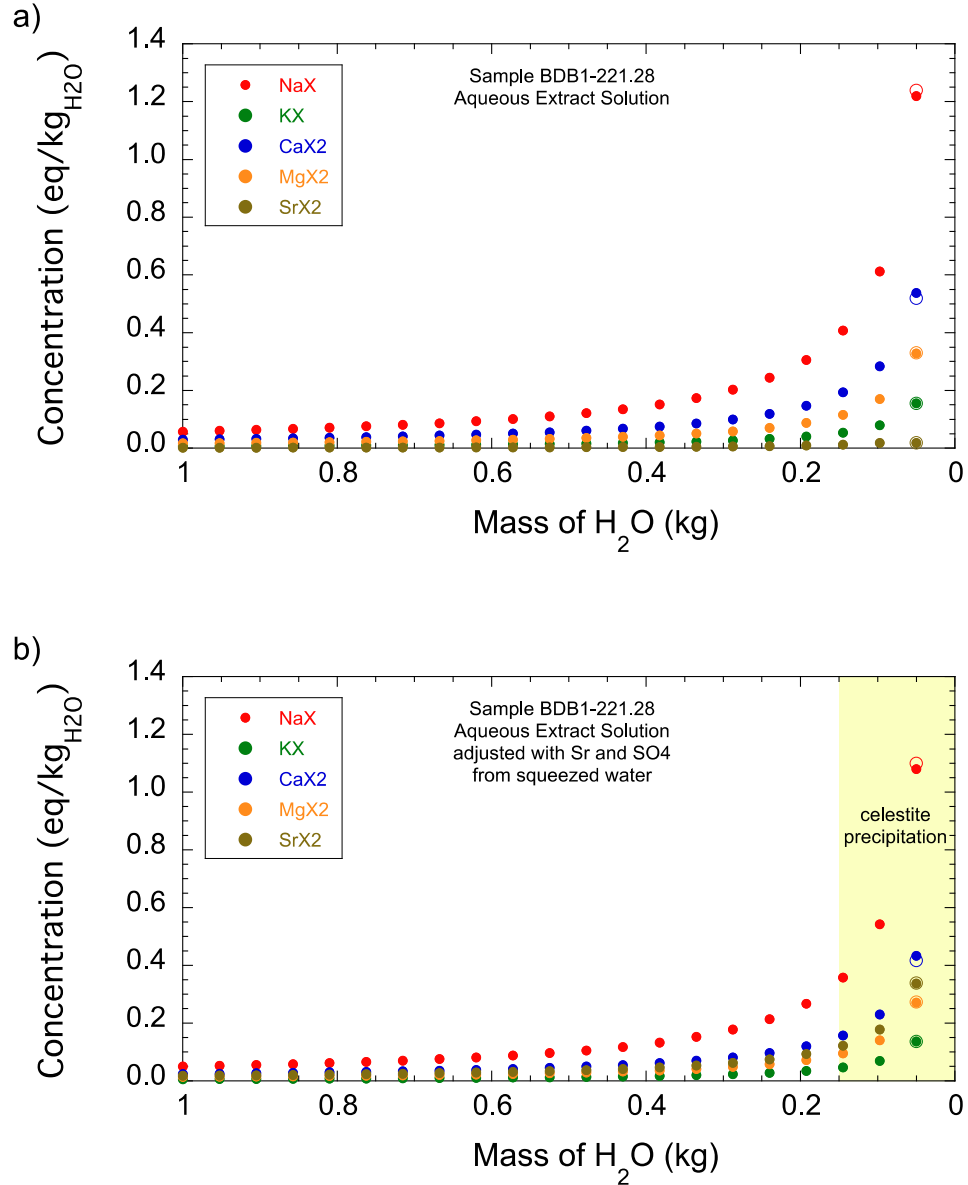
Notes: a) aqueous extract solution, b) aqueous extract solution with Sr and S<sup>VI</sup> from squeezed water adapted to the dilution used in aqueous extraction. Note that the aqueous solution just reaches celestite saturation at its measured water content (a) whereas this is reached earlier with Sr and S<sup>VI</sup> from squeezed water (b) during water removal. Open symbols indicate the adjustment of the final solution to a log pCO<sub>2</sub> of -2.5.

**Figure 8-13: Behaviour of Mineral Saturation Indices During Removal of Water from Aqueous Extract Conditions (mass H<sub>2</sub>O = 1) to the Measured Water Content of Sample BDB1-221.28.**



Notes: a) aqueous extract solution, b) aqueous extract solution with Sr and S<sup>VI</sup> from squeezed water adapted to the dilution used in aqueous extraction. Note and that dissolved concentrations of SO<sub>4</sub><sup>2-</sup> in the aqueous solution (a) are not affected during water removal in spite of much higher concentrations until the measured water content whereas these are lowered by celestite precipitation when Sr and S<sup>VI</sup> from squeezed water (b) are used. Open symbols indicate the adjustment of the final solution to a log pCO<sub>2</sub> of -2.5.

**Figure 8-14: Behaviour of Total Dissolved S and S-species During Removal of Water from Aqueous Extract Conditions (mass H<sub>2</sub>O = 1) to the Measured Water Content of Sample BDB1-221.28.**



Notes: a) aqueous extract solution, b) aqueous extract solution with Sr and  $S^{VI}$  from squeezed water adapted to the dilution used in aqueous extraction. Note the different sequence in exchanged cations in the final solution and the higher amount of exchanged  $Sr^{+2}$  when Sr and  $S^{VI}$  from squeezed water are used (b). Open symbols indicate the adjustment of the final solution to a log  $pCO_2$  of -2.5.

**Figure 8-15: Exchanged Cation Concentrations During Removal of Water from Aqueous Extract Conditions (mass  $H_2O = 1$ ) to the Measured Water Content of Sample BDB1-221.28.**

#### 8.6.4 Discussion and Summary About Origin of Sulphate

The BDB-1 borehole provided a unique opportunity to collect rock samples for porewater characterisation at a high frequency across the entire section from the Passwang Fm in the

hanging wall to the Staffelegg Fm in the footwall of the Opalinus Clay. Equal time periods for individual samples for collection, storage time and preparation in the laboratory aimed to minimise induced artefacts. Combined with the high frequency of samples, this allows a more sound interpretation of chemically reactive dissolved components, such as sulphate.

Evaluation of ion-ion ratios, comparison with independent parameters and observations, and geochemical modelling exercises reveal that the observed increase in  $\text{SO}_4^{-2}$  concentrations in aqueous extract solutions of rock samples from the Opalinus Clay to the Staffelegg Fm mimic an increase in porewater  $\text{SO}_4^{-2}$  concentrations. Model calculations indicate that the effect of celestite dissolution are minimal and below the analytical uncertainty of the chemical analyses. Rapid sample processing (maximum exposure of sample material to air of 5 minutes) ensures minimal oxidation of sulphur-minerals (e.g., pyrite) for the aqueous extraction technique.

The present study does not attempt to derive the  $\text{SO}_4^{-2}$  concentration of the porewater itself. In contrast to  $\text{Cl}^-$  and  $\text{Br}^-$  this cannot be done by simple back-calculation of  $\text{SO}_4^{-2}$  concentrations measured in aqueous extract solutions to a  $\text{SO}_4^{-2}$ -accessible porosity. This because at the elevated ionic strength of the porewater,  $\text{SO}_4^{-2}$  does not only occur as free ion, but up to 40 % or more also as monovalent or neutral complexes. Nevertheless, it can be stated that the porewater in the Opalinus Clay at Mont Terri has higher  $\text{SO}_4^{-2}$  concentrations than observed in borehole water and squeezed water and that the porewater concentrations might surpass 4 g/L at the bottom of the Opalinus Clay.

As shown in Figure 8-16, the  $\text{SO}_4/\text{Cl}$  and  $\text{Br}/\text{Cl}$  ratios of aqueous extract solutions from the Opalinus Clay and Staffelegg Fm lie between those of seawater and deep, evolved groundwater from the Triassic Keuper and Muschelkalk aquifers in Switzerland. Such groundwaters typically have  $\text{Br}/\text{Cl}$  ratios lower than seawater and a large range of  $\text{SO}_4/\text{Cl}$  ratios, depending on their evolution and the amount of halite dissolution (e.g., Waber et al. 2014). Porewater in these lithologies can be expected to have similar ion-ion ratios to the groundwater and to be at or close to equilibrium with the surrounding rock. A possible scenario for the elevated  $\text{SO}_4^{-2}$  concentrations and  $\text{SO}_4/\text{Cl}$  and  $\text{Br}/\text{Cl}$  ratios observed in the aqueous extract solutions of rocks from the Opalinus Clay and Staffelegg Fm is the migration of ground- or porewater from these underlying lithologies into the overlying argillaceous Jurassic units. Notably, exchange of  $\text{SO}_4^{-2}$  between the low-permeability rocks of the Opalinus Clay and Staffelegg Fm (or "Lias", respectively) has also been proposed for the Benken site in Northern Switzerland based on similarly elevated  $\text{SO}_4/\text{Cl}$  ratios in aqueous extract solutions and evidence from porewater isotope compositions (Nagra 2001; Waber et al. 2003b).

Two processes are envisaged to account for migration of  $\text{SO}_4^{-2}$  from underlying evaporite layers into the Opalinus Clay. These are exchange by diffusion along concentration gradients over extended geologic time periods, and upward migration of  $\text{SO}_4^{-2}$  induced by the folding and thrusting of the Jura Mountains.

Exchange by diffusion over extended geologic time essentially has started since the time of deposition of the sediments. The sabkha-type sediments of the Gipskeuper in Northern Switzerland contain abundant gypsum and anhydrite that has formed under subaqueous and supra-aqueous conditions, combined with eolian processes (Dronkert et al. 1990). Subaqueous precipitation occurs when the brine reaches gypsum saturation in shallow lagoons and isolated ponds. Supra-aqueous formation of sulphate minerals occurs through capillary enrichment of the porewater in such sabkha environments. In the Gipskeuper of Northern Switzerland, evaporation during the Gipskeuper seems not to have proceeded until the formation of halides, but such occurrences are known to occur in the French Jura (Dronkert et al. 1990). In any case,

evaporation of seawater-derived brines also results in enrichment of dissolved halides besides sulphate.

Since Liassic times, marine conditions prevailed (i.e., during the sedimentation of the Staffelegg Fm and the younger Opalinus Clay). The concentration of  $\text{SO}_4^{-2}$  in the initial porewater of these argillaceous rocks was that of seawater. Bacterial degradation of organic matter during the sedimentation phase resulted in reduction of  $\text{SO}_4^{-2}$  dissolved in porewater and the formation of the ubiquitous framboidal pyrite (and other minor sulphide phases). These processes continued during diagenesis until either the organic and/or the  $\text{SO}_4^{-2}$ -metal pools were exhausted. As a result, the  $\text{SO}_4/\text{Cl}$  was lowered compared to that of seawater. In addition, a strong chemical gradient was established in concentrations of  $\text{SO}_4^{-2}$  and  $\text{Cl}^-$  in porewater of the argillaceous, marine sediments and those of pore- and/or groundwater of the underlying sulphate-bearing Keuper lithologies. Such a gradient persists presently and it seems likely that diffusive exchange between these rock sequences occurred over Cretaceous and Tertiary times leading to upward migration of evaporite-derived  $\text{SO}_4^{-2}$  and  $\text{Cl}^-$  into the marine argillaceous rock sequences. During the two burial phases, such exchange would have increased, particularly diffusion in association with the elevated temperatures, and transport possibly could have included an advective component as well.

Alternatively, the upward migration of  $\text{SO}_4^{-2}$  (and  $\text{Cl}^-$ ) may have essentially been forced during the folding and thrusting of the Jura Mountains. Folding and thrusting seems likely to have resulted in expulsion of porewater from the central evaporite lithologies to the distal argillaceous lithologies in the anticline. At Mont Terri, such migration might have occurred sometime between 10.5 to 3 Ma ago (Becker 2000).

For both scenarios, it is unimportant if the source for  $\text{SO}_4^{-2}$  and  $\text{Cl}^-$  is porewater from diffusion-controlled, low-permeability evaporite sequences or from flowing groundwater in the continental sandy deposits of the Upper Keuper. Groundwater collected from these Upper Keuper lithologies (mainly Stubensandstein and Schilfsandstein) are known to have higher  $\text{SO}_4^{-2}$  concentrations and in many cases also higher  $\text{Cl}^-$  concentrations compared to those of the present-day Opalinus Clay porewater at the bottom of the formation (Biehler et al. 1993; Waber et al. 2014).

Both of these scenarios are further supported by the observed isotope composition of the water (*cf.* Chapter 10), dissolved  $\text{Cl}^-$  and its isotope composition (*cf.* Chapter 9), and the noble gas concentrations and isotopes in porewater (*cf.* Chapter 11). They are also consistent with model simulations of solute exchange between the Opalinus Clay and water-conducting zones in its hanging and footwall over the past few millions of years (Mazurek et al. 2011). However, these scenarios are inconsistent with the long-term scenario by Mazurek and de Haller (2017) who propose an infiltration of evaporated Tertiary seawater across the Jurassic limestone into the Opalinus Clay.

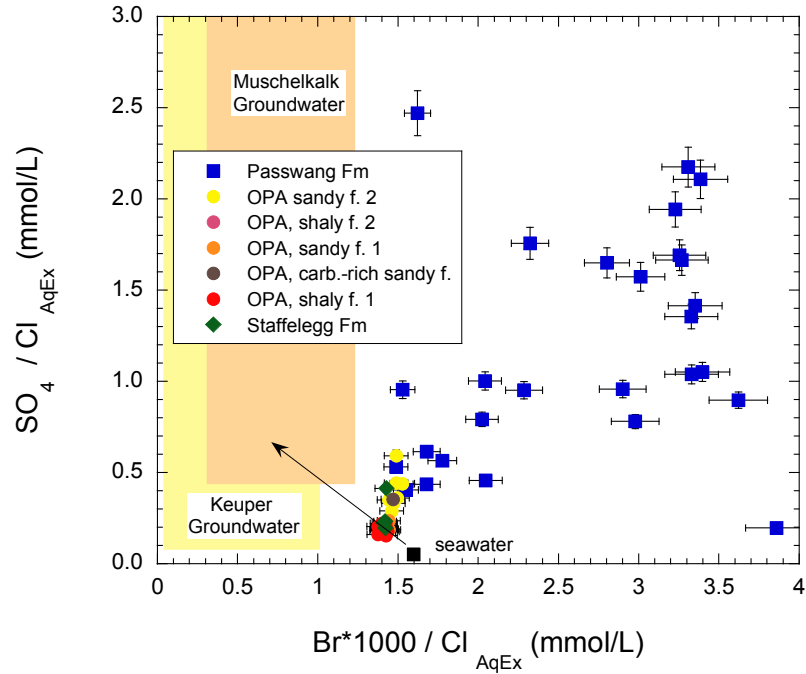


**Figure 8-16: Molar  $\text{Sr}/\text{SO}_4$  Ratio vs  $\text{Br}/\text{Cl}$  Ratios of Aqueous Extract Solutions of Rock Samples from Borehole BDB-1 and Compared to the Seawater Ratio and Ranges Given by Deep Groundwater in Triassic Lithologies.**

**Table 8-2: Modelled Ion Exchange Populations and Mineral Mass Transfer During Evaporation to Water-loss Porosity of Original Aqueous Extract Solutions and Aqueous Extract Solutions Adjusted with Sr<sup>+2</sup> and SO<sub>4</sub><sup>-2</sup> from Squeezed Water**

Sample	BDB1-114.80	BDB1-114.80	BDB1-115.35	BWS-E3	BDB1-189.71	BDB1-189.71	BWS-A6	BDB1-221.28	BDB1-221.28	BDB1-221.50	BWS-A6
OPA Facies	sandy facies 2	sandy facies 2	sandy facies 2	sandy facies 2	carbonate- rich sandy facies	carbonate- rich sandy facies	shaly facies 1	shaly facies 1	shaly facies 1	shaly facies 1	shaly facies 1
Type of solution	Aqueous Extract	mod. AqEx & SQ	Squeezed Water	Waber et al., 2003	Aqueous Extract	mod. AqEx & SQ	Waber et al., 2003	Aqueous Extract	mod. AqEx & SQ	Squeezed Water	Waber et al., 2003
<b>Concentrations in input solution</b>											
pH		9.08	9.08		8.28	–		8.96	8.96		
Na	mg/L	157	157		180	–		340.1	340.1		
K	mg/L	8.16	8.16		13.35	–		8.75	8.75		
NH <sub>4</sub>	mg/L	2.28	2.28		1.85	–		2.81	2.81		
Mg	mg/L	0.53	0.53		3.54	–		0.97	0.97		
Ca	mg/L	1.6	1.6		11.57	–		1.81	1.81		
Sr	mg/L	0.177	0.445		0.441	–		0.172	2.102		
F	mg/L	6.4	6.4		0.58	–		4.81	4.81		
Cl	mg/L	71.5	71.5		87.6	–		298.3	298.3		
Br	mg/L	0.24	0.24		0.29	–		0.94	0.94		
SO <sub>4</sub>	mg/L	85.8	21.1		83.9	–		178.5	44.2		
Alkalinity	meq/L	3.03	3.03		4.64	–		2.98	2.98		
<b>Concentrations at water-loss porosity</b>											
Cl		1774		1180	5666		7174	6307			7174
Br		6.0			18.8			19.9			
Sr		4.4			28.5			3.6			
SO <sub>4</sub>		2128			5425			3774			
<b>Concentrations in squeezed water</b>											
Cl				3245						11182	
Br				10.7						41.9	
Sr				10.7						36.1	
SO <sub>4</sub>				957.5						1658.1	
<b>Cation exchange capacity adjusted to clay content of samples</b>											
Total CEC	meq/kg <sub>rock</sub>	87	87		17	17		120	120		
<b>Concentrations in evaporated solution and in equilibrium with CEC (PhreeqC calculation)</b>											
Cl	mg/kg <sub>H<sub>2</sub>O</sub>	1721	1721		5672			5945	5945		
Br	mg/kg <sub>H<sub>2</sub>O</sub>	5.8	5.8		18.8			18.7	18.7		
Sr	mg/kg <sub>H<sub>2</sub>O</sub>	12.0	46.7		11.9			14.7	282		
SO <sub>4</sub>	mg/kg <sub>H<sub>2</sub>O</sub>	1354	409		4046			2745	136		
<b>Cation fractional occupancy in evaporated solution and in equilibrium with CEC</b>											
NaX	fraction	0.360	0.341	0.324	0.435		0.477	0.547	0.484		0.477
KX	fraction	0.087	0.083	0.103	0.075		0.067	0.069	0.060		0.067
CaX <sub>2</sub>	fraction	0.380	0.361	0.269	0.305		0.239	0.230	0.185		0.239
MgX <sub>2</sub>	fraction	0.150	0.144	0.263	0.181		0.179	0.146	0.121		0.179
SrX <sub>2</sub>	fraction	0.023	0.071	0.041	0.004		0.009	0.008	0.150		0.009
<b>Mass transfer during evaporation to water-loss porosity</b>											
Calcite	mg/kg <sub>H<sub>2</sub>O</sub>	49	45		38			50	49		
Celestite	mg/kg <sub>H<sub>2</sub>O</sub>	0	7.9		0			0	72		
Fluorite	mg/kg <sub>H<sub>2</sub>O</sub>	0	12.9		0			0	9.5		
Gypsum	mg/kg <sub>H<sub>2</sub>O</sub>	0	0		0			0	0		

## 9. POREWATER CHEMICAL CONCENTRATIONS

Solute concentrations of the in-situ porewater have to be derived differently depending on their chemical nature. Chemically conservative (mobile) elements can be calculated from aqueous extract concentrations using their in-situ accessible porosity (geochemical or ion-specific accessible porosity; e.g., Pearson 1999; Pearson et al. 2003; Appelo et al. 2008, 2010). The ion-specific accessible porosity can be assessed in different ways. Most straightforward is the comparison of the concentrations of conservative solutes in aqueous extract solutions with those in experimental solutions obtained from high-pressure squeezing or advective displacement technique or long-term in-situ sampling. This comparison delivers the fraction of water-loss porosity that is accessible, or rather inaccessible, to the solute (e.g., Pearson 1999; Pearson et al. 2003). More demanding are approaches using diffusion experiments with HTO traced water and different solutes in the laboratory or in-situ (e.g., HTO and  $\text{Cl}^-$ ; e.g., van Loon et al. 2003, 2005; van Loon and Mibus 2015) or theoretical approaches using geochemical modelling strategies that account for the effects of the diffusive double layer in clay minerals (e.g., Appelo et al. 2008, 2010).

Concentrations of all reactive compounds in the porewater have to be assessed by geochemical modelling. Different approaches of equilibrium modelling to derive the complete in-situ porewater composition in the Opalinus Clay at Mont Terri have been conducted (e.g., Pearson et al. 2003; Mäder 2009). For the porewater in the rocks of the Passwang and Stafflegg Fm, however, such model approaches are still pending. The derivation of the complete porewater compositions is also outside the scope of the present report.

Based on comparison of concentrations of conservative solutes in aqueous extract solutions with those of water collected over long time periods from boreholes and/or water squeezed under high pressure, Pearson et al. (2003; Table A10.4) derived an average fraction of the water-loss porosity accessible to  $\text{Cl}^-$  of  $0.57 \pm 0.06$ . Based on early data from Mont Terri, Pearson (1999) suggested an average fraction of  $0.54 \pm 0.04$ . Pearson et al. (2003) also recognised differences between the different facies, with the largest variation for individual samples observed for the shaly facies (fraction between 0.50 and 0.74). This large variation was partly ascribed to artefacts and a bias toward the larger number of samples available from the shaly facies.

Comparison of  $\text{Cl}^-$  concentrations in aqueous extract solutions and water squeezed at the lowest pressure from samples collected adjacent in the BDB-1 borehole (data from Mazurek et al. 2017) delivers ranges of the  $\text{Cl}^-$  accessible porosity fraction of 0.53–0.59 for the sandy facies ( $n=3$ ) and 0.54–0.61 for the shaly facies ( $n=4$ ). The average values calculated for the sandy and shaly facies were used here to convert  $\text{Cl}^-$  concentrations in aqueous extract solution to porewater  $\text{Cl}^-$  concentrations according to equation (17). The same procedure was applied to the  $\text{Br}^-$  concentrations.

Such average values for the  $\text{Cl}^-$  accessible porosity fraction is, however, inapplicable for the rocks of the carbonate-rich sandy facies of the Opalinus Clay and the Passwang Fm, which have significantly lower clay contents. Data from squeezed water from the Passwang Fm are only available at very high pressure (300–500 MPa; Mazurek et al. 2017), at which induced artefacts are well known to occur (e.g., Waber and Oyama 2000; Fernández et al. 2003; Mazurek et al. 2017). In the absence of direct information, Waber (2005, 2010) proposed

scaling of the experimentally-derived Cl<sup>-</sup>-accessible porosity fraction with the clay content for clay-poor rocks such as sandy marl, sandstone and limestone.

Unfortunately, neither the total clay content, nor the clay mineralogy, nor an estimate of the clay content based on geophysical logging, is available for a large section across the Passwang Fm in borehole BDB-1. Therefore, an alternative solution was chosen: the anion-accessible porosity is a function of the diffusive double layer thickness on clay minerals. This thickness depends on the type of clay as well as on the ionic strength of the porewater. A trend is commonly observed between the anion-accessible porosity and the clay content, with the anion-accessible porosity becoming larger at lower clay contents. The rocks of the BDB-1 borehole display rather small variation in the clay mineralogy and there exists a well-developed correlation between clay content and water content in the Opalinus Clay, and indication for such correlation to be applicable to rocks of the Passwang Fm (*cf.* Chapter 6 and 7). In the absence of additional data, the Cl<sup>-</sup> accessible porosity fraction in the rocks of the Passwang Fm and the carbonate-rich sandy facies were estimated based on their water content. Clay-poor samples, with water-loss porosity between 5 wt.% and 15 wt.%, were assigned a Cl<sup>-</sup> accessible porosity fraction of 0.7, and those with water-loss porosity <5wt.% with one of 0.9. It is recognised that the uncertainty introduced by this approach is considerable; however, the general trends in the spatial distribution of porewater Cl<sup>-</sup> concentrations across the Passwang Fm are captured using this approach because the rather low porewater Cl<sup>-</sup> concentrations in most of the Passwang Fm are not strongly affected by the scaling factor (see sections 9.1 and 9.4).

## 9.1 CHLORIDE CONCENTRATIONS IN POREWATER

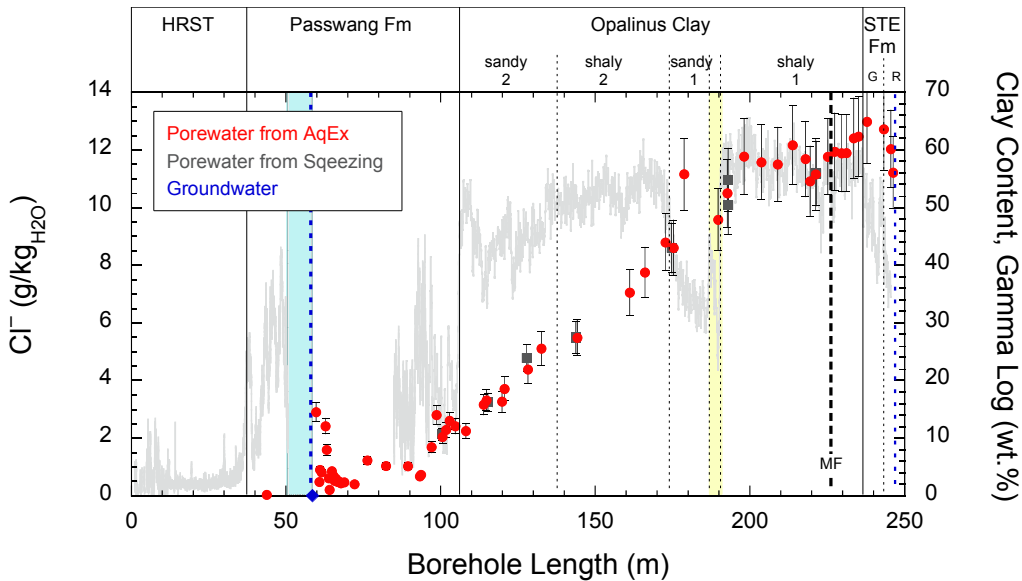
Porewater Cl<sup>-</sup> concentrations derived from aqueous extraction data and the Cl<sup>-</sup>-accessible porosity vary between 36 mg/kg<sub>H<sub>2</sub>O</sub> and 2,904 mg/kg<sub>H<sub>2</sub>O</sub> in the Passwang Fm, between 2,251 mg/kg<sub>H<sub>2</sub>O</sub> and 12,463 mg/kg<sub>H<sub>2</sub>O</sub> in the Opalinus Clay and between 11,201 mg/kg<sub>H<sub>2</sub>O</sub> and 12,973 mg/kg<sub>H<sub>2</sub>O</sub> in the Staffelegg Fm (Table 9-1).

In the Passwang Fm, porewater Cl<sup>-</sup> concentrations display an irregular spatial distribution without correlation to the clay content or other lithological characteristics (Figure 9-1). This irregular distribution is not associated with the estimated scaling factor for the Cl<sup>-</sup>-accessible porosity, as the same pattern is apparent when using the water-loss porosity without scaling. At least some of the variation has to be attributed to the lack of knowledge of the in-situ accessible porosity for Cl<sup>-</sup> (or anions in general) in these rocks. However, concentration differences may reach more than a factor of 2 on the metre scale, which seems difficult to obtain by differences in anion-accessible porosity alone. More likely, a significant contribution is due to the heterogeneity of the hydraulic properties of the rock formation that did not allow establishment of a well-defined diffusion profile, as observed for the more homogenous Opalinus Clay. This is also indicated by the disequilibrium between the groundwater collected at 58.6 m BHL and the porewater samples closest to this water-conducting zone. Whereas the sample adjacent to the water-conducting zone (BDB1-59.75) appears to have been impacted by the drilling process and water sampling campaign, the following samples have more than ten times higher Cl<sup>-</sup> concentrations than the groundwater (Figure 9-1, Table 9-1). If real, such high gradients could indicate too short of a time for exchange with the sampled groundwater to attain equilibrium, or exchange with a differently composed groundwater at a different location. This issue will be explored in more detail in the following Sections and Chapters.

In the Opalinus Clay, porewater Cl<sup>-</sup> concentrations increase from the bottom of the Passwang formation rocks to the top of shaly facies 1 in an almost linear manner from about 2.2 g/kg<sub>H<sub>2</sub>O</sub> to

about 11.7 g/kg<sub>H<sub>2</sub>O</sub> before they reach some sort of a plateau that extends into the Staffelegg Fm (Figure 9-1). The plateau extends across the Main Fault in the Opalinus Clay without notable change in Cl<sup>-</sup> concentrations outside the propagated uncertainty band. This suggests that no fluid of a Cl<sup>-</sup> concentration different from that of the porewater has percolated into the Main Fault in more recent geological times. The small excursion toward lower values in two samples just above the Main Fault might, however, indicate that, at a certain time in the past, in the evolution of the porewater Cl<sup>-</sup> concentration profile, fluid with lower Cl<sup>-</sup> concentration did percolate into the Main Fault. Notably, Cl<sup>-</sup> concentrations obtained from aqueous extract solutions in this area match those of squeezed water (Figure 9-1).

Porewater Cl<sup>-</sup> concentrations derived from aqueous extraction of Opalinus Clay rock samples compare well with those obtained by squeezing for the differently composed facies. This supports the approach of specific Cl<sup>-</sup>-accessible porosity fractions for the different facies. The necessity of sample-specific Cl<sup>-</sup>-accessible porosity fractions seems to be indicated by one sample of sandy facies 1 and the carbonate-rich sandy facies. Calculated with the average Cl<sup>-</sup>-accessible porosity fraction for the sandy facies, sample BDB1-178.73 obtains a Cl<sup>-</sup> porewater concentration that is outside of the uncertainty band and above the concentration profile given by the other samples (Figure 9-1). All isotope tracer results (i.e., δ<sup>18</sup>O, δ<sup>2</sup>H, δ<sup>37</sup>Cl) for this sample show no evidence of excursion and fall on the trend lines given by surrounding samples (cf. Figure 9-3 and Chapter 10). This suggests that the average Cl<sup>-</sup>-accessible porosity fraction for the sandy facies is too low for this sample and the lithology at this location has a somewhat larger anion-accessibility. This is consistent with the clay content of this sample (25 wt.%) compared to the average of the sandy facies of about 40 ± 8 wt.% (cf. Chapter 6).



Notes: Error bars are propagated error for Cl<sup>-</sup> derived from aqueous extraction and ±10 % for squeezed water concentrations. The grey curve displays the clay content estimated from the gamma log.

**Figure 9-1: Chloride Concentrations in Porewater Across the Passwang Fm, Opalinus Clay and Staffelegg Fm in Rock Samples from Borehole BDB-1 at the Mont Terri URL.**

Less clear is the small excursion of the  $\text{Cl}^-$  porewater concentration obtained for sample BDB1-189.71 of the carbonate-rich facies. This  $\text{Cl}^-$  concentration seems to be below the concentration profile given by the other samples, but is within the propagated uncertainty band. However, the sample has also  $\delta^{18}\text{O}$  and  $\delta^2\text{H}$  values that fall off the general trend (*cf.* Chapter 10) and elevated total He and Ar concentrations (*cf.* Chapter 11). In the absence of porosity-independent data, it cannot be decided if this somehow aberrant behaviour of different, independent tracers can be attributed to the sample's very low water-loss porosity (4.17 vol.%) and clay content (8 wt.%), or if it has to be attributed to circulation of a differently composed fluid in the carbonate-rich sandy facies over some time period.

Porewater in the Staffelegg Fm displays the highest overall  $\text{Cl}^-$  concentrations between about 11.2 g/kg<sub>H<sub>2</sub>O</sub> and 12.9 g/kg<sub>H<sub>2</sub>O</sub>. Porewater concentrations seem to slightly increase from the bottom of the Opalinus Clay into the Gross Wolf Member before they appear to slightly decrease in the Riethelm Member. These trends are, however, within the propagated uncertainty of the data and not really conclusive. This further means that the lower boundary of the  $\text{Cl}^-$  concentration profile in porewater across the Opalinus Clay was not encountered in borehole BDB-1.

Borehole BDB-1 did not encounter a water-conducting zone in the Staffelegg Fm, but was terminated due to moist zones in the Riethelm Member (former Posidonia shale) around 244 m BHL. It is unknown, but well conceivable, that this moist zone corresponds to that observed at the tunnel level. There, the tunnel construction allowed discharge of previously stagnant,  $^3\text{H}$ -free water with a  $\text{Cl}^-$  concentration of about 8.5 g/L in December 1988 (Gautschi et al. 1993). Some 18 months later, the same seepage water contained  $^3\text{H}$  and the concentration had dropped to about 2 g/L (*cf.* Figure 6.3 in Bath et al. 2003). The only porewater sample at this location is an aqueous extract solution that delivers a porewater  $\text{Cl}^-$  concentration of about 8.3 g/L (Waber et al. 2003) and thus seems to have been in equilibrium with the stagnant seepage water (*cf.* Figure 6.1 in Bath et al. 2003). A similar observation was made in a short borehole drilled some 14 m away from the above location in the Riethelm Member (former Posidonia shale) where the seepage water was  $^3\text{H}$ -bearing already at its first collection in 1998 and  $\text{Cl}^-$  concentration dropped from about 1 g/L to 0.25 g/L by 1999 (Griffault et al. 2003).

Further down in the footwall of the Opalinus Clay, observation points for porewater and seepage water are limited to two locations in the tunnel. The first is located in the Obtusus Clay where a porewater  $\text{Cl}^-$  concentration of around 4 g/kg<sub>H<sub>2</sub>O</sub> was derived from squeezed water and aqueous extraction data (*cf.* Figure 6.3 in Bath et al. 2003). The second location is located in the Gryphaea limestone at the interface of the Staffelegg Fm with the evaporate lithologies of the Keuper. There, water seeps at variable flow rates and  $\text{Cl}^-$  concentrations vary between 0.01 g/L – 1.3 g/L (Griffault et al. 2003); aqueous extraction data indicate similarly low  $\text{Cl}^-$  concentrations (Waber et al. 2003 and Figure 6.3 in Bath et al. 2003). This location is commonly regarded as the lower boundary of the solute concentration profiles across the Opalinus Clay. At the tunnel level, these two locations are about 50 m distant from the lower boundary of the Opalinus Clay. Converted to the BDB-1 borehole depths, the interface of the Staffelegg Fm – Keuper might be expected some 40 m BHL deeper than the maximum depth of BDB-1.

To conclude, porewater  $\text{Cl}^-$  concentrations in borehole BDB-1 describe a well-defined profile across the Opalinus Clay with the upper boundary condition in the Passwang being poorly defined with respect to locality, and the lower boundary in the Staffelegg Fm (or lower) being

undefined. The concentration profile yields no indication that the lower boundary would be near the bottom depth of the borehole.

**Table 9-1: Concentrations of Cl<sup>-</sup> and Br<sup>-</sup> from Aqueous Extract Solutions Calculated to the Water-loss Porosity and to Porewater Concentrations Using Facies-specific Anion-accessible Porosity**

Sample	Depth	Strati- graphie	Member / Facies	Lithology	Cl @ WL-P	prop.	Br @ WL-P	prop.	Cl PW @	prop.	Br PW @	prop.	Anion- accessible Porosity fraction	$\delta^{37}\text{Cl}$ PW	
					(mg/L)	error	(mg/L)	error	facies Cl-P	error	facies Cl-P	error		% SMOC	1 $\sigma$
	m BHL				mg/kg <sub>H2O</sub>		% SMOC	% SMOC							
BDB1-36.19	36.19	HRST	Brüggli - Mb.	sa lst	1005	52	10.16	0.53	1117	126	11.28	1.27	0.90		
BDB1-43.78	43.78	PAF	Waldenburg - Mb.	sa lst	20	1	b.d.	b.d.	36	4	b.d.	b.d.	0.54		
BDB1-59.75	59.75	PAF	Waldenburg - Mb.	sa lst	2614	131	22.74	1.14	2904	325	25.26	2.82	0.90	-0.74	0.22
BDB1-60.79	60.79	PAF	Waldenburg - Mb.	sa lst	261	13	1.71	0.09	483	54	3.16	0.35	0.54	-0.52	0.21
BDB1-61.00	61.00	PAF	Waldenburg - Mb.	sa lst	636	32	4.27	0.21	908	102	6.10	0.68	0.70		
BDB1-61.52	61.52	PAF	Waldenburg - Mb.	sa lst	442	22	3.32	0.17	819	92	6.15	0.69	0.54		
BDB1-62.80	62.80	PAF	Waldenburg - Mb.	lst	2179	109	17.79	0.89	2421	271	19.76	2.21	0.90		
BDB1-63.15	63.15	PAF	Waldenburg - Mb.	lst	1116	56	8.55	0.43	1594	178	12.21	1.37	0.70		
BDB1-63.80	63.80	PAF	Waldenburg - Mb.	sa lst	427	21	3.20	0.16	610	68	4.57	0.51	0.70		
BDB1-64.11	64.11	PAF	Waldenburg - Mb.	sa lst	146	7	1.10	0.05	209	23	1.56	0.17	0.70		
BDB1-64.88	64.88	PAF	Waldenburg - Mb.	lst	771	39	5.61	0.28	857	96	6.23	0.70	0.90		
BDB1-65.34	65.34	PAF	Waldenburg - Mb.	lst	489	24	3.69	0.19	698	78	5.28	0.59	0.70		
BDB1-65.70	65.70	PAF	Waldenburg - Mb.	sa lst	367	18	2.80	0.14	524	59	4.00	0.45	0.70		
BDB1-66.15	66.15	PAF	Waldenburg - Mb.	sa lst	418	21	3.08	0.15	597	67	4.40	0.49	0.70		
BDB1-66.70	66.70	PAF	Waldenburg - Mb.	sa lst	339	17	2.53	0.13	484	54	3.61	0.40	0.70		
BDB1-67.30	67.30	PAF	Waldenburg - Mb.	sa lst	343	17	1.25	0.06	490	55	1.8	0.20	0.70		
BDB1-67.80	67.80	PAF	Waldenburg - Mb.	sa lst	233	12	1.71	0.09	432	48	3.17	0.35	0.54		
BDB1-68.90	68.90	PAF	Waldenburg - Mb.	sa lst	329	16	2.23	0.11	470	53	3.19	0.36	0.70		
BDB1-72.20	72.20	PAF	Waldenburg - Mb.	sa lst	220	11	1.39	0.07	407	46	2.57	0.29	0.54	-0.85	0.31
BDB1-76.30	76.30	PAF	Himichopf - Mb.	sa lst	861	43	4.51	0.23	1230	138	6.44	0.72	0.70	-0.71	0.16
BDB1-82.30	82.30	PAF	Himichopf - Mb.	lst	726	36	3.74	0.19	1037	116	5.34	0.60	0.70	-1.01	0.33
BDB1-89.45	89.45	PAF	Himichopf - Mb.	li sst	557	28	2.56	0.13	1031	115	4.75	0.53	0.54		
BDB1-93.24	93.24	PAF	Himichopf - Mb.	sa ma	365	18	1.26	0.06	676	76	2.33	0.26	0.54	-0.44	0.18
BDB1-93.65	93.65	PAF	Himichopf - Mb.	sa ma	395	20	1.33	0.07	732	82	2.45	0.27	0.54		
BDB1-97.10	97.10	PAF	Sissach - Mb.	lst	1182	59	5.45	0.27	1688	189	7.79	0.87	0.70		
BDB1-98.68	98.68	PAF	Sissach - Mb.	sa lst	2521	126	11.51	0.58	2801	313	12.78	1.43	0.90	0.37	0.11
BDB1-100.63	100.63	PAF	Sissach - Mb.	sa ma	1433	72	5.74	0.29	2048	229	8.20	0.92	0.70		
BDB1-101.80	101.80	PAF	Sissach - Mb.	sa ma	1600	80	6.05	0.30	2286	256	8.65	0.97	0.70		
BDB1-102.93	102.93	PAF	Sissach - Mb.	sa ma	1403	70	4.90	0.25	2597	290	9.07	1.01	0.54		
BDB1-104.78	104.78	PAF	Sissach - Mb.	sa ma	1307	65	4.95	0.25	2420	271	9.16	1.02	0.54		

**Notes:**

See text for derivation of anion-accessible porosity fraction; shaded samples were used for inter-laboratory comparison. PW = porewater, WL-P = Water-loss porosity; Cl-P = chloride-accessible porosity; values in italics are less reliable due to analytical problems. PAF = Passwang Formation, OPA = Opalinus Clay, STF = Staffelegg Formation. Field lithology after Hostettler et al. (2017): li sst = limy sandstone, sa ma = sandy marl, lst = limestone; sa lst = sandy limestone, clst = claystone, silt clst = silty claystone, clst & lst la = claystone with limestone layers, clst & sst la = claystone with sandstone layers, arg ma = argillaceous marl, bit ma = bituminous marl.

Table 9-1: (cont.)

Sample	Depth	Stratigraphie	Member / Facies	Lithology	Cl @ WL-P	prop. error	Br @ WL-P	prop. error	Cl PW @ facies Cl-P	prop. error	Br PW @ facies Cl-P	prop. error	Anion-accessible Porosity fraction	$\delta^{37}\text{Cl PW}$	$1\sigma$
					(mg/L)		(mg/L)		(mg/L)		(mg/L)			% SMOC	% SMOC
					mg/kg <sub>H2O</sub>										
BDB1-108.24	108.24	OPA	sandy facies 2	clst & lst la	1207	60	4.15	0.21	2251	252	7.75	0.87	0.54	0.98	0.11
BDB1-113.88	113.88	OPA	sandy facies 2	clst & lst la	1694	85	5.69	0.28	3160	353	10.61	1.19	0.54		
BDB1-114.80	114.80	OPA	sandy facies 2	clst & lst la	1774	89	5.95	0.30	3310	370	11.11	1.24	0.54		
BDB1-119.86	119.86	OPA	sandy facies 2	clst & lst la	1752	88	5.70	0.29	3268	365	10.63	1.19	0.54		
BDB1-120.68	120.68	OPA	sandy facies 2	clst & lst la	1989	99	6.60	0.33	3712	415	12.32	1.38	0.54		
BDB1-128.24	128.24	OPA	sandy facies 2	clst & lst la	2351	118	7.74	0.39	4387	490	14.45	1.62	0.54	1.27	0.18
BDB1-132.63	132.63	OPA	sandy facies 2	clst & lst la	2739	137	9.24	0.46	5110	571	17.23	1.93	0.54		
BDB1-144.17	144.17	OPA	shaly facies 2	silt clst	3366	168	10.80	0.54	5486	613	17.60	1.97	0.61	1.36	0.11
BDB1-161.18	161.18	OPA	shaly facies 2	silt clst	4328	216	13.75	0.69	7054	789	22.40	2.50	0.61	1.21	0.17
BDB1-166.08	166.08	OPA	shaly facies 2	silt clst	4759	238	15.36	0.77	7755	867	25.03	2.80	0.61		
BDB1-172.70	172.70	OPA	shaly facies 2	silt clst	5394	270	17.23	0.86	8790	983	28.08	3.14	0.61	1.01	0.13
BDB1-175.33	175.33	OPA	sandy facies 1	clst & sst la	5086	254	16.55	0.83	8601	962	27.99	3.13	0.59		
BDB1-178.73	178.73	OPA	sandy facies 1	clst & sst la	6595	330	21.47	1.07	11154	1247	36.31	4.06	0.59	1.07	0.08
BDB1-189.71	189.71	OPA	carb.-rich sandy f.	lst	5666	284	18.76	0.94	9583	1072	31.74	3.55	0.59		
BDB1-192.68	192.68	OPA	shaly facies 1	clst	5935	297	19.07	0.95	10496	1174	33.71	3.77	0.57	0.97	0.16
BDB1-198.13	198.13	OPA	shaly facies 1	clst	6655	333	20.65	1.03	11768	1316	36.51	4.08	0.57		
BDB1-203.68	203.68	OPA	shaly facies 1	clst	6546	327	21.18	1.06	11575	1294	37.44	4.19	0.57	0.92	0.20
BDB1-209.00	209.00	OPA	shaly facies 1	clst	6501	325	20.88	1.04	11496	1285	36.93	4.13	0.57		
BDB1-213.85	213.85	OPA	shaly facies 1	clst	6879	344	21.94	1.10	12163	1360	38.79	4.34	0.57	1.08	0.15
BDB1-217.98	217.98	OPA	shaly facies 1	clst	6609	331	20.91	1.05	11686	1307	36.97	4.13	0.57		
BDB1-219.49	219.49	OPA	shaly facies 1	clst	6170	309	19.79	0.99	10911	1220	35.00	3.91	0.57		
BDB1-221.28	221.28	OPA	shaly facies 1	clst	6307	315	19.88	0.99	11153	1247	35.15	3.93	0.57		
BDB1-225.18	225.18	OPA	shaly facies 1	clst	6652	333	20.63	1.03	11763	1315	36.47	4.08	0.57		
BDB1-227.43	227.43	OPA	shaly facies 1	clst	6750	338	21.51	1.08	11936	1335	38.04	4.25	0.57	1.10	0.07
BDB1-229.68	229.68	OPA	shaly facies 1	clst	6720	336	21.27	1.06	11883	1329	37.61	4.21	0.57		
BDB1-231.18	231.18	OPA	shaly facies 1	clst	6727	336	21.22	1.06	11895	1330	37.52	4.20	0.57		
BDB1-233.63	233.63	OPA	shaly facies 1	clst	7017	351	22.60	1.13	12407	1387	39.97	4.47	0.57	0.99	0.06
BDB1-235.14	235.14	OPA	shaly facies 1	clst	7048	352	22.15	1.11	12463	1394	39.17	4.38	0.57	0.93	0.04
BDB1-237.88	237.88	STF	Gross Wolf Mb.	arg ma	7337	367	23.52	1.18	12973	1451	41.58	4.65	0.57		
BDB1-243.37	243.37	STF	Gross Wolf Mb.	lst	8905	454	28.66	1.46	12721	1428	40.94	4.60	0.70	0.96	0.17
BDB1-245.54	245.54	STF	Rietheim Mb.	bit ma	6806	340	21.64	1.08	12035	1346	38.27	4.28	0.57	1.46	0.37
BDB1-246.34	246.34	STF	Rietheim Mb.	bit ma	6340	317	20.30	1.02	11210	1253	35.90	4.01	0.57	1.18	0.00

## 9.2 CHLORINE STABLE ISOTOPES ( $\delta^{37}\text{Cl}$ ) IN POREWATER

The stable isotope composition of chlorine is expressed as  $\delta^{37}\text{Cl}$  in per mil relative to the Standard Mean Ocean Water standard (SMOC). It serves as a tracer for the origin of  $\text{Cl}^-$  dissolved in porewater and the transport processes that such porewater was subjected to during its evolution. By definition, modern seawater has a  $\delta^{37}\text{Cl}$  value of 0 ‰ SMOC. Over Phanerozoic times the  $\delta^{37}\text{Cl}$  value of seawater remained essentially constant around this value with  $\delta^{37}\text{Cl} = 0.0 \pm 0.5$  ‰ SMOC (Eastoe et al. 2007). More recent investigations suggest, however, that while there is only a small variation in the  $\delta^{37}\text{Cl}$  value of seawater between 0 ‰ and 0.05 ‰ back to Cretaceous times, older seawater appears to have been significantly enriched in  $^{37}\text{Cl}$  with  $\delta^{37}\text{Cl}$  values between 0.1 ‰ and 0.15 ‰ SMOC during Jurassic and Triassic times, and  $>0.15$  ‰ SMOC during Palaeozoic times (Eggenkamp et al. 2016). Phanerozoic evaporite minerals in sedimentary basins around the globe typically vary within  $\pm 1$  ‰ of the seawater value, with a tendency toward positive enrichment in halite-dominated deposits (e.g., Eggenkamp et al. 1995; Eastoe et al. 2001, 2007). Larger variation in both directions is observed when including  $\text{Cl}^-$  from the potash facies and recrystallized halides. An even larger variation is introduced during transport of chloride in low-permeability rocks. Diffusion of  $\text{Cl}^-$  was observed to induce fractionation of the  $\text{Cl}^-$  isotopes up to several per mil (e.g., Desaulniers et al. 1986; Eggenkamp et al. 1994; Hendry et al. 2000; Waber et al. 2001; Gimmi and Waber 2004; Lavastre et al. 2005; Eggenkamp and Coleman 2009). Ion-filtration was theoretically shown to fractionate  $\text{Cl}^-$  isotopes (Phillips and Bentley 1987) and proposed to have occurred in nature (Waber et al. 2013).

Chlorine isotope data of porewater in the Opalinus Clay have been determined previously during the WS-Experiment (Coleman et al. 2000, 2003). These authors analysed the  $\text{Cl}^-$  stable isotope composition of aqueous extract solutions and water that accumulated in borehole over long periods of time. At a given location, the two types of solutions have overlapping  $\delta^{37}\text{Cl}$  values within the analytical uncertainty. The  $\delta^{37}\text{Cl}$  values display a rather symmetrically curved profile across the Opalinus Clay, ranging from +0.33 ‰ SMOC to +1.31 ‰ SMOC (*cf.* Figure A7.1 in Coleman et al. 2003). In the hanging wall of the Opalinus Clay, the Passwang Fm, a negative signature of  $-0.35$  ‰ SMOC was obtained for an extract solution, whereas the lowest value in the footwall stems from seepage water collected in the Riethelm Member (Posidonia Shale, respectively; erroneously labelled “JM” for Jurensis Marl) with a  $\delta^{37}\text{Cl}$  value of +0.14 ‰ SMOC.

### 9.2.1 Chlorine Isotopes During High-pressure Squeezing

In a feasibility study during the WS-Experiments at the Mont Terri URL, it was shown that step-wise squeezing (from 200 MPa to 500 MPa) of rock samples collected from the Opalinus Clay shaly facies in borehole BWS-A6 resulted in decreased  $\text{Cl}^-$  concentration in the squeezed water by about 25–30 % with increasing pressure (Waber & Oyama 2000; *cf.* also Fernández et al. 2003). Whereas the concentrations of  $\text{Cl}^-$  and  $\text{Br}^-$  appeared to be mainly affected by the squeezing layout and process, all other chemical compounds were affected by reactions in the rock and also with the material of the squeezing apparatus. Comparison with data obtained in other laboratories at lower pressure, but longer squeezing time suggested that the  $\text{Cl}^-$  concentration obtained for the first water squeezed does not only depend on pressure, but also on squeezing time, the time of pressure increments, and the geometry of the sample and squeezing device. In this respect it is important to recall that high-pressure squeezing delivers

only a fraction of the total porewater present in the core, in this case only about 12–14 %. Most important was the finding that squeezing under high-pressure of two samples collected adjacent to each other did not deliver identical concentrations of  $\text{Cl}^-$  and  $\text{Br}^-$ . Waber & Oyama (2000) interpreted this as an effect of the rock's mineralogy and texture in addition to the dependencies mentioned above. They concluded that squeezing under high-pressure will not, a priori, deliver the in-situ  $\text{Cl}^-$  and  $\text{Br}^-$  concentrations.

The processes leading to the observed decrease in concentrations of mobile elements during squeezing are complex and not yet understood in a quantitative way. Different working hypotheses, such as increased liberation of water bound in the diffusive double layer (DDL), ion-filtration, osmotic and diffusion processes, exist (e.g., Appelo 1977; Chilingarian et al. 1994; Fernández et al. 2014; Mazurek et al. 2015).

A second feasibility study conducted during the PC-C Experiment at the Mont Terri URL in 2004 attempted to shed some more light on this issue. In this previously not reported study, two adjacent samples collected from the shaly facies of the Opalinus Clay in borehole BPC-C1 were subjected to step-wise squeezing from 100 MPa to 500 MPa by T. Oyama at the CRIEPI laboratories. The samples were conditioned in the field and laboratory in the same way as the samples from borehole BWS-A6 (i.e., vacuum-sealed in the field, ambient conditions in the lab). However, the squeezing rig at CRIEPI was improved in the meantime with respect to dead volume, materials used in the sampling system of the rig, and a controlled atmosphere during squeezing. In this study, the  $\text{Cl}^-$  isotope composition was analysed for the first time on the small sample volumes of squeezed water in order to obtain information about the possible  $\text{Cl}^-$  isotope fractionation effects during high-pressure squeezing.

The results of these tests are given in Table 9-2 and shown in Figure 9-2. Due to the small volumes of squeezed water, total  $\text{Cl}^-$  concentrations were only analysed for the squeezed waters from sample BPC-C1-SQ2, whereas the total volume of squeezed water was used for the adaption of the  $\delta^{37}\text{Cl}$  analysis to small volumes at the University of Waterloo, Canada. For sample BPC-C1-SQ2, total  $\text{Cl}^-$  concentrations in water squeezed at 100 MPa are higher by about 7% compared to water squeezed at 200 MPa. An even larger decrease of about 26 % is observed for the  $\text{Br}^-$  concentrations obtained at 100 MPa and 200 MPa, although the  $\text{Br}^-$  data show irregular behaviour and seem less reliable.

The  $\text{Cl}^-$  and  $\text{Br}^-$  concentrations obtained at 100 MPa compare with the average values of shaly facies 1 from borehole BDB-1 ( $11,685 \pm 545 \text{ mg/kg}_{\text{H}_2\text{O}}$ ,  $37.1 \pm 1.7 \text{ mg/kg}_{\text{H}_2\text{O}}$ ,  $n=14$ ) which corresponds to the location of borehole BPC-C1 (Table 9-2). This suggests that the  $\text{Cl}^-$  and  $\text{Br}^-$  concentrations squeezed at 100 MPa are closer to the in-situ porewater composition compared to the water squeezed at 200 MPa. However, it has to be kept in mind that the concentrations calculated from the BDB-1 aqueous extract data are not an independent comparison, as they have been calculated using an anion-accessible porosity derived from squeezing data at 200 MPa. Accounting for the difference in  $\text{Cl}^-$  concentrations in squeezed waters from 100 MPa and 200 MPa, the anion-accessible porosity become lower and the  $\text{Cl}^-$  concentrations derived from aqueous extract concentration become larger. This indicates that the in-situ porewater  $\text{Cl}^-$  concentrations in borehole BDB-1 could be underestimated by about 7–10 %.

Support in this direction comes from the  $\text{Cl}^-$ -isotope data obtained during step-wise squeezing. In both samples from the BPC-C1 borehole, the  $\delta^{37}\text{Cl}$  values systematically decrease from about 0.6 ‰ SMOC in water squeezed at 100 MPa to about 0.2–0.3 ‰ SMOC in water squeezed at 500 MPa (Figure 9-2, Table 9-2). Interestingly, the  $\delta^{37}\text{Cl}$  value in water squeezed at 100 MPa is already lower by about 0.4 ‰ compared to the average value of aqueous extract

solutions of shaly facies 1 rock samples from borehole BDB-1 ( $1.0 \pm 0.08$  ‰ SMOC). This suggests that fractionation of  $\text{Cl}^-$  isotopes has already occurred in the very first squeezing step up to 100 MPa. Furthermore, the decrease in  $\delta^{37}\text{Cl}$  values in water squeezed at increasing pressure is opposite to what theory predicts for  $\text{Cl}^-$  isotope fractionation during ion-filtration (Phillips and Bentley 1987). These data, therefore, suggest that ion-filtration is not the dominant process producing the observed behaviour of  $\text{Cl}^-$  and its isotopes (and other porewater solutes) during squeezing of Opalinus Clay rock at increasing pressure.

**Table 9-2: Concentrations of  $\text{Cl}^-$ ,  $\text{Br}^-$  and  $\text{I}^-$  and  $\delta^{37}\text{Cl}$  of Water Squeezed at Different Pressures from Shaly Facies Opalinus Clay in Borehole BPC-C1**

Sample No	BHL (m)	Squeezing Pressure	Mass squeezed water g	Cl mg/kg <sub>H2O</sub>	Br mg/kg <sub>H2O</sub>	I mg/kg <sub>H2O</sub>	SO <sub>4</sub> mg/kg <sub>H2O</sub>	$\delta^{37}\text{Cl}$ ‰ SMOC
PC-C1-SQ1-0	12.55 - 12.77	100	syringe leak	n.a.	n.a.	n.a.	n.a.	0.62
PC-C1-SQ1-1	12.55 - 12.77	200	0.380	n.a.	n.a.	n.a.	n.a.	0.59
PC-C1-SQ1-2	12.55 - 12.77	300	0.788	n.a.	n.a.	n.a.	n.a.	0.54
PC-C1-SQ1-3	12.55 - 12.77	400	0.674	n.a.	n.a.	n.a.	n.a.	0.24
PC-C1-SQ1-4	12.55 - 12.77	500	0.688	n.a.	n.a.	n.a.	n.a.	0.23
PC-C1-SQ2-1	12.99 - 13.00	100	0.756	11461	39.2	1.040		0.61
PC-C1-SQ2-2	12.99 - 13.00	200	2.864	10624	29.1	1.595	1812	0.57
PC-C1-SQ2-3	12.99 - 13.00	300	1.348	9841	32.4	1.530	1831	0.56
PC-C1-SQ2-4	12.99 - 13.00	400	1.150	9303	29.9	1.605	1816	0.4
PC-C1-SQ2-5	12.99 - 13.00	500	1.127	8706	36.4	1.356	1662	0.31

Squeezing Time: Sample PC-C1-SQ1 from 10.5.-2.5.2004, sample PC-C1-SQ1 from 10.5.-2.6.2004

**Notes:**

Squeezing was performed by T. Oyama at CRIEPI, Japan, Cl and SO<sub>4</sub> analyses by IC at RWI, University of Bern, Switzerland, Br and I analyses by ICP-MS at BGS, Keyworth, UK, Cl-isotope analyses by MS at University of Waterloo, Canada.

### 9.2.2 Spatial Distribution of $\delta^{37}\text{Cl}$ in Porewater Across the Opalinus Clay

The stable isotope composition of chloride,  $\delta^{37}\text{Cl}$ , in aqueous extract solutions is suggested to represent that of the porewater, as extraction occurred with chloride-free water and Cl-bearing, readily-dissolvable minerals are not present in the rocks from the Passwang Fm to the Staffelegg Fm.

In porewater of the Passwang Fm,  $\delta^{37}\text{Cl}$  values range from -1.01 to +0.37 ‰ SMOC (Table 9-1). From the water-conducting zone at 58.6 m BHL, values tend to first increase and then decrease to about 80 m BHL, though the values do overlap within their uncertainty (Figure 9-3). From there to the Opalinus Clay interface  $\delta^{37}\text{Cl}$  becomes increasingly enriched and the  $\delta^{37}\text{Cl}$  values change from negative to positive.

The analysis of the groundwater collected from the water-conducting zone in the Passwang Fm is still pending. But the porewater sample adjacent to this zone has an identical negative  $\delta^{37}\text{Cl}$  value as seepage water from the Passwang Fm collected in the nearby borehole, BPC-C2. This suggests that the exchange between porewater and groundwater at this location is in steady-

state. However, further down in the Passwang Fm, more negative  $\delta^{37}\text{Cl}$  values occur, indicating a more complex behaviour than simple exchange between Opalinus Clay porewater and the present water-conducting zone (*cf.* Section 9.4).

In the Opalinus Clay porewater,  $\delta^{37}\text{Cl}$  values increase first from 1 ‰ to about 1.36 ‰ across sandy facies 2 into shaly facies 2 before they decline again and form a plateau with values around 1 ‰ down to the interface with the Staffelegg Fm (Figure 9-3; Table 9-1). The absolute  $\delta^{37}\text{Cl}$  values and their distribution across the Opalinus Clay is in general agreement and overlap within the uncertainty of those values reported by Coleman et al. (2003). In the two studies, different analytical protocols were used, and the overlap of the data provides evidence that the enrichment in  $^{37}\text{Cl}$  in the Opalinus Clay porewater by about 1 ‰ compared to the original seawater is real.

The plateau described by the  $\delta^{37}\text{Cl}$  values in the Opalinus Clay continues into the Gross Wolf Member of the Staffelegg Fm before more enriched values occur again in the Riethelm Member. However, the most enriched value at 245.54 m BHL shows large variation in the triplicate analysis, resulting in an uncertainty of  $\pm 0.37$  ‰ ( $1\sigma$ , Figure 9-3). Therefore, the present data are inconclusive as to whether or not an enrichment of  $^{37}\text{Cl}$  also occurs in the Staffelegg Fm. Further, the data neither support nor reject the decrease in  $\delta^{37}\text{Cl}$  values observed by Coleman et al. (2003; Fig. A7.1) in one aqueous extract sample and in seepage waters in the rocks of the Staffelegg Fm at the Mont Terri URL level.

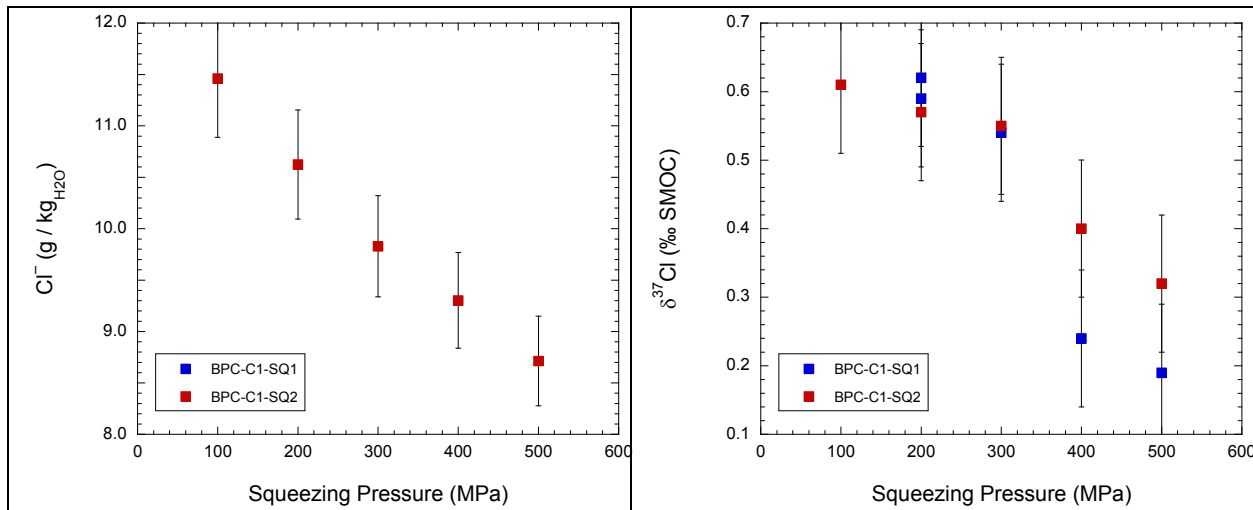
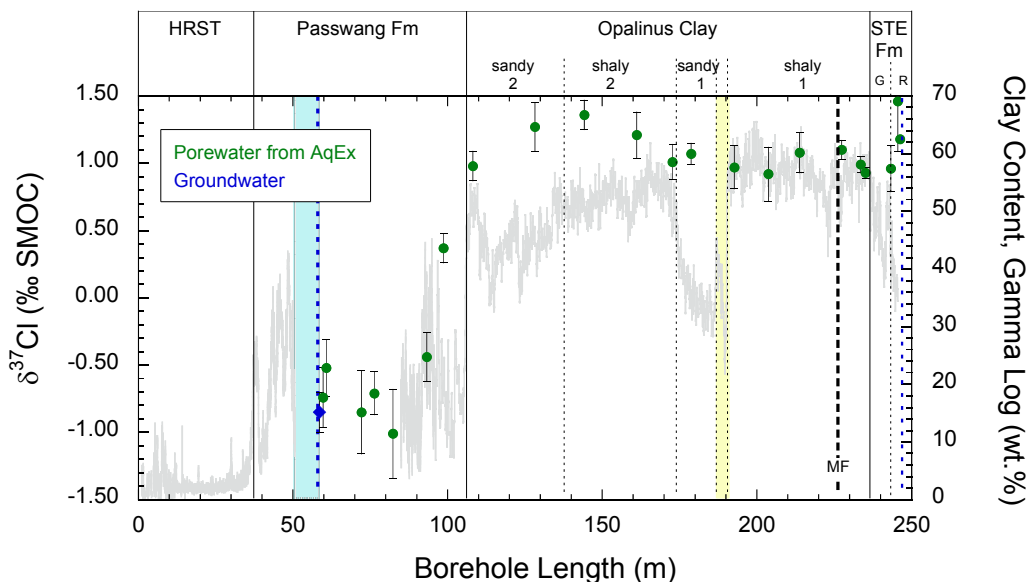


**Figure 9-2: Cl Concentration and  $\delta^{37}\text{Cl}$  of Water Squeezed Under Increasing Pressure of Two Rock Samples from Shaly Facies 1 of the Opalinus Clay in Borehole BPC-C1.**



Notes: Error bars are  $1\sigma$  of multiple measurements. The grey curve displays the clay content estimated from the gamma log.

**Figure 9-3: Chloride Stable Isotope Composition ( $\delta^{37}\text{Cl}$ ) in Porewater Across the Passwang Fm, Opalinus Clay and Staffelegg Fm in Rock Samples from Borehole BDB-1 at the Mont Terri URL.**

### 9.2.3 Evolution of $\delta^{37}\text{Cl}$ in Porewater Across the Opalinus Clay

Different processes may have resulted in the observed enrichment in  $^{37}\text{Cl}$  of dissolved  $\text{Cl}^-$  in porewater of the Opalinus Clay compared to its initial seawater value. These include fractionation during transport by diffusion, ion filtration of  $\text{Cl}^-$  across the Opalinus Clay, and/or migration of  $\text{Cl}^-$  already enriched in  $^{37}\text{Cl}$  into the Opalinus Clay.

Based on the  $\text{Cl}^-$  data alone it appears that ion filtration as a single process can hardly account for the observed distribution of  $\text{Cl}^-$  concentrations and isotope composition in the Opalinus Clay at Mont Terri. Whereas ion filtration is theoretically capable to enrich  $^{37}\text{Cl}$  in the residual solution in the low-permeability units to a large degree, it will also lead to an enrichment of the total  $\text{Cl}^-$  concentration. Present-day porewater in the Opalinus Clay at Mont Terri has, however, lower  $\text{Cl}^-$  concentration and higher  $\delta^{37}\text{Cl}$ -values compared to its initial porewater (i.e., seawater). If ion filtration would have been the major process responsible for the present-day chemistry, the Opalinus Clay porewater would have had to be replaced with dilute or moderately-mineralised water with a  $\delta^{37}\text{Cl}$  value of around 0 ‰ SMOC before filtration began. However, such groundwater types commonly have negative  $\delta^{37}\text{Cl}$  values (e.g., Koehler and Wassenaar 2010), and the degree of ion filtration to attain present  $\text{Cl}^-$  concentration and  $\delta^{37}\text{Cl}$  values would have to be unreasonably high. Thus, ion filtration alone seems an unlikely process to have produced the present-day situation in the Opalinus Clay at Mont Terri.

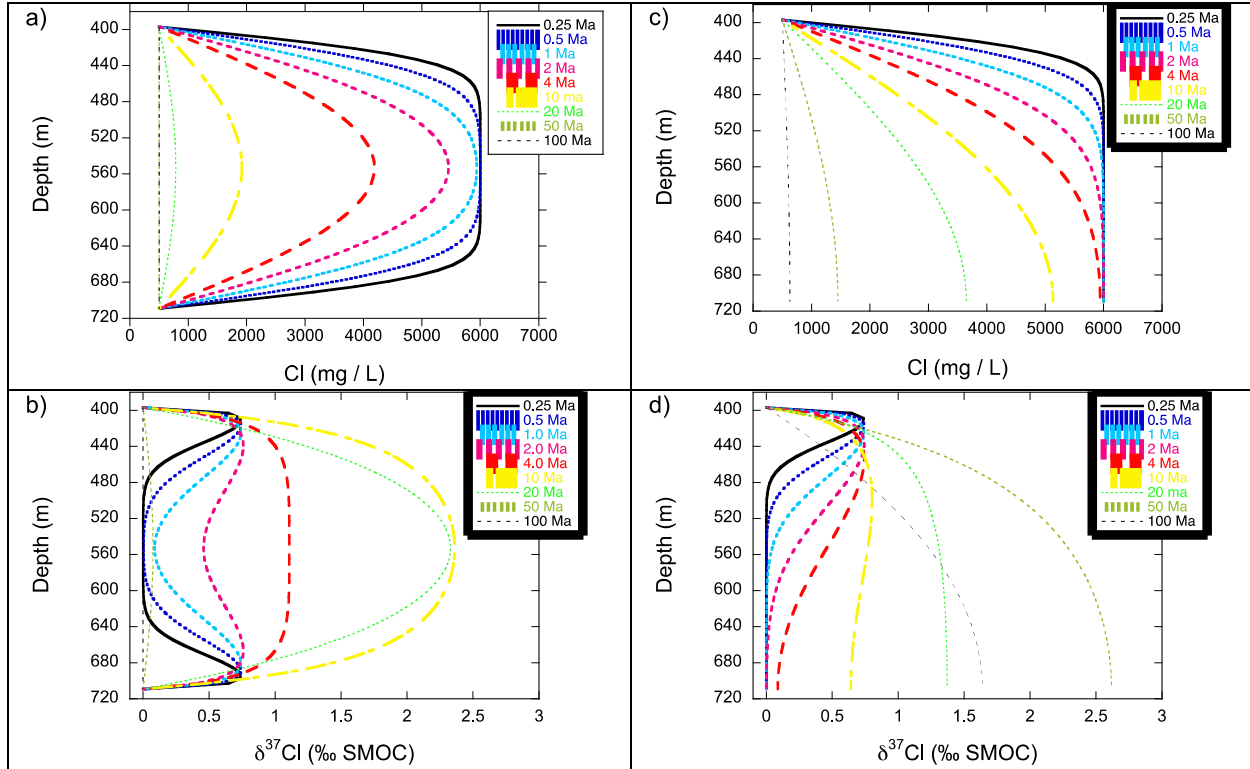
The spatial distribution of  $\delta^{37}\text{Cl}$  values across the Opalinus Clay mimics, quite nicely, the shape of a profile that would be generated over time by out-diffusion of  $\text{Cl}^-$  into bounding groundwater

with low  $\text{Cl}^-$  concentrations. As shown by Gimmi and Waber (2004) the diffusive exchange of porewater in a low-permeability formation and groundwater in adjacent aquifer(s) results in elevated  $\delta^{37}\text{Cl}$  values at the rims and a plateau of lower values in the centre of the low-permeability formation (Figure 9-4). With increasing time, the  $\delta^{37}\text{Cl}$  values will describe a simple curved profile with a maximum in the centre of the low-permeability formation similar to that of the total  $\text{Cl}^-$  concentrations. In the Opalinus Clay of borehole BDB-1 at the Mont Terri URL, such a profile seems to be developed toward the overlying Passwang Fm (Figures 9-1 and 9-3). The time period over which an enrichment in  $^{37}\text{Cl}$  evolves and persists at the interface of a low permeability rock unit to the bounding aquifer(s) is on the order of a few million years according to the theoretical calculation performed by Gimmi and Waber (2004) using the parameters of Opalinus Clay in the Benken borehole, Northern Switzerland (Figure 9-4a, b). However, over this time period, the enrichment in  $^{37}\text{Cl}$  in the centre of the low-permeability formation is lower than what is observed in the Opalinus Clay at Mont Terri. To obtain  $\delta^{37}\text{Cl}$  values of about 1 ‰ SMOC in the central part, an order of magnitude longer diffusion time would be required, and the enrichment of  $^{37}\text{Cl}$  at the rims would disappear. Similar arguments are indicated for one-sided diffusion (Figure 9-4c, d). It thus appears that the observed concentration profile of  $\text{Cl}^-$  and  $\text{Cl}^-$  isotopes in porewater of the Opalinus Clay at Mont Terri cannot be explained alone by out-diffusion of  $\text{Cl}^-$  toward the bounding aquifer.

Unfortunately, the lower boundary in the Staffelegg Fm or deeper was not encountered by borehole BDB-1 which prevents drawing conclusions as to whether or not out-diffusion occurs in both directions (e.g., upwards and downwards) or just upwards toward the Passwang Fm. In this context, it might be worth mentioning that the observed decline of porewater solute concentrations in the rocks of the Staffelegg Fm (or "Lias" in Pearson et al. 2003) is based on only two observation points with porewater samples and two water inflows at the tunnel level, the latter of which were both activated by the tunnel construction – as indicated by their evolution in  $\text{Cl}^-$  concentrations and  $^3\text{H}$  contents (cf. Pearson et al. 2003 and Griffault et al. 2003).

A third mechanism for enrichment of  $^{37}\text{Cl}$  in the porewater is the migration of  $\text{Cl}^-$  already enriched in  $^{37}\text{Cl}$  into the Opalinus Clay. Chloride enriched in the heavy isotope can be generated by the dissolution of halite- or other  $\text{Cl}^-$ -bearing minerals in evaporites (e.g., Eggenkamp et al. 1995). Such lithologies are known to occur below the Opalinus Clay in the Triassic Keuper and Muschelkalk units. For instance, halite from the "Salzlager" in the Middle Muschelkalk of Northern Switzerland has  $\delta^{37}\text{Cl}$  values of 0.07–0.69 ‰ SMOC ( $n=4$ ; Waber et al. 2003b). Dissolution of such halite and migration of a certain portion of saline water into the Opalinus Clay can, however, not explain the even more enriched porewater  $\delta^{37}\text{Cl}$  values observed today. Similarly, infiltration of evaporated seawater cannot explain the high values. Evaporation only leads to  $\text{Cl}^-$  isotope fractionation when salts start to precipitate and the residual water becomes depleted in  $^{37}\text{Cl}$ . It thus appears that the observed concentration pattern evolved from a combination of different mechanisms.

In this context, it is interesting to note that porewater in the Opalinus Clay in northern Switzerland has  $\delta^{37}\text{Cl}$  values of 0.37–0.52 ‰ SMOC in the central plateau and around 1 ‰ SMOC at the rims of the low-permeability rock sequence (Waber et al. 2003b; Gimmi and Waber 2004). This indicates that dissolved  $\text{Cl}^-$  and its isotope composition evolved differently in the Mont Terri area and in Northern Switzerland.



Notes: a) and b) constant concentrations on both sides of the low-permeability domain; c) and d) constant concentration at top and zero gradient at bottom. Boundary conditions:  $C_{Cl} = 500 \text{ mg/L}$ ,  $\delta^{37}\text{Cl} = 0$  at both sides in a) and b) and at top in c) and d).

**Figure 9-4: Theoretical Profiles of Chloride and  $\delta^{37}\text{Cl}$  During Diffusion Across a Low-permeability Rock Formation (from Gimmi and Waber 2004)**

To conclude, the  $\text{Cl}^-$  concentration and  $\text{Cl}^-$  isotope signature of porewater in the Oplains Clay at Mont Terri suggests a complex, multi-stage evolution that includes migration of  $\text{Cl}^-$  enriched in  $^{37}\text{Cl}$  into the formation before out-diffusion toward the bounding aquifer commenced. Porewater from an underlying evaporite formation might serve as a possible source for isotopically enriched  $\text{Cl}^-$ . Such a scenario could also help to explain the observed elevated  $\text{SO}_4$ -concentrations, as these evaporate formations contain abundant readily dissolvable sulphate mineral phases, and porewater is likely to be in equilibrium with these phases. A possible mechanism forcing such saline porewater upwards into the Opalinus Clay could have been the folding of the Jura Mountains. Once erosion established infiltration pathways for fresh water into the carbonate lithologies in the hanging wall and footwall, out-diffusion of  $\text{Cl}^-$  in the Opalinus Clay porewater was initiated, leading to the concentration profiles observed today. Such a scenario, however, can only further be resolved by applying transport model calculations, which are outside the scope of this study.

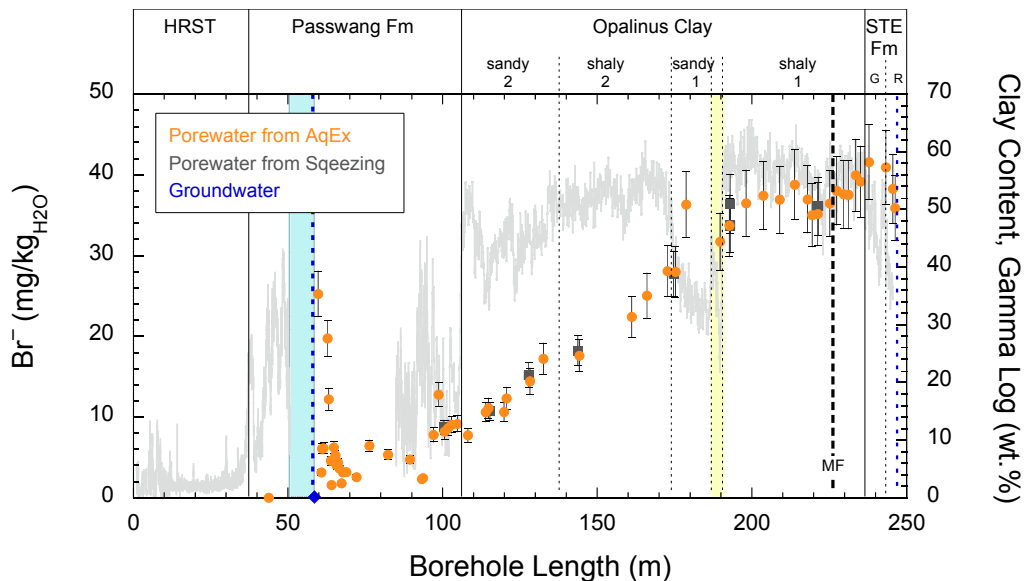
### 9.3 BROMIDE CONCENTRATIONS IN POREWATER

Dissolved bromine in aqueous solutions mainly occurs as bromide ( $\text{Br}^-$ ) and is generally considered to behave conservatively, just as dissolved  $\text{Cl}^-$ . Exceptions from this rule are

environments with elevated organic matter contents. There, bromine may be retarded by sorption and complexation with organic substances (e.g., Gilfedder et al. 2011).

So far, there is little or no evidence that dissolved bromide in porewater of the Opalinus Clay and lithologies in the hanging and footwall would not behave conservatively, and that it occurs mainly, if not exclusively, as dissolved  $\text{Br}^-$ . This allows treating the  $\text{Br}^-$  concentrations obtained from aqueous extract solutions in the same manner as the  $\text{Cl}^-$  concentrations. Furthermore, the  $\text{Br}/\text{Cl}$  ratio in aqueous extract solution corresponds to that of the porewater, as the concentrations of both components are calculated with the same water-loss porosity and anion-accessible porosity fraction. The latter is, however, still an assumption, as only limited direct data exist on the  $\text{Br}$ -accessible porosity. The same accounts for the diffusion coefficient of  $\text{Br}^-$  in the Opalinus Clay.

In the Passwang Fm, porewater  $\text{Br}^-$  concentrations vary in a similar way as the  $\text{Cl}^-$  contents and cover a large range between 1.6  $\text{mg}/\text{kg}_{\text{H}_2\text{O}}$  and 25.3  $\text{mg}/\text{kg}_{\text{H}_2\text{O}}$  (Figure 9-5). As for the porewater  $\text{Cl}^-$  concentrations, at least some of this scatter has to be attributed to the uncertainty attached to the anion-accessible porosity (*cf.* Section 1). Porewater  $\text{Br}^-$  concentrations close to the water-conducting zone are more than one order of magnitude higher than those in the groundwater, which has a  $\text{Br}^-$  concentration around the detection limit (*cf.* Chapter 12), indicating disequilibrium as already observed for  $\text{Cl}^-$ . Across the Passwang Fm, porewater  $\text{Br}^-$  concentrations correlate with the  $\text{Cl}^-$  concentrations, also with different slopes for different borehole metre sections (*cf.* Figure 8-6a). This results in molar  $\text{Br}/\text{Cl}$  ratios above 0.003 in the first decametre after the water-conducting zone before they continuously decrease to values below the molar  $\text{Br}/\text{Cl}$  ratio of seawater (*cf.* Fig. 8-7).



Notes: Error bars are propagated error for  $\text{Br}^-$  derived from aqueous extraction and  $\pm 10\%$  for squeezed water concentrations. The grey curve displays the clay content estimated from the gamma log.

**Figure 9-5: Bromide Concentrations in Porewater Across the Passwang Fm, Opalinus Clay and Staffelegg Fm in Rock Samples from Borehole BDB-1 at the Mont Terri URL.**

In the Opalinus Clay, porewater  $\text{Br}^-$  concentrations increase from the bottom of the Passwang Fm to the top of shaly facies 1 in an almost linear manner from about 7.6 mg/kg $_{\text{H}_2\text{O}}$  to about 33.7 mg/kg $_{\text{H}_2\text{O}}$  before they reach some sort of a plateau that extends into the Staffelegg Fm (Figure 9-5). Similar to what is observed for the  $\text{Cl}^-$  concentrations, porewater  $\text{Br}^-$  concentrations are identical across the Main Fault within the propagated uncertainty band and the  $\text{Br}^-$  concentrations obtained from aqueous extract solutions in this area match those of water squeezed at 150 MPa (Figure 9-5). Most remarkable is the fact that the  $\text{Br}/\text{Cl}$  ratios slightly, but constantly, decrease with increasing depth and are below the  $\text{Br}/\text{Cl}$  ratio of seawater from the top of shaly facies 2 down to the bottom of the Opalinus Clay (*cf.* Figure 8-7).

Porewater  $\text{Br}^-$  concentrations derived from aqueous extraction of Opalinus Clay rock samples compare well with those obtained for water squeezed at the lowest pressure (100–150 MPa) of adjacent samples in the differently composed facies. As observed for the  $\text{Cl}^-$  concentrations, porewater  $\text{Br}^-$  concentrations of samples BDB1-178.73, and to a lesser degree sample BDB1-189.71, fall off the general trend given by surrounding samples. As shown in Section 9.1, the deviation in sample BDB1-178.73 can most likely be attributed to the lack of the sample-specific anion-accessible porosity in the clay-poor sample rather than to ingress of differently composed water, as none of the isotope tracers of this sample displays an excursion from the general profile. In contrast, for sample BDB1-189.71, the  $\text{Br}^-$  concentration also may indicate a percolation of differently-composed water in the carbonate-rich sandy facies at some time in the evolution of the concentration profile, as indicated by the porewater  $\delta^{18}\text{O}$  and  $\delta^2\text{H}$  values and noble gas concentrations (*cf.* Section 9.1).

Porewater in the Staffelegg Fm displays the overall highest  $\text{Br}^-$  concentrations, around 41 mg/kg $_{\text{H}_2\text{O}}$  in the Gross Wolf Member adjacent to the Opalinus Clay before they tend to slightly decrease to 36 mg/kg $_{\text{H}_2\text{O}}$  in the Riethelm Member, similar to the  $\text{Cl}^-$  concentrations (*cf.* Section 9.1). As for the  $\text{Cl}^-$  concentrations, the trend is, however, within the propagated uncertainty of the data and not really conclusive, indicating that lower boundary of the porewater concentration profile across the Opalinus Clay was not encountered by borehole BDB-1. This is also supported by the  $\text{Br}/\text{Cl}$  ratio, which remains constant and below that of seawater across the entire rock section in the Staffelegg Fm (*cf.* Figure 8-7).

To conclude, porewater  $\text{Br}^-$  concentrations in borehole BDB-1 mimic the well-defined profile across the Opalinus Clay given by the porewater  $\text{Cl}^-$  concentrations, with  $\text{Br}/\text{Cl}$  ratios in porewater of the Opalinus Clay and the Staffelegg Fm that are below that of seawater and slightly, but consistently, decrease with depth.

#### 9.4 $\text{Cl}^-$ AND $\text{Br}^-$ ACROSS THE PASSWANG FM – OPALINUS CLAY INTERFACE

As mentioned in Section 9.1 and 9.3, the derivation of porewater concentrations of even the chemically conservative compounds, such as  $\text{Cl}^-$  and  $\text{Br}^-$ , is rather uncertain in rocks of the Passwang Fm. The reason is the poorly established anion-accessible porosity to-date for these rocks. In the absence of data about the mineralogy and total clay content, and the failure of squeezing to deliver water at low pressure, the anion-accessible porosity had to be estimated based on the water content for most of the samples of the Passwang Fm (*cf.* Section 9-1).

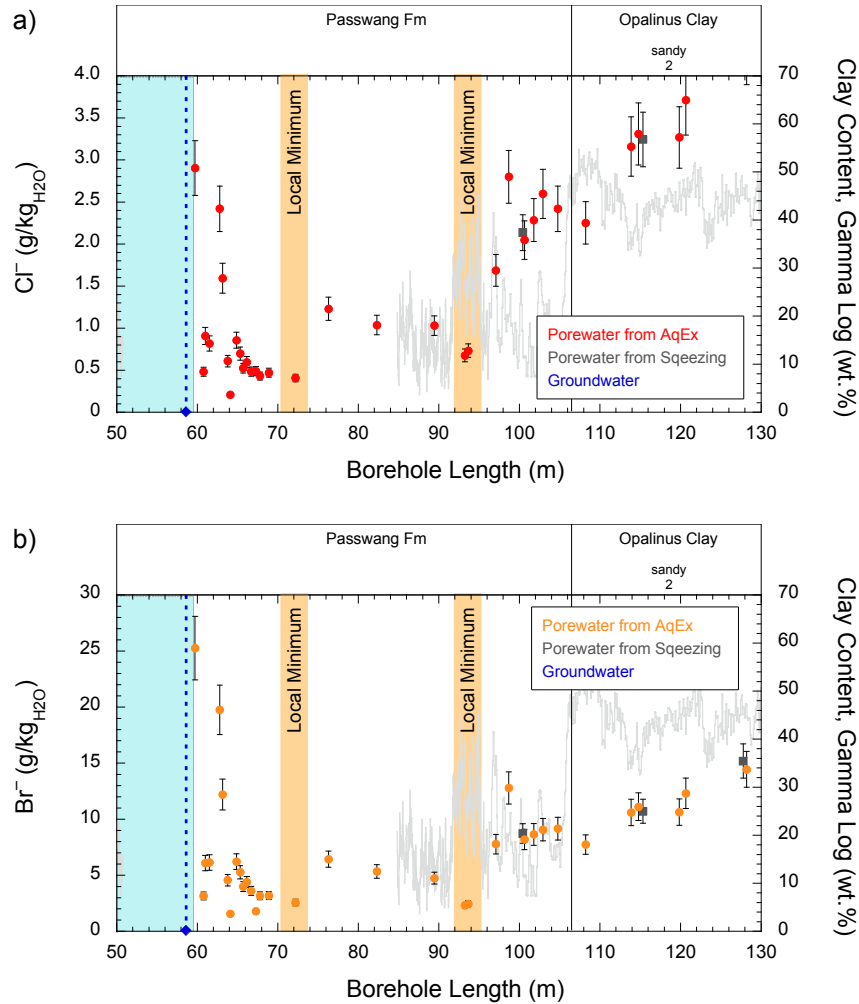
Nevertheless, some more or less supported statements can be made. Most supported is the established disequilibrium in  $\text{Cl}^-$  and  $\text{Br}^-$  concentrations between groundwater in the water conducting zone at 58.6 m BHL and the porewater samples in the adjacent 4 metres into the Passwang Fm. Porewater  $\text{Cl}^-$  and  $\text{Br}^-$  concentrations are higher by 2–3 orders of magnitude

when compared to the groundwater (Figure 9-6a, b). Such large differences cannot be explained by adjusting the anion-accessible porosity to a fraction of 1 (i.e., to the water-loss porosity). Similarly, elevated porewater concentrations observed at 62–63 m BHL appear to be real, as these persist when the aqueous extract concentrations are converted using the water-loss porosity. From 63 m BHL, there appears a general trend toward lower porewater  $\text{Cl}^-$  and  $\text{Br}^-$  concentrations down to a depth of about 72 m BHL, where these concentrations reach a minimum (Figure 9-6). From 72 m BHL down to the interface of the Opalinus Clay, the water-loss porosity of the porewater samples is above 5 vol.%, except for one sample at 98.68 m BHL. The value of 5 vol.% of water-loss porosity was used as a threshold value for applying a scaling factor of 0.7 (above 5 vol.%) and 0.9 (below 5 vol.%) for the anion-accessible porosity (*cf.* Section 9-1). Starting with about 5 times higher concentrations at 76 m BHL compared to the local minimum,  $\text{Cl}^-$  and  $\text{Br}^-$  concentrations first tend to decrease further down to about 93–94 m BHL before they gradually increase toward the interface to the values observed in the Opalinus Clay. The deviation toward higher values indicated for the sample at 98.68 m BHL might be associated with a scaling factor that is too high, as this sample was scaled using 0.9 compared to 0.7 (which was used for all other samples in this depth interval). An excursion toward higher concentrations would, however, still remain when using the lower scaling factor.

Porewater  $\text{Cl}^-$  and  $\text{Br}^-$  concentrations in the rocks of the Passwang Fm appear to have two local minima, one at around 72 m BHL and one at around 93–94 m BHL, and possibly a local maximum at around 98 m BHL (Figure 9-6a, b). It is interesting to note that, at two of these locations, an accumulation of open fractures was observed, though no moist zones were observed around 98 m BHL where borehole logs are available (*cf.* Section 6.3).

In the case of uncertain porosity values, isotope and ion-ion ratios are often better suited than total concentrations to evaluate concentration differences of dissolved solutes in porewater across a rock formation. Such ratios are independent of porosity and, thus, indicate true concentration variation in the porewater. Obviously, this is strictly only valid again for chemically conservative compounds, but ion-ion ratios of reactive compounds also can deliver some information.

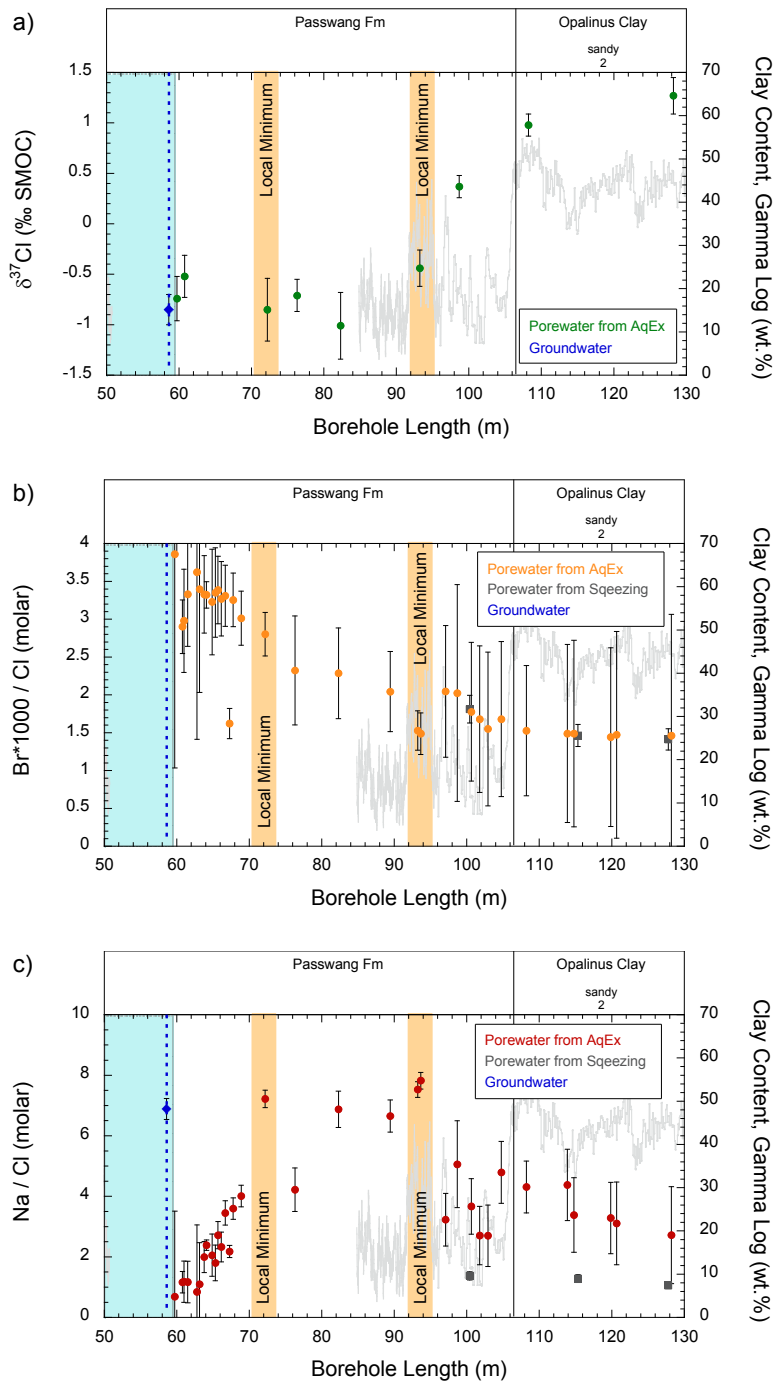
As shown in Figure 9-7a, porewater  $\delta^{37}\text{Cl}$  values do weakly support the local minimum indicated by the porewater  $\text{Cl}^-$  and  $\text{Br}^-$  concentrations at 72 m BHL, but not that at 98 m BHL, though they are not actually in contradiction due to the complexity of Cl isotope diffusion. In contrast to the total concentrations, however, porewater and groundwater at 58.6 m BHL have equal  $\delta^{37}\text{Cl}$  values, indicating that the chloride in the groundwater stems from the porewater.



**Notes:** Note the local concentration minima suggested at 72 m and 98 m BHL. Error bar are propagated error for Cl, Br derived from aqueous extraction and  $\pm 10\%$  for squeezed water concentrations. The grey curve displays the clay content estimated from the gamma log.

**Figure 9-6: Close-up of the  $\text{Cl}^-$  (a) and  $\text{Br}^-$  (b) Concentrations in Porewater Across the Passwang Fm – Opalinus Clay Interface in Borehole BDB-1 at the Mont Terri URL.**

Molar ratios of Br/Cl in porewater do not show deviation from the general trend given around the local minimum at 72 m BHL. In turn, they tend to be lower at the minima located at 98 m BHL (Figure 9-7b). Interestingly, both localities with local minima indicated by the porewater  $\text{Cl}^-$  and  $\text{Br}^-$  concentrations also display differences in the molar Na/Cl ratio of the aqueous extract solutions (Figure 9-7c). The molar Na/Cl in porewater at these locations is similar to that in the groundwater at 58.6 m and significantly higher than in porewater of the Passwang Fm above and below, as well as higher than in the Opalinus Clay sandy facies 2 (Figure 9-7c).



Notes: Local minima are those indicated by the total Cl and Br concentrations. The grey curve displays the clay content estimated from the gamma log.

**Figure 9-7: Close-up of Cl-isotope Ratios ( $\delta^{37}\text{Cl}$ ) in Porewater (a) and Molar Br/Cl (b) and Na/Cl (c) Ratios in Aqueous Extract Solutions Across the Passwang Fm – Opalinus Clay Interface in Borehole BDB-1 at the Mont Terri URL.**

Total concentrations, isotopes and ion-ion ratios of porewater and aqueous extract solutions thus confirm that the rocks of the Passwang Fm cannot be regarded as a homogenous rock sequence such as the Opalinus Clay. Excursion in porewater concentration profiles associated with the occurrence of open fractures indicate that fluids of different compositions percolated into these zones over geologic time, or may even circulate at low velocity at present. Further support in this direction comes from the water stable isotope composition (*cf.* Chapter 10) and the porewater noble gas composition (*cf.* Chapter 11).

This renders the localisation of boundary conditions for the diffusive exchange between the Opalinus Clay and the overlying Passwang Fm difficult. The data indicate that the localities of the bounding water-conducting zone, and also the composition of the fluid in that zone, has varied over time scales of a few millions of years.

## 10. $\delta^{18}\text{O}$ and $\delta^2\text{H}$ IN POREWATER

The porewater stable water isotope composition was determined by the isotope diffusive exchange technique on a total of 63 samples across the profile from the Hauptrogenstein to the Staffelegg Fm in borehole BDB-1 (Table 10-1). Inspection of the many-fold experimental parameters revealed evaporation of two samples during the exchange experiments and these were excluded from further interpretation. The two samples consist of limestone layers from the Hauptrogenstein (BDB1-36-19) and Staffelegg Fm (BDB1-243.37) with water-loss porosities of less than 2 vol. %.

As discussed in Section 7.3.2, the water content obtained from the isotope diffusive exchange technique displays a systematic deviation of up to about 10 % compared to the gravimetric water content obtained by drying the originally saturated samples to stable weight conditions. The deviation is positively correlated with the total clay content and might be due to some exchange with water of different isotopic composition bound on the clay surfaces. However, the difference in water content is balanced by a change of not more than 0.1 ‰ in  $\delta^{18}\text{O}$  and 1 ‰ in  $\delta^2\text{H}$  in the porewater isotope composition. Such small change lies within the propagated uncertainty of the porewater  $\delta^{18}\text{O}$  and  $\delta^2\text{H}$  values ( $0.19 \pm 0.04$  ‰ and  $1.99 \pm 0.67$  ‰ VSMOW, respectively). Therefore, the  $\delta^{18}\text{O}$  and  $\delta^2\text{H}$  values obtained by the diffusive exchange technique can be regarded as very similar to the in-situ porewater isotope composition.

An important characteristic of the derivation of the porewater O- and H-isotope composition is their independence of any porosity value, which is in contrast to the derivation of solute concentrations.

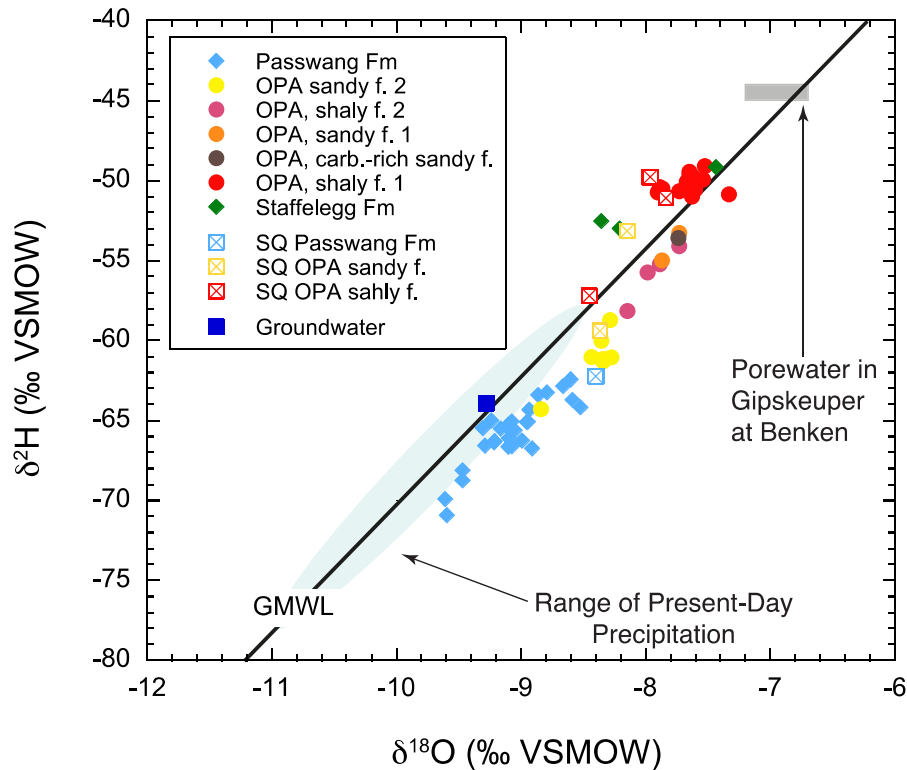
### 10.1 ORIGIN OF WATER COMPONENT

The original porewater in the marine sediments of the Passwang Fm, Opalinus Clay and Staffelegg Fm was seawater. To what degree the water isotope composition of seawater varied from Mesozoic to Quaternary times is an on-going discussion. General agreement exists about short-term fluctuations, such as the observed increase in  $\delta^{18}\text{O}$  of marine carbonate at the Cretaceous/Tertiary time boundary, which is interpreted as general climatic cooling, leaving the Tertiary seawater enriched in  $^{18}\text{O}$  (e.g., Corfield et al. 1991; Savin 1977). From the Lower to the Upper Mesozoic, Veizer et al. (1997) propose a change in  $\delta^{18}\text{O}$  of seawater from  $-2.1$  ‰ to  $0.9$  ‰ VSMOW at an average temperature of  $25$  °C. This is consistent with a change of  $2$  ‰ based on model calculations of the global ridge system evolution as proposed by Gregory (1991).

The distinction between water derived from marine and meteoric sources of ground- and porewater samples is commonly made based on comparison of the measured isotope composition with the Global Meteoric Water Line, GMWL (Craig 1961; updated by Rozanski et al. 1993). The GMWL represent a global average of meteoric water around the planet earth in the time period of about 1960–1990. It is recognised that the slope of this meteoric water depends on the local climatic conditions and moisture sources, and changes significantly between tropical, mediterranean, (semi-) arid and arctic climate areas (e.g., Clark and Fritz 1999). Whereas the GMWL may serve as a base assumption for the distinction of meteoric and marine palaeo-fluids, its exact trend during pre-Quaternary time is unknown, similar to the seawater isotope composition.

Porewater  $\delta^{18}\text{O}$  and  $\delta^2\text{H}$  values in the Passwang Fm and the Opalinus Clay sandy facies 1 fall within the large range given by modern precipitation in northern Switzerland and then become increasingly enriched in  $^{18}\text{O}$ , and especially  $^2\text{H}$ , further down in the Opalinus Clay and Staffelegg Fm (Fig. 10-1). In the Passwang Fm and the Opalinus Clay, down to shaly facies 1, porewater  $\delta^{18}\text{O}$  and  $\delta^2\text{H}$  values are linearly correlated and plot along a line parallel to and below the GMWL, with a shift of about 0.3 ‰ in  $\delta^{18}\text{O}$  (Figure 10-1). Porewater of the Opalinus Clay shaly facies 1 and the Staffelegg Fm plot onto or slightly above the GMWL. Water squeezed at the lowest pressure from borehole BDB-1 displays more scatter and a 'less regular' distribution of the  $\delta^{18}\text{O}$  and  $\delta^2\text{H}$  values compared to those obtained by the diffusive exchange method, but are in line with the trends given by the diffusive exchange method.

Groundwater collected from the water-conducting zone at 58.6 m BHL in the Passwang Fm plots onto the GMWL, with  $\delta^{18}\text{O}$  and  $\delta^2\text{H}$  values in the middle of the range given by porewaters from the Passwang Fm (Figure 10-1).



**Notes:** Error bars are omitted for legibility reasons, but given in the following figures. Data of squeezed water (SQ) from Mazurek et al. (2017). Range of present-day precipitation in Northern Switzerland from Waber et al. (2014). Porewater range of the Gipskeuper from the Benken borehole in Northern Switzerland (Rübel and Sonntag 2000; Nagra 2001) is shown for comparison to indicate meteoric-type porewater isotope signatures in these lithologies at other locations.

**Figure 10-1:  $\delta^{18}\text{O}$  vs.  $\delta^2\text{H}$  of Porewater, Groundwater and Recent Infiltration in Borehole BDB-1 at the Mont Terri URL.**

The exact trend of the GMWL during pre-Quaternary time is not known, however the correlation between the present-day GMWL and porewater from the Passwang Fm to the Staffelegg Fm allows inference that the porewater is of meteoric origin. A small percentage of marine component cannot be excluded based on the water isotope composition alone, but is also not required.

The difference in  $\delta^{18}\text{O}$  and  $\delta^2\text{H}$  values of porewater in the upper and lower (i.e., shaly facies 1) Opalinus Clay and the Staffelegg Fm seems real, as indicated by comparing isotope composition and mineralogy of the Opalinus Clay shaly facies 2 with that of shaly facies 1. Porewater in the rocks of these two facies differ in spite of their equal total clay content and clay mineral distribution (*cf.* Chapter 6, Figs. 6-2 to 6-4). Not known, however, is if the change of about 30 % in ionic strength of the porewater, as indicated by the different  $\text{Cl}^-$  concentrations, could have an effect on the determined isotope values. Changes in ionic strength affect the thickness of the diffusive double layer on the clay minerals and possibly the ease of isotope exchange with water molecules in the DDL. However, no data exist to-date for such small changes in porewater ionic strength, and it seems difficult to conceive that such small change would affect the isotope diffusive exchange data to the degree observed.

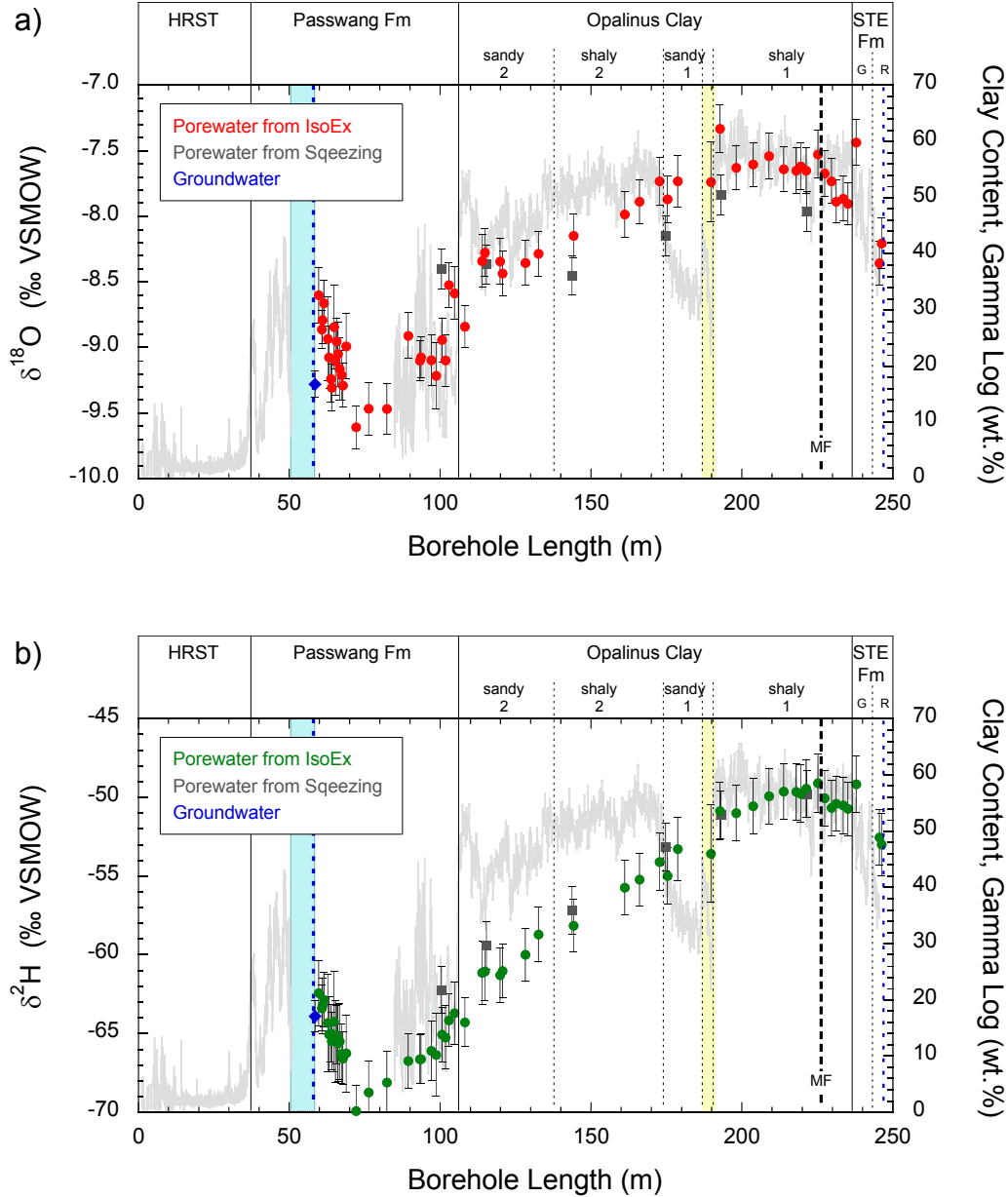
The difference in  $\delta^{18}\text{O}$  and  $\delta^2\text{H}$  values between porewater in the section from the Passwang Fm to the carbonate-rich sandy facies in the Opalinus Clay, and in the section from shaly facies 1 in the Opalinus Clay down to the Staffelegg Fm, thus needs to be explained in a different way. One possible source for such isotopically composed water is porewater from underlying Triassic sediments of mainly terrestrial origin. As shown in Figure 10-1, porewater in the Gipskeuper of northern Switzerland has  $\delta^{18}\text{O}$  and  $\delta^2\text{H}$  values that plot slightly above the GMWL, are enriched in  $^{18}\text{O}$  and  $^2\text{H}$ , and could potentially serve as an end member for the signatures observed in the Opalinus Clay shaly facies 1 and the Staffelegg Fm. Such origin from the Triassic sediment in the centre of the Mont Terri anticline would also be consistent with the addition of sulphate and isotopically-enriched chloride from such lithologies (*cf.* Sections 8.6 and 9.2).

## 10.2 SPATIAL DISTRIBUTION OF WATER ISOTOPES

Porewater  $\delta^{18}\text{O}$  and  $\delta^2\text{H}$  values show well-defined profiles across the low-permeability rock sequence from the Passwang Fm to the Opalinus Clay to the Staffelegg Fm (Figure 10-2, Table 10-1). The large scatter in the  $\delta^{18}\text{O}$  data compared to the  $\delta^2\text{H}$  data is of subjective value, taking into account the different scales.

In the Passwang Fm, there is clear evidence that porewater adjacent to the water-conducting zone at 58.6 m BHL differs from that of groundwater collected from this zone – in that they are enriched in  $^{18}\text{O}$  and  $^2\text{H}$ . As all these values plot on a line parallel to the GMWL (Figure 10-1), this enrichment can be interpreted in terms of a memory (i.e., residual impact on the signature) in the porewater of exchange with groundwater that infiltrated during warmer climate conditions than the groundwater collected today. From the water-conducting zone downwards, porewater  $\delta^{18}\text{O}$  and  $\delta^2\text{H}$  values first decrease by more than 1 ‰ and 5 ‰, respectively, to about 72 m BHL before they increase again to similar values to the water-conducting zone toward the interface with the Opalinus Clay. As shown in Section 10.3, neither the decrease nor the following increase is continuous and displays a great deal of scatter – though the scatter is primarily within the propagated uncertainty.

Squeezed water from rock of the Passwang Fm could only be obtained at high pressure of 300 MPa. This delivers the isotope composition of such squeezed water as non-representative for the porewater, as shown by the large deviation outside the propagated uncertainty from the isotope values obtained by the isotope diffusive exchange technique.



Notes: Error bars indicate the propagated error for the isotope diffusive exchange (IsoEx) technique and the analytical error for squeezed water and groundwater. Data of water squeezed at lowest pressure are from Mazurek et al. (2017).

**Figure 10-2: Distribution of Porewater  $\delta^{18}\text{O}$  (a) and  $\delta^2\text{H}$  (b) Across the Passwang Fm, Opalinus Clay and Staffelegg Fm in Borehole BDB-1 at the Mont Terri URL.**

In the Opalinus Clay, the shape of the  $\delta^{18}\text{O}$  and  $\delta^2\text{H}$  profiles becomes much more smooth (Figure 10-2). The  $\delta^{18}\text{O}$  and  $\delta^2\text{H}$  values increase from sandy facies 2 to the top of shaly facies 1 in an almost linear way from  $-8.84$  ‰ to  $-7.73$  ‰ VSMOW and  $-64.3$  ‰ to  $-50.9$  ‰ VSMOW, respectively. The porewater isotope composition of the carbonate-rich facies seems to be slightly below the general trend, although the values are within the propagated uncertainty. Because the same feature is also observed in the porewater chemical tracers (*cf.* Sections 9.1 and 9.3) and the chemistry of the aqueous extract solution (*cf.* Chapter 8), circulation of differently composed water cannot be excluded in this zone at some time during the more recent geologic past.

In shaly facies 1 of the Opalinus Clay, porewater  $\delta^{18}\text{O}$  and  $\delta^2\text{H}$  values reach a plateau with only very small variation of  $-7.66 \pm 0.15$  ‰ VSMOW in  $\delta^{18}\text{O}$  and  $-50.2 \pm 0.6$  ‰ VSMOW in  $\delta^2\text{H}$  over a distance of more than 40 m across the Opalinus Clay (Figure 10-2). Toward the base of shaly facies 1, the  $\delta^{18}\text{O}$  and  $\delta^2\text{H}$  values tend to become slightly more negative again, although the trend is not significantly outside of the range of the propagated uncertainty. Maximum values of  $-7.33$  ‰ in  $\delta^{18}\text{O}$  and  $-49.1$  ‰ in  $\delta^2\text{H}$  are clearly below the seawater isotope composition and also significantly more negative than in Opalinus clay at the Benken site ( $\delta^{18}\text{O}_{\text{max}} = -4.59$  ‰,  $\delta^2\text{H}_{\text{max}} = -39.3$  ‰; Rübél and Sonntag 2000) and the Schlattingen site ( $\delta^{18}\text{O}_{\text{max}} = -5.51$  ‰,  $\delta^2\text{H}_{\text{max}} = -45.2$  ‰; Wersin et al. 2013) in northern Switzerland.

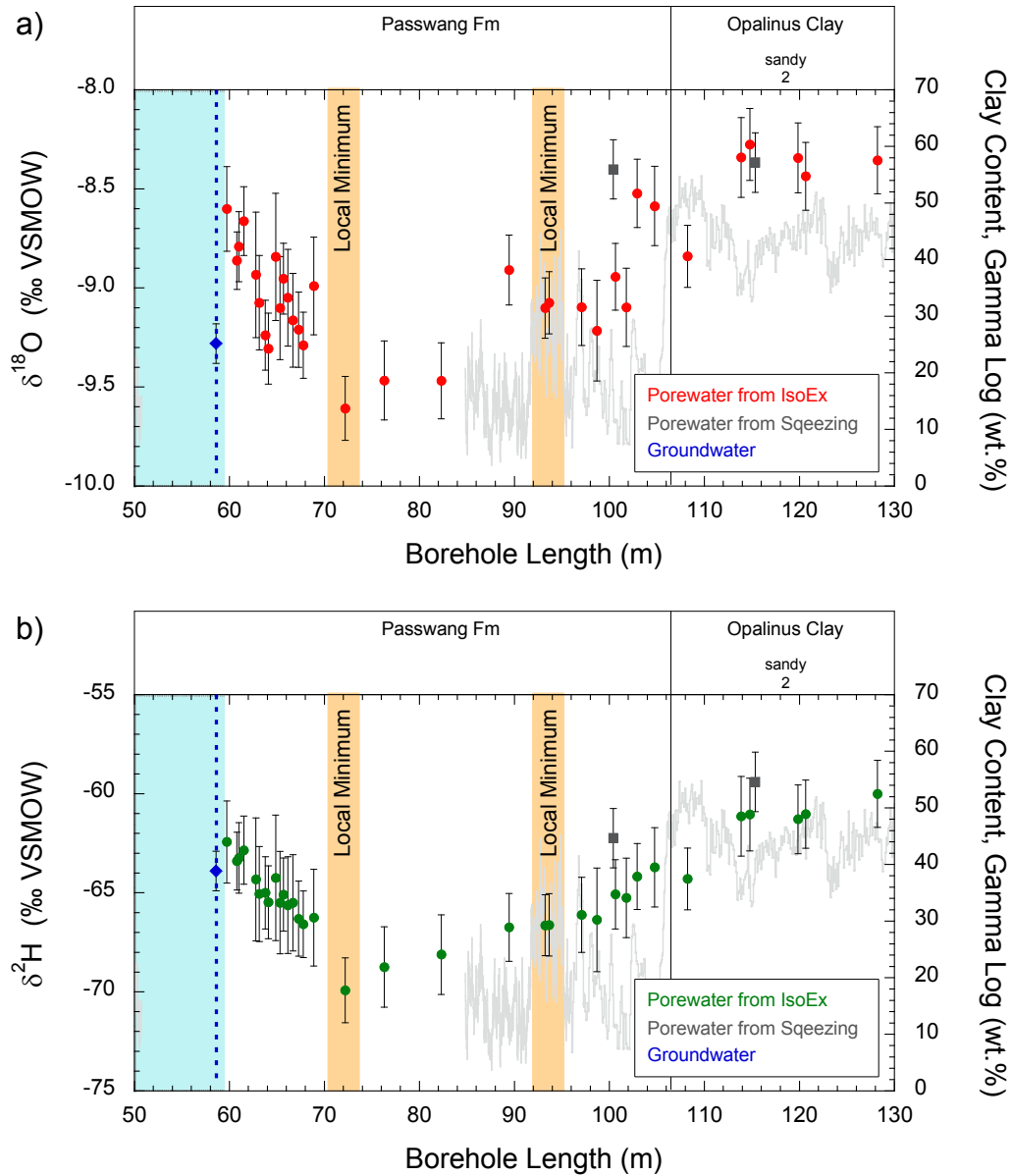
Water squeezed at the lowest pressure (100–150 MPa) from Opalinus Clay samples systematically underestimates the  $\delta^{18}\text{O}$  values outside the propagated uncertainty, except for the sample from sandy facies 2 (Figure 10-2a). In contrast, better agreement is obtained for the  $\delta^2\text{H}$  values (Figure 10-2b). To what degree the difference is associated with induced pressure solution of carbonate or other reactions during high pressure squeezing is the subject of further investigations.

In the Staffelegg Fm, the indicated trend toward negative  $\delta^{18}\text{O}$  and  $\delta^2\text{H}$  values at the bottom of shaly facies 1 in the Opalinus Clay is first interrupted at the sample adjacent to the Opalinus Clay and then continues further down into the Riethelm Member at the end of borehole BDB-1 (Figure 10-2). The trend is more pronounced than in the chemical tracers (*cf.* Figures 9-1, 9-3 and 9-5). As shown in Section 6.3, an accumulation of open fractures and moist zones occurred around 243 m BHL (*cf.* Figure 6-10), which is where from the two deepest samples of the Staffelegg Fm come. The present data do not allow a final conclusion, but indicate that in these zones a water of different isotopic composition, with a chemical composition not significantly different to the porewater, might be present.

### 10.3 $\delta^{18}\text{O}$ AND $\delta^2\text{H}$ ACROSS THE PASSWANG FM – OPALINUS CLAY INTERFACE

The porewater isotope composition in the Passwang Fm displays a less homogeneous distribution as a function of distance from the water-conducting zone compared to that observed in the Opalinus Clay. More scatter is observed in the  $\delta^{18}\text{O}$  values compared to those of  $\delta^2\text{H}$ , although the variation is only about 1 ‰ in  $\delta^{18}\text{O}$  and 8 ‰ in  $\delta^2\text{H}$  (Figure 10-3). From the water-conducting zone at 58.6 m BHL,  $\delta^{18}\text{O}$  and  $\delta^2\text{H}$  in porewater decrease towards a minimum at about 72 m BHL. This minimum coincides with that observed in the profiles of the chemical tracers (*cf.* Chapter 9).

Based on this multi-tracer evidence, and the observed accumulation of fractures in this zone (*cf.* Section 6.3), it is likely that groundwater of different composition percolated into this zone over a certain time period. Given the lack of geophysical and other borehole logs in this depth interval, it might well be that groundwater circulation at low hydraulic conductivity still takes place today in this zone. As a consequence, and based on the changes in chemical and isotopic concentration profile, it appears that this zone at about 72 m BHL most likely forms the upper boundary for the diffusive exchange of porewater solutes between the Opalinus Clay and the Passwang Fm. In contrast, no excursion in the  $\delta^{18}\text{O}$  and  $\delta^2\text{H}$  profile is observed at the second local minimum indicated by the porewater chemical tracers at around 92–95 m BHL (Figure 10- 3). Similarly, no excursion is observed at 98 m BHL where the chemical tracers suggest a local maximum. This could either be due to the different diffusion of water and its isotopes, or due to an artefact of the poorly-known ion-accessible porosity used for the calculation of the porewater concentrations of chemical tracers. Which of these possibilities comes closer to reality will have to be investigated by conducting transport model calculations.



Notes: Local minima as derived from porewater  $\text{Cl}^-$  and  $\text{Br}^-$  concentrations. Error bars indicate the propagated error for the isotope diffusive exchange (IsoEx) technique and the analytical error for squeezed water and groundwater. Data of water squeezed at lowest pressure are from Mazurek et al. (2017).

**Figure 10-3: Close-up of the  $\delta^{18}\text{O}$  (a) and  $\delta^2\text{H}$  (b) Values in Porewater Across the Passwang Fm – Opalinus Clay Interface in Borehole BDB-1 at the Mont Terri URL.**

**Table 10-1: Porewater  $\delta^{18}\text{O}$  and  $\delta^2\text{H}$  Derived by the Isotope Diffusive Exchange Technique**

Sample	Depth m BHL	Strati- graphie	Member / Facies	Lithology	$\delta^{18}\text{O}$ PW ‰ VSMOW	prop. error	$\delta^2\text{H}$ PW ‰ VSMOW	prop. error
BDB1-36.19	36.19	HRST	Brüggli - Mb.	sa lst	-9.38	0.43	-70.5	4.6
BDB1-43.78	43.78	PAF	Waldenburg - Mb.	sa lst	-9.59	0.16	-70.9	1.6
BDB1-59.75	59.75	PAF	Waldenburg - Mb.	sa lst	-8.60	0.21	-62.4	2.1
BDB1-60.79	60.79	PAF	Waldenburg - Mb.	sa lst	-8.86	0.15	-63.4	1.5
BDB1-61.00	61.00	PAF	Waldenburg - Mb.	sa lst	-8.79	0.18	-63.2	1.8
BDB1-61.52	61.52	PAF	Waldenburg - Mb.	sa lst	-8.66	0.17	-62.8	1.7
BDB1-62.80	62.80	PAF	Waldenburg - Mb.	lst	-8.93	0.32	-64.3	3.1
BDB1-63.15	63.15	PAF	Waldenburg - Mb.	lst	-9.07	0.24	-65.1	2.4
BDB1-63.80	63.80	PAF	Waldenburg - Mb.	sa lst	-9.24	0.18	-65.0	1.8
BDB1-64.11	64.11	PAF	Waldenburg - Mb.	sa lst	-9.31	0.18	-65.5	1.8
BDB1-64.88	64.88	PAF	Waldenburg - Mb.	lst	-8.84	0.32	-64.2	3.2
BDB1-65.34	65.34	PAF	Waldenburg - Mb.	lst	-9.10	0.26	-65.5	2.6
BDB1-65.70	65.70	PAF	Waldenburg - Mb.	sa lst	-8.95	0.18	-65.1	1.8
BDB1-66.15	66.15	PAF	Waldenburg - Mb.	sa lst	-9.05	0.24	-65.6	2.4
BDB1-66.70	66.70	PAF	Waldenburg - Mb.	sa lst	-9.16	0.24	-65.5	2.4
BDB1-67.30	67.30	PAF	Waldenburg - Mb.	sa lst	-9.21	0.19	-66.3	1.9
BDB1-67.80	67.80	PAF	Waldenburg - Mb.	sa lst	-9.29	0.17	-66.6	1.7
BDB1-68.90	68.90	PAF	Waldenburg - Mb.	sa lst	-8.99	0.25	-66.3	2.4
BDB1-72.20	72.20	PAF	Waldenburg - Mb.	sa lst	-9.61	0.16	-69.9	1.6
BDB1-76.30	76.30	PAF	Himichopf - Mb.	sa lst	-9.47	0.20	-68.7	2.0
BDB1-82.30	82.30	PAF	Himichopf - Mb.	lst	-9.47	0.19	-68.1	2.0
BDB1-89.45	89.45	PAF	Himichopf - Mb.	li sst	-8.91	0.18	-66.7	1.7
BDB1-93.24	93.24	PAF	Himichopf - Mb.	sa ma	-9.10	0.15	-66.6	1.5
BDB1-93.65	93.65	PAF	Himichopf - Mb.	sa ma	-9.07	0.16	-66.6	1.6
BDB1-97.10	97.10	PAF	Sissach - Mb.	lst	-9.10	0.19	-66.1	1.9
BDB1-98.68	98.68	PAF	Sissach - Mb.	sa lst	-9.22	0.25	-66.4	2.6
BDB1-100.63	100.63	PAF	Sissach - Mb.	sa ma	-8.94	0.17	-65.1	1.7
BDB1-101.80	101.80	PAF	Sissach - Mb.	sa ma	-9.10	0.20	-65.3	2.0
BDB1-102.93	102.93	PAF	Sissach - Mb.	sa ma	-8.52	0.17	-64.2	1.7
BDB1-104.78	104.78	PAF	Sissach - Mb.	sa ma	-8.59	0.20	-63.7	2.0

**Notes:**

PW = porewater; values in italics are less reliable due to analytical problems. PAF = Passwang Formation, OPA = Opalinus Clay, STF = Stafflegg Formation. Field lithology after Hostettler et al. (2017): li sst = limy sandstone, sa ma = sandy marl, lst = limestone; sa lst = sandy limestone, clst = claystone, silt clst = silty claystone, clst & lst la = claystone with limestone layers, clst & sst la = claystone with sandstone layers, arg ma = argillaceous marl, bit ma = bituminous marl. Shaded samples were used for inter-laboratory comparison.

Table 10-1: (cont.)

Sample	Depth	Strati- graphie	Member / Facies	Lithology	$\delta^{18}\text{O}$ PW	prop. error	$\delta^2\text{H}$ PW	prop. error
					‰ SMOC	‰ SMOC	‰ SMOC	‰ SMOC
BDB1-108.24	108.24	OPA	sandy facies 2	clst & lst la	-8.84	0.16	-64.3	1.6
BDB1-113.88	113.88	OPA	sandy facies 2	clst & lst la	-8.34	0.20	-61.1	2.0
BDB1-114.80	114.80	OPA	sandy facies 2	clst & lst la	-8.28	0.18	-61.0	1.8
BDB1-119.86	119.86	OPA	sandy facies 2	clst & lst la	-8.34	0.18	-61.3	1.7
BDB1-120.68	120.68	OPA	sandy facies 2	clst & lst la	-8.44	0.17	-61.0	1.7
BDB1-128.24	128.24	OPA	sandy facies 2	clst & lst la	-8.36	0.17	-60.0	1.7
BDB1-132.63	132.63	OPA	sandy facies 2	clst & lst la	-8.28	0.17	-58.7	1.7
BDB1-144.17	144.17	OPA	shaly facies 2	silt clst	-8.15	0.17	-58.1	1.7
BDB1-161.18	161.18	OPA	shaly facies 2	silt clst	-7.98	0.17	-55.7	1.7
BDB1-166.08	166.08	OPA	shaly facies 2	silt clst	-7.89	0.17	-55.2	1.7
BDB1-172.70	172.70	OPA	shaly facies 2	silt clst	-7.73	0.18	-54.1	1.8
BDB1-175.33	175.33	OPA	sandy facies 1	clst & sst la	-7.87	0.18	-55.0	1.8
BDB1-178.73	178.73	OPA	sandy facies 1	clst & sst la	-7.73	0.20	-53.3	2.0
BDB1-189.71	189.71	OPA	carb.-rich sandy f.	lst	-7.74	0.30	-53.6	3.1
BDB1-192.68	192.68	OPA	shaly facies 1	clst	-7.33	0.18	-50.9	1.8
BDB1-198.13	198.13	OPA	shaly facies 1	clst	-7.63	0.17	-51.0	1.8
BDB1-203.68	203.68	OPA	shaly facies 1	clst	-7.60	0.17	-50.6	1.7
BDB1-209.00	209.00	OPA	shaly facies 1	clst	-7.54	0.17	-49.9	1.8
BDB1-213.85	213.85	OPA	shaly facies 1	clst	-7.64	0.17	-49.6	1.8
BDB1-217.98	217.98	OPA	shaly facies 1	clst	-7.65	0.17	-49.6	1.8
BDB1-219.49	219.49	OPA	shaly facies 1	clst	-7.62	0.18	-49.8	1.8
BDB1-221.28	221.28	OPA	shaly facies 1	clst	-7.65	0.18	-49.4	1.8
BDB1-225.18	225.18	OPA	shaly facies 1	clst	-7.53	0.18	-49.1	1.9
BDB1-227.43	227.43	OPA	shaly facies 1	clst	-7.67	0.17	-50.1	1.8
BDB1-229.68	229.68	OPA	shaly facies 1	clst	-7.73	0.17	-50.7	1.7
BDB1-231.18	231.18	OPA	shaly facies 1	clst	-7.89	0.16	-50.4	1.8
BDB1-233.63	233.63	OPA	shaly facies 1	clst	-7.87	0.17	-50.5	1.8
BDB1-235.14	235.14	OPA	shaly facies 1	clst	-7.90	0.16	-50.7	1.7
BDB1-237.88	237.88	STF	Gross Wolf Mb.	arg ma	-7.44	0.17	-49.2	1.8
BDB1-243.37	243.37	STF	Gross Wolf Mb.	lst	-6.58	0.59	-48.1	6.3
BDB1-245.54	245.54	STF	Rietheim Mb.	bit ma	-8.36	0.17	-52.5	1.8
BDB1-246.34	246.34	STF	Rietheim Mb.	bit ma	-8.21	0.19	-53.0	2.0

**Notes:**

PW = porewater; values in italics are less reliable due to analytical problems. PAF = Passwang Formation, OPA = Opalinus Clay, STF = Stafflegg Formation. Field lithology after Hostettler et al. (2017): li sst = limy sandstone, sa ma = sandy marl, lst = limestone; sa lst = sandy limestone, clst = claystone, silt clst = silty claystone, clst & lst la = claystone with limestone layers, clst & sst la = claystone with sandstone layers, arg ma = argillaceous marl, bit ma = bituminous marl. Shaded samples were used for inter-laboratory comparison.

## 11. NOBLE GAS CONCENTRATIONS AND ISOTOPES IN POREWATER

### 11.1 EVALUATION OF AIR CONTAMINATION

The purified and analysed gas extracted from the sample container consists of the gas volume, which has degassed from the porewater (the “porewater gas”) and - possibly – variable amounts of contaminant gas, such as air. The degree of air contamination of a measured gas is commonly determined via its Ne content (e.g., Bigler et al. 2005; Rübél & Sonntag 2000; Rübél et al. 2002; Waber 2012). With negligible in-situ geogenic productions ( $^{20}\text{Ne} = 1.5 \times 10^{-21}$ ,  $^{22}\text{Ne} = 5.2 \times 10^{-21}$  ccSTP/(g<sub>rock</sub> a); Leya & Wieler 1999), any excess Ne<sub>H<sub>2</sub>O</sub> concentration above that of air-saturated water (Ne<sub>asw</sub> approximately  $1.9 \times 10^{-7}$  ccSTP/g<sub>H<sub>2</sub>O</sub>; Weiss 1971) - which was brought into the system during the infiltration of surface water - is interpreted as being derived from air contamination. Using the relative atmospheric abundances of Ne (Ne<sub>air</sub> = 18.18 ppmv), He (He<sub>air</sub> = 5.24 ppmv) and Ar (Ar<sub>air</sub> = 0.934 vol.%), the total amount of air that has contaminated the sample, as well as the corresponding amounts of He and Ar brought into it by this contaminant air, can be determined from the excess Ne as:

$$air_{contaminant} = \frac{(Ne_{H_2O} - Ne_{asw})}{Ne_{air}} \quad [ccSTP/g_{H_2O}] \quad (29)$$

$$(He, Ar)_{air\ derived} = air_{contaminant} \times (He, Ar)_{air} \quad [ccSTP/g_{H_2O}] \quad (30)$$

With this, the corrected  $^4\text{He}_{PW}$ ,  $(^3\text{He}/^4\text{He})_{PW}$ ,  $Ar_{PW}$  and  $(^{40}\text{Ar}/^{36}\text{Ar})_{PW}$  values can be calculated from the respective measured “<sub>H<sub>2</sub>O</sub>” values according to:

$$(^4\text{He}, Ar)_{pw} = (^4\text{He}, Ar)_{H_2O} - (^4\text{He}, Ar)_{air\ derived} \quad [ccSTP/g_{H_2O}] \quad (31)$$

$$\left(\frac{^3\text{He}}{^4\text{He}}\right)_{pw} = \frac{\left(\frac{^3\text{He}}{^4\text{He}}\right)_{H_2O} - \left(\left(\frac{^3\text{He}}{^4\text{He}}\right)_{air} \times \frac{^4\text{He}_{air\ derived}}{^4\text{He}_{H_2O}}\right)}{1 - \frac{^4\text{He}_{air\ derived}}{^4\text{He}_{H_2O}}} \quad (32)$$

$$\left(\frac{^{40}\text{Ar}}{^{36}\text{Ar}}\right)_{pw} = \frac{\left(\frac{^{40}\text{Ar}}{^{36}\text{Ar}}\right)_{H_2O} - \left(\left(\frac{^{40}\text{Ar}}{^{36}\text{Ar}}\right)_{air} \times \frac{Ar_{air\ derived}}{Ar_{H_2O}}\right)}{1 - \frac{Ar_{air\ derived}}{Ar_{H_2O}}} \quad (33)$$

Air is – relative to the average porewater gas composition – strongly depleted in He and enriched in Ar, both of which also have a less radiogenic isotope signature in air than in the porewater gas. This means that He and Ar in porewater-derived gas are very differently affected if this gas comes into contact with air.

This is illustrated when a representative porewater gas (parameterised in Table 11-1) is taken as the (uncontaminated) starting composition for a sample gas that is increasingly contaminated by an admixture of air, with the degree of contamination being represented by the fraction of the contaminant air in the (now contaminated) sample gas. The *total amount* of helium in the

increasingly contaminated sample gas is hardly affected due to the large difference of more than two orders of magnitude between the He-rich uncontaminated porewater gas and the He-poor air (Table 11-1, lower panel of Figure 11-1). The induced deviation from the initial He content of the sample gas would exceed the analytical uncertainty only at a contamination of more than 60 % air. In contrast, the amount of argon in the increasingly contaminated sample gas shows a drastic increase even at low degrees of contamination, as the Ar concentration in air is generally significantly higher than in the uncontaminated porewater gas. As a result, the Ar amounts of the contaminated sample gas already deviate for more than the analytical uncertainty from the uncontaminated value at less than 1 % of air contamination and reach three times the uncontaminated value at around 7 % air contamination (upper panel of Figure 11-1).

**Table 11-1: Representative He and Ar Compositions of a BDB-1 Porewater Gas and Air**

	$C_{\text{He}}$ [ppmv]	$C_{\text{Ar}}$ [vol.%]	$^3\text{He}/^4\text{He}$	$^{40}\text{Ar}/^{36}\text{Ar}$	$R/R_{\text{air}}$
porewater gas	110	0.03	$3.4 \times 10^{-7}$	320	1.07
Air	5.24	0.93	$1.36 \times 10^{-6}$	298.56	1.00

	$C_{\text{He}_{\text{pw}}}$ [ccSTP/g <sub>pw</sub> ]	$C_{\text{Ar}_{\text{pw}}}$ [ccSTP/g <sub>pw</sub> ]	$m_{\text{pw}}$ [g]	$n_{\text{sample gas}}$ [ccSTP]	
porewater	$6.0 \times 10^{-5}$	$1.8 \times 10^{-4}$	17.6	9.6	

**Notes:**

Porewater gas values are a representative estimate for the range of BDB-1 samples for which air contamination could be corrected, calculated with the tabled representative porewater values ( $n_{\text{sample gas}}$  based on an average gas pressure of 50 mbar and an average gas volume of 206 cm<sup>3</sup> in the sample container). Air values: concentrations from Prinn (2004);  $^3\text{He}/^4\text{He}$  from de Laeter (2003);  $^{40}\text{Ar}/^{36}\text{Ar}$  from Lee et al. (2006);  $R/R_{\text{air}} = ^{40}\text{Ar}/^{36}\text{Ar}$  of analyte relative to  $^{40}\text{Ar}/^{36}\text{Ar}$  ratio of air.

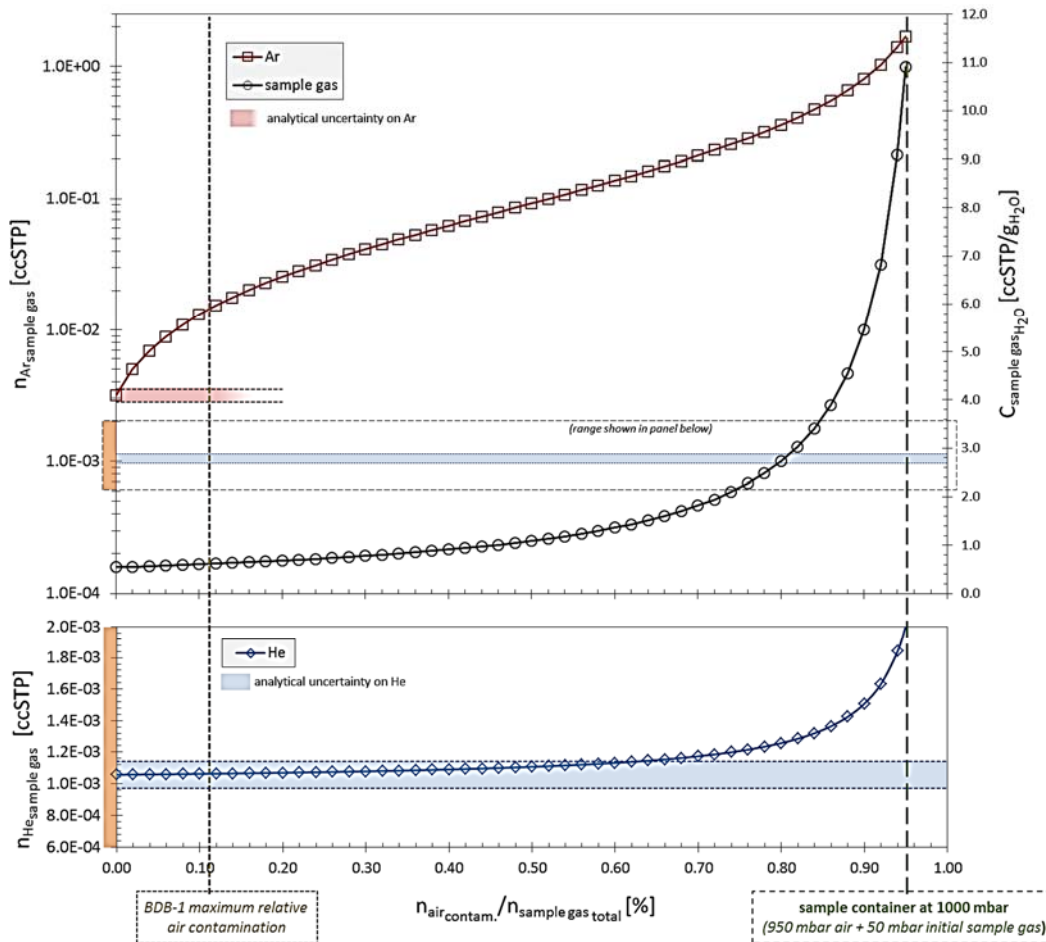
The isotope ratios of  $^3\text{He}/^4\text{He}$  and  $^{40}\text{Ar}/^{36}\text{Ar}$  are affected by air contamination, much like the elemental concentrations (Figure 11-2). In accordance with the impact of contamination on absolute amounts,  $^3\text{He}/^4\text{He}$  values are less affected by an admixture of air than  $^{40}\text{Ar}/^{36}\text{Ar}$  ratios due to the difference between the two gases in terms of their abundance in air. This effect is, however, to some degree counteracted by the far larger difference in  $^3\text{He}/^4\text{He}$  isotope ratio in air relative to porewater (up to one order of magnitude) when compared to the difference in  $^{40}\text{Ar}/^{36}\text{Ar}$  (roughly 5-20 %). In consequence,  $^3\text{He}/^4\text{He}$  ratios of the increasingly contaminated sample gas show no deviation within analytical uncertainty from the uncontaminated value, up to a relative air contamination of 15 %, whereas for  $^{40}\text{Ar}/^{36}\text{Ar}$ , a significant deviation is already reached at a relative air contamination of approximately 5 %.

For the BDB-1 samples  $\text{Ne}_{\text{H}_2\text{O}}$  concentrations in porewater were determined to be between  $8.6 \times 10^{-8}$  (below LOC, see section 11.1.1) and  $1.9 \times 10^{-6}$  ccSTP/g<sub>H<sub>2</sub>O</sub>. This range is comparable to the values of  $1.3 \times 10^{-7}$  to  $2.0 \times 10^{-7}$  ccSTP/g measured by Rübél and Lehmann (in Pearson et al. 2003) for the Opalinus Clay at Mont Terri. It is somewhat lower than the ranges of  $4.7 \times 10^{-7}$  to  $1.8 \times 10^{-5}$  ccSTP/g and  $1.0 \times 10^{-7}$  to  $5.6 \times 10^{-5}$  ccSTP/g<sub>H<sub>2</sub>O</sub> obtained for the Callovo-Oxfordian Clay at the Bure site in the Paris Basin (Waber 2012; Smith 2010) and the range of  $3.3 \times 10^{-8}$  to

$9.9 \times 10^{-5}$  ccSTP/g<sub>H<sub>2</sub>O</sub> measured on samples from the PH4 borehole at the Tournemire URL (Bensenouci et al. 2011). All these samples were collected using the same general sampling technique.

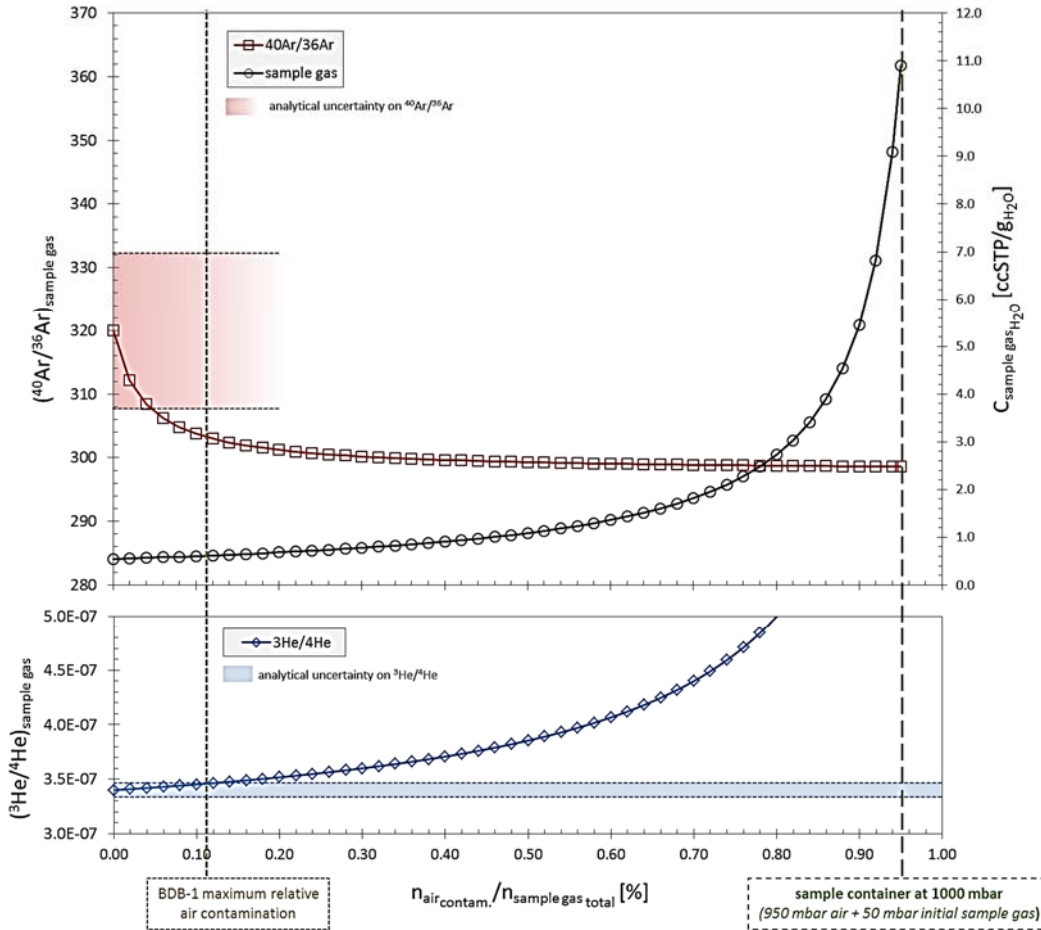
In 9 samples, Ne<sub>H<sub>2</sub>O</sub> concentrations could not be adequately determined due to analytical problems or because the measured Ne amounts are below the limit of calibration (*cf.* Table 5-1, Section 5.5.3).

In the other analysed BDB-1 samples, Ne<sub>H<sub>2</sub>O</sub> concentrations, with an average measured <sup>20</sup>Ne/<sup>22</sup>Ne ratio of  $8.95 \pm 0.97$ , indicate contamination by air between 0.03 and 0.09 ccSTP/g<sub>H<sub>2</sub>O</sub>, equivalent to a fraction of 1.5 - 11.2 vol.% of air in gas present in the sample containers.



**Notes:** The analytical uncertainty on the He and Ar amounts of the uncontaminated sample gas are given by the shaded horizontal bars. The ordinate range of the lower panel is marked on the ordinate axis of the upper panel by the vertical grey bar. For the uncontaminated sample gas composition see Table 11-1.

**Figure 11-1: Ar and He Amount in an Increasingly Contaminated Sample Gas as a Function of Relative Air Contamination.**



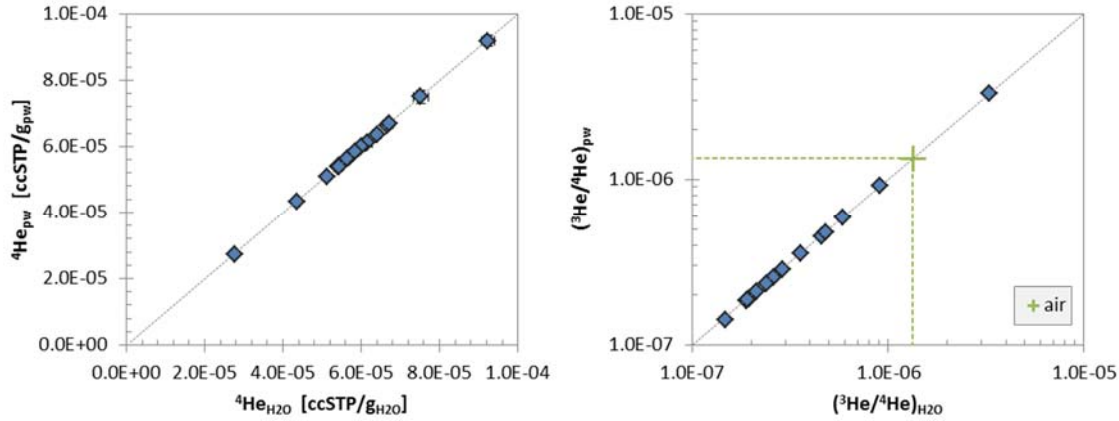
**Notes:** The ranges of analytical uncertainty on the  ${}^3\text{He}/{}^4\text{He}$  and  ${}^{40}\text{Ar}/{}^{36}\text{Ar}$  isotope ratios of the uncontaminated sample gas are indicated by the shaded horizontal bars. For the uncontaminated sample gas composition see Table 11-1.

**Figure 11-2:  ${}^{40}\text{Ar}/{}^{36}\text{Ar}$  and  ${}^3\text{He}/{}^4\text{He}$  Isotope Ratios in an Increasingly Contaminated Sample Gas as a Function of Relative Air Contamination.**

For He, the corresponding relative addition of  $\text{He}_{\text{air derived}}$  to the total measured He is below 0.8 % for all samples, resulting in air contamination corrected and uncorrected values being identical, within uncertainty, both for  ${}^4\text{He}$  concentrations and for  ${}^3\text{He}/{}^4\text{He}$  isotope ratios (Figure 11-3).

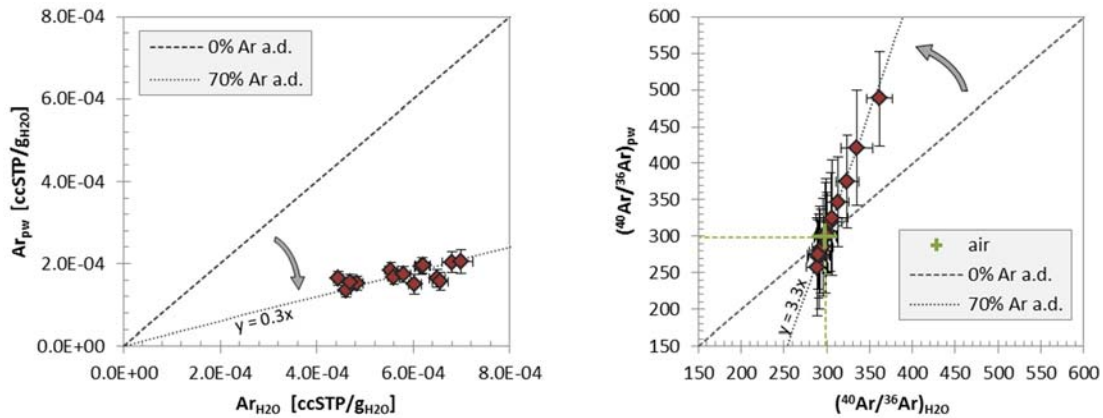
For Ar the corresponding relative addition of  $\text{Ar}_{\text{air derived}}$  to the measured Ar is 63-77 %, resulting in air contamination corrections of up to a factor of 4.2 for Ar concentrations and up to 35 % on  ${}^{40}\text{Ar}/{}^{36}\text{Ar}$  isotope ratios (Figure 11-4). The steep slope of the calculated  $({}^{40}\text{Ar}/{}^{36}\text{Ar})_{\text{pw}}$  vs.  $({}^{40}\text{Ar}/{}^{36}\text{Ar})_{\text{H}_2\text{O}}$  line for the exemplary case of 70 % air-derived Ar shows how sensitive, in particular, corrected  $({}^{40}\text{Ar}/{}^{36}\text{Ar})_{\text{pw}}$  values are to both the accurate measurement of the Ne concentration (from which the degree of air contamination and therefore the slope of the correction line is calculated) and the uncertainty of the  $({}^{40}\text{Ar}/{}^{36}\text{Ar})_{\text{H}_2\text{O}}$  measurement. While the attained relative analytical precision is similar for both  $\text{Ar}_{\text{H}_2\text{O}}$  and  $({}^{40}\text{Ar}/{}^{36}\text{Ar})_{\text{H}_2\text{O}}$  measurements (5 % and 3.9 %, respectively, on long-term reproducibility), the increasingly steeper slope of the isotope ratio correction line with increasing air contamination leads to very large uncertainties on

the corrected  $^{40}\text{Ar}/^{36}\text{Ar}$  values, far exceeding the relative increase in uncertainty on the corrected Ar concentration values – where the slope of the correction line becomes smaller with increasing air contamination (Figure 11-4).



Notes: Error bars are within symbols.

**Figure 11-3:  $^4\text{He}$  (left) and  $^3\text{He}/^4\text{He}$  Isotope Ratios (right) in an Increasingly Contaminated Sample Gas as a Function of Relative Air Contamination.**

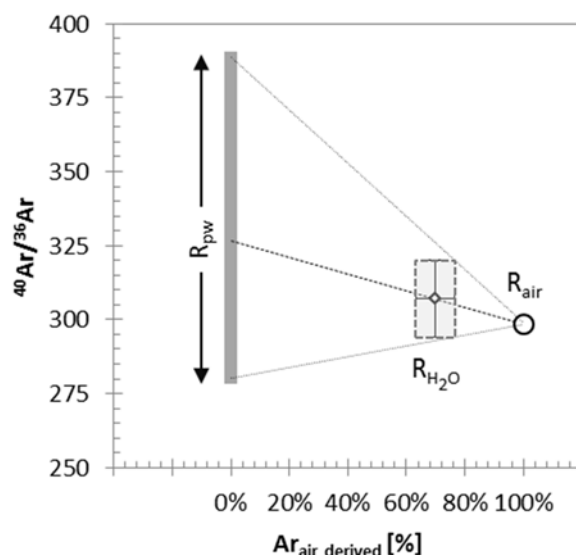


Notes: The dashed and dotted lines indicate calculated  $\text{Ar}_{\text{pw}}$  as function of  $\text{Ar}_{\text{H}_2\text{O}}$  for 0 %  $\text{Ar}_{\text{air}}$  derived and 70 %  $\text{Ar}_{\text{air}}$  derived. These lines of increasing air derived Ar contamination pivot around the origin for Ar concentrations and around the air value for  $^{40}\text{Ar}/^{36}\text{Ar}$  ratios.

**Figure 11-4: Comparison of Air Contamination Corrected and Uncorrected Concentration Values of Ar (left) and Ar-Isotope Ratio (right) for the BDB-1 Samples.**

As the air contamination corrected He concentrations and isotope ratios are equal within their analytical uncertainty to the uncorrected values, all He values – including those for which no correction could be calculated due to missing Ne values – are reported as  $\text{He}_{\text{pw}}$  and  $(^3\text{He}/^4\text{He})_{\text{pw}}$ .

For Ar concentrations as well as isotope ratios, however, the corrected values are dominantly controlled by the air contamination correction. The correction-induced changes in concentration values are on average over 30 times, and on isotope ratios over 2 times, higher than the corresponding analytical uncertainty of the long-term reproducibility. For the isotope ratios, the unreasonable upscaling of the uncertainty from the uncorrected to the corrected value for high degrees of air-derived Ar has to be considered as well (Figure 11-5).



**Notes:** The measured isotope signature of the sample ( $R_{H_2O}$ ) is  $305 \pm 13$  ( $1 \sigma$ ), which is the average of the BDB-1 dataset;  $A_{air\ derived}$  is  $70 \% \pm 7 \%$ , which represents the range of the BDB-1 dataset (63 – 77 %);  $R_{air}$  is  $298.56 \pm 0.31$  (Lee et al. 2006).

**Figure 11-5: The Problem of Unrealistic Upscaling of the Maximal Uncertainties on Air-contamination-corrected  $^{40}\text{Ar}/^{36}\text{Ar}$  Values for High Degrees of Air-derived Ar.**

### 11.1.1 Samples with Elevated Gas Concentrations

While detection and quantitative determination of air contamination is usually done by means of the Ne concentration as described above, the admixture of a contaminant gas phase (which might or might not be air) to the porewater gas also increases the overall amount of gas in the sample container, which is detectable by an increased gas pressure in the sample container. As increased gas amounts in the sample container can also simply be due to elevated sample porosity, and therefore a larger porewater reservoir providing more porewater gas, only the case of adding an extrinsic gas phase would concomitantly also increase the gas concentration in the porewater. As such, diverging, high gas concentrations in porewater can act as a qualitative proxy pointing to a potential addition of a contaminant gas phase to the porewater gas.

Below the Passwang Fm, several BDB-1 samples show roughly 3 to 7 times higher gas concentrations in porewater relative to lithologically comparable samples from similar depth. There is, however, no correlation between gas concentrations and Ne concentrations in the

porewater for these samples. If they have suffered from addition of an extrinsic gas phase, this contaminant gas has therefore either not been air, or the determination of Ne (as the air proxy) on these samples is incorrect.

Looking at the composition of the gas extracted from the sample container (Table 11-2), it is evident that the samples with elevated gas concentrations in the porewater unanimously have lower He fractions in the gas. At the same time, the absolute amount of He in the gas of these samples does not show this kind of aberrant behaviour (Figure 11-6). This is in agreement with a contamination of the porewater gas by a gas with a low He partial pressure (such as air), leading to a dilution of He in the sample container. Sample BDB1-144.49-NG shows the strongest dilution effect, in accordance with it having the highest gas concentration in the porewater. Sample BDB1-114.08-NG shows the least dilution, with the least elevated gas concentration of the samples. While the He fraction in these potentially contaminated gases do trend toward the air value, the fractions of Ne and Ar do not. These species show, similar to He, the same effects of dilution in the potentially contaminated samples, without clearly divergent absolute amounts in the sample containers (Figures 11-7 and 11-8).

With air as the contaminant phase (and therefore, as a corollary, assuming Ne determination to be incorrect), Ar fractions would have to increase toward the air value (roughly one order of magnitude higher) instead of decrease. Under the same premise, absolute Ar amounts in these high-gas-content samples would have to be roughly between 0.1 – 0.6 ccSTP in the sample containers, over one order of magnitude higher than the observed values. Furthermore, with the substantial addition of air-derived Ar by such contamination, the He/Ar ratio of the gas in the sample container would have to trend toward the atmospheric ratio, which is over 2 orders of magnitude lower than the value observed in these gas-rich samples. Neither the He/Ar nor the He/Ne or Ar/Ne ratios do, however, change with increasing gas contents in the sample gas containers (Figure 11-9), but stay similar to the corresponding values of their neighbouring samples (Figure 11-10).

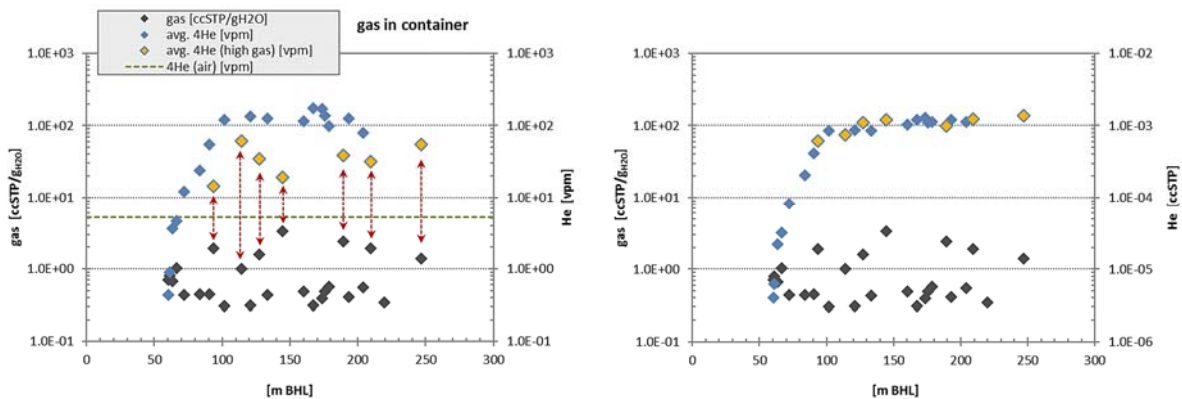
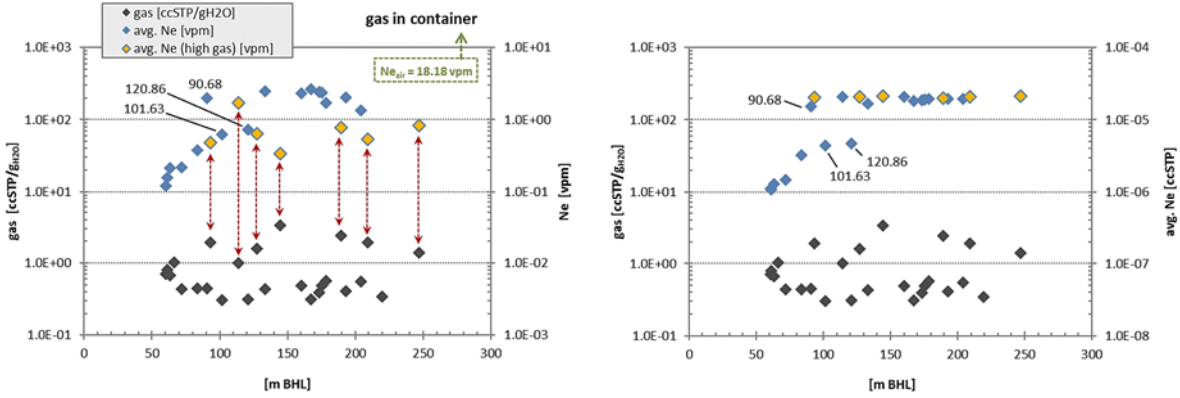
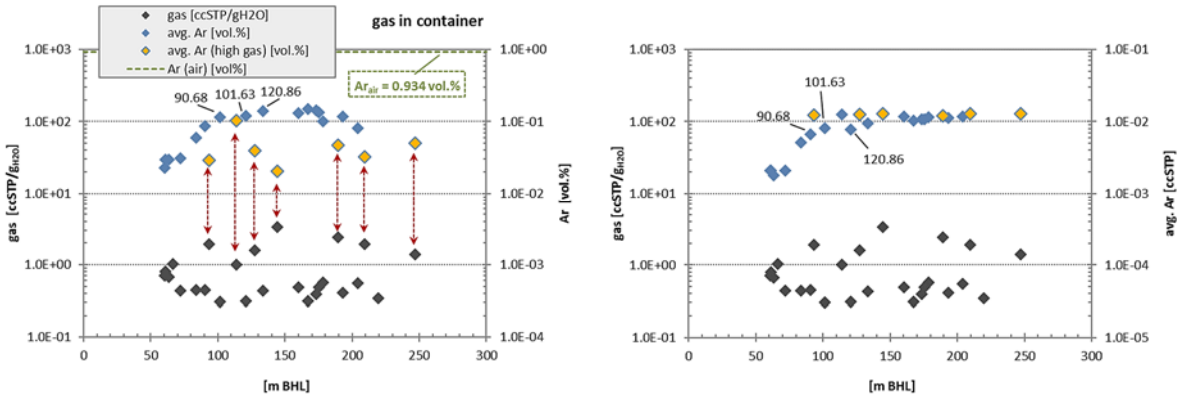


**Figure 11-6: Fractions of He (left) and Absolute He Amounts (right) in the Sample Container Gas, Together with Sample Container Gas Concentrations in the Porewater as a Function of Borehole Depth.**



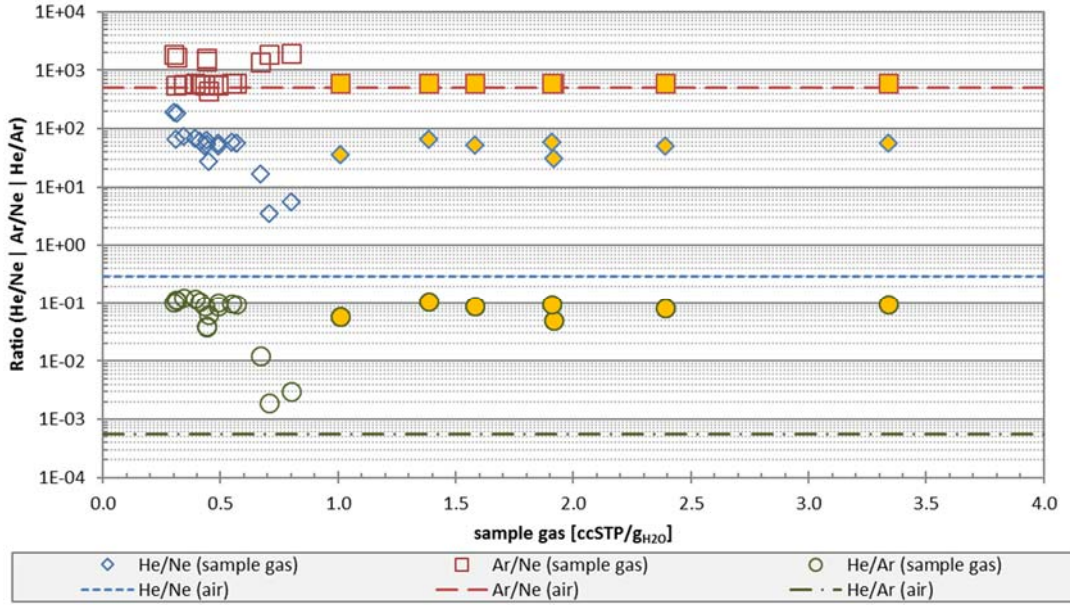
Notes: See Section 11.1.2 for discussion of labelled samples.

**Figure 11-7: Fractions of Ne (left) and Absolute Ne Amounts (right) in the Sample Container Gas, Together with Sample Container Gas Concentrations in the Porewater as a Function of Borehole Depth.**



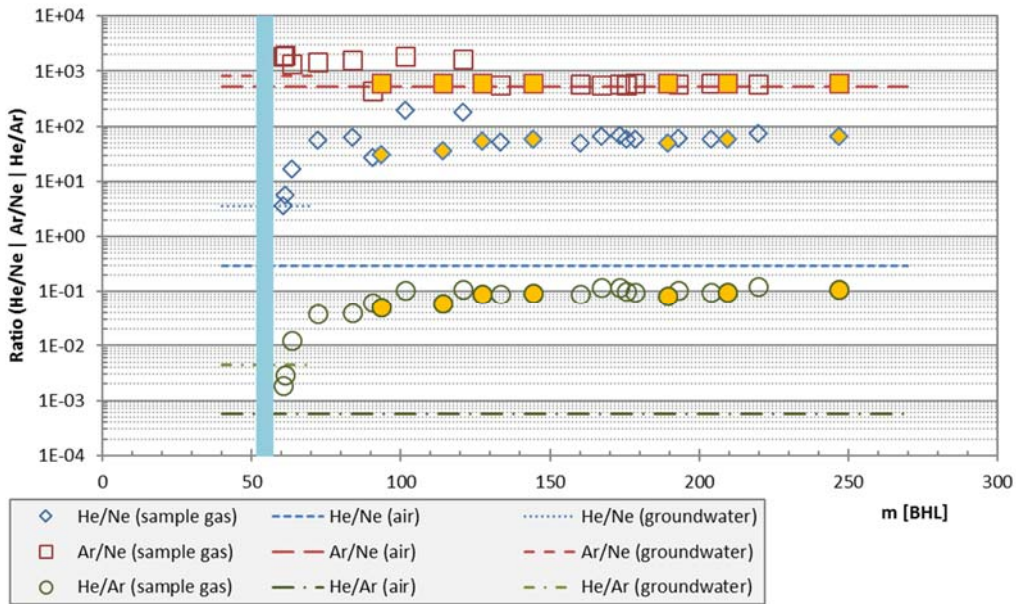
Notes: See Section 11.1.2 for discussion of labelled samples

**Figure 11-8: Fractions of Ne (left) and Absolute Ne Amounts (right) in the Sample Container Gas, Together with Sample Container Gas Concentrations in the Porewater as a Function of Borehole Depth.**



Notes: Filled symbols indicate samples with elevated gas concentrations (c.f. Figures 11-16 to 11-18).

**Figure 11-9: Ar/Ne, He/Ne and He/Ar Ratios of the BDB-1 Samples as Function of Sample Container Gas Concentration in Porewater.**



Notes: Filled symbols indicate samples with elevated gas concentrations (c.f. Figures 11-16 to 11-18); the vertical blue bar indicates the interval where the groundwater was sampled.

**Figure 11-10: Ar/Ne, He/Ne and He/Ar Ratios of the BDB-1 Samples as Function of Borehole Depth.**

This demonstrates that these samples have a) suffered from addition of a gas phase different to their porewater gas, and b) that the contaminant gas phase had a composition different from air and was depleted in He, Ne and Ar.

The type and origin of this gas phase is at the moment unknown. The contaminant phase during drilling would be air, as it would be during sampling of the core and later storage of the sample container (through leakage). The only contact of the sample with a gas phase dissimilar to air happens during flushing of the sample cylinder with N<sub>2</sub>, which would also satisfy the criteria of low noble gas abundances in this contaminant phase. The amounts of N<sub>2</sub>, which would have to have been added this way, are very roughly between 20 and 50 ccSTP, equivalent of an N<sub>2</sub> pressure in the sample containers between 100 and 270 mbar. This is far too much to be explained by insufficient pumping during sampling, as pumping times are similar to the other samples and the attained pressures after each pumping cycle was below 10 mbar (Appendix A3). It is also irreconcilable with impregnation of the sample material with N<sub>2</sub> during flushing, as the calculated N<sub>2</sub> amounts do not correlate with the sample porosity, but do rather surpass the limit of solubility in the available porewater by roughly one order of magnitude.

A hypothetical source for the contaminant gas phase could be bacterial production during storage, though only one of these samples was stored for 490 instead of less than 183 days (Appendix A3). As no reactive gas analyses are available for these samples, this hypothesis cannot currently be tested.

Nonetheless, with the contaminant gas phase not contributing to any of the investigated noble gas species, these samples can be used for hydrogeochemical evaluations in the same manner as the other samples.

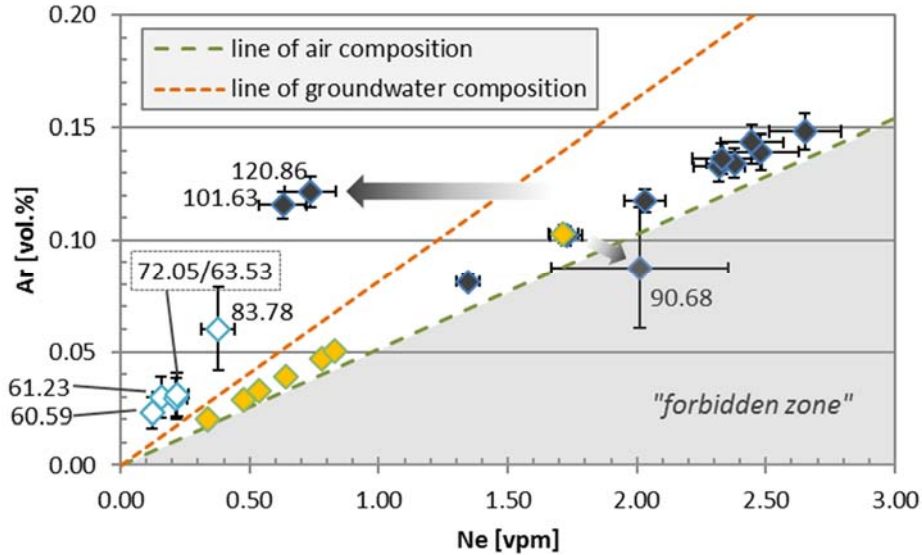
#### **11.1.2 Samples From Below 83.78 m and From 90.68 m, 101.63 m and 120.86 m BHL**

Considering that at minor degrees of air contamination both the resulting Ne and Ar in the sample container are dominantly derived from this air contamination (*cf.* Section 11.1.1), the relationship between these two species in the sample gas can be used to assess potential analytical problems or limits.

For the BDB-1 samples, roughly 90 % of the measured Ne and 30 % of the measured Ar is derived from air. As such, these samples lie roughly in a straight line above the air composition line when plotting the Ar fraction in the gas against the Ne fraction as the abscissa (Figure 11-11). The samples with elevated gas concentrations are shifted along this sample line toward the origin due to the equivalent relative dilution of both Ar and Ne (as discussed in section 11.1.1).

The 5 shallowest samples (60.59 – 83.78 m BHL) lie above both the line defined by the bulk of the samples, as well as above the line defined by the groundwater composition, ostensibly indicating either an Ar enrichment or Ne depletion. With the proximity of these samples to the groundwater conducting zone, and taking into account their low air contamination (qualitatively indicated by the low Ar fraction of less than 0.06 vol.% in the sample container gas), it would be expected that these samples plot between the sample composition line and (probably near to) the line defined by the groundwater composition. While there is no independent criterion to assess the accuracy of the Ar determination, it has already been indicated in Section 11.1.1 that the Ne measurements of these samples is below the limit of calibration and that they show Ne concentrations in the porewater below the value for air saturated water (and also below the Ne

concentration in the groundwater), suggesting that Ne might potentially be underestimated in these samples. As a consequence, these Ne concentrations are not considered for air-contamination correction.

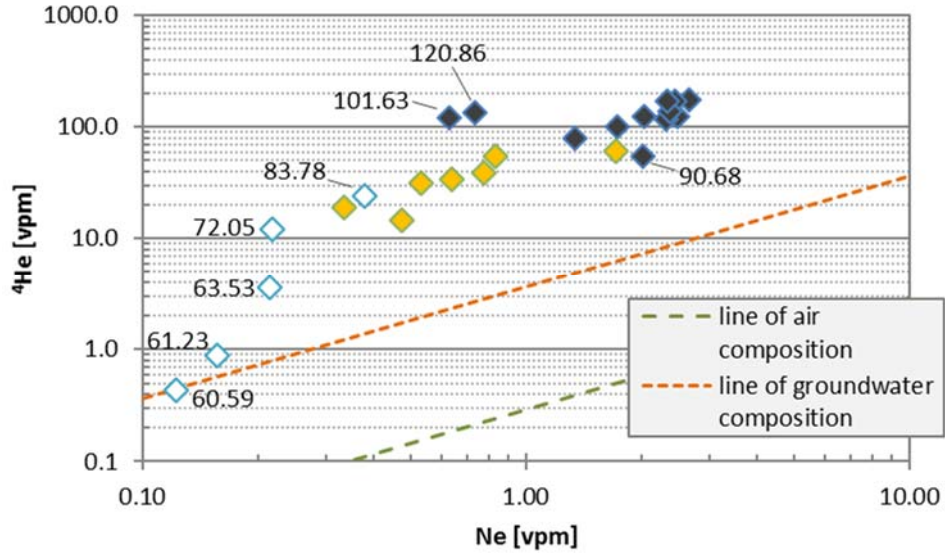


**Notes:** Empty diamonds indicate samples for which Ne is below the limit of calibration; light yellow diamonds indicate samples with elevated gas content. Error bars for samples low in Ne and Ar are within the symbols.

**Figure 11-11: Ar Fraction as Function of the Ne Fraction in the Sample Container Gas of the BDB-1 Samples.**

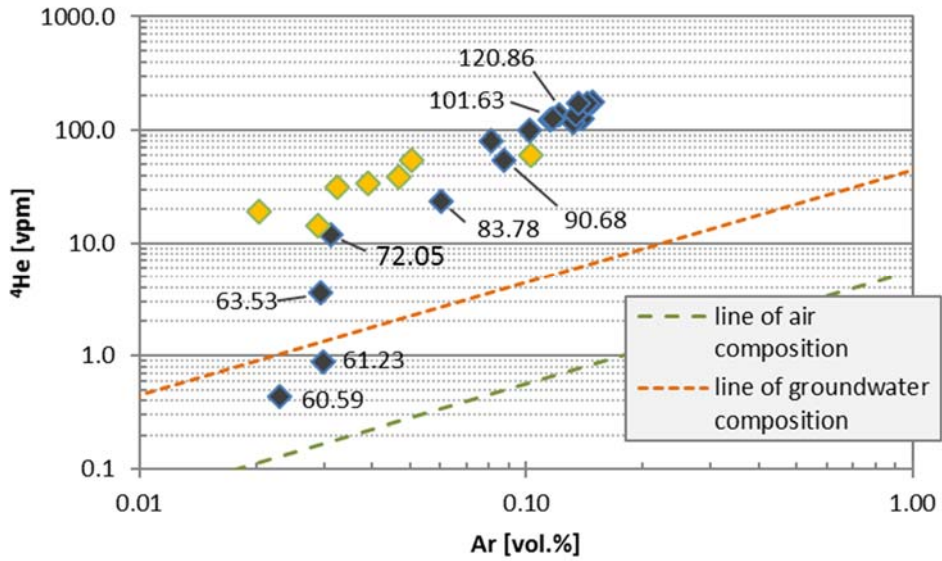
Sample BDB1-90.68-NG plots below the air composition line, which would require admixture of a Ne-enriched/Ar-depleted component. With no plausible source for such a component in the present geological system, this suggests a quantitative mis-determination of either of the two species, despite no indication to this effect during the analysis. Looking at the relative and absolute abundance of Ne and Ar (Figures 11-7 and 11-8), as well as the He/Ne and He/Ar ratios (Figures 11-12 and 11-13) of this sample in the context of its neighbouring samples, only a potential overestimation of Ne becomes manifest. In consequence, the noble gas data of sample BDB1-90.68-NG is – similar to the 5 shallowest samples – given without air-contamination correction.

Samples BDB1-101.63-NG and BDB1-120.86-NG also indicate either overestimation of Ar or underestimation of Ne, with the relative and absolute abundances of both species (Figures 11-7 and 11-8) as well as their relationship to He (Figures 11-12 and 11-13), suggesting the latter. As for BDB1-90.68-NG, the noble gas data for these samples are therefore given without air-contamination correction.



Notes: Empty diamonds indicate samples for which Ne is below the limit of calibration; light yellow diamonds indicate samples with elevated gas content. No error bars shown.

**Figure 11-12: <sup>4</sup>He Fraction as Function of the Ne Fraction in the Sample Container Gas of the BDB-1 Samples**



Notes: Light yellow diamonds indicate samples with elevated gas content. No error bars shown.

**Figure 11-13: <sup>4</sup>He Fraction as Function of the Ar Fraction in the Sample Container Gas of the BDB-1 Samples.**

**Table 11-2: Gas Pressure in Sample Containers, Ne and Gas Concentration in Porewater, He, Ne and Ar Concentration in Gas and  $^{20}\text{Ne}/^{22}\text{Ne}$  Ratio in Gas of BDB-1 Samples**

Sample	Depth	Stratigraphic	Member / Facies	Lithology	P	Gas <sub>H2O</sub>	1σ	Ne <sub>gas</sub>	Ne <sub>gas</sub>	1σ	$^{20}\text{Ne}/^{22}\text{Ne}$	1σ	He <sub>gas</sub>	1σ	Ar <sub>gas</sub>	1σ	aircontam.	R <sub>He/Ne</sub>	R <sub>Ar/Ne</sub>	R <sub>He/Ar</sub>
	m BHL				mbar	ccSTP/g <sub>H2O</sub>		ccSTP/g <sub>H2O</sub>	ppmv				ppmv		vol.%		vol.%			
estimated uncertainty (1σ)																				
BDB1-60.59-NG	60.59	PAF	Waldenburg - Mb.	sa lst	43	0.71	0.03						0.4	0.03	0.02	0.007	-	3.6	1889	1.90E-03
BDB1-61.23-NG	61.23	PAF	Waldenburg - Mb.	sa lst	34	0.8	0.04						0.9	0.1	0.03	0.009	-	5.7	1917	3.00E-03
BDB1-63.53-NG	63.53	PAF	Waldenburg - Mb.	sa lst	33	0.67	0.04						3.6	0.2	0.03	0.009	-	16.8	1368	1.20E-02
BDB1-66.40-NG	66.4	PAF	Waldenburg - Mb.	sa lst	32	1.03	0.05						4.6	0.5	0.03	0.002	-	-	-	1.60E-02
BDB1-72.05-NG	72.05	PAF	Waldenburg - Mb.	sa lst	33	0.44	0.02						12	0.7	0.03	0.01	-	55.3	1435	3.90E-02
BDB1-83.78-NG	83.78	PAF	Waldenburg - Mb.	mst	43	0.44	0.02						23.8	1.3	0.06	0.018	-	62.8	1586	4.00E-02
BDB1-90.68-NG	90.68	PAF	Himichopf - Mb.	li sst	41	0.45	0.02						54.5	2.9	0.09	0.027	8.7	27.1	435	6.20E-02
BDB1-93.40-NG	93.4	PAF	Himichopf - Mb.	sa ma	236	1.91	0.04	9.10×10-07	0.48	0.01	8.5	0.3	14.4	0.4	0.03	0.001	2.1	30.4	609	5.00E-02
BDB1-101.63-NG	101.63	PAF	Sissach - Mb.	sa ma	42	0.3	0.01						121	6.2	0.12	0.006	0.01	192.4	1840	1.00E-01
BDB1-114.08-NG	114.08	OPA	sandy facies 2	clst & lst la	61	1.01	0.03	1.73×10-06	1.71	0.06	8.9	0.3	61.1	2.3	0.1	0.004	8.4	35.6	600	5.90E-02
BDB1-120.86-NG	120.86	OPA	sandy facies 2	clst & lst la	35	0.31	0.02						134	7.2	0.12	0.007	0.7	182.4	1656	1.10E-01
BDB1-127.33-NG	127.33	OPA	sandy facies 2	clst & lst la	168	1.58	0.03	1.01×10-06	0.64	0.02	8.7	0.3	34.2	0.9	0.04	0.001	2.9	53.3	608	8.80E-02
BDB1-133.46-NG	133.46	OPA	sandy facies 2	clst & lst la	32	0.43	0.02	1.07×10-06	2.48	0.15	9.8	1.7	125.6	7	0.14	0.008	11.2	50.7	562	9.00E-02
BDB1-144.49-NG	144.49	OPA	shaly facies 2	silt clst	319	3.34	0.06	1.12×10-06	0.34	0.01	8.5	0.3	19.2	0.5	0.02	0.001	1.5	57.2	608	9.40E-02
BDB1-160.25-NG	160.25	OPA	shaly facies 2	silt clst	43	0.49	0.02	1.14×10-06	2.32	0.1	9	0.5	116.3	5.1	0.13	0.006	10.6	50.2	572	8.80E-02
BDB1-167.38-NG	167.38	OPA	shaly facies 2	silt clst	37	0.31	0.01	8.24×10-07	2.65	0.14	9.3	0.8	174.4	8.8	0.15	0.008	11.2	65.8	559	1.20E-01
BDB1-173.47-NG	173.47	OPA	shaly facies 2	silt clst	38	0.39	0.02	9.55×10-07	2.45	0.12	10.1	1	170.6	8.3	0.14	0.007	10.8	69.8	587	1.20E-01
BDB1-175.53-NG	175.53	OPA	sandy facies 1	clst & sst la	43	0.49	0.02	1.16×10-06	2.38	0.11	9.1	0.8	137.1	6.1	0.13	0.006	11	57.6	564	1.00E-01
BDB1-178.53-NG	178.53	OPA	sandy facies 1	clst & sst la	66	0.57	0.02	9.82×10-07	1.73	0.06	9.1	0.4	99.3	3.6	0.1	0.004	7.7	57.5	591	9.70E-02
BDB1-189.52-NG	189.52	OPA	carb.-rich sandy f.	lst	147	2.39	0.06	1.86×10-06	0.78	0.02	8.5	0.3	38.7	1.1	0.05	0.002	3.8	49.7	604	8.20E-02
BDB1-193.13-NG	193.13	OPA	shaly facies 1	clst	55	0.41	0.01	8.36×10-07	2.03	0.08	8.5	0.4	124.4	5	0.12	0.005	8.6	61.2	578	1.10E-01
BDB1-204.09-NG	204.09	OPA	shaly facies 1	clst	88	0.55	0.02	7.36×10-07	1.35	0.04	8.8	0.3	79.5	2.8	0.08	0.003	5.5	59.1	604	9.80E-02
BDB1-209.37-NG	209.37	OPA	shaly facies 1	clst	200	1.91	0.04	1.02×10-06	0.53	0.01	8.7	0.3	31.5	0.8	0.03	0.001	2.4	59	609	9.70E-02
BDB1-219.66-NG	219.66	OPA	shaly facies 1	clst	43	0.34	0.02	8.02×10-07	2.33	0.12	9.6	0.8	170	8	0.14	0.007	9.8	73	585	1.20E-01
BDB1-246.99-NG	246.99	STF	Rietheim Mb.	bit ma	127	1.39	0.03	1.15×10-06	0.83	0.02	8.6	0.4	54.3	1.7	0.05	0.002	3.8	65.3	607	1.10E-01
air value									18.18		9.782		5.24	0.005	0.934	0.0009		0.29	513.8	5.60E-04

**Notes:**

PAF = Passwang Formation, OPA = Opalinus Clay, STF = Stafflegg Formation. Field lithology after Hostettler et al. (2017): li sst = limy sandstone, sa ma = sandy marl, mst = marlstone, lst = limestone; sa lst = sandy limestone, clst = claystone, silt clst = silty claystone, clst & lst la = claystone with limestone layers, clst & sst la = claystone with sandstone layers, arg ma = argillaceous marl, bit ma = bituminous marl. Shaded samples were used for inter-laboratory comparison.

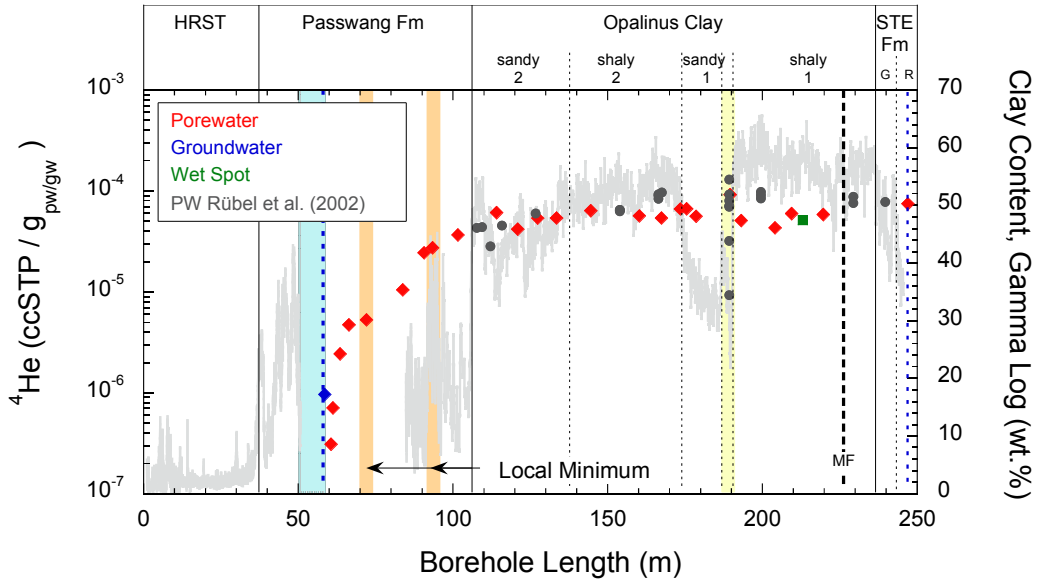
## 11.2 $^4\text{He}$ CONCENTRATION AND $^3\text{He}/^4\text{He}$ RATIO IN POREWATER

The BDB-1 samples have  $^4\text{He}$  concentrations between  $4.19 \times 10^{-5}$  and  $9.19 \times 10^{-5}$  ccSTP/g<sub>pw</sub> in the Opalinus Clay and the Staffelegg Fm, while concentrations in the Passwang Fm go as low as  $< 1 \times 10^{-6}$  ccSTP/g<sub>pw</sub> toward the groundwater-conducting feature near the boundary between the Brüggli- and Waldenburg-Member (Table 11-3, Figure 5-18). These concentrations are as much as 3 orders of magnitude higher than air-saturated water (approximately  $4.6 \times 10^{-8}$  ccSTP/g<sub>H<sub>2</sub>O</sub>, Kipfer et al. 2002), giving evidence to the accumulation of radiogenic  $^4\text{He}$  produced underground. For the Opalinus Clay, the measured  $^4\text{He}$  concentrations from the BDB-1 samples are comparable to porewater  $^4\text{He}$  values, ranging from  $2.8 \times 10^{-5}$  to  $9.8 \times 10^{-5}$  ccSTP/g in samples recovered from various boreholes of the WS experiment (Rübel et al. 2002) and  $3.3\text{--}4.8 \times 10^{-5}$  ccSTP/g measured by Mainault et al. (2013) from the undisturbed part of a borehole into the sandy facies underlying the upper shaly facies at the level of the rock laboratory. The values are also near identical to the  $^4\text{He}$  concentration of  $5.14 \times 10^{-4}$  ccSTP/g determined on water obtained from a wet spot in the Opalinus Clay (D. Traber, *pers. comm.* 2016). Compared to  $^4\text{He}$  concentrations in the Opalinus Clay from the Schlattingen borehole, SLA-1 ( $2.7 \times 10^{-4}$  to  $10.2 \times 10^{-4}$  ccSTP/g; Rufer and Waber 2015) and Benken ( $1.9 \times 10^{-4}$  ccSTP/g; NAGRA 2001; Rübel and Sonntag 2000), the BDB-1 values are roughly one order of magnitude lower, reflecting the different geological setting of the Opalinus Clay at Mont Terri from that in Northeastern Switzerland.

As a function of depth,  $^4\text{He}$  concentrations are very similar throughout the Opalinus Clay, within approximately a factor of 2, showing a flat profile over the entire unit, again comparable to the data by Rübel et al. (2002) (Figure 11-14). Above the Opalinus Clay, and upward through the limestones of the Passwang Fm, the  $^4\text{He}$  concentrations show a clear decrease of more than one order of magnitude, from values similar to the Opalinus Clay to values  $< 1 \times 10^{-6}$  ccSTP/g<sub>pw</sub> close to the water-conducting feature at 58.6 m BHL. These lower values coincide with the  $^4\text{He}$  concentration measured in the groundwater (*cf.* Chapter 12).

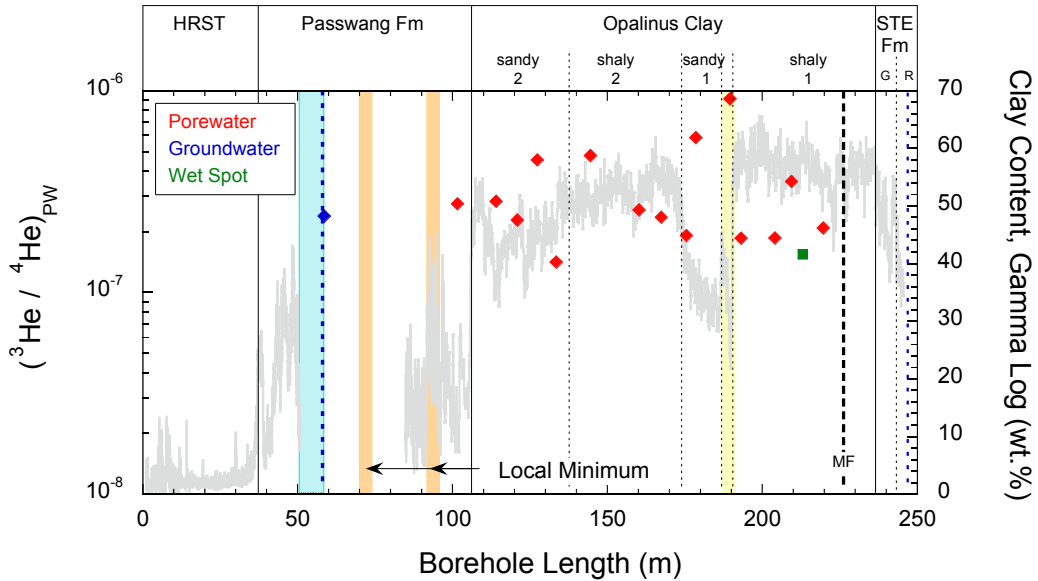
Measured  $^3\text{He}/^4\text{He}$  isotope ratios of the BDB-1 samples range from  $1.42 \times 10^{-7}$  to  $9.12 \times 10^{-7}$  throughout the Opalinus Clay and the topmost Passwang Fm. The data forms a flat profile with depth, with values scattering roughly around the  $^3\text{He}/^4\text{He}$  value of  $2.39 \times 10^{-7}$  determined on the groundwater (Figure 11-15). Compared to a single  $^3\text{He}/^4\text{He}$  value of  $1.54 \times 10^{-7}$  determined on a wet spot in the Opalinus Clay (D. Traber, *pers. comm.* 2016; sample wa,447,113), the isotope ratios of the BDB-1 samples are within the same order of magnitude, though on average roughly a factor of 2 higher.

No correlation exists between clay mineral content and the  $^4\text{He}$  concentration or the  $^3\text{He}/^4\text{He}$  isotope ratio for the samples from the Opalinus Clay, except for sample BDB1-189.52-NG from the sandy carbonate-rich facies. This low clay-mineral content sample shows both the highest  $^4\text{He}$  concentration ( $9.19 \times 10^{-5}$  ccSTP/g<sub>pw</sub>) and the highest  $^3\text{He}/^4\text{He}$  ratio ( $9.14 \times 10^{-7}$ ) of all samples analysed.



Notes: The blue shaded area is the depth interval in which the groundwater was sampled. Error bars are within symbol size [except for data by Rbel et al. (2002) where no error is given].

**Figure 11-14: Distribution <sup>4</sup>He Concentration in Porewater Across the Passwang Fm, Opalinus Clay and Staffelegg Fm in Borehole BDB-1 at the Mont Terri URL.**



Notes: The blue shaded area is the depth interval in which the groundwater was sampled. Error bars are within symbol size.

**Figure 11-15: Distribution of <sup>3</sup>He/<sup>4</sup>He Isotope Ratio in Porewater Across the Passwang Fm, Opalinus Clay and Staffelegg Fm in Borehole BDB1 at the Mont Terri URL.**

**Table 11-3:  $^4\text{He}$  and Ar Concentration and  $^3\text{He}/^4\text{He}$  and  $^{40}\text{Ar}/^{36}\text{Ar}$  Isotope Ratio in Porewater of BDB-1 Samples**

Sample	Depth m BHL	Strati- graphy	Member / Facies	Lithology	$^4\text{He}$ PW ccSTP/g <sub>PW</sub>	$\sigma$	$^3\text{He}/^4\text{He}$ PW ccSTP/g <sub>H<sub>2</sub>O</sub>	$A_{\text{H}_2\text{O}}$	$^{40}\text{Ar}/^{36}\text{Ar}_{\text{H}_2\text{O}}$	$R/R_{\text{air}}$
estimated uncertainty ( $1\sigma$ )					$\sigma = 0.3 - 2\%$					
BDB1-60.59-NG	60.59	PAF	Waldenburg - Mb.	sa lst	3.09E-07 <sup>a)</sup>		n.a.	1.63E-04	319	1.07
BDB1-61.23-NG	61.23	PAF	Waldenburg - Mb.	sa lst	7.09E-07 <sup>a)</sup>		n.a.	2.39E-04	302	1.01
BDB1-63.53-NG	63.53	PAF	Waldenburg - Mb.	sa lst	2.43E-06	7.70E-08	n.a.	1.97E-04	314	1.05
BDB1-66.40-NG	66.4	PAF	Waldenburg - Mb.	sa lst	4.72E-06	4.22E-07	n.a.	<sup>c)</sup>		
BDB1-72.05-NG	72.05	PAF	Waldenburg - Mb.	sa lst	5.29E-06	1.61E-07	n.a.	1.37E-04	324	1.08
BDB1-83.78-NG	83.78	PAF	Waldenburg - Mb.	mst	1.05E-05	3.61E-07	n.a.	2.65E-04	304	1.02
BDB1-90.68-NG	90.68	PAF	Himichopf - Mb.	li sst	2.44E-05	7.40E-07	n.a.	3.92E-04	298	1
BDB1-93.40-NG	93.4	PAF	Himichopf - Mb.	sa ma	2.74E-05	5.99E-07	n.a.	5.54E-04	362	1.21
BDB1-101.63-NG	101.6	PAF	Sissach - Mb.	sa ma	3.67E-05	9.44E-07	2.75E-07	3.51E-04	304	1.02
BDB1-114.08-NG	114.1	OPA	sandy facies 2	clst & lst la	6.11E-05	1.25E-06	2.83E-07	1.04E-03	295	0.99
BDB1-120.86-NG	120.9	OPA	sandy facies 2	clst & lst la	4.19E-05	7.70E-07	2.28E-07	3.80E-04	314	1.05
BDB1-127.33-NG	127.3	OPA	sandy facies 2	clst & lst la	5.39E-05	9.04E-07	4.53E-07	6.18E-04	301	1.01
BDB1-133.46-NG	133.5	OPA	sandy facies 2	clst & lst la	5.41E-05	1.03E-06	1.42E-07	6.03E-04	299	1
BDB1-144.49-NG	144.5	OPA	shaly facies 2	silt clst	6.37E-05	1.06E-06	4.78E-07	6.81E-04	335	1.12
BDB1-160.25-NG	160.3	OPA	shaly facies 2	silt clst	5.67E-05	9.65E-07	2.56E-07	6.50E-04	291	0.98
BDB1-167.38-NG	167.4	OPA	shaly facies 2	silt clst	5.40E-05	9.08E-07	2.36E-07	4.61E-04	305	1.02
BDB1-173.47-NG	173.5	OPA	shaly facies 2	silt clst	6.64E-05	1.12E-06	<sup>b)</sup>	5.60E-04	313	1.05
BDB1-175.53-NG	175.5	OPA	sandy facies 1	clst & sst la	6.68E-05	1.13E-06	1.91E-07	6.56E-04	298	1
BDB1-178.53-NG	178.5	OPA	sandy facies 1	clst & sst la	5.62E-05	9.58E-07	5.85E-07	5.81E-04	291	0.97
BDB1-189.52-NG	189.5	OPA	carb.-rich sandy f.	lst	9.19E-05	1.65E-06	9.12E-07	1.12E-03	289	0.97
BDB1-193.13-NG	193.1	OPA	shaly facies 1	clst	5.10E-05	8.69E-07	1.86E-07	4.84E-04	293	0.98
BDB1-204.09-NG	204.1	OPA	shaly facies 1	clst	4.33E-05	7.49E-07	1.86E-07	4.45E-04	290	0.97
BDB1-209.37-NG	209.4	OPA	shaly facies 1	clst	5.98E-05	1.01E-06	3.55E-07	6.21E-04	300	1
BDB1-219.66-NG	219.7	OPA	shaly facies 1	clst	5.84E-05	1.02E-06	2.09E-07	4.69E-04	324	1.08
BDB1-246.99-NG	247	STF	Rietheim Mb.	bit ma	7.49E-05	1.84E-06	n.a.	6.99E-04	306	1.03

**Notes:**

Ar data is considered semi-quantitative and is given without uncertainties;  $R_{\text{air}} = 298.56$ .

n.a.”= not analysed, <sup>a)</sup> values below limit of calibration (section 5.1.1) are given without uncertainty, <sup>b)</sup> no values due to analytical problems, <sup>c)</sup> analysed, discarded due to analytical problems. PAF = Passwang Formation, OPA = Opalinus Clay, STF = Stafflegg Formation. Field lithology after Hostettler et al. (2017): li sst = limy sandstone, sa ma = sandy marl, mst = marlstone, lst = limestone; sa lst = sandy limestone, clst = claystone, silt clst = silty claystone, clst & lst la = claystone with limestone layers, clst & sst la = claystone with sandstone layers, arg ma = argillaceous marl, bit ma = bituminous marl. Shaded samples were used for inter-laboratory comparison.

### 11.3 EVOLUTION OF THE $^4\text{He}$ POREWATER PROFILE

#### 11.3.1 In-situ Production of He in the Rock and Transfer to the Porewater

Helium and Ar parent radionuclide data (U, Th, Li and K) were measured on the rock material of 8 noble gas sample pieces over the entire core length, with 5 of those samples originating from the Opalinus Clay Formation.  $^4\text{He}$  concentrations and  $^3\text{He}/^4\text{He}$  ratios in the rock matrix were also determined, with the latter representing an upper limit given without measure of uncertainty, as the  $^3\text{He}$  concentrations were at or below the limit of measurement (Table 11-4).

For the Opalinus Clay Formation, the average measured helium parent nuclide concentrations are U = 2.63 ppm, Th = 12.7 ppm and Li = 124 ppm (Table 11-4), which is comparable to the average values of 2.65 ppm, 13 ppm and 141 ppm, respectively, reported by Lehmann and Tolstikhin (1999) and Rubel et al. (2002) for Opalinus Clay in the Benken borehole, Northern Switzerland.

Based on these values, a formation average annual  $^4\text{He}$  production rate ( $^4\text{He}_P$ ) can be calculated according to Ballentine & Burnard (2002) as:

$$^4\text{He}_P = (3.115 \times 10^6 + 1.272 \times 10^5) \times U + 7.710 \times 10^5 \times Th \quad \left[ \frac{\text{atoms}}{g_{\text{rock}} \times a} \right] \quad (34)$$

which is recalculated in ccSTP/( $g_{\text{rock}} \times a$ ) according to :

$$^4\text{He}_P [\text{ccSTP } g_{\text{rock}}^{-1} a^{-1}] = \frac{^4\text{He}_P \left[ \frac{\text{atoms}}{g_{\text{rock}} \times a} \right]}{6.022 \times 10^{23}} \times 22711 \quad (35)$$

where  $6.022 \times 10^{23}$  is Avogadro's number and the factor 22711 is the molar gas volume in ccSTP/mole.

Multiplying the annual  $^4\text{He}$  production with the average sedimentation age ( $t_{\text{sedim.}}$ ) of 172 Ma for the Opalinus Clay Formation (ICS International Chronostratigraphic Chart 2013) yields the maximal produced  $^4\text{He}$  since the time of deposition ( $^4\text{He}_{P \text{ max}}$ ) as:

$$^4\text{He}_{P \text{ max}} = ^4\text{He}_P \times t_{\text{sedim.}} \quad [\text{ccSTP } g_{\text{rock}}^{-1}] \quad (36)$$

For the Opalinus Clay at Mont Terri, the formation average annual radiogenic  $^4\text{He}$  production calculates to  $6.9 \times 10^{-13}$  ccSTP/( $g_{\text{rock}} a$ ) and the maximal produced  $^4\text{He}$  over the last 172 Ma to  $1.2 \times 10^{-4}$  ccSTP/ $g_{\text{rock}}$ , which is comparable to values obtained on Opalinus Clay rock samples from the Schlattingen borehole, SLA-1 ( $1.0 \times 10^{-4}$  to  $1.8 \times 10^{-4}$  ccSTP/ $g_{\text{rock}}$ ; Rufer and Waber 2015).

Based on  $^4\text{He}_{P \text{ max}}$  and the average He concentration measured in the Opalinus Clay at Mont Terri ( $^4\text{He}_{\text{rock}} = 8.6 \times 10^{-6}$  ccSTP/ $g_{\text{rock}}$ , Table 11-6), the amount of  $^4\text{He}$  that has maximally been lost from the rock to the porewater since its deposition can be calculated as:

$$^4\text{He}_{\text{loss max}} = ^4\text{He}_{P \text{ max}} - ^4\text{He}_{\text{rock}} \quad [\text{ccSTP } g_{\text{rock}}^{-1}] \quad (37)$$

With a calculated formation average,  ${}^4\text{He}_{\text{loss max}}$  of  $1.11 \times 10^{-4}$  ccSTP/g<sub>rock</sub>, the Opalinus Clay at Mont Terri has lost 93 % of the in-situ produced  ${}^4\text{He}$  to the porewater, which is well within the range of identically calculated values for Opalinus Clay from the deep borehole at Benken (>95 %, Lehmann et al. 2001) and Schlattingen (93-98 %, Rufer and Waber 2015).

When assuming no loss of gas from the porewater into the atmosphere (i.e., a hypothetical closed-system condition), the maximal accumulation (i.e., of  ${}^4\text{He}$  in the porewater of the Opalinus Clay since the time of deposition ( ${}^4\text{He}_{\text{accum. max}}$ )) can be calculated as:

$${}^4\text{He}_{\text{accum. max}} = {}^4\text{He}_{\text{loss max}} \times \frac{\rho_{\text{grain}}}{\rho_{\text{PW}}} \times \frac{1-\phi_{\text{WL}}}{\phi_{\text{WL}}} \quad [\text{ccSTP } g_{\text{PW}}^{-1}] \quad (38)$$

where  $\rho_{\text{grain}} = 2.70$  is the average grain density of the Opalinus Clay samples (Table 7-1),  $\rho_{\text{PW}} =$  density of the porewater (taken as  $1.0 \text{ g cm}^{-3}$ ) and  $\phi_{\text{WL}} = 13 \text{ vol.}\%$  is the average water-loss porosity of the Opalinus Clay samples (Tables 7-1 and 7-2).

The formation-specific maximum accumulation,  ${}^4\text{He}_{\text{accum. max}}$ , value for the Opalinus Clay at Mont Terri is calculated to be  $2.1 \times 10^{-3}$  ccSTP/g<sub>pw</sub>, which is again similar to the values obtained for the Opalinus Clay at Schlattingen ( $3.0 \times 10^{-3}$  ccSTP/g<sub>pw</sub>; Rufer and Waber 2015).

The  ${}^3\text{He}$  production in the rock is dominated by thermal neutron capture by  ${}^6\text{Li}$  in the reaction:



Lehmann and Rubel (in Pearson et al. 2003) calculated the maximal produced  ${}^3\text{He}$  since the time of deposition ( ${}^3\text{He}_{\text{p max}}$ ) in several Opalinus Clay samples based on their measured Li concentrations in the rock and “assuming a representative neutron flux for clay” (no numerical value is given). Recalculating their  ${}^3\text{He}_{\text{p max}}$  into an annual  ${}^3\text{He}$  production rate as a function of Li concentration gives an average value of  ${}^3\text{He}_{\text{p}} = 5.8 \times 10^{-15}$  ccSTP g<sub>rock</sub><sup>-1</sup> a<sup>-1</sup> [Li]<sub>ppm</sub><sup>-1</sup>. This allows a comparative calculation of annual  ${}^3\text{He}$  production for the BDB-1 samples by multiplying the calculated average rate from Lehmann and Rubel with the measured Li concentrations from the BDB-1 samples. This results in annual  ${}^3\text{He}$  production rates between  $0.7 \times 10^{-20}$  and  $3.3 \times 10^{-20}$  ccSTP g<sub>rock</sub><sup>-1</sup> a<sup>-1</sup> and in  ${}^3\text{He}/{}^4\text{He}$  production ratios of  $1.6 \times 10^{-8}$  to  $4.6 \times 10^{-8}$  for the Opalinus Clay (Table 11-6). These values are comparable to those calculated with the data given by Rubel and Lehmann (2003): average  ${}^3\text{He}_{\text{p}}$  of  $2.3 \times 10^{-20}$  ccSTP g<sub>rock</sub><sup>-1</sup> a<sup>-1</sup> and average ( ${}^3\text{He}/{}^4\text{He}$ )<sub>p</sub> of  $3.0 \times 10^{-8}$ .

While the listed  ${}^3\text{He}/{}^4\text{He}$  ratios in the rock matrix for the BDB-1 samples only represent an approximate (maximum) value due to analytical limitations in determining  ${}^3\text{He}$  concentrations, their range ( $2.9 \times 10^{-8}$  to  $5.3 \times 10^{-8}$ , Table 11-6) overlaps with the range of measured  ${}^3\text{He}/{}^4\text{He}$  ratios in the rock given by Rubel and Lehmann (2003;  $1.8 \times 10^{-8}$  to  $7.3 \times 10^{-8}$ ).

Comparing the average BDB-1 Opalinus Clay  ${}^3\text{He}/{}^4\text{He}$  production ratios ( $2.9 \times 10^{-8}$ ) with the determined  ${}^3\text{He}/{}^4\text{He}$  ratios in the rock matrix ( $3.9 \times 10^{-8}$ ) and in the porewater ( $3.4 \times 10^{-7}$ ), a shift from isotopically heavier to increasingly lighter ratios is observed, with the porewater being on the order of one magnitude lighter than the other two ratios. The same phenomenon of increasingly lighter  ${}^3\text{He}/{}^4\text{He}$  signatures from the in-situ production ratio to the rock He inventory to the porewater has already been observed at Benken (Lehmann et al. 2001; Rubel and

Sonntag 2000), Schlattingen (Rufer and Waber 2015) and Weiach (no porewater data; Tolstikhin et al. 2005, 2011).

For Mont Terri, Rübél and Lehmann (2003) propose that the difference observed in their data between the isotopically heavier He in the rock (average of  $4.3 \times 10^{-8}$ ) and the lighter He in the porewater ( $> 1 \times 10^{-7}$ ) could be explained by isotope fractionation during the release of He from the rock matrix<sup>7</sup>. However, while a lighter  $^3\text{He}/^4\text{He}$  rock ratio relative to the production ratio would require that the He released from the rock into the porewater must be enriched in  $^4\text{He}$ , the opposite would be required in order to explain the even more  $^3\text{He}$ -enriched porewater signature.

As such, the increasingly lighter He signatures in these three reservoirs cannot be solely explained by fractionation during the release from the rock matrix, but requires at least one other process. For the Benken and Schlattingen site, addition of a small fraction of isotopically light, mantle-type He has been proposed by Lehmann et al. (2001), Waber et al. (2003) and Rufé and Waber (2015), respectively.

### 11.3.2 Quantitative Assessment of the He Porewater Profile

Comparing the measured present day  $^4\text{He}_{\text{pw}}$  concentration with  $^4\text{He}_{\text{accum max}}$  shows that the current He inventory in the Opalinus Clay porewater constitutes only roughly 3 % of the maximum possible accumulation of  $^4\text{He}$  in the porewater since the time of sedimentation. Contrary to the previously discussed intrinsic values of the rock-porewater system, the retained He fraction in the porewater of the Opalinus Clay is much lower at Mont Terri than at Schlattingen (10 – 45 %; Rufé and Waber 2015), clearly mirroring the different geological history of the two sites.

The minimum time that would be required to produce the presently observed porewater He inventory exclusively by in-situ production in the rocks (i.e., under closed system conditions; no in- and outflux from the rock-porewater system), can be assessed by:

$$t_{\min} = \frac{{}^4\text{He}_{\text{pw}}}{{}^4\text{He}_{\text{accum max}}} \times t_{\text{sedim.}} \quad (40)$$

For the Opalinus Clay at Mont Terri,  $t_{\min}$  calculates to 4.9 Ma using the formation average  $^4\text{He}_{\text{pw}}$  of  $5.9 \times 10^{-5}$  ccSTP/g<sub>pw</sub>. If the maximal measured  $^4\text{He}_{\text{pw}}$  ( $9.2 \times 10^{-5}$  ccSTP/g<sub>pw</sub>) is used,  $t_{\min}$  equals 7.7 Ma. This is comparable to the (identically calculated) value of 9.1 Ma obtained by Rübél et al. (2002), with the difference being primarily attributable to the difference in water-loss porosity  $\phi_{\text{WL}}$  (recalculating the present data with the  $\phi_{\text{WL}} = 16$  vol.% of Rübél et al. (2002) gives a  $t_{\min}$  of 10.1 Ma).

The He concentrations from the water-conducting fracture in the Passwang Fm, and down and across the Opalinus Clay, depict a diffusion profile with the groundwater He concentration as an approximate boundary condition and little to no gradient in the lower part of the Opalinus Clay.

<sup>7</sup> The cited text erroneously states (based on the  $^3\text{He}/^4\text{He}$  ratios of the rock matrix and the porewater) that the **heavier**  $^4\text{He}$  isotope is released preferentially, but this would lead to a  $^4\text{He}$  depletion in the rock with the corresponding enrichment in the porewater. As a result, the rock would show a higher and the porewater a lower  $^3\text{He}/^4\text{He}$  ratio, diametrically opposite to what is stated in the text and is evident in the data.

**Table 11-4: Radionuclide and <sup>4</sup>He Concentration, <sup>3</sup>He/<sup>4</sup>He Isotope Ratio and Helium Production Rates and Ratios in the Rock Matrix of BDB-1 Samples**

Sample	Depth	Stratigraphy	Member / Facies	Lithology	U	Th	K	Li
	m BHL				[ppm]	[ppm]	[wt. %]	[ppm]
estimated uncertainty (1σ)					σ = 10%	σ = 10%	σ = 3%	σ = 20%
BDB1-63.53-NG	63.53	PAF	Waldenburg - Mb.	sa lst	0.58	11.90	0.45	9
BDB1-93.40-NG	93.4	PAF	Himichopf - Mb.	sa ma	2.62	12.10	2.46	103
BDB1-127.33-NG	127.3	OPA	sandy facies 2	clst & lst la	3.07	15.00	2.50	135
BDB1-160.25-NG	160.3	OPA	shaly facies 2	silt clst	2.92	15.40	2.49	177
BDB1-178.53-NG	178.5	OPA	sandy facies 1	clst & sst la	2.77	13.10	2.22	70
BDB1-189.52-NG	189.5	OPA	carb.-rich sandy f.	lst	1.54	7.20	0.92	39
BDB1-209.37-NG	209.4	OPA	shaly facies 1	clst	2.87	13.00	2.44	201
BDB1-246.99-NG	247	STF	Rietheim Mb.	bit ma	4.38	6.60	1.52	24
<i>OPA</i>	<i>average</i>				2.63	12.7	2.11	124

Sample	Depth	Stratigraphy	Member / Facies	Lithology	<sup>4</sup> He <sub>rock</sub>	<sup>3</sup> He/ <sup>4</sup> He <sub>rock</sub>	<sup>4</sup> He <sub>p</sub>	<sup>3</sup> He <sub>p</sub>	<sup>3</sup> He/ <sup>4</sup> He <sub>p</sub>
	m BHL				ccSTP/g <sub>rock</sub>	(upper limit)	ccSTP g <sub>rock</sub> <sup>-1</sup> a <sup>-1</sup>	ccSTP g <sub>rock</sub> <sup>-1</sup> a <sup>-1</sup>	
estimated uncertainty (1σ)					σ = 10%				
BDB1-63.53-NG	63.53	PAF	Waldenburg - Mb.	sa lst	10.5×10 <sup>-6</sup>	4.5×10 <sup>-8</sup>	4.17×10 <sup>-13</sup>	0.16×10 <sup>-20</sup>	0.4×10 <sup>-8</sup>
BDB1-93.40-NG	93.4	PAF	Himichopf - Mb.	sa ma	8.4×10 <sup>-6</sup>	2.4×10 <sup>-8</sup>	6.72×10 <sup>-13</sup>	1.71×10 <sup>-20</sup>	2.5×10 <sup>-8</sup>
BDB1-127.33-NG	127.3	OPA	sandy facies 2	clst & lst la	4.5×10 <sup>-6</sup>	5.3×10 <sup>-8</sup>	8.12×10 <sup>-13</sup>	2.25×10 <sup>-20</sup>	2.8×10 <sup>-8</sup>
BDB1-160.25-NG	160.3	OPA	shaly facies 2	silt clst	4.3×10 <sup>-6</sup>	4.8×10 <sup>-8</sup>	8.05×10 <sup>-13</sup>	2.95×10 <sup>-20</sup>	3.7×10 <sup>-8</sup>
BDB1-178.53-NG	178.5	OPA	sandy facies 1	clst & sst la	10.0×10 <sup>-6</sup>	2.9×10 <sup>-8</sup>	7.20×10 <sup>-13</sup>	1.17×10 <sup>-20</sup>	1.6×10 <sup>-8</sup>
BDB1-189.52-NG	189.5	OPA	carb.-rich sandy f.	lst	11.2×10 <sup>-6</sup>	3.4×10 <sup>-8</sup>	3.98×10 <sup>-13</sup>	0.65×10 <sup>-20</sup>	1.6×10 <sup>-8</sup>
BDB1-209.37-NG	209.4	OPA	shaly facies 1	clst	12.8×10 <sup>-6</sup>	3.1×10 <sup>-8</sup>	7.29×10 <sup>-13</sup>	3.34×10 <sup>-20</sup>	4.6×10 <sup>-8</sup>
BDB1-246.99-NG	247	STF	Rietheim Mb.	bit ma	6.2×10 <sup>-6</sup>	3.6×10 <sup>-8</sup>	7.29×10 <sup>-13</sup>	3.96×10 <sup>-20</sup>	0.5×10 <sup>-8</sup>
<i>OPA</i>	<i>average</i>				8.6×10 <sup>-6</sup>	3.9×10 <sup>-8</sup>	6.93×10 <sup>-13</sup>	2.07×10 <sup>-20</sup>	2.9×10 <sup>-8</sup>

**Notes:**

<sup>3</sup>He/<sup>4</sup>He ratios are maximum values and given without measure of uncertainty. Production rates (<sup>4</sup>He<sub>p</sub>, <sup>3</sup>He<sub>p</sub>) and production ratios (<sup>3</sup>He<sub>p</sub>/<sup>4</sup>He<sub>p</sub>) are calculated according to section 11.3.1. PAF = Passwang Formation, OPA = Opalinus Clay, STF = Staffelegg Formation. Field lithology after Hostettler et al. (2017): sa ma = sandy marl, lst = limestone; sa lst = sandy limestone, clst = claystone, silt clst = silty claystone, clst & lst la = claystone with limestone layers, clst & sst la = claystone with sandstone layers, arg ma = argillaceous marl, bit ma = bituminous marl. Shaded samples were used for inter-laboratory comparison.

### 11.3.2.1 Assessment of Steady-state of the Porewater – Groundwater System

If – analogous to the work of Rübél et al. (2002) – the He concentrations are, as a first assumption, taken to be in steady-state between in-situ production and diffusive loss to the groundwater, the profile can be described by the differential equation:

$$D_p \times \frac{\partial^2 C}{\partial x^2} = -A_{is}, \quad (41)$$

with  $D_p$  being the pore diffusion coefficient for He,  $C$  the He concentration in the porewater,  $x$  the distance along borehole from the groundwater and  $A_{is}$  the in-situ accumulation rate of He in the porewater, calculated as

$$A_{is} = \frac{{}^4\text{He}_{accum.max}}{t_{sedim.}} [ccSTP g_{PW}^{-1} a^{-1}]. \quad (42)$$

Integrating equation (41) using the boundary conditions

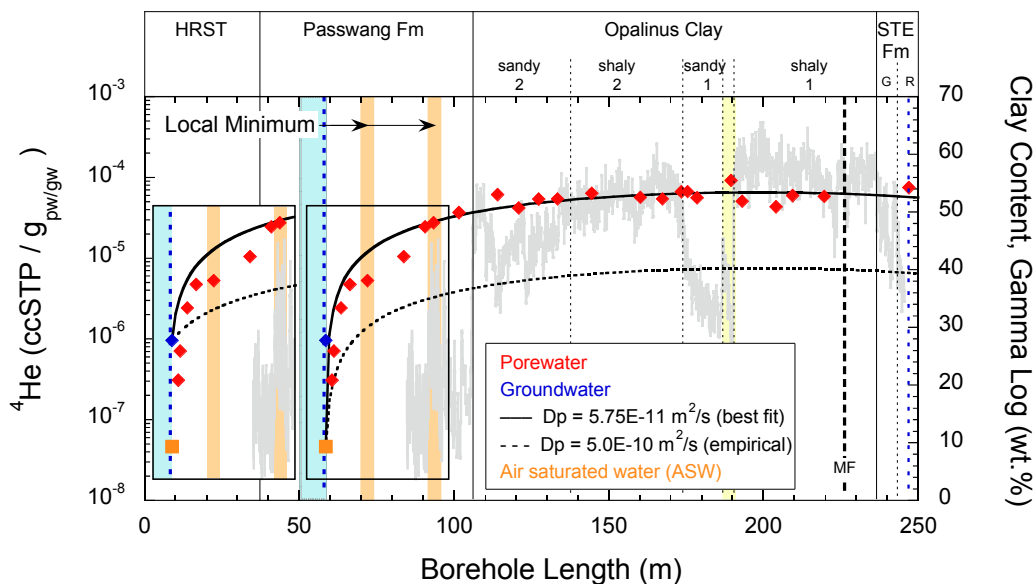
$$C|_{x=0} = C_0 \quad \text{and} \quad \left. \frac{\partial C}{\partial x} \right|_{x=L} = 0 \quad (43)$$

yields the parabolic porewater He concentration profile

$$C(x) = -\frac{A_{is} \times x^2}{2 \times D_p} + \frac{A_{is} \times L \times x}{D_p} + C_0 [ccSTP g_{PW}^{-1}] \quad (44)$$

with  $C_0$  being the He concentration at the boundary and  $L$  the half thickness of the diffusive layer. The latter is, in this case, postulated to be the low-permeability sequence between the observed water-conducting fracture at 58.6 m BHL and potentially flowing groundwater in the Liassic Gryphaea Limestone at a projected borehole length of approximately 340 m BHL. This is based on the stratigraphic thicknesses along the tunnel and a dip of the bedding planes of 44°, resulting in a total thickness of  $2 \times L = 280$  m perpendicular to bedding. It must be stressed that in this simplistic model, both  $D_p$  and  $A_{is}$  were taken as constant throughout the formation. That is, they were set equal in the Opalinus Clay and in the the Passwang Fm limestones, as either parameter is currently undetermined for the latter.

With fixed parameters,  $A_{is} = 1.19 \times 10^{-11}$  ccSTP/g<sub>pw</sub>/a,  $L = 140$  m and  $C_0 = 4.65 \times 10^{-8}$  ccSTP/g (He concentration in air-saturated water at 20 °C; Weiss 1971), the best fit to the measured data is obtained with a  $D_p$  of  $5.7 \times 10^{-11}$  m<sup>2</sup>/s (Figure 11-16), which is similar to the best fit  $D_p$  of  $3.5 \times 10^{-11}$  m<sup>2</sup>/s obtained by Rübél et al. (2002). In contrast, experimentally derived  $D_p$  perpendicular to bedding of Opalinus Clay from the deep borehole SLA-1 at Schlattingen ( $7.13 \times 10^{-10}$  m<sup>2</sup>/s at a porosity of 9.6 vol.%; Jacops et al. 2016) and from Mont Terri ( $5.4 \times 10^{-10}$  m<sup>2</sup>/s at a porosity of 12 vol.%; Jacops et al. 2013) are one order of magnitude higher than the fitted values.



**Notes:** The solid and dashed lines are the model profiles obtained using the best fit  $D_p$  and the experimentally derived  $D_p$ , respectively, calculated for boundary concentrations of air-saturated water (main plot) and the measured groundwater concentration (inset).

**Figure 11-16: Modelled Steady-state He Concentration Profiles from the Water-conducting Feature in the Passwang Fm Through the Opalinus Clay into the Staffelegg Fm.**

On the one hand this seems to suggest that the fitted  $D_p$  of  $5.7 \times 10^{-11} \text{ m}^2/\text{s}$  is severely underestimated and that the assumption of steady state is indeed questionable, as already discussed by Mazurek et al. (2011) and Jacobs et al. (2013). Calculating equation (44) using a conservative  $D_p$  of  $5.0 \times 10^{-10} \text{ m}^2/\text{s}$  (equally assuming the same  $D_p$  for the Opalinus Clay as well as for the Passwang Fm) would result in a steady state profile with approximately one order of magnitude lower porewater concentrations. This profile also shows negligible sensitivity concerning the boundary concentration being selected as representative for air-saturated water ( $C_{\text{He}} = 4.65 \times 10^{-8} \text{ ccSTP/g}$ ), or for the measured groundwater value ( $C_{\text{He}} = 9.6 \times 10^{-7} \text{ ccSTP/g}$ ) (Figure 11-16). This would suggest that the observed He porewater concentration profile has not yet reached steady state since its last disturbance and is still in a transient state from an anterior undisturbed situation with more elevated He concentrations in the Opalinus Clay.

On the other hand, the provisional assumption of an identical  $D_p$  for both formations is clearly debatable. A lower  $D_p$  in the limestones of the Passwang Fm would cause them to act as a diffusive barrier, both impeding and controlling the rate of diffusive loss of He from the Opalinus Clay toward the groundwater. This would, in consequence, shift the steady-state He concentrations in the center of the aquitard to higher values than those anticipated by a steady-state model which assumes an identical  $D_p$  along the entire diffusion pathway. As a corollary, He concentration gradients in the Passwang Fm would have to be steeper than those predicted by the model using a singular  $D_p$ . While this could be argued for in the lower part of the Passwang Fm (below approximately 65 m BHL), where the gradient of the measured porewater He concentrations away from the Opalinus Clay is steeper than predicted by the singular  $D_p$  model (Figure 11-16), the porewater He concentrations rebound onto the model

curve closer to the groundwater. This could indicate either an additional heterogeneity within the Passwang Fm, with the lowest  $D_p$  values around approximately 90 m BHL, or that the evolution of the He profile in the Passwang Fm is (or at least was in the past) influenced by other factors as well.

### 11.3.2.2 1D Diffusion Model for the Evolution of the Porewater Helium Profile

In order to estimate the evolution time of the presently observed porewater He concentrations, a simple one-dimensional diffusion model can be formulated as:

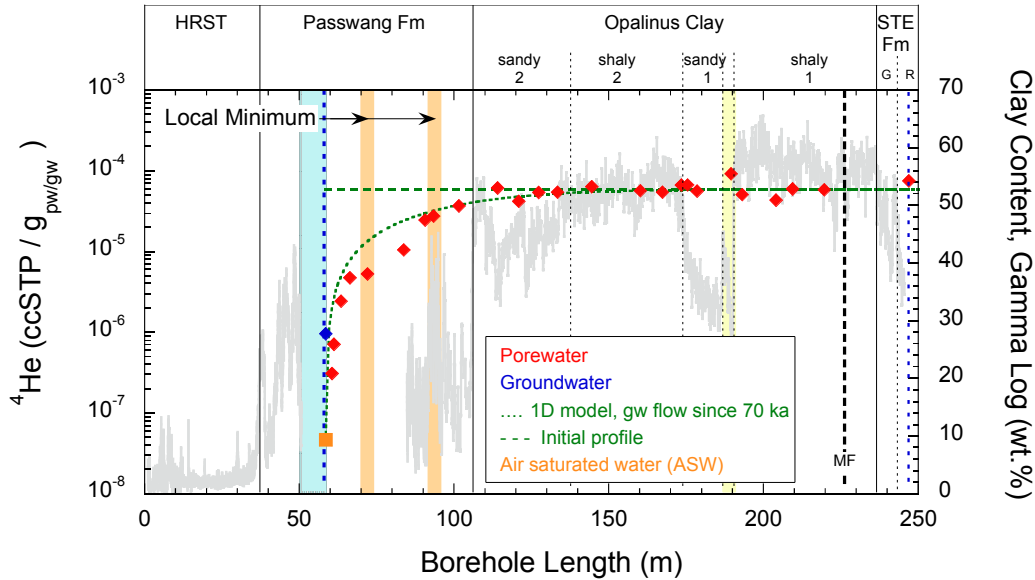
$$C(x, t) = C_0 + C_{OPA}(t) \times \operatorname{erf}\left(\frac{x}{2\sqrt{D_p \times t}}\right) [ccSTP \ g_{PW}^{-1}] \quad (45)$$

with  $\operatorname{erf}()$  being the error-function,  $t$  being the age at which diffusion started and He began to evolve from a perfectly flat initial profile into the observed diffusion profile, and  $C_{OPA}(t)$  is the average He concentration in the Opalinus Clay at age,  $t$ , calculated as:

$$C_{OPA}(t) = C_{OPA}(t = 0) - t \times A_{is} [ccSTP \ g_{PW}^{-1}] \quad (46)$$

with  $C_{OPA}(t = 0) = 5.9 \times 10^{-5}$  ccSTP/g<sub>pw</sub>, the measured present day average He concentration in the Opalinus Clay. For the model, the boundary concentration  $C_0$  is not a function of  $t$ , but is maintained at the He concentration of air-saturated water, simulating quantitative removal of He by flowing groundwater with very short residence time. The modelling assumption of a 'semi-infinite reservoir medium' is argued by the following points: a) the lower half of the Opalinus Clay He profile shows a flat continuation into the Staffelegg Fm; b) the assumed distal boundary in the Gryphaea Limestone at approximately 340 m BHL is over 90 m away, a distance over which the observed He concentration profile on the proximal end has nearly reached the flat part in the center of the Opalinus Clay (this argument is augmented by the geological restraint that – due to the erosion history of the area - freshwater infiltration into the upper boundary has been possible since > 1.2 Ma ago, whereas the activation of the lower boundary happened no sooner than 0.5 Ma ago [Bossart and Wermeille 2003], resulting in even shorter penetration depth of a diffusive signal); and c) a posteriori, by the relative short simulation times, during which the central/lower part of the He profile is barely affected and, thus, the type or position of the lower boundary condition is not yet relevant.

Calculating porewater He concentrations using these model parameters results in a best fit between the model curve and the measured He concentration profile for an onset of diffusion at  $t = 70$  ka, with an initial  $C_{OPA}(t)$  of  $5.77 \times 10^{-5}$  ccSTP/g<sub>pw</sub> (Figure 11-17).



**Notes:** A homogeneous porewater He concentration over the entire depth is assumed at that time and the boundary concentration is kept constant at the He concentration of air-saturated water, whereas the He concentration in the porewater is influenced by both diffusion toward the boundary and in situ accumulation of He.

**Figure 11-17: Simplified One-dimensional He Diffusion Profile for BDB-1 Resulting from Hypothetical Opening of the Water-conducting Fracture 70 ka Ago.**

This is in contrast to the interpretation by Mazurek et al. (2011), based on the data from Rübél et al. (2002), which are nearly identical to those elaborated upon here for rock material from borehole BDB-1. These authors do not interpret the profile in the lower part of the Opalinus Clay as predominantly flat and, therefore, can neither use this Opalinus Clay He concentration as a fixed initial concentration for their diffusion model (consequently treating it as a fitting parameter), nor use a single boundary, semi-infinite model geometry (consequently using a one-dimensional model with diffusion toward two boundaries). Based on the results from fitting the Cl<sup>-</sup> concentration profile and the prerequisite assumption of identical palaeo-hydrogeological evolution in both cases, the evolution time was set for the time since the activation of the upper aquifer,  $t = 6$  Ma, and assuming an opening of the lower aquifer at 0.5 Ma. Using a slightly lower  $D_p$  of  $2.5 \times 10^{-10}$ , they obtain a best fit for the He profile if an initial porewater He concentration of  $4.7 \times 10^{-4}$  ccSTP/g<sub>pw</sub> is assumed (Table 11-7).

Calculating  $t_{\min}$  (eq. 40) for this value gives a minimum time of 38 Ma during which closed-system conditions would have been required to prevail in order build up such a high initial He concentration in the porewater. This is on the order of  $t_{\min}$  values determined for the Opalinus Clay at Schlattingen ( $t_{\min} = 47$  Ma; Rufer and Waber 2015) and about twice as high as for Benken ( $t_{\min} = 17$  Ma for the entire sequence 'Brauner Dogger' to Staffelegg Fm; Lehmann et al. 2001). Considering the different geological setting, such as the overall thinner low-permeability sequence and the geodynamic activity (e.g., structural imprint due to the Oligocene opening of the Rhine Graben and the folding of the Jura mountains some between 10.5 and 3 Ma; Becker 2000) at Mont Terri compared to NE-Switzerland, such a long minimal build-up time for the porewater He inventory is, at least, open for debate. This is also acknowledged by Mazurek et

al. (2011), who state the “low predictive value in the calculation” and primarily conclude that the current porewater He concentration profile has not yet reached steady-state conditions.

The validity of the assumption of a semi-infinite model geometry, whose initial He concentration has not yet been pervasively disturbed by the latest variation in the boundary condition, hinges on the interpretation that the lower part of the observed profile is indeed flat. This can of course be disputed based on the scatter (though small) in the data in this part of the profile.

However, re-establishing a nearly flat profile from a curved diffusion profile with a gradient of roughly  $5 \times 10^{-5}$  ccSTP/gpw over 50 m BHL (as observed in the data and the modelled diffusion profiles for both the model used in this study as well as by Mazurek et al. (2011)) can be achieved in much less than 100 ka, if temporary stagnant conditions in the groundwater are assumed, with He concentrations diffusively equilibrating from the aquitard (where in-situ He accumulation continues) into the aquifer. As a consequence, disturbances in the hydrological system on even relatively short timescales of a few ten thousand years could potentially obscure any information about the distribution and history of a pre-existing He porewater inventory, allowing insight into only the results of the most recent hydrological change (Figure 11-18).

**Table 11-5: Overview of Best-fit Model Parameters for Modelling the He Concentration Profile over the Opalinus Clay and Bounding Units at Mont Terri Obtained in this Work and by Mazurek et al. (2011)**

	<b>this work</b>	<b>Mazurek et al. (2011)</b>	
$D_p$	$5.0 \times 10^{-10}$	$2.5 \times 10^{-10}$	[m <sup>2</sup> /s]
$C_0$	$4.65 \times 10^{-8}$ (a.s.w.)	not given (assumed 0 - $4.65 \times 10^{-8}$ )	[ccSTP/g]
$C_{OPA}(t)$	$5.8 \times 10^{-5}$	$4.7 \times 10^{-4}$	[ccSTP/g]
$t$	<i>0.07</i>	6	[Ma]
model geometry	1D, semi-infinite	1D, two boundaries	

Notes: Values given in italics are the best fit results of the respective fitting parameters

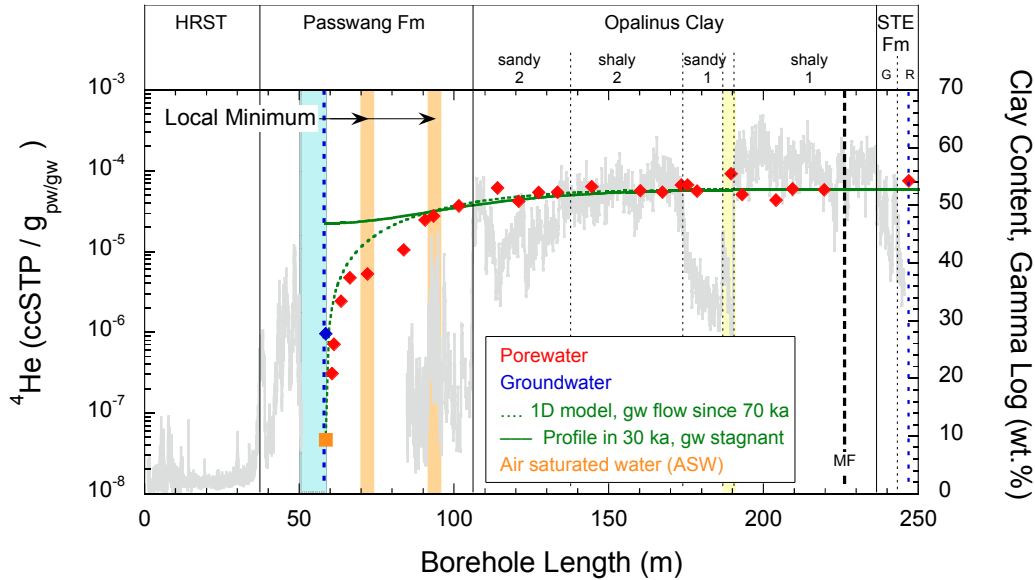


**Figure 11-18: Modern and Projected He Diffusion Profiles Along BDB-1 Modelled for Evolution with Open Boundary Conditions for the Last 70 ka (modern profile) and Assuming Continued Evolution Under Stagnant Boundary Conditions for the Next 30 ka (projected profile).**

In this context, the local minima observed at around 72 m and 92–94 m BHL in the chemical and isotope tracers suggest a variation in boundary conditions in space and time (*cf.* Chapters 9 and 10). Although hardly outside the total uncertainty, the  $^4\text{He}$  data also indicate a local minimum at the 72 m BHL (Figure 11-18). As shown above, the present profile shape requires flowing groundwater, with essentially air-saturated water concentrations of  $^4\text{He}$ , at the currently observed water-conducting zone at 58.6 m BHL (where the groundwater was sampled). This contrasts the  $^{14}\text{C}$  activity measured on the sampled groundwater, which suggests that these waters infiltrated about 25–29 ka ago when corrected for carbonate reactions (*cf.* Chapter 12). Based on the model calculations above, water which infiltrates through strata overlying the Opalinus Clay (e.g., within the Passwang Formation) from the surface down to the level of the gallery over such a duration will have its  $^4\text{He}$  concentration raised from air-saturated water concentration to values which would be one to two orders of magnitude higher than what is currently observed in the sampled groundwater and the porewater samples most proximal to it. The resulting diffusion profile would be almost flat over the Passwang Fm (*cf.* projected profile in Figure 11-18). The excursion of  $^4\text{He}$  concentrations around the local minimum at 72 m BHL from the present-day observed profile suggests an inherited signature of a once-flowing groundwater with a surface water  $^4\text{He}$  signature in the past at this location. This would have first resulted in a drawdown of  $^4\text{He}$  concentrations at this location. After cessation of groundwater flow in this zone, the  $^4\text{He}$  concentration would rapidly rebound. The accumulation of  $^4\text{He}$  in the porewater would, however, be asymmetrical based on the higher  $^4\text{He}$  in-situ production in the Opalinus Clay compared to the Passwang Fm. The present-day concentrations would develop within a few tens of thousands to a few hundred thousands of years after cessation of groundwater flow. The  $^4\text{He}$  concentrations profile also supports moving boundary conditions over recent geological time, as observed from independent chemical and isotope tracers.

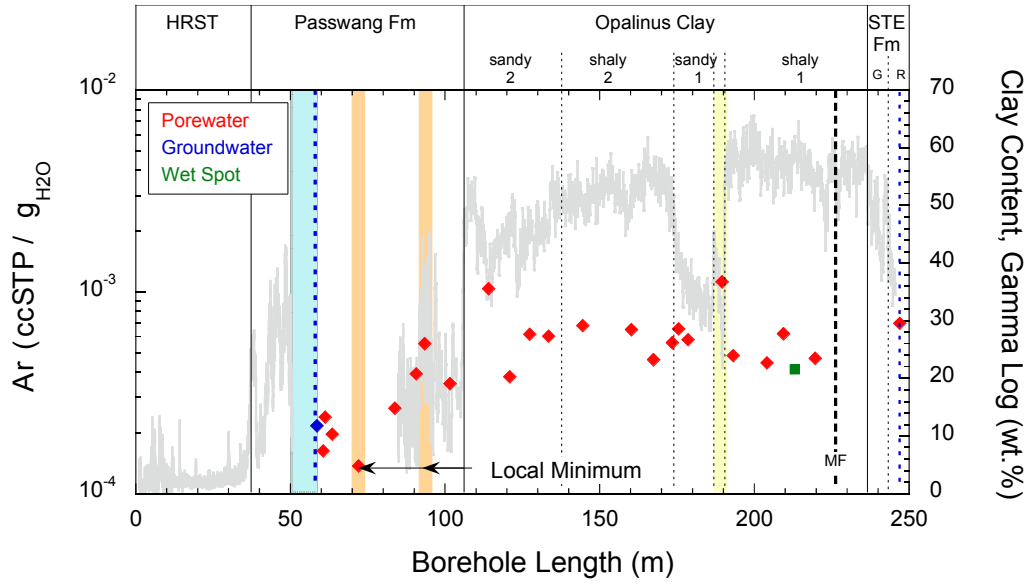
## 11.4 Ar CONCENTRATION AND $^{40}\text{Ar}/^{36}\text{Ar}$ ISOTOPE RATIO IN POREWATER

Due to the dominating effects of the air-contamination correction on Ar values (*cf.* Section 11.1), both  $\text{Ar}_{\text{H}_2\text{O}}$  concentrations and  $(^{40}\text{Ar}/^{36}\text{Ar})_{\text{H}_2\text{O}}$  isotope ratios determined on BDB-1 porewater are conservatively taken as semi-quantitative and are given here without a measure of uncertainty. The tabulated concentrations are considered to represent maximum, and the  $^{40}\text{Ar}/^{36}\text{Ar}$  ratios to represent minimum, values (*cf.* Section 11.1).

The determined  $\text{Ar}_{\text{H}_2\text{O}}$  concentrations of the BDB-1 porewater range from  $1.4 \times 10^{-4}$  to  $1.1 \times 10^{-3}$  ccSTP/g<sub>pw</sub> (Table 11-5). As a function of depth, there is a trend toward higher values from the Passwang Fm down into the Opalinus Clay – similar to the  $^4\text{He}_{\text{pw}}$  concentration profile (Figure 11-19). Close to the water-conducting zone,  $\text{Ar}_{\text{H}_2\text{O}}$  concentrations in the porewater are nearly equal to the value of  $2.2 \times 10^{-4}$  ccSTP/g<sub>H<sub>2</sub>O</sub> determined for the groundwater, while in the Opalinus Clay the porewater  $\text{Ar}_{\text{H}_2\text{O}}$  concentrations scatter around  $6 \times 10^{-4}$  ccSTP/g<sub>pw</sub>, which is comparable to the value determined on a wet spot in the Opalinus Clay (D. Traber, *pers. comm.* 2016). The highest  $\text{Ar}_{\text{H}_2\text{O}}$  concentrations were determined on samples BDB1-114.08-NG and BDB1-189.52-NG from the upper and lower sandy, bioclast-rich facies. Both samples also exhibit elevated  $^4\text{He}_{\text{pw}}$  concentrations with respect to their position along the profile (Figure 11-14), in particular BDB1-189.52-NG, which also has the highest  $^3\text{He}/^4\text{He}$  ratio of all samples (Figure 11-16 and discussion in Section 11.2).

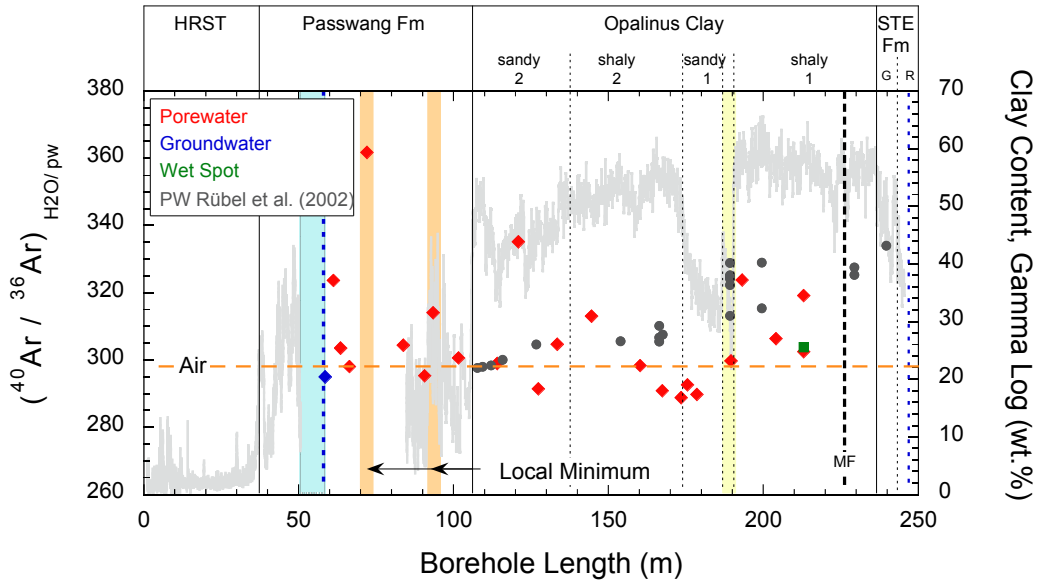
Measured  $(^{40}\text{Ar}/^{36}\text{Ar})_{\text{H}_2\text{O}}$  values range from 289 to 361 with a median value of 303, which coincides with the value determined for the groundwater ( $^{40}\text{Ar}/^{36}\text{Ar} = 295$ ) as well as for a wet spot in the Opalinus Clay ( $^{40}\text{Ar}/^{36}\text{Ar} = 304$ ; sample wa,447,113; D. Traber, *pers. comm.* 2016). These values indicate an overall slightly radiogenic signature for the porewater Ar, and are in general agreement with the data from Rübél et al. (2002), who reported values between 297 and 334. While Rübél et al. (2002) suggest that there is a tendency toward more radiogenic signatures with depth, the scatter in the present dataset does not allow deduction of a potential trend.

While the Ar and He concentration profiles seem to exhibit some similarities, it is not possible to directly compare them due to the semi-quantitative nature of the Ar data, and the potential for using Ar to model porewater evolution is currently not given.



Notes: The blue shaded area is the depth interval in which the groundwater was sampled. No error bars given.

Figure 11-19: Ar Concentration of Porewater from the BDB-1 Borehole as a Function of Depth.



Notes: The blue shaded area is the depth interval in which the groundwater was sampled. No error bars given.

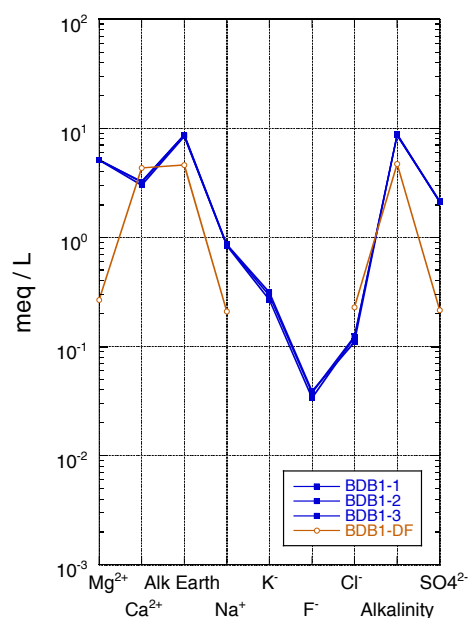
Figure 11-20:  $^{40}\text{Ar}/^{36}\text{Ar}$  Isotope Ratio of Porewater from the BDB-1 Borehole as a Function of Depth.

## 12. GROUNDWATER COMPOSITION AND EVOLUTION

Groundwater could be successfully collected from a packed-off interval enclosing a water-conducting zone at 58.6 m BHL in the Passwang Fm. In addition, artesian groundwater from the near-by borehole, BDS-2 in the Hauptrogenstein, which was used as drilling fluid across this interval, was also analysed. Details about the sampling procedure and analyses performed are given in Chapter 4 and the field sampling protocol is provided in Appendix A4.

Groundwater samples collected over three consecutive days from the Passwang Fm displayed constant chemical and isotope composition (Table 12-1). The groundwater is of the chemical Mg-Ca-HCO<sub>3</sub>-(SO<sub>4</sub>) type with a total mineralisation of about 817 mg/L (Figure 12-1). In contrast, groundwater from the Hauptrogenstein (i.e., the drilling fluid) differs in its chemical and isotope composition and is of Ca-HCO<sub>3</sub> type with a lower total mineralisation of 413 mg/L.

Groundwater from the Passwang Fm is characterised by its elevated concentrations in earth alkaline elements, HCO<sub>3</sub><sup>-</sup> and SO<sub>4</sub><sup>2-</sup>, and low Cl<sup>-</sup> contents of only about 4 mg/L (Table 12-1). It has a pH value around neutral and is mildly reducing (Eh<sub>Ag/AgCl</sub> ≈ -40 mV). At the pH value measured in the field, the groundwater is at saturation with respect to calcite, dolomite, quartz, barite, and probably also with respect to siderite as indicated by the first sample collected (Table 12-2). The groundwater is close to saturation with respect to strontianite (SrCO<sub>3</sub>), but under-saturated with respect to celestite (SrSO<sub>4</sub>) and gypsum. Overall, the chemical composition is indicative of an evolved groundwater that has reached almost complete equilibrium with the carbonate-bearing lithologies from which it was sampled.

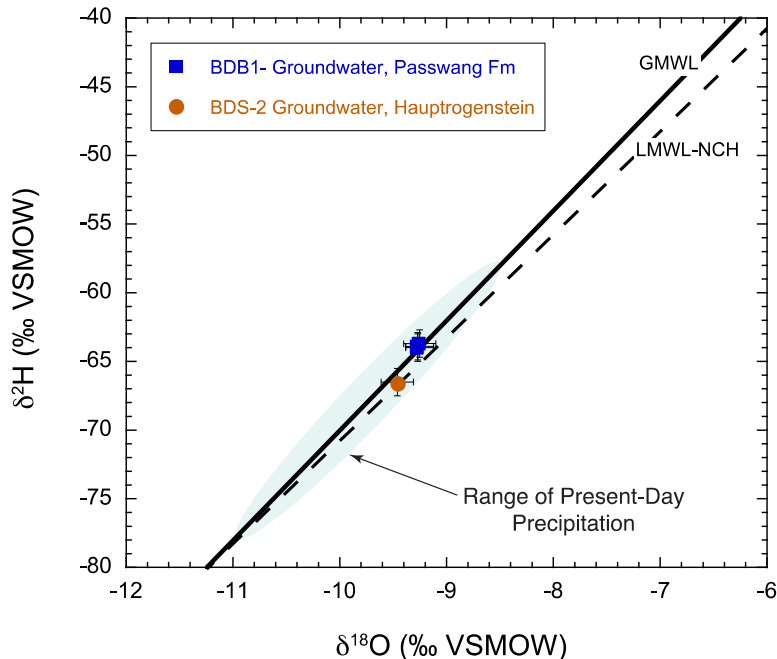


**Notes:** The artesian groundwater from the Hauptrogenstein was used as drilling fluid (concentrations of K<sup>+</sup> and F<sup>-</sup> are below detection limit in this groundwater).

**Figure 12-1: Schoeller-Diagram of Groundwater from the Passwang Fm in Borehole BDB-1 and the Hauptrogenstein in Borehole BDS-2 at the Mont Terri URL.**

The advanced chemical evolution of the groundwater is in accordance with its isotopic composition. The Passwang groundwater is of meteoric origin, as indicated by its  $\delta^{18}\text{O}$  and  $\delta^2\text{H}$  values that plot on the global meteoric water line, GMWL. It is, however, enriched in  $^{18}\text{O}$  and  $^2\text{H}$  compared to the groundwater from the Hauptrogenstein, which plots in the  $\delta^{18}\text{O}$ – $\delta^2\text{H}$  diagram on the local meteoric water line for precipitation in Northern Switzerland (Figure 12-2). This latter groundwater has a high  $^3\text{H}$ -activity, indicating a residence time in the underground of a few years at maximum. In contrast, the Passwang Fm groundwater has no measurable  $^3\text{H}$  and a low  $^{14}\text{C}$ -activity (see below), which, in combination with the  $\delta^{18}\text{O}$  and  $\delta^2\text{H}$  values, suggests that this groundwater infiltrated under different, and possibly warmer, conditions compared to present-day.

The difference in  $^3\text{H}$ -activity being high in the Hauptrogenstein groundwater, which was used as drilling fluid, and being absent in the Passwang Fm water also indicates that the latter is not contaminated by drilling fluid to a measurable degree.



**Notes:** The artesian groundwater from the Hauptrogenstein was used as drilling fluid; LMWL-NCH from Kullin & Schmassmann (1991); range of present-day precipitation in Northern Switzerland from Waber et al. (2014).

**Figure 12-2:  $\delta^{18}\text{O}$  vs.  $\delta^2\text{H}$  of Groundwater from the Passwang Formation in Borehole BDB-1 and the Hauptrogenstein in Borehole BDS-2 at the Mont Terri URL.**

The absence of  $^3\text{H}$  in the Passwang Fm groundwater is corroborated by a low  $^{14}\text{C}$ -activity of only 1.1 pmc. The  $\delta^{13}\text{C}_{\text{DIC}}$  value of  $-1.29$  ‰ PDB indicates that the groundwater is also in C-isotopic equilibrium with the marine limestone rocks of the Passwang Fm. Correcting the measured  $^{14}\text{C}$ -activity for mineral carbonate dissolution, until chemical equilibrium is observed, and using the carbon stable isotopes as additional constraint, yields a  $^{14}\text{C}$  residence time of about 25–29 ka for the Passwang Fm groundwater at 58.6 m BHL in borehole BDB-1. Such long residence time indicates an infiltration of the groundwater during an interglacial period,

before the last glaciation, and is consistent with the chemical evolution and the water stable isotope composition.

The indicated long residence time of the Passwang Fm water is also corroborated by the elevated  $^4\text{He}$  concentration and the  $^3\text{He}/^4\text{He}$  isotope ratio (Table 12-1). The  $^4\text{He}$  concentration of  $9.6 \times 10^{-7}$  ccSTP/g $_{\text{H}_2\text{O}}$  in the groundwater is more than one order of magnitude higher than that of air-saturated water ( $0.46 \times 10^{-7}$  ccSTP/g $_{\text{H}_2\text{O}}$ ), suggesting a rather long accumulation of He from the surrounding rock and porewater. This is supported by the lower  $^3\text{He}/^4\text{He}$  isotope ratio ( $2.4 \times 10^{-7}$ ) compared to that of air-saturated water ( $13.8 \times 10^{-7}$ ), which also indicates the accumulation of radiogenic  $^4\text{He}$  from the surrounding rock. In turn, the  $^{40}\text{Ar}/^{36}\text{Ar}$  ratio is still that of air-saturated water indicating that the groundwater resided not yet long enough in the underground to accumulate radiogenic  $^{40}\text{Ar}$ .

The evolved chemical and isotope composition of the Passwang Fm groundwater, combined with its indicated long  $^{14}\text{C}$  residence time, the elevated  $^4\text{He}$  concentration and the low  $^3\text{He}/^4\text{He}$  isotope ratios indicate, in combination with the low  $\text{Cl}^-$  concentration and an  $^{40}\text{Ar}/^{36}\text{Ar}$  ratio absent of radiogenic  $^{40}\text{Ar}$  input, that this groundwater resided mainly in limestone environments and was not in the system long enough to exchange with porewater generated in silicate-rich rocks such as the Opalinus Clay. Chemical, isotope and noble gas composition of the groundwater are consistent with a long-term evolution without significant contribution from exchange with Opalinus Clay porewater. The groundwater, therefore, does not seem to have acted as the boundary condition for such exchange over extended time periods. This is consistent with observations made for the various chemical, isotope and noble gas porewater tracers, which suggest interaction over long periods of time with a boundary closer to the Passwang Fm – Opalinus Clay interface (*cf.* Chapter 8 to 11).

**Table 12-1: Chemical and Isotope Composition of Groundwater Sampled from the Water-conducting Zone in the Passwang Fm of Borehole BDB-1**

SAMPLE	Lab	Method	Unit	BDB1-1 BDB1 Passwang- Fm	BDB1-2 BDB1 Passwang- Fm	BDB1-3 BDB1 Passwang- Fm	BDB1-DF BDS Hauptrogen- stein
Borehole							
Geology							
Type of sample				groundwater	groundwater	groundwater	groundwater as drilling fluid at inflow
Date Sampled				14-Dec-2013	15-Dec-2013	16-Dec-2013	14-Dec-2013
Sampling Interval (m BHL)				51.0–59.7 m	51.0–59.7 m	51.0–59.7 m	artesian
Water Pressure				7 bar	8.5 bar	8.4	
How Sampled				outflow from singlepacker interval	outflow from singlepacker interval	outflow from singlepacker interval	artesian outflow
Sampling				HDPE/Inox	HDPE/Inox	HDPE/Inox	HDPE
<b>GROUNDWATER TYPE</b>				<u>Mg-Ca-HCO<sub>3</sub>-(SO<sub>4</sub>)</u>	<u>Mg-Ca-HCO<sub>3</sub>-(SO<sub>4</sub>)</u>	<u>Mg-Ca-HCO<sub>3</sub>-(SO<sub>4</sub>)</u>	<u>Ca-HCO<sub>3</sub></u>
<b>FIELD MEASUREMENTS</b>							
pH (field)			-log (H <sup>+</sup> )	7.24	7.20	7.22	–
Electrical Conductivity	RWI, UniBern		µs/cm	715	704	689	–
Eh (Ag/AgCl)	RWI, UniBern		mV	-30	-45	-42	–
Dissolved Oxygen (O <sub>2</sub> )	RWI, UniBern		mg/L	1.6	1.6	2.65	–
Temperature at wellhead	RWI, UniBern		°C	12.9	12.5	11.3	–
Turbidity sensoric	RWI, UniBern		turbid		very turbid	turbid	clear
Smell sensoric	RWI, UniBern		none		none	none	none
Color	RWI, UniBern		colourless		colourless	colourless	colourless
<b>LAB MEASUREMENTS</b>							
Date analysed				18.12.13	18.12.13	18.12.13	18.12.13
pH (lab)	RWI, UniBern		-log (H <sup>+</sup> )	7.25	7.24	7.26	7.55
Sample Temperature	RWI, UniBern		°C	22	22	22	
<b>DISSOLVED CONSTITUTENTS</b>							
Sodium (Na <sup>+</sup> )	RWI, UniBern	IC	mg/L	19.6	19.8	19.4	4.8
Potassium (K <sup>+</sup> )	RWI, UniBern	IC	mg/L	11.5	12.3	10.5	<1
Ammonium (NH <sub>4</sub> <sup>+</sup> )	RWI, UniBern	IC	mg/L	1	<1	<1	<1
Magnesium (Mg <sup>+2</sup> )	RWI, UniBern	IC	mg/L	62.4	62.3	62.6	3.3
Calcium (Ca <sup>+2</sup> )	RWI, UniBern	IC	mg/L	60.6	65.2	64.6	87.2
Strontium (Sr <sup>+2</sup> )	RWI, UniBern	IC	mg/L	13.3	13.6	12.5	0.097
Barium (Ba <sup>+2</sup> )	RWI, UniBern	ICP-OES	mg/L	0.034	0.039	0.032	0.007
Total Iron (Fe tot)	RWI, UniBern	ICP-OES	mg/L	0.623	0.496	0.002	<0.001
Manganese (Mn tot)	RWI, UniBern	ICP-OES	mg/L	0.031	0.026	0.066	<0.001
Aluminium (Al)	RWI, UniBern	ICP-OES	mg/L	0.007	<0.005	0.029	<0.005
Silica (Si)	RWI, UniBern	Colorimetry	mg/L	4.34	4.26	4.31	2.30
Fluoride (F <sup>-</sup> )	RWI, UniBern	IC	mg/L	0.72	0.74	0.64	<0.06
Chloride (Cl <sup>-</sup> )	RWI, UniBern	IC	mg/L	4.4	3.9	4.3	8.1
Bromide (Br <sup>-</sup> )	RWI, UniBern	IC	mg/L	0.080	0.080	0.080	<0.08
Sulfate (SO <sub>4</sub> <sup>-2</sup> )	RWI, UniBern	IC	mg/L	102.9	101.5	102.5	10.3
Nitrate (NO <sub>3</sub> <sup>-</sup> )	RWI, UniBern	IC	mg/L	0.080	<0.08	<0.08	5.78
Alkalinity (m-value, lab)	RWI, UniBern	Titration	meq/L	8.69	8.83	8.71	4.74
Alkalinity (HCO <sub>3</sub> <sup>-</sup> )	RWI, UniBern	calc.	mg/L	530.2	538.8	531.5	289.2
<b>SUMMARY PARAMETERS</b>							
TDS	RWI, UniBern		mg/L	812	824	814	413
Charge Balance	RWI, UniBern		%	-6.45	-5.59	-5.62	-3.60
<b>ISOTOPES</b>							
delta 18O H <sub>2</sub> O	RWI, UniBern	CRDS	‰ VSMOW	-9.28	-9.28	-9.26	-9.47
delta D H <sub>2</sub> O	RWI, UniBern	CRDS	‰ VSMOW	-63.9	-64.0	-63.7	-66.5
3H	Hydroisotop	LSC (enr.)	TU	<0.6	–	–	8.5±0.7
14C	Hydroisotop	AMS	pmC	1.10±0.12	–	–	–
13C-DIC	Hydroisotop	IRMS	‰ VPDB	-1.29	–	–	-14.96
					error		
<b>NOBLE GASES</b>							
Helium (He)	EAWAG	MS	ccSTP/g	9.61E-07	2E-08	–	–
Neon (Ne)	EAWAG	MS	ccSTP/g	2.66E-07	7E-09	–	–
Argon (Ar)	EAWAG	MS	ccSTP/g	2.17E-04	5E-06	–	–
Krypton (Kr)	EAWAG	MS	ccSTP/g	4.96E-08	1E-09	–	–
Xenon (Xe)	EAWAG	MS	ccSTP/g	7.72E-09	2E-10	–	–
3He/4He	EAWAG	MS		2.39E-07	2E-08	–	–
20Ne/22Ne	EAWAG	MS		9.776	0.003	–	–
40Ar/36Ar	EAWAG	MS		295.0	0.4	–	–

**Table 12-2: Modelled Parameters of Groundwater Sampled from the Water-conducting Zone in the Passwang Fm of Borehole BDB-1**

<b>SAMPLE</b>	<b>Unit</b>	<b>BDB1-1</b>	<b>BDB1-2</b>	<b>BDB1-3</b>	<b>BDB1-DF</b>
Borehole		BDB1	BDB1	BDB1	BDS
Geology		Passwang-groundwater	Passwang-groundwater	Passwang-groundwater	Hauptrogen-groundwater
Type of sample		groundwater	groundwater	groundwater	groundwater
Date Sampled		14-Dec-2013	15-Dec-2013	16-Dec-2013	14-Dec-2013
Sampling Interval (m BHL)		51.0–59.7 m	51.0–59.7 m	51.0–59.7 m	artesian
Water Pressure		7 bar	8.5 bar	8.4	
How Sampled		outflow from singlepacker interval	outflow from singlepacker interval	outflow from singlepacker interval	artesian outflow
Sampling		HDPE/Inox	HDPE/Inox	HDPE/Inox	HDPE
<b>GROUNDWATER TYPE</b>		<u>Mg-Ca-HCO<sub>3</sub>-(SO<sub>4</sub>)</u>	<u>Mg-Ca-HCO<sub>3</sub>-(SO<sub>4</sub>)</u>	<u>Mg-Ca-HCO<sub>3</sub>-(SO<sub>4</sub>)</u>	<u>Ca-HCO<sub>3</sub></u>
<b>CARBONATE SYSTEM</b>					
<b>MEASURED VALUES</b>					
pH (field)	-log (H <sup>+</sup> )	7.24	7.2	7.22	7.55
Alkalinity	meq/L	8.69	8.83	8.71	4.74
<b>MODELLED USING MEASURED pH</b>					
Total Dissolved CO <sub>2</sub>	molality	9.856E-03	1.014E-02	9.975E-03	5.062E-03
SI calcite		0.02	0.01	0.00	0.29
log P(CO <sub>2</sub> )	log bars	-1.62	-1.57	-1.60	-2.18
<b>MODELLED USING pH ADJUSTED FOR CALCITE SATURATION</b>					
pH	-log (H <sup>+</sup> )	–	–	–	7.26
Total dissolved CO <sub>2</sub> (TIC)	molality	–	–	–	5.401E-03
log P(CO <sub>2</sub> )	log bars	–	–	–	-1.89
<b>MINERAL SATURATION INDICES</b>					
Calcite		0.02	0.01	0.00	0.00
Dolomite		0.22	0.17	0.14	-1.28
Magnesite		-0.33	-0.38	-0.40	-1.81
Siderite		0.10	-2.43	-2.44	
Fluorite		-1.33	-1.39	-1.38	-3.14
Gypsum		-1.75	-1.73	-1.72	-2.44
Strontianite		-0.12	-0.15	-0.18	-2.42
Witherite		-3.62	-3.72	-3.67	-4.43
Celestite		-0.71	-0.71	-0.73	-3.69
Barite		0.02	-0.05	0.03	-1.44
Quartz		0.03	0.02	0.04	-0.22
Fe(OH) <sub>3</sub> (a)		-2.37	-5.25	-5.17	

**Notes:**

Model calculations performed with PhreeqC, Wateq4F TDB (Parkhurst and Appelo 1999; v. 2.18, 2011).

### 13. SUMMARY AND CONCLUSIONS

At the Mont Terri URL, borehole BDB-1 is the first borehole that cross-cuts the Opalinus Clay in its entire thickness. It cuts across the Jurassic sediment sequence of low-permeability from the Hauptrogenstein across the Passwang Fm and Opalinus Clay, and into the rocks of the Staffelegg Fm. Across the Hauptrogenstein and Passwang Fm, the borehole was water-drilled with low-mineralised, recent groundwater from the Hauptrogenstein as drilling fluid. Across the Opalinus Clay and into the Staffelegg Fm, the borehole was air-drilled. Groundwater could be collected from a water-conducting zone in the Passwang Fm at 58.6m BHL, but was not encountered in the lithologies in the footwall of the Opalinus Clay.

For porewater characterisation, borehole BDB-1 provided unique opportunities in several aspects. First, the borehole allowed collection of drill-core samples at a high spatial frequency within the Opalinus Clay and at the Passwang Fm – Opalinus Clay interface. Second, all samples experienced the same drilling conditions, allowing better comparison of obtained results and identification of possible artefacts induced by the drilling process. Third, all drill-core samples were subjected to the same strict sampling protocol, including time monitoring of the different steps and aiming to reduce/minimize exposure of the samples to air and, thus, the reduction of induced artefacts such sample desiccation and oxidation. Fourth, samples could be collected adjacent to each other for inter-laboratory comparison, allowing identification of pros and cons of different indirect porewater extraction techniques and artefacts induced during the laboratory treatment of the samples. Finally, optimised porewater sampling and extraction techniques could be applied based on experience gained over the past 20 years.

The above unique opportunities allowed optimisation of indirect porewater extraction techniques and identification of induced artefacts, and expansion of our understanding of evolution and origin of porewater solutes compared to the work presented in Pearson et al. (2003). The conclusions presented in Pearson et al. (2003) had to be based, in many cases, on the "best knowledge practice" at that time. Their conclusions were hampered by the fact that results had to be compared from boreholes drilled with different techniques (e.g., N<sub>2</sub> vs. air), drill-core samples conditioned in different ways (if at all), drill-core samples stored for largely differing time periods (days to years), and from extraction techniques that were still in the early development state. All of this resulted in relatively large spread of data that required the assumption of some concepts in order to allow interpretation in terms of porewater evolution and the origin of solutes. Some of the concepts and interpretations presented in Pearson et al. (2003) are supported by the findings made on behalf of rock material from the BDB-1 borehole, while others are revised.

Across the entire profile, more than 110 samples were collected for porewater investigations at RWI, University of Bern. Subsets of these samples were subjected to aqueous extraction, isotope diffusive exchange, noble gas extraction and high-pressure squeezing techniques, in addition to mineralogical and petrophysical investigations. Special emphasis was given to connect results obtained about the porewater composition to the variable mineralogy and texture of the rocks and to the spatial distribution of components dissolved in porewater, as well as to the (so far, only poorly defined) interface between the Passwang Fm and the Opalinus Clay. A subset of 34 samples was further used for inter-laboratory comparison to elaborate potential differences between different indirect porewater extraction techniques and to identify artefacts induced by the techniques. The results of this comparison are reported in Mazurek et al. (2017).

The rocks of the Passwang Fm consist of an alternation of limestone, marl and sandstone, with highly variable contents of silt, sand and clay. This variation in mineralogical composition is also reflected in the petrophysical properties of the Passwang Fm rocks. The clay mineral content in the Passwang Fm is generally lower than that in the Opalinus Clay and varies between less than 10 wt.% and more than 40 wt.%. In the 29 investigated samples, the water content varies between about 1.5 wt.% and 7.7 wt.%, corresponding to water-loss porosities between 4.1 vol.% and 18.6 vol.%. The pycnometer porosity is generally higher (at low water-loss porosities, up to 10 % or more) indicating pore space in these rocks that is not accessible to porewater (e.g., mainly mineral fluid inclusions). The large variation in porosity and the rheology of the Passwang Fm rocks render it difficult to define an anion-accessible porosity as well, as only high-pressure squeezing yields water at a very high pressures, when the porewater solute concentrations have already been modified by the squeezing process. Clearly, a unique average value for the anion-accessible porosity is not applicable for these differently-composed rock types. Here, alternative techniques need to be considered such as out- or through-diffusion and should be applied to a series of samples.

The Opalinus Clay is more homogeneous from a mineralogical and petrophysical point of view, although significant differences exist between the individual sedimentary facies. The clay content in the 28 samples generally increases with increasing depth (33 – 63 wt.%), except for sandy facies 1 (15 – 29 wt.%) and the carbonate-rich sandy facies at about half-way through the formation, the latter containing sections of exceptionally low clay content (8 wt.%). Although the total clay content varies, the proportions of the individual clay minerals are very similar across the entire Opalinus Clay. A general increase from top to bottom of the Opalinus Clay is also observed for the water content (4.1 – 6.1 wt.%) and the water-loss porosity (10.3 – 14.8 vol.%), again with the exception of sandy facies 1 (4.3 – 4.7 wt.% and 10.8 – 11.8 vol.%) and the carbonate-rich sandy facies (1.7 wt.% and 4.4 vol.%). Water-loss porosity and pycnometer porosity are similar, except for carbonate-rich samples from sandy facies 1 and the carbonate-rich sandy facies. There exists a positive correlation between the N<sub>2</sub> specific surface area and the clay content, again with the above mentioned exceptions.

The differences in mineralogy, texture and porosity also manifest in the transport of porewater in the Opalinus Clay. Thus, moist zones were observed in borehole image logs in the both sandy facies and the carbonate-rich facies after just a few days of drilling, whereas such moist zones remained almost absent in both of the shaly facies.

The few rock samples from the Staffelegg Fm are composed similar to the bottom of the Opalinus Clay, except for the much higher sulphur contents (i.e., pyrite) and a higher organic carbon fraction in the Rietheim Member (former Posidonia Shale). The clay-rich rocks of the Staffelegg Fm have water-loss porosity values (11.5 – 13.9 vol.%) in the range of those of the Opalinus Clay, with the exception of a limestone layer with very low clay content, water content (0.7 wt.%) and water-loss porosity (2 vol.%).

The different natural tracers in the porewater (Cl<sup>-</sup>, δ<sup>37</sup>Cl, Br<sup>-</sup>, δ<sup>18</sup>O, δ<sup>2</sup>H, He, <sup>3</sup>He/<sup>4</sup>He, Ar) all describe well-defined concentration profiles from the Staffelegg Fm across the Opalinus Clay into the Passwang Fm. Although so far only quantified for He, the concentration profiles of all tracers indicate diffusion as the dominant solute transport process across the Opalinus Clay. The shapes of the tracer concentration profiles resemble those described in Pearson et al. (2003) and quantitatively assessed using transport modelling by Mazurek et al. (2009, 2011), although the decrease in tracer concentrations in the footwall was not encountered by borehole BDB-1. The decline from highest concentrations in shaly facies 1 at the bottom of the Opalinus Clay towards lower concentrations at the Passwang Fm – Opalinus Clay interface is attributed

to the diffusive exchange triggered by the concentration gradients toward pore- and groundwater in the overlying rocks of the Passwang Fm. It represents the most recent evolutionary trend of the porewater in the Opalinus Clay, i.e., over the past few millions of years. Differences in the profile shape are associated with the different pore-diffusion coefficients of the different tracers. This might also explain the minor excursions from the general concentrations profiles that are observed in sandy facies 1 and the carbonate-rich facies for some tracers (e.g.,  $\text{Cl}^-$ ,  $\text{Br}^-$ , He,  $^3\text{He}/^4\text{He}$ ), but not preserved for others ( $\delta^{18}\text{O}$ ,  $\delta^2\text{H}$ ).

In the rocks of the Passwang Fm, the concentrations profiles of the porewater tracers display much more complex shapes, except for He and  $^3\text{He}/^4\text{He}$ . For porewater  $\text{Cl}^-$  and  $\text{Br}^-$  concentrations this is at least partly due to the large uncertainty associated with the anion-accessible porosity of these often low-porosity rocks. However, porosity-independent tracers such as  $\delta^{18}\text{O}$  and  $\delta^2\text{H}$  display a complex profile shape in the Passwang Fm as well. In common to all tracers, and in spite of the scatter, two local concentration minima are observed in porewater at two locations (72 m and 94 m BHL) closer to the Opalinus Clay than to the water-conducting zone from which groundwater could be collected. This indicates that the location of the boundary condition (i.e., flowing groundwater) in the Passwang Fm for the diffusive exchange of solutes between Opalinus Clay and Passwang Fm has changed in the more recent geologic past. This is not surprising given the karstic nature of the Passwang Fm limestone rocks. Most likely, such change(s) occurred since the time direct infiltration has been facilitated by exposure of the the Passwang Fm through erosion, which occurred  $\sim 1.2$  Ma ago (Bossart and Wermeille 2003). Given the long  $^{14}\text{C}$ -residence time of the collected groundwater (25-29 ka), and a quantitative assessment of the  $^4\text{He}$  concentration profile, it is possible that surface-derived groundwater could have flowed through the feature at 72 m BHL up until a few tens to hundreds of thousands of years before present.

The improved sampling, sampling treatment, extraction and analytical techniques applied to the rocks encountered in borehole BDB-1 further allows better assessment of the origin of the porewater solutes and, thus, the porewater evolution. Besides the porewater tracer concentration profiles, ion-ion ratios in aqueous extract solutions reveal well-defined profiles across the Opalinus Clay into the Passwang Fm. Ratios of  $\text{Br}/\text{Cl}$  and  $\text{SO}_4/\text{Cl}$  are below and above, respectively, those of modern seawater, indicating that the largest component in the Opalinus Clay porewater is not of residual marine origin. This contrasts the conclusions drawn by Pearson and Waber (2001) and Pearson et al. (2003) who argued for a mainly marine origin of the Opalinus Clay porewater. These authors were, however, aware of the scatter in the available data and their conclusions were based on "best knowledge practice" at that time.

Furthermore, the present data, combined with geochemical modelling, indicate that the  $\text{SO}_4^{2-}$  concentrations are more compatible with the geochemical properties of the Opalinus Clay rocks, such as the cation exchange properties and mineral equilibria, compared to  $\text{SO}_4^{2-}$  concentrations obtained by high-pressure squeezing and water accumulated over long time periods from boreholes. It is concluded that the  $\text{SO}_4^{2-}$  concentration obtained from aqueous extraction serves as a suitable proxy for the in-situ porewater  $\text{SO}_4^{2-}$  concentration, which might be higher by a factor of 2 – 4 relative to that measured from squeezed and borehole water. Currently, the conversion of measured hexavalent sulphur in the experimental solutions to  $\text{SO}_4^{2-}$  concentrations in porewater is hampered by the unknown  $\text{SO}_4^{2-}$ -accessible porosity and by the similarly unknown activity of  $\text{SO}_4^{2-}$  in porewater, which differs from the hexavalent sulphur measured in experimental solutions and expressed as  $\text{SO}_4^{2-}$  concentration. For future modelling of the porewater composition in the Opalinus Clay at Mont Terri, it is recommended to use the  $\text{SO}_4/\text{Cl}$  ratio obtained in cautiously-prepared aqueous extract solutions instead of the

seawater  $\text{SO}_4/\text{Cl}$  ratio or fixation of the  $\text{SO}_4^{2-}$  concentration by mineral solubility controls (as used in earlier studies).

Consistent with all natural tracers ( $\text{Cl}^-$ ,  $\delta^{37}\text{Cl}$ ,  $\text{Br}^-$ ,  $\delta^{18}\text{O}$ ,  $\delta^2\text{H}$ ,  $\text{He}$ ,  $^3\text{He}/^4\text{He}$ ,  $\text{Ar}$ ) and ion-ion ratios ( $\text{Br}/\text{Cl}$  and  $\text{SO}_4/\text{Cl}$ ), it is concluded that the largest portion (if not all) of solutes in the porewater of the Opalinus Clay at the Mont Terri URL are of non-marine origin. The most likely origin of the solutes and isotope in Opalinus Clay porewater is pore- and groundwater from the underlying Triassic evaporite rocks. Chemical gradients established between evaporite pore- and groundwater and the originally marine porewater in the Opalinus Clay have been favourable for solute exchange since the deposition of these sediments. Possible enhancement of the upward migration of  $\text{SO}_4^{2-}$  and  $\text{Cl}^-$  (based on its isotope composition) from underlying evaporites may have occurred during the folding and thrusting of the Jura Mountains some 10.5 – 3 Ma ago (Becker 2000). This tectonic activity likely resulted in the expulsion of pore- and groundwater from the central evaporite lithologies to the distal argillaceous lithologies in the Mont Terri anticline. Such a scenario is compatible with the meteoric origin of the Opalinus Clay porewater, as indicated by its  $\delta^{18}\text{O}$  and  $\delta^2\text{H}$  values. Such origin is supported by the isotope composition of porewater in the lithologies of the Keuper in Northern Switzerland (Rübel and Sonntag 2000; Nagra 2001), which is similar to that observed for the porewater at the base of the Opalinus Clay at Mont Terri. Another argument for such evaporite origin of dissolved halides and  $\text{SO}_4^{2-}$  in the Opalinus Clay porewater is the chlorine isotope composition. The observed  $\delta^{37}\text{Cl}$  values, strongly enriched in  $^{37}\text{Cl}$ , cannot be derived by fractionation during diffusive transport alone, but the chlorine isotope signature must have been enriched compared to that of seawater before the transport of dissolved  $\text{Cl}^-$ .

It is acknowledged that the proposed evolution of porewater in the Opalinus Clay at Mont Terri is in contrast to conclusions drawn earlier by Pearson and Waber (2001) and Pearson et al. (2003) and to the long-term evolution scenario proposed by Mazurek and de Haller (2017). The latter scenario does require assumptions about climatic, hydraulic and geochemical conditions over tens of millions of years that are difficult to quantify. In the context of this work, the scenario proposed by Mazurek and de Haller (2017) could not explain the observations made on porewater samples from borehole BDB-1 with respect to ion-ion ratios ( $\text{Br}/\text{Cl}$  and  $\text{SO}_4/\text{Cl}$ ), solute concentrations ( $\text{Cl}^-$ ,  $\text{Br}^-$  and  $\text{SO}_4^{2-}$  and cations) and isotope composition ( $\delta^{37}\text{Cl}$ ). The scenario of a mainly evaporite origin of the porewater, as proposed here, is consistent with the argument for Sr-isotope ratios used by Mazurek and de Haller (2017).

The proposed long-term evolution of porewater in the Opalinus Clay at Mont Terri is, however, not in conflict with the more recent evolution, indicating solute exchange by diffusion between the Opalinus Clay and the overlying rocks of the Passwang Fm over the past few millions of years, as quantified by Mazurek et al. (2009, 2011). The present data, therefore, support the tightness of the Opalinus Clay over very long time periods with diffusion being the dominant transport process.

**ACKNOWLEDGEMENTS**

The authors would like to thank David Jaeggi and his team Linda Wymann, Mauro Häusler, M. Hoffmann and M. Kern (all swisstopo) for their great support on-site during drilling, sampling and drill-core description of the BDB-1 borehole. The authors further greatly acknowledge the excellent analytical work carried out by the RWI lab staff, Priska Bähler and Stefan Weissen. Financial support by NWMO and Nagra for field work, data production and interpretation is highly appreciated. The porewater characterisation work of the BDB-1 borehole was carried out within the Mont Terri Project DB-A Experiment financed by swisstopo, NWMO, Nagra, and IRSN.

## REFERENCES

- Appelo, C.A.J. 1977. Chemistry of water expelled from compacting clay layers: a model based on Donnan equilibrium. *Chem. Geol.* **19**, 91–98.
- Appelo, C.A.J., A. Vinsot, S. Mettler and S. Wechner. 2008. Obtaining the porewater composition of a clay rock by modeling the in- and out-diffusion of anions and cations from an in-situ experiment. *Journal of Contaminant Hydrology* **101**, 67-76.
- Appelo, C.A.J., L.R. Van Loon and P. Wersin. 2010. Multicomponent diffusion of a suite of tracers (HTO, Cl, Br, I, Na, Sr, Cs) in a single sample of Opalinus Clay. *Geochimica et Cosmochimica Acta* **74**(4), 1201-1219.
- Bath, A., A. Gautschi, T. Gimmi, F.J. Pearson and A. Rübél. Chapter 6: Geochemical Evolution. *In: F.J. Pearson et al. (2003). Mont Terri Project - Geochemistry of Water in the Opalinus Clay Formation at the Mont Terri Rock Laboratory. Reports of the Federal Office of Water and Geology (FOWG), Geology Series No 5. Federal Office of Topography (swisstopo), Wabern, Switzerland, 105-118, (available at [www.mont-terri.ch](http://www.mont-terri.ch)).*
- Becker, A. 2000. The Jura Mountains – An active foreland fold-and-thrust belt? *Tectonophysics* **321**, 381-406.
- Becker, J. 2014. VA Experiment: Mineralogical analyses of the BDB-1 drillcore (rawdata). Mont Terri Project Technical Note TN 2014-38.
- Bensenouci, F., J.L. Michelot, J.M. Matray, S. Savoye, B. Lavielle, B. Thomas and P. Dick. 2011. A Profile of helium-4 concentration in pore-water for assessing the transport phenomena through an argillaceous formation (Tournemire, France). *Phys. Chem. Earth* **36**, 1521-1530.
- Beyerle, U., W. Aeschbach-Hertig, D.M. Imboden, H. Baur, T. Graf, T and R. Kipfer. 2000. A mass spectrometric system for the analysis of noble gases and tritium from water samples. *Environ. Sci. Technol.* **34**(10), 2042–2050.
- Biehler, D., H. Schmassmann, K. Schneemann and J. Sillanpää. 1993. Hydrochemische Synthese Nordschweiz: Dogger-, Lias-, Keuper- und Muschelkalk-Aquifere. Nagra Technical Report NTB 92-08, Nagra, Wettingen, Switzerland.
- Bigler, T. 2003. Heliummessung im Porenwasser gering durchlässiger Gesteinsschichten. Diploma Thesis, Institute of Physics, University of Bern, Bern Switzerland.
- Bigler, T., B. Ihly, B.E. Lehmann and H.N. Waber. 2005. Helium Production and Transport in the Low-Permeability Callovo-Oxfordian Shale at the Site Meuse/Haute Marne, France. Nagra Working Report NAB 05-07, Nagra, Wettingen, Switzerland
- Bossart, P. and S. Wermeille. 2003. Paleohydrological study of the Mont Terri rock laboratory. *In: Heitzmann, P. and Tripet, J.P. (eds.), Mont Terri Project – Geology, paleohydrogeology and stress field of the Mont Terri region. Reports of the Federal Office of Water and Geology (FOWG), Geology Series No 4, 4546 Federal Office of Topography (swisstopo), Wabern, Switzerland.*
- Brunauer, S., P.H. Emmett and E. Teller. 1938. Adsorption of gases in multimolecular layers. *J. Am. Chem. Soc.* **60**, 309-319.
- Chilingarian, G.V., H.H. Rieke and A. Kazi. 1994. Chemistry of Pore Water. *In: W.H. Fertl, R.E. Chapman and R. O. Hotz (eds.), Studies in Abnormal Pressures. Developments in Petroleum Science* **38**, 107-153.

- Clark, I. and P. Fritz. 1999. Environmental Isotopes in Hydrogeology. Lewis Publishers, New York, USA.
- Coleman, M., M. Isaacs and D. Thornley. 2000. WS-E Experiment: Chlorine stable isotopes through the Jurensis Marl, Opalinus Clay and "Blaukalk", Mont Terri Rock Laboratory, Switzerland. Mont Terri Project Technical Note TN 99-02. Federal Office of Topography (swisstopo), Wabern, Switzerland.
- Coleman, M., M. Isaacs and D. Thornley. 2003. Stable Chlorine Isotopic Analyses. *In*: F.J. Pearson et al. (2003). Mont Terri Project - Geochemistry of Water in the Opalinus Clay Formation at the Mont Terri Rock Laboratory. Reports of the Federal Office of Water and Geology (FOWG), Geology Series No 5. Federal Office of Topography (swisstopo), Wabern, Switzerland, 263-268, (available at [www.mont-terri.ch](http://www.mont-terri.ch)).
- Corfield R.M., J.E. Cartlige, I. Premoli-Silva and R.A. Hously. 1991. Oxygen and carbon isotope stratigraphy of the Palaeogene and Cretaceous limestones in the Bottaccione Gorge and the Contessa Highway sections, Umbria, Italy. *Terra Nove* **3**, 414-422.
- Craig, H. 1961. Isotopic variation in meteoric waters. *Science* **133**, 1702-1703.
- de Haller, A., M. Mazurek, J. Spangenberg and A. Möri. 2014. SF, Self sealing of fault and paleo-fluid flow: Synthesis report. Mont Terri Project Technical Report TR 2008-2. Federal Office of Topography (swisstopo), Wabern, Switzerland.
- de Laeter, J. R., J.K. Böhlke, P. de Bièvre, H. Hidaka, H.S. Peiser, K.J.R. Rosman and P.D.P. Taylor. 2003. Atomic weights of the elements (Review 2000 - IUPAC Technical Report). *Pure and Appl. Chem.* **75**(6), 683-800.
- Desaulniers, D.E., R.S. Kaufmann, J.A. Cherry and H.W. Bentley. 1986.  $^{37}\text{Cl}$ - $^{35}\text{Cl}$  variations in a diffusion-controlled groundwater system. *Geochim. Cosmochim. Acta* **50**, 1757-1764.
- Dronkert, H., H.R. Bläsi and A. Matter. 1990. Facies and Origin of Triassic Evaporites from the Nagra Boreholes, Nortehr Switzerland. Nagra Technical Report NTB 87-02, Nagra, Wettingen, Switzerland.
- Eggenkamp, H.G.M., J.J. Middleburg and R. Kreulen. 1994. Preferential diffusion of  $^{35}\text{Cl}$  relative to  $^{37}\text{Cl}$  in sediments of Kau Bay, Halmahera, Indonesia. *Chem. Geol.* **116**, 317-325.
- Eggenkamp, H.G.M., R. Kreulen and A.F. Koster van Groos. 1995. Chlorine stable isotope fractionation in evaporites. *Geochim. Cosmochim. Acta* **59**, 5169-5175.
- Eggenkamp, H.G.M. and M.L. Coleman. 2009. The effect of aqueous diffusion on the fractionation of chlorine and bromine stable isotopes. *Geochim. Cosmochim. Acta* **73**, 3539-3548.
- Eggenkamp, H.G.M., M. Bonifacie, M. Ader and P. Agrinier. 2016. Experimental determination of stable chlorine and bromine isotope fractionation during precipitation of salt from a saturated solution. *Chem. Geol.* **433**, 46-56.
- Eastoe, C.J., A. Long, L.S. Land and J.R. Kyle. 2001. Stable chlorine isotopes in halite and brine from the Gulf Coast Basin: brine genesis and evolution. *Chem. Geol.* **176**, 343-360.
- Eastoe, C.J., T.M. Peryt, O.Y. Petrychenko and S. Geisler-Cussey. 2007. Stable chlorine isotopes in Phanerozoic evaporites. *Appl. Geochem.* **22**, 575-588.
- Fernández, A.M., A. Bath, H.N. Waber and T. Oyama. 2003. Water Sampling by Squeezing Drillcore. *In*: F.J. Pearson et al. (2003). Mont Terri Project - Geochemistry of Water in

- the Opalinus Clay Formation at the Mont Terri Rock Laboratory. Reports of the Federal Office of Water and Geology (FOWG), Geology Series No 5. Federal Office of Topography (swisstopo), Wabern, Switzerland, 171-199, (available at [www.mont-terri.ch](http://www.mont-terri.ch)).
- Fernández, A.M., D.M. Sánchez-Ledesma, C. Tournassat, A. Melón, E.C. Gaucher, J. Astudillo and A. Vinsot. 2014. Applying the squeezing technique to highly consolidated clayrocks for pore water characterisation: Lessons learned from experiments at the Mont Terri Rock Laboratory. *Appl. Geochem.* 49, 2-21.
- Fischer, D. 2014. DB experiment: Borehole Logging Mont Terri Test Site, in the borehole BDB1 18.12.2013, 13.1.2014 and 30.1.2014. Mont Terri Project Technical Note, TN 2014-19, Federal Office of Topography (swisstopo), Wabern, Switzerland.
- Füchtbauer, H. 1988. Sedimente und Sedimentgesteine. Schweizerbart Verlagsbuchhandlung, Stuttgart, 1141 p.
- Gaucher, E.C., A.M. Fernández and H.N. Waber. 2003. Rock and Mineral Characterisation of the Opalinus Clay Formation. *In*: F.J. Pearson et al. (2003). Mont Terri Project - Geochemistry of Water in the Opalinus Clay Formation at the Mont Terri Rock Laboratory. Reports of the Federal Office of Water and Geology (FOWG), Geology Series No 5. Federal Office of Topography (swisstopo), Wabern, Switzerland, 281-303, (available at [www.mont-terri.ch](http://www.mont-terri.ch)).
- Gautschi, A., C. Ross and A. Scholtis. 1993. Pore water – groundwater relationships in Jurassic shales and limestones of northern Switzerland. *In*: D.A.C. Manning, P.L. Hall and C.R. Hughes. (eds.): Geochemistry of clay – pore fluid interactions. Chapman & Hall, London, 412–422.
- Gilfedder, B.S., M. Petri, M. Wessels and H. Biester. 2011. Bromine species fluxes from Lake Constance's catchment, and a preliminary lake mass balance. *Geochim. Cosmochim Acta* 75, 3385-3401.
- Gimmi, T. and H.N. Waber. 2004. Modelling of tracer profiles in pore water of argillaceous rocks in the Benken borehole: Stable water isotopes, chloride, and chlorine isotopes. Nagra Technical Report NTB 04-05, Nagra, Wettingen, Switzerland.
- Gimmi, T., O.X. Leupin, J. Eikenberg, M. Glaus, L.R. Van Loon, H.N. Waber, P. Wersin, H.A.O. Wang, D. Grolimund, C.N. Borcaa, S. Dewonck and C. Wittebroodt. 2014. Anisotropic diffusion at the field scale – I: A four-year multi-tracer diffusion and retention experiment at the Mont Terri URL (Switzerland). *Geochim Cosmochim Acta* 125, 373–393.
- Gregory, R.T. 1991. Oxygen isotope history of seawater revisited: Timescales for boundary event changes in the oxygen isotope composition of seawater. Taylor, H.P. Jr., O'Neil, J.R. and Kaplan, I.R. (eds.), *Stable Isotope Geochemistry: A tribute to Samuel Epstein*. The Geochemical Society Special Publication.
- Griffault, L., C. Bauer, H.N. Waber, F.J. Pearson, T. Fierz, A. Scholtis, C. Degueldre and L. Eichinger. 2003. Water Sampling and Analyses for Boreholes and Seepages. *In*: F.J. Pearson et al. (2003). Mont Terri Project - Geochemistry of Water in the Opalinus Clay Formation at the Mont Terri Rock Laboratory. Reports of the Federal Office of Water and Geology (FOWG), Geology Series No 5. Federal Office of Topography (swisstopo), Wabern, Switzerland, 142-172, (available at [www.mont-terri.ch](http://www.mont-terri.ch)).

- Hendry, M.J., L.I. Wassenaar and T. Kotzer. 2000. Chloride and chlorine isotopes ( $^{36}\text{Cl}$  and  $\delta^{37}\text{Cl}$ ) as tracers of solute migration in a thick, clay-rich aquifer system. *Water Resources Research* **36**(1), 285–296.
- Hobbs, M.Y. and H.N. Waber. 2002. Pore water chemistry (PC) experiment: Evaluation of the diffusive exchange method for the determination of  $\delta^{18}\text{O}$  and  $\delta^2\text{H}$  in Opalinus Clay pore water from Mont Terri. Mont Terri Project Technical Note, TN 2002-24, Federal Office of Topography (swisstopo), Wabern, Switzerland.
- Horita, J., D.J. Wesolowski and D.R. Cole. 1993. The activity-composition relationship of oxygen and hydrogen isotopes in aqueous salt solutions: I. Vapor-liquid water equilibration of single salt solutions from 50 to 100°C. *Geochim. Cosmochim. Acta* **57**, 2797-2817.
- Hostettler, B., A.G. Reisdorf, D. Jaeggi, G. Deplazes, H.-R. Bläsi, A. Morard, S. Feist-Burkhardt, A. Waltschew, V. Dietze and U. Menkveld-Gfeller. 2017. Litho- and biostratigraphy of the Opalinus Clay and bounding formations in the Mont Terri rock laboratory (Switzerland). *Swiss Journal of Geosciences* **110**. DOI:10.1007/s00015-016-0250-3.
- Hydroisotop GmbH. 2016. GD-Experiment: Chlorine-Isotopes in porewater samples from the BDB-1 borehole (data report). Mont Terri Project Technical Note, TN 2014-106, Swisstopo Switzerland.
- Jacops, E., A. Grade, J. Govaerts and N. Maes. 2013. Measuring the diffusion coefficient for He in Opalinus Clay. SCK•CEN External Report 238, SCK•CEN, Mol, Belgium.
- Jacops, E., N. Maes, C. Bruggeman and A. Grade. 2016. Measuring diffusion coefficients of dissolved He and Ar in three potential clay host formations: Boom Clay, Callovo-Oxfordian Clay and Opalinus Clay. *In*: Norris, S., Bruno, J., Van Geet, M., and Verhoef, E. (eds.), *Radioactive Waste Confinement: Clays in Natural and Engineered Barriers*. Geological Society, London, Special Publications, London, United Kingdom
- Jäggi, D., N. Kern, M. Häusler, M. Hoffmann and L. Wymann. 2016. DB (Deep inclined borehole through the Opalinus Clay) Experiment, Borehole BDB-1 (247.5 m), Report of on-site operations, geological core mapping, sampling, installation of multipacker system and first results. Mont Terri Project Technical Note, TN 2015-14, Federal Office of Topography (swisstopo), Wabern, Switzerland.
- Kipfer, R., W. Aeschbach-Hertig, F. Peeters and M. Stute. 2002. Noble gases in lakes and ground waters. *Noble Gases in Lakes and Groundwater. Reviews in Mineralogy and Geochemistry* **47**, 615-700. *Geochem Soc. Am.*, Washington D.C., USA.
- Koehler, G. and L.I. Wassenaar. 2010. The stable isotopic composition ( $^{37}\text{Cl}/^{35}\text{Cl}$ ) of dissolved chloride in rainwater. *App. Geochem.* **25**, 91-96.
- Kullin, M. and H. Schmassmann. 1991. Isotope Composition of Modern Recharge. *In*: F.J. Pearson et al. (eds) *Applied Isotope Hydrogeology – A case study in northern Switzerland*. *Studies in Environmental Science* **43**, 65-89. Elsevier, Amsterdam.
- Lavastre V., N. Jendrzewski, P. Agrinier, M. Javoy and M. Evrard. 2005. Chlorine transfer out of a very low permeability clay sequence (Paris Basin, France):  $^{35}\text{Cl}$  and  $^{37}\text{Cl}$  evidence. *Geochim. Cosmochim. Acta* **69**, 4949–4961
- Lee, J.Y., K. Marti, J.P. Severinghaus, K. Kawamura, H.S. Yoo, J.B. Lee and J.S. Kim. 2006. A redetermination of the isotopic abundances of atmospheric Ar. *Geochim. Cosmochim. Acta* **70**, 4507-4512.

- Lehmann, B. E., H.H. Loosli and I. Tolstikhin. 2001. Sondierbohrung Benken: Radioelements (U, Th, K) and noble gases ( $^4\text{He}$ ,  $^3\text{He}/^4\text{He}$ ,  $^{40}\text{Ar}$ ,  $^{40}\text{Ar}/^{36}\text{Ar}$ ) in rocks. Nagra Internal Report NIB, Nagra, Wettingen, Switzerland.
- Lehmann, B. E. and I.N. Tolstikhin. 1999. Noble gases and isotopes from porewaters and rocks, Part II: Helium and Argon Isotopes in Rock Samples. *In*: Thury, M. and Bossart, P., Mont Terri rock Laboratory – Results of the hydrogeological, geochemical and geotechnical experiments performed in 1996 and 1997. Geological Reports Swiss National Hydrological and Geological Survey 23, 148-151.
- Lerouge, C. S. Gaboreau, P. Blanc, C. Guerrot, H. Haas, V. Jean-Prost, S. Touzelet and G. Wille. 2010. PC-C Experiment: Mineralogy and geochemistry of cores of the BPC-C2 borehole. Mont Terri Project Technical Note TN 2010-05, Federal Office of Topography (swisstopo), Wabern, Switzerland.
- Leya, I. and R. Wieler. 1999. Nucleogenic production of Ne isotopes in Earth's crust and upper mantle induced by alpha particles from the decay of U and Th. *J. Geophys. Res. Solid Earth* 104(B7), 15439-15450.
- Mäder, U. 2009. Reference pore water for the Opalinus Clay and "Brown Dogger" for the provisional safety-analysis in the framework of the sectorial plan - interim results (SGT-ZE). Nagra Working Report (NAB). Wettingen, Switzerland.
- Maineult, A., B. Thomas, C. Nussbaum, K. Wieczorek, D. Gibert, B. Lavielle, B. Kergosien, F. Nicollin, K. Mahiouz and N. Lesparre. 2013. Anomalies of noble gases and self-potential associated with fractures and fluid dynamics in a horizontal borehole, Mont Terri Underground Laboratory. *Eng. Geol.* 165, 46-57.
- Mazurek M., P. Alt-Epping, A. Bath, T. Gimmi and H.N. Waber. 2009. Natural tracer profiles across argillaceous formations: The CLAYTRAC project. OECD/NEA Report 6253, OECD Nuclear Energy Agency, Paris, France, 358 pp. available at [www.nea.fr](http://www.nea.fr)
- Mazurek, M., P. Alt-Epping, A. Bath, T. Gimmi, H.N. Waber, S. Buschaert, P.D. Cannière, M.D. Craen, A. Gautschi, S. Savoye, A. Vinsot, I. Wemaere and L. Wouters. 2011. Natural tracer profiles across argillaceous formations. *App. Geochem.* 26, 1035-1064.
- Mazurek, M., T. Oyama, P. Wersin and P. Alt-Epping. 2015. Pore-water squeezing from indurated shales. *Chem. Geol.* 400, 106-121.
- Mazurek, M., T. Al, M. Celejewski, I.D. Clark, A.M. Fernández, L. Kennell-Morrison, J.M. Matray, S. Murseli, T. Oyama, S. Qiu, D. Rufer, G. St-Jean, H.N. Waber and C. Yu. 2017. Mont Terri Project: Mont Terri DB-A Experiment: Comparison of Pore-water Investigations Conducted by Several Research Groups on Core Materials from the BDB-1 Borehole. Technical Report for the Nuclear Waste Management Organization, NWMO-TR-2017-09. (also published as *Mont Terri TR 2017-01*).
- Mazurek, M. and A. de Haller. 2017. Porewater evolution and solute transport mechanism in Opalinus Clay at Mont Terri and Mont Russelin (Canton Jury, Switzerland). *Swiss Journal of Geosciences* 110. DOI:10.1007/s00015-016-0249-9.
- McNaught, A. D. and A. Wilkinson. 1997. IUPAC - Compendium of Chemical Terminology. Blackwell Scientific Publications, Oxford, UK.
- Nagra. 2001. Sondierbohrung Benken, Untersuchungsbericht. Nagra Technical Report NTB 00-01, Nagra, Wettingen, Switzerland.
- Nordstrom, D.K., L.N. Plummer, T.M.L. Wigley, T.J. Wolery, J.W. Ball, E.A. Jenne, R.L. Bassett, D.A. Crerar, T.M. Florence, B. Fritz, M. Hoffman, G.R. Holdren, Jr., G.M. Lafon, S.V.

- Mattigod, R.E. McDuff, F. Morel, M.M. Reddy, G. Sposito and J. Thraillkill. 1979. A comparison of computerized chemical models for equilibrium calculations in aqueous systems. *In* Jenne, E.A. (ed.), *Chemical Modeling in aqueous systems, speciation, sorption, solubility, and kinetics*. American Chemical Society, Series 93, 857-892.
- Norton, D. and R. Knapp. 1977. Transport Phenomena in Hydrothermal Systems: The Nature of Porosity. *American Journal of Science* 277, 913-936.
- Nussbaum, C., P. Bossart, F. Amann and C. Aubourg. 2011. Analysis of tectonic structures and excavation induced fractures in the Opalinus Clay, Mont Terri underground rock laboratory (Switzerland). *Swiss J Geosci* 104, 187–210.
- Osenbrück, K., J. Lippmann and C. Sonntag. 1998. Dating very old pore waters in impermeable rocks by noble gas isotopes. *Geochim. Cosmochim. Acta* 62, 3041-3045.
- Parkhurst, D.L. and C.A.J. Appelo. 1999. User's guide to PHREEQC (Version 2) – A computer program for speciation, batch reaction, one-dimensional transport, and inverse geochemical calculations. U.S. Geological Survey Water-Resources Investigations Report 99-4259.
- Pearson, F.J. 1999. What is the porosity of a mudrock? *In*: A.C. Aplin, A.J. Fleet and J.H. S. Macquaker (eds), *Muds and Mudstones: Physical and Fluid Flow Properties*. Geol. Soc. Spec. Publ. 158. London, UK, 9-21.
- Pearson, F.J. and H.N. Waber. 2001. Origin and evolution of pore-water solutes in the very-low permeability Opalinus Clay, Switzerland. *In*: Cidu R. (ed.): *Proceedings of the 10<sup>th</sup> International Symposium on Water-Rock Interaction WRI-10*, Villasimius, Italy, A.A. Swets&Zeitlinger, Lisse, ISBN 90 2651 824 2, 1355-1358.
- Pearson, F.J. and A. Bath. 2003. Chapter 4: Perturbing Effects. *In*: F.J. Pearson et al. 2003. *Mont Terri Project - Geochemistry of Water in the Opalinus Clay Formation at the Mont Terri Rock Laboratory*. Reports of the Federal Office of Water and Geology (FOWG), Geology Series No 5. Federal Office of Topography (swisstopo), Wabern, Switzerland, 54-66, (available at [www.mont-terri.ch](http://www.mont-terri.ch)).
- Pearson, F.J., D. Arcos, A. Bath, J.-Y. Boisson, A.M. Fernández, H.-E. Gäbler, E. Gaucher, A. Gautschi, L. Griffault, P. Hernán and H.N. Waber. 2003. *Mont Terri Project - Geochemistry of Water in the Opalinus Clay Formation at the Mont Terri Rock Laboratory*. Reports of the Federal Office of Water and Geology (FOWG), Geology Series No 5. Federal Office of Topography (swisstopo), Wabern, Switzerland, 319pp, (available at [www.mont-terri.ch](http://www.mont-terri.ch)).
- Pearson, F.J., C. Tournassat and E.C. Gaucher. 2011. Biogeochemical processes in a clay formation in situ experiment: Part E – Equilibrium controls on chemistry of pore water from the Opalinus Clay, Mont Terri Underground Research Laboratory, Switzerland. *Appl. Geochem.* 26, 990-1008.
- Phillips, F.M. and H.W. Bentley. 1987. Isotopic fractionation during ion filtration: I. Theory. *Geochim. Cosmochim. Acta* 51, 683-695.
- Poole, J.C., G.W. McNeill, S.R. Langman and F. Dennis. 1997. Analysis of noble gases in water using a quadrupole mass spectrometer in static mode. *App. Geochem.* 12, 707-714.
- Reisdorf, A.G., B. Hostettler, D. Jaeggi, G. Deplazes, H.R. Bläsi, A. Morard, S. Feist-Burkhardt, A. Waltschew, V. Dietze and U. Menkveld-Gfeller. 2016. Litho- and biostratigraphy of

- the 250 m-deep Mont Terri BDB-1 borehole through the Opalinus Clay and bounding formations, St-Ursanne, Switzerland. Mont Terri Project Technical Report TR 2016-02.
- Rogge, T. 1997. Eine molekular-diffusive Methode zur Bestimmung des Porenwassergehaltes und der Zusammensetzung von stabilen Isotopen im Porenwasser von Gestein. Diploma thesis, University of Heidelberg, Germany (unpublished).
- Rozanski, K., L. Araguás-Araguás and R. Gonfiantini. 1993. Isotopic patterns in modern global precipitation. *In: Continental Indicators of climate*, American Geophysical Union Monograph.
- Rufer, D. and H.N. Waber, H.N. 2015. Noble and reactive gas data of porewaters and rocks from the Schlattingen borehole SLA-1. Nagra Working Report NAB 15-12, Nagra, Wettingen, Switzerland.
- Rübel, A.P. 2000. Stofftransport in undurchlässigen Gesteinsschichten – Isotopenuntersuchungen im Grund- und Porenwasser. PhD Thesis, Institut für Umweltphysik, University of Heidelberg, Der Andere Verlag, Osnabrück, Germany.
- Rübel A. and C. Sonntag. 2000. Sondierbohrung Benken: Profiles of pore water content, stable isotopes and dissolved noble gas content in the pore water of samples from argillaceous rocks. Nagra Internal Report NIB, Nagra, Wettingen, Switzerland.
- Rübel, A.P., C. Sonntag, J. Lippmann, F.J. Pearson and A. Gautschi. 2002. Solute transport in formations of very low permeability: Profiles of stable isotope and dissolved noble gas contents of pore water in the Opalinus Clay, Mont Terri, Switzerland. *Geochim. Cosmochim. Acta* **66**, 1311–1321.
- Rübel, A. and B.E. Lehmann. 2003. Extraction and Analyses of Noble Gases in Pore Waters and Minerals. *In: F.J. Pearson et al. (2003). Mont Terri Project - Geochemistry of Water in the Opalinus Clay Formation at the Mont Terri Rock Laboratory. Reports of the Federal Office of Water and Geology (FOWG), Geology Series No 5. Federal Office of Topography (swisstopo), Wabern, Switzerland, 245-254, (available at [www.mont-terri.ch](http://www.mont-terri.ch)).*
- Savin S.M. 1977. The history of the earth's surface temperature during the past 100 million years. *Ann. Rev. Earth Planet. Sci.* **5**, 319-355.
- Smith, T. 2010. Transfert vertical des gaz rares à l'échelle des différentes formations de la zone de transposition du site de Meuse/Haute-Marne et à l'échelle des eaux poreuses de l'argilite du Callovo-Oxfordien. PhD Thesis, University of Bordeaux I, Bordeaux, France.
- Sültenfuss, J., W. Roether and M. Rhein. 2009. The Bremen mass spectrometric facility for the measurement of helium isotopes, neon, and tritium in water. *Isotope in Environmental and Health Studies* **45**, 83-95.
- Tolstikhin, I., M. Gannibal, S. Tarakanov, B. Pevzner, B. Lehmann, B. Ihly and H.N. Waber. 2005. Helium transfer from water into quartz crystals: A new approach for porewater dating. *Earth Planet. Sci. Letters* **238**, 31-41.
- Tolstikhin, I., H.N. Waber, I. Kamensky, H.H. Loosli, V. Skiba and M. Gannibal. 2011. Production, redistribution and loss of helium and argon isotopes in a thick sedimentary aquitard-aquifer system (Molasse Basin, Switzerland). *Chem. Geol.* **286**, 48-58.
- Traber, D. 2004. Ventilation Experiment in Opalinus Clay (VE" Experiment): Geochemical Characterisation of Core Samples from Boreholes BVE85 and BVE86 (post desaturation

- phase) – Geochemical Process Evaluation. Project Deliverable D5c&d/D22 EC contract FIKW-CT2001-00126, Final Report prepared for Nagra, Nagra, Wettingen Switzerland.
- Van Geldern, R. and J.A.C. Barth. 2012. Optimization of instrument setup and post-run corrections for oxygen and hydrogen stable isotope measurements of water by isotope ratio infrared spectroscopy (IRIS). *Limnol. Oceanogr.: Methods* 10, 1024–1036.
- Van Loon, L.R., J.M. Soler and M.H. Bradbury. 2003. Diffusion of HTO,  $^{36}\text{Cl}$  and  $^{125}\text{I}$  in Opalinus Clay samples from Mont Terri: Effect of confining pressure. *J. Contam. Hydrol.* 61, 73-83.
- Van Loon, L.R., W. Müller and K. Iijima. 2005. Activation energies of the self-diffusion of HTO,  $^{22}\text{Na}^+$  and  $^{36}\text{Cl}^-$  in a highly compacted argillaceous rock (Opalinus Clay). *Appl. Geochem.* 20, 961-972.
- Van Loon, L.R. and J. Mibus. 2015. A modified version of Archie's law to estimate effective diffusion coefficients of radionuclides in argillaceous rocks and its application in safety analysis studies. *Appl. Geochem.* 59, 85-94.
- Veizer J., P. Bruckschen, F. Pawellek, A. Diener, O.G. Podlaha, G.A.F. Carden, T. Jaspe, C. Korte, H. Strauss, K. Azmy and D. Ala. 1997. Oxygen isotope evolution of Phanerozoic sea- water. *Palaeogeography, Palaeoclimatology, Palaeoecology* 132, 159-172.
- Waber, H.N. 1999. Mont Terri Project: Phase 3 Hydrochemical Data Review. *In: Pearson, F. J. (ed.), Geochemical Modelling and Synthesis (GM) Task: Results of Phase 4 Activities. Mont Terri Project Technical Note 99-51*, 11-26.
- Waber, H.N. 2001. Mont Terri Project: Phase 4 & 5 Hydrochemical Data Review. *In: Pearson F.J. et al., Geochemical Modelling and Synthesis (GM) Task: Compilation of Aqueous Geochemistry Data Collected During Phases 4 and 5, Rock Property Data from All Phases and Results of Phase 5 Geochemical Modelling. Mont Terri Project Technical Note 2000-36*, 5-52.
- Waber, H.N. 2005. Laboratoire de Recherche Souterrain Meuse / Haute-Marne - Chloride,  $\delta^{18}\text{O}$  and  $\delta^2\text{H}$  in Pore Water of the Callovo-Oxfordian and Surrounding Rock Formations. Nagra Working Report NAB 05-02, Nagra, Wettingen, Switzerland.
- Waber, H.N. 2012. Laboratoire de Recherche Souterrain Meuse / Haute-Marne - Geochemical Data of Borehole EST433. Working Report NAB 09-16, Nagra, Wettingen, Switzerland.
- Waber, H.N. and T. Oyama. 2000. WS-A Experiment: Feasibility Study of Porewater Squeezing as a Function of Pressure. Mont Terri Project Technical Note TN 2000-23, Federal Office of Topography (swisstopo), Wabern, Switzerland.
- Waber, H.N. and R. Schürch. 2000. WS-A Experiment: Fracture Mineralogy and Geochemistry as Constraints on Porewater Composition. Mont Terri Project Technical Note TN 99-83, Federal Office of Topography (swisstopo), Wabern, Switzerland.
- Waber, H.N., S.K. Frape and A. Gautschi. 2001. Cl-isotopes as indicator for a complex paleohydrogeology in Jurassic argillaceous rocks, Switzerland. *In: R. Cidu (ed.), Proceedings of the 10<sup>th</sup> Int. Symp. on Water-Rock Interaction WRI-10, Villasimius, Italy, A.A. Balkema Publisher. 2*, 1403-1406.
- Waber, H.N., E.C. Gaucher, A.M. Fernández and A. Bath. 2003a. Aqueous Leachates and Cation Exchange Properties of Mont Terri Claystones. *In: F.J. Pearson et al. (2003). Mont Terri Project - Geochemistry of Water in the Opalinus Clay Formation at the Mont Terri Rock Laboratory. Reports of the Federal Office of Water and Geology (FOWG),*

- Geology Series No 5. Federal Office of Topography (swisstopo), Wabern, Switzerland, 200-237, (available at [www.mont-terri.ch](http://www.mont-terri.ch)).
- Waber, H.N., F.J. Pearson, M.Y. Hobbs and T. Oyama. 2003b. Sondierbohrung Benken, Characterisation of Porewater from Argillaceous Rocks. Nagra Internal Report NIB, Wettingen, Switzerland.
- Waber, H.N., M.Y. Hobbs and S.K. Frape. 2013. Assessing Initial Conditions for Chloride Transport Across Low- permeability Argillaceous Rocks, Wellenberg, Switzerland. Proc. Earth Plan. Sci. 7, 875-879.
- Weiss, R. F. 1970. The solubility of nitrogen, oxygen and argon in water and seawater. Deep-Sea Research 17, 15.
- Weiss, R. F. 1971. Solubility of Helium and Neon in Water and Seawater. J. Chem. Eng. Data 16, 235-241.
- Wersin, P., M. Mazurek, H.N. Waber, U.K. Mäder, T. Gimmi, D. Rufer and A. de Haller. 2013. Rock and porewater characterisation on drillcores from the Schlattingen borehole. Nagra Working Report (NAB), Wettingen, Switzerland.
- Willenberg-Spillmann, H. 2015. Bohrung BDB-1 (Mont Terri): Abschätzung des Tonmineralgehaltes aus geophysikalischen Bohrlochlogs. Appendix in Reisdorf et al. (2016), Litho- and biostratigraphy of the 250 m-deep Mont Terri BDB-1 borehole through the Opalinus Clay and bounding formations, St-Ursanne, Switzerland. Mont Terri Project Technical Report TR 2016-02.



**APPENDIX A:  
SAMPLING PROTOCOLS**

**CONTENTS**

	<u>Page</u>
<b>A.1</b>	<b>POREWATER SAMPLE INVENTORY OF BORHEOLE BDB-1.....189</b>
<b>A.2</b>	<b>FIELD SAMPLING TIME LOGS POREWATER SAMPLES .....191</b>
<b>A.3</b>	<b>TIME RECORD OF CORE SAMPLING .....192</b>
<b>A.4</b>	<b>GROUNDWATER SAMPLING PROTOCOL.....195</b>





-Page left intentionally blank-

A.2 FIELD SAMPLING TIME LOGS POREWATER SAMPLES

DB/DB-A sampling log of 1m core section v2.0 | 15.11.2013 / DRU

**IMPORTANT: Use separate form for each core section (1m on plastic trencher) --> 3 forms per core**

Core:  -  m BHL Date:  core recovery:  [hh:mm]

Section:  -  m BHL 1<sup>st</sup> sealing:  re-exposure:  [hh:mm]

Comment: \_\_\_\_\_

**Samples (to be) taken in this section:**

Owner:	Type:	Sample depth a.b.:	avg. (calc.)	Placeholder / Strati-slab	Start sawing: (hh:mm)	Salami sealing: (hh:mm)	Alu/final sealing: (hh:mm)	Checked: (signed)
<input type="text" value="RWI"/>	<input type="text" value="SQ"/>	<input type="text" value="174.60"/> - <input type="text" value="174.80"/>	<input type="text" value="174.70"/>	<input checked="" type="checkbox"/> / <input checked="" type="checkbox"/>	<input type="text" value="10:30"/>	<input type="text" value="10:34"/>	<input type="text" value="10:51"/>	<input type="text" value="DRU"/>
<input type="text" value="UO"/>	<input type="text" value="VD"/>	<input type="text" value="174.80"/> - <input type="text" value="175.00"/>	<input type="text" value="174.90"/>	<input checked="" type="checkbox"/> / <input checked="" type="checkbox"/>	<input type="text" value="10:27"/>	<input type="text" value="10:33"/>	<input type="text" value="10:38"/>	<input type="text" value="DRU"/>
<input type="text" value="UNB"/>	<input type="text"/>	<input type="text" value="175.00"/> - <input type="text" value="175.20"/>	<input type="text" value="175.10"/>	<input checked="" type="checkbox"/> / <input checked="" type="checkbox"/>	<input type="text" value="10:26"/>	<input type="text" value="10:30"/>	<input type="text" value="10:36"/>	<input type="text" value="DRU"/>
<input type="text" value="RWI"/>	<input type="text" value="AQ"/>	<input type="text" value="175.20"/> - <input type="text" value="175.45"/>	<input type="text" value="175.33"/>	<input checked="" type="checkbox"/> / <input checked="" type="checkbox"/>	<input type="text" value="10:28"/>	<input type="text" value="10:32"/>	<input type="text" value="10:41"/>	<input type="text" value="DRU"/>
<input type="text"/>	<input type="text"/>	<input type="text"/>	<input type="text"/>	<input type="checkbox"/> / <input type="checkbox"/>	<input type="text"/>	<input type="text"/>	<input type="text"/>	<input type="text"/>
<input type="text"/>	<input type="text"/>	<input type="text"/>	<input type="text"/>	<input type="checkbox"/> / <input type="checkbox"/>	<input type="text"/>	<input type="text"/>	<input type="text"/>	<input type="text"/>

Fig. A.2-1: Example of a Core Sampling Log Filled Out During the BDB-1 Sampling Campaign

**BDB1 - Noble gas sampling log (RWI-NG)**

#	Date	Depth <sub>avg</sub> [m.00]	"Salami sealing" [hh:mm]	Start sawing [hh:mm]	End sawing [hh:mm]	m <sub>field wet</sub> [g.00]	Start pumping [hh:mm]	1 <sup>st</sup> pumping [s]	P <sub>1st</sub> pumping [mbar.0]	2 <sup>nd</sup> pumping [s]	P <sub>2nd</sub> pumping [mbar.0]	3 <sup>rd</sup> pumping [s]	P <sub>3rd</sub> pumping [mbar.0]	4 <sup>th</sup> pumping [s]	P <sub>final</sub> [mbar]	t <sub>final</sub> sealing [hh:mm]	T <sub>ambient</sub> [°C]	RH <sub>ambient</sub> [%]
17	27.01.2014	173.47	#N/A	09:39	09:42	337.37	09:45	45	7.2	30	6.9	30	6.8	40	6.5	09:48	15.3	60
Comment: _____																		
18	27.01.2014	175.53	#N/A	10:45	10:46	388.11	10:49	35	6.6	30	6.3	30	6.1	40	5.8	10:52	15.3	61
Comment: _____																		
19	27.01.2014	178.53	#N/A	11:38	11:40	411.46	11:43	30	7.7	30	7.2	30	6.9	40	6.6	11:46	15.5	62
Comment: _____																		
20	28.01.2014	189.53	#N/A	08:45	08:47	434.86	08:50	50	5.4	30	4.9	30	4.6	45	4.1	08:54	15.1	60
Comment: _____																		
21	28.01.2014	193.13	#N/A	09:45	09:49	407.65	09:54	35	7.5	35	7.1	30	6.9	40	6.6	09:55	15.1	60
Comment: _____																		
22	28.01.2014	204.09	#N/A	18:39	18:41	427.6	18:45	35	7.7	30	7.4	30	7.2	40	7	18:48	16	58
Comment: _____																		
23	28.01.2014	209.37	#N/A	20:51	20:53	351.33	20:56	45	7.1	30	7.0	30	6.8	45	6.55	20:59	16	56
Comment: _____																		
24	29.01.2014	219.66	#N/A	10:28	10:30	416.38	10:33	30	7.1	30	6.8	30	6.6	45	6.3	10:36	16	57
Comment: _____																		
25	30.01.2014	246.99	#N/A	11:20	11:24	22.04	10:27	45	5.7	30	5.6	30	5.2	50	5.7	11:32	15	59
Comment: _____																		

Fig. A.2-2: Example of a Noble Gas Sampling Log Filled Out During the BDB-1 Sampling Campaign

### A.3 TIME RECORD OF CORE SAMPLING OF SAMPLES PROCESSES AT RWI-IfG, UNIVERSITY OF BERN

Sample	Stratigraphie	Member / Facies	Lithology	Sample top	Sample bottom	Aver. Depth	Sampling date	Core recovery	Core sealing	Core re-exposure	Start of sample sawing	Duration of sample sawing	First sealing / start pumping	Total pumping duration	Final pressure	Final sealing	Total core exposure duration	Sample exposure duration	Notes
				m BHL	m BHL	m BHL	dd.mm.yy	hh:mm	hh:mm	hh:mm	hh:mm	minutes	hh:mm	seconds	mbar	hh:mm	minutes	minutes	
BDB1-36.19-AQ	HRST	Brüggli - Mb.	sa lst	36.08	36.30	36.19	12.12.13	12:52	13:04	13:10	13:12		13:15			13:22	17	3	Re-sealed 16:22
BDB1-43.78-AQ	PAF	Waldenburg - Mb.	sa lst	43.65	43.90	43.78	12.12.13	19:07	19:13	19:19	19:21		19:33			19:37	20	12	
BDB1-51.78-SQ	PAF	Waldenburg - Mb.	mst	51.65	51.90	51.78	13.12.13	10:11	10:19	10:25	10:27		10:30			10:33	13	3	
BDB1-52.28-SQ	PAF	Waldenburg - Mb.	mst	52.15	52.40	52.28	13.12.13	11:50	12:00	12:07	12:08		12:12			12:16	15	4	
BDB1-59.75-AQ	PAF	Waldenburg - Mb.	sa lst	59.67	59.83	59.75	16.12.13	09:55	09:58	10:02	10:03		10:08			10:10	9	5	
BDB1-60.59-NG	PAF	Waldenburg - Mb.	sa lst	60.54	60.64	60.59	16.12.13	09:55	09:58	10:02	10:09	4	10:27	182	5.8	10:29	28	18	
BDB1-60.79-AQ	PAF	Waldenburg - Mb.	sa lst	60.70	60.87	60.79	16.12.13	10:57	11:01	11:13	11:15		11:18			11:21	9	3	
BDB1-61.00-AQ	PAF	Waldenburg - Mb.	sa lst	60.87	61.13	61.00	16.12.13	10:57	11:01	11:13	11:17		11:22			11:25	13	5	
BDB1-61.23-NG	PAF	Waldenburg - Mb.	sa lst	61.15	61.30	61.23	16.12.13	10:57	11:01	11:13	11:22	7	11:33	140	5.7	11:37	24	11	
BDB1-61.52-AQ	PAF	Waldenburg - Mb.	sa lst	61.42	61.62	61.52	16.12.13	10:57	11:01	11:13	11:20		11:24			11:30	15	4	
BDB1-62.39-AQ	PAF	Waldenburg - Mb.	sa lst	62.32	62.46	62.39	16.12.13	11:45	12:00	12:15	12:17		12:25			12:29	25	8	
BDB1-62.80-AQ	PAF	Waldenburg - Mb.	lst	62.70	62.90	62.80	16.12.13	11:45	12:00	12:15	12:20		12:23			12:28	23	3	
BDB1-63.15-AQ	PAF	Waldenburg - Mb.	lst	63.06	63.24	63.15	16.12.13	11:45	12:04	12:25	12:29		12:35			n.r.	29	6	
BDB1-63.53-NG	PAF	Waldenburg - Mb.	sa lst	63.45	63.60	63.53	16.12.13	11:45	12:04	12:25	12:33	8	12:43	150	3.3	12:46	37	10	
BDB1-63.80-AQ	PAF	Waldenburg - Mb.	sa lst	63.71	63.89	63.80	16.12.13	11:45	12:04	12:25	12:28		12:31			n.r.	25	3	
BDB1-64.11-AQ	PAF	Waldenburg - Mb.	sa lst	64.00	64.22	64.11	16.12.13	13:34	13:42	13:48	13:50		13:56			13:59	16	6	
BDB1-64.88-AQ	PAF	Waldenburg - Mb.	lst	64.76	65.00	64.88	16.12.13	13:34	13:44	13:54	13:55		14:00			14:05	16	5	
BDB1-65.34-AQ	PAF	Waldenburg - Mb.	lst	65.20	65.48	65.34	16.12.13	13:34	13:44	13:54	14:00		14:04			14:08	20	4	
BDB1-65.70-AQ	PAF	Waldenburg - Mb.	sa lst	65.60	65.80	65.70	16.12.13	14:25	14:30	14:48	14:51		14:55			14:58	12	4	
BDB1-66.15-AQ	PAF	Waldenburg - Mb.	sa lst	66.05	66.25	66.15	16.12.13	14:25	14:30	14:48	14:56		15:00			15:04	17	4	Re-sealed 15:35
BDB1-66.40-NG	PAF	Waldenburg - Mb.	sa lst	66.35	66.45	66.40	16.12.13	14:25	14:40	15:00	15:07	6	15:15	135	2.8	15:18	30	8	
BDB1-66.70-AQ	PAF	Waldenburg - Mb.	sa lst	66.60	66.80	66.70	16.12.13	14:25	14:40	15:00	15:04		15:08			15:10	23	4	
BDB1-67.30-AQ	PAF	Waldenburg - Mb.	sa lst	67.20	67.40	67.30	16.12.13	15:30	15:35	15:55	16:00		16:10			16:15	20	10	
BDB1-67.80-AQ	PAF	Waldenburg - Mb.	sa lst	67.70	67.90	67.80	16.12.13	15:30	15:35	15:55	16:00		16:08			16:12	18	8	
BDB1-68.25-SQ	PAF	Waldenburg - Mb.		68.15	68.35	68.25	16.12.13	15:30	15:37	16:17	16:21		16:24			16:28	14	3	
BDB1-68.45-SQ	PAF	Waldenburg - Mb.		68.35	68.55	68.45	16.12.13	15:30	15:37	16:17	16:23		16:27			16:33	17	4	
BDB1-68.90-AQ	PAF	Waldenburg - Mb.	sa lst	68.80	69.00	68.90	16.12.13	17:50	17:55	18:12	18:13		18:20			18:23	13	7	
BDB1-69.50-SQ	PAF	Waldenburg - Mb.		69.40	69.60	69.50	16.12.13	17:50	17:55	18:12	18:19		18:23			18:25	16	4	
BDB1-70.30-AQ	PAF	Waldenburg - Mb.		70.20	70.40	70.30	16.12.13	18:58	19:04	19:10	19:13		19:17			19:20	13	4	
BDB1-72.05-NG	PAF	Waldenburg - Mb.	sa lst	72.00	72.10	72.05	16.12.13	20:03	20:08	20:15	20:18	n.r.	20:24	125	6.5	20:27	14	6	
BDB1-72.20-AQ	PAF	Waldenburg - Mb.	sa lst	72.10	72.30	72.20	16.12.13	20:03	20:08	20:15	20:16		20:21			20:25	11	5	
BDB1-74.30-AQ	PAF	Himichopf - Mb.		74.20	74.40	74.30	17.12.13	06:40	06:46	06:55	06:57		07:00			07:02	11	3	
BDB1-76.30-AQ	PAF	Himichopf - Mb.	sa lst	76.20	76.40	76.30	17.12.13	08:46	08:52	09:00	09:02		09:05			09:08	11	3	
BDB1-79.30-AQ	PAF	Himichopf - Mb.	sa ma	79.20	79.40	79.30	17.12.13	11:11	11:15	11:22	11:24		11:27			11:30	9	3	
BDB1-82.30-AQ	PAF	Himichopf - Mb.	lst	82.20	82.40	82.30	17.12.13	14:43	14:52	15:00	15:03		15:06			15:08	15	3	
BDB1-82.50-SQ	PAF	Himichopf - Mb.	sa lst	82.40	82.60	82.50	17.12.13	14:43	14:52	15:00	15:03		15:08			15:11	17	5	
BDB1-82.70-SQ	PAF	Himichopf - Mb.	mst	82.60	82.80	82.70	17.12.13	14:43	14:52	15:00	15:03		15:10			15:14	19	7	
BDB1-83.78-NG	PAF	Himichopf - Mb.	mst	83.70	83.85	83.78	17.12.13	15:52	15:59	16:11	16:16	3	16:22	140	6.4	16:25	18	6	
BDB1-83.95-AQ	PAF	Himichopf - Mb.	mst	83.85	84.05	83.95	17.12.13	15:52	15:59	16:11	16:15		16:19			16:20	15	4	
BDB1-86.90-AQ	PAF	Himichopf - Mb.	sa lst	86.80	87.00	86.90	17.12.13	18:26	18:33	18:38	18:42		18:44			18:46	13	2	
BDB1-89.45-AQ	PAF	Himichopf - Mb.	li sst	89.35	89.55	89.45	17.12.13	19:52	19:59	20:06	20:08		20:12			20:16	13	4	

#### Notes:

AQ = samples for aqueous extraction etc.; NG = samples for noble gas analyses; SQ = samples for high-pressure squeezing. HRST = Hauptrogenstein, PAF = Passwang Formation, OPA = Opalinus Clay, STF = Stafflegg Formation; Lithology according to Hostettler et al. (2017).

## A.3 (cont.)

Sample	Stratigraphie	Member / Facies	Lithology	Sample top	Sample bottom	Aver. Depth	Sampling date	Core recovery	Core sealing	Core re-exposure	Start of sample sawing	Duration of sample sawing	First sealing / start pumping	Total pumping duration	Final pressure	Final sealing	Total core exposure duration	Sample exposure duration	Notes
				m BHL	m BHL	m BHL	dd.mm.yy	hh:mm	hh:mm	hh:mm	hh:mm	minutes	hh:mm	seconds	mbar	hh:mm	minutes	minutes	
BDB1-90.68-NG	PAF	Himichopf - Mb.	li sst	90.60	90.75	90.68	18.12.13	07:23	07:29	07:34	07:40	2	07:45	155	6.6	07:49	17	5	
BDB1-90.85-AQ	PAF	Himichopf - Mb.	sa ma	90.75	90.95	90.85	18.12.13	07:23	07:29	07:34	07:37		07:41			07:43	13	4	
BDB1-92.75-SQ	PAF	Himichopf - Mb.	sa ma	92.65	92.85	92.75	18.12.13	10:13	10:19	10:33	10:39		10:44			10:49	17	5	
BDB1-92.95-SQ	PAF	Himichopf - Mb.	sa lst	92.85	93.05	92.95	18.12.13	10:13	10:19	10:33	10:42		10:47			10:51	20	5	
BDB1-93.24-AQ	PAF	Himichopf - Mb.	sa ma	93.15	93.33	93.24	18.12.13	10:13	10:19	10:33	10:36		10:38			10:43	11	2	
BDB1-93.40-NG	PAF	Himichopf - Mb.	sa ma	93.33	93.46	93.40	18.12.13	10:13	10:19	10:33	10:34	1	10:38	145	6.5	10:41	11	4	
BDB1-93.65-AQ	PAF	Himichopf - Mb.	sa ma	93.55	93.75	93.65	18.12.13	10:13	10:20	10:52	10:56		10:58			11:01	13	2	
BDB1-97.10-AQ	PAF	Sissach - Mb.	lst	97.00	97.20	97.10	18.12.13	12:49	12:57	13:05	13:10		13:16			13:21	19	6	
BDB1-98.68-AQ	PAF	Sissach - Mb.	sa lst	98.55	98.80	98.68	15.01.14	09:15	09:28	09:41	09:47		09:51			10:11	23	4	
BDB1-100.43-SQ	PAF	Sissach - Mb.	sa ma	100.30	100.55	100.43	15.01.14	11:32	11:44	11:47	11:56		12:08			12:16	33	12	
BDB1-100.63-AQ	PAF	Sissach - Mb.	sa ma	100.50	100.75	100.63	15.01.14	11:32	11:44	11:47	11:52		11:58			12:18	23	6	Re-sealed 12:58
BDB1-101.63-NG	PAF	Sissach - Mb.	sa ma	101.55	101.70	101.63	15.01.14	11:32	11:45	12:02	12:08	2	12:12	220	6.4	12:17	23	4	
BDB1-101.80-AQ	PAF	Sissach - Mb.	sa ma	101.70	101.90	101.80	15.01.14	11:32	11:45	12:02	n.r.		12:14			12:28	25	<12	
BDB1-102.93-AQ	PAF	Sissach - Mb.	sa ma	102.80	103.05	102.93	15.01.14	14:08	14:15	14:24	14:28		14:32			14:35	15	4	
BDB1-104.78-AQ	PAF	Sissach - Mb.	sa ma	104.65	104.90	104.78	15.01.14	14:08	14:18	14:31	14:34		14:38			14:40	17	4	
BDB1-108.24-AQ	OPA	sandy facies 2	clst & lst l	108.10	108.38	108.24	22.01.14	07:30	07:48	07:56	07:58		08:06			08:12	28	8	
BDB1-113.88-AQ	OPA	sandy facies 2	clst & lst l	113.75	114.00	113.88	22.01.14	11:03	11:11	11:29	11:33		11:40			11:44	19	7	
BDB1-114.08-NG	OPA	sandy facies 2	clst & lst l	114.00	114.15	114.08	22.01.14	11:03	11:11	11:29	11:34	2	11:40	160	5.05	11:43	19	6	
BDB1-114.80-AQ	OPA	sandy facies 2	clst & lst l	114.70	114.90	114.80	22.01.14	11:03	11:16	11:34	n.r.		n.r.			11:53	<33	<29	
BDB1-115.35-SQ	OPA	sandy facies 2	clst & lst l	115.25	115.45	115.35	22.01.14	11:03	11:18	11:40	n.r.		n.r.			12:21	<55	<41	
BDB1-119.86-AQ	OPA	sandy facies 2	clst & lst l	119.75	119.97	119.86	22.01.14	15:35	15:40	16:02	16:10		16:12			16:20	15	2	
BDB1-120.10-SQ	OPA	sandy facies 2	clst & lst l	120.00	120.20	120.10	22.01.14	15:35	15:43	16:14	16:16		16:23			16:33	17	7	
BDB1-120.68-AQ	OPA	sandy facies 2	clst & lst l	120.55	120.80	120.68	22.01.14	15:35	15:43	16:14	16:17		16:27			16:36	21	10	
BDB1-120.86-NG	OPA	sandy facies 2	clst & lst l	120.80	120.92	120.86	22.01.14	15:35	15:43	16:14	16:17	2	16:22	155	6.3	16:25	16	5	
BDB1-127.33-NG	OPA	sandy facies 2	clst & lst l	127.25	127.40	127.33	22.01.14	17:37	17:48	18:13	18:14	2	18:19	135	6.7	18:22	17	5	
BDB1-127.80-SQ	OPA	sandy facies 2	clst & lst l	127.70	127.90	127.80	22.01.14	17:37	17:52	18:21	18:25		18:28			18:33	22	3	
BDB1-128.24-AQ	OPA	sandy facies 2	clst & lst l	128.10	128.38	128.24	22.01.14	17:37	17:52	18:21	18:27		18:29			18:36	23	2	
BDB1-132.63-AQ	OPA	sandy facies 2	clst & lst l	132.50	132.75	132.63	22.01.14	19:40	19:47	19:59	20:04		20:08			20:14	16	4	
BDB1-133.46-NG	OPA	sandy facies 2	clst & lst l	133.40	133.52	133.46	22.01.14	19:40	19:49	20:10	20:11	2	20:16	150	6.4	20:19	15	5	
BDB1-143.75-SQ	OPA	shaly facies 2	silt clst	143.65	143.84	143.75	23.01.14	12:02	12:14	13:00	13:03		13:05			13:10	17	2	
BDB1-144.17-AQ	OPA	shaly facies 2	silt clst	144.06	144.27	144.17	23.01.14	12:02	12:14	13:00	13:03		13:11			13:25	23	8	
BDB1-144.49-NG	OPA	shaly facies 2	silt clst	144.41	144.57	144.49	23.01.14	12:02	12:15	12:36	12:43	5	12:50	200	5.7	12:54	27	7	
BDB1-160.30-NG	OPA	shaly facies 2	silt clst	160.25	160.35	160.30	24.01.14	14:14	14:24	14:55	14:56	2	15:02	155	6	15:05	17	6	
BDB1-161.18-AQ	OPA	shaly facies 2	silt clst	161.05	161.30	161.18	24.01.14	14:14	14:21	14:37	14:40		14:43			14:51	13	3	
BDB1-166.08-AQ	OPA	shaly facies 2	silt clst	165.95	166.20	166.08	27.01.14	07:14	07:23	07:32	07:35		07:37			07:39	14	2	
BDB1-167.38-NG	OPA	shaly facies 2	silt clst	167.30	167.45	167.38	27.01.14	07:14	07:25	07:39	07:43	2	07:48	195	6.1	07:53	20	5	
BDB1-172.70-AQ	OPA	shaly facies 2	silt clst	172.60	172.80	172.70	27.01.14	09:15	09:23	09:39	09:41		09:45			09:51	14	4	
BDB1-173.47-NG	OPA	shaly facies 2	silt clst	173.38	173.55	173.47	27.01.14	09:15	09:23	09:39	09:39	3	09:45	145	6.5	09:48	14	6	
BDB1-174.70-SQ	OPA	sandy facies 1	clst & sst l	174.60	174.80	174.70	27.01.14	10:07	10:13	10:23	10:30		10:34			10:51	17	4	
BDB1-175.33-AQ	OPA	sandy facies 1	clst & sst l	175.20	175.45	175.33	27.01.14	10:07	10:13	10:23	10:28		10:32			10:41	15	4	
BDB1-175.53-NG	OPA	sandy facies 1	clst & sst l	175.45	175.60	175.53	27.01.14	10:07	10:14	10:42	10:45	1	10:49	135	5.8	10:52	14	4	

## Notes:

AQ = samples for aqueous extraction etc.; NG = samples for noble gas analyses; SQ = samples for high-pressure squeezing. HRST = Hauptrogenstein, PAF = Passwang Formation, OPA = Opalinus Clay, STF = Stafflegg Formation; Lithology according to Hostettler et al. (2017).

## A.3 (cont.)

Sample	Stratigraphie	Member / Facies	Lithology	Sample top	Sample bottom	Aver. Depth	Sampling date	Core recovery	Core sealing	Core re-exposure	Start of sample sawing	Duration of sample sawing	First sealing / start pumping	Total pumping duration	Final pressure	Final sealing	Total core exposure duration	Sample exposure duration	Notes
				m BHL	m BHL	m BHL	dd.mm.yy	hh:mm	hh:mm	hh:mm	hh:mm	minutes	hh:mm	seconds	mbar	hh:mm	minutes	minutes	
BDB1-178.35-SQ	OPA	sandy facies 1	clst & sst l	178.25	178.45	178.35	27.01.14	11:00	11:16	11:36	11:37		11:43			11:46	23	6	
BDB1-178.53-NG	OPA	sandy facies 1	clst & sst l	178.45	178.60	178.53	27.01.14	11:00	11:16	11:36	11:38	2	11:43	130	6.6	11:46	23	5	
BDB1-178.73-AQ	OPA	sandy facies 1	clst & sst l	178.60	178.85	178.73	27.01.14	11:00	11:14	11:28	11:21		11:36			11:49	22	15	
BDB1-189.52-NG	OPA	sandy facies 1	lst	189.45	189.58	189.52	28.01.14	08:19	08:27	08:42	08:45	2	08:50	155	4.1	08:54	16	5	
BDB1-189.71-AQ	OPA	carb.-rich sandy f.	limestone	189.58	189.83	189.71	28.01.14	08:19	08:27	08:42	08:49		08:52			08:59	18	3	
BDB1-192.68-AQ	OPA	shaly facies 1	clst	192.55	192.80	192.68	28.01.14	09:22	09:29	09:36	09:42		09:44			09:55	15	2	
BDB1-192.95-SQ	OPA	shaly facies 1	clst	192.85	193.05	192.95	28.01.14	09:22	09:32	09:45	09:46		09:51			09:59	16	5	
BDB1-193.13-NG	OPA	shaly facies 1	clst	193.05	193.20	193.13	28.01.14	09:22	09:32	09:45	09:45	4	09:54	140	6.6	09:55	19	9	
BDB1-198.13-AQ	OPA	shaly facies 1	clst	198.00	198.25	198.13	28.01.14	11:07	11:15	11:25	11:29		11:31			11:35	14	2	
BDB1-198.45-SQ	OPA	shaly facies 1	clst	198.35	198.55	198.45	28.01.14	11:07	11:15	11:25	11:28		11:30			11:32	13	2	
BDB1-203.68-AQ	OPA	shaly facies 1	clst	203.55	203.80	203.68	28.01.14	18:00	18:09	18:18	18:23		18:24			18:32	15	1	
BDB1-204.09-NG	OPA	shaly facies 1	clst	204.02	204.15	204.09	28.01.14	18:00	18:11	18:37	18:39	2	18:45	135	7	18:48	19	6	
BDB1-204.51-SQ	OPA	shaly facies 1		204.42	204.60	204.51	28.01.14	18:00	18:11	18:37	18:41		18:44			18:50	18	3	
BDB1-209.00-AQ	OPA	shaly facies 1	clst	208.88	209.12	209.00	28.01.14	20:23	20:29	20:40	20:44	2	20:46	150	6.55	20:49	12	2	
BDB1-209.37-NG	OPA	shaly facies 1	clst	209.32	209.41	209.37	28.01.14	20:23	20:30	20:50	20:51		20:56			20:59	13	5	
BDB1-209.73-SQ	OPA	shaly facies 1	clst	209.63	209.83	209.73	28.01.14	20:23	20:30	20:50	20:55		20:59			21:02	16	4	
BDB1-213.85-AQ	OPA	shaly facies 1	clst	213.75	213.95	213.85	29.01.14	07:55	08:02	08:16	08:18		08:20			08:24	11	2	
BDB1-214.05-SQ	OPA	shaly facies 1	clst	213.95	214.15	214.05	29.01.14	07:55	08:02	08:16	08:20		08:22			08:28	13	2	
BDB1-217.98-AQ	OPA	shaly facies 1	clst	217.85	218.10	217.98	29.01.14	08:48	08:57	09:03	09:08		09:10			09:11	16	2	
BDB1-219.49-AQ	OPA	shaly facies 1	clst	219.38	219.60	219.49	29.01.14	09:55	10:09	10:27	10:30		10:33			10:37	20	3	
BDB1-219.66-NG	OPA	shaly facies 1	clst	219.60	219.72	219.66	29.01.14	09:55	10:09	10:27	10:28	2	10:33	135	6.3	10:36	20	5	
BDB1-221.28-AQ	OPA	shaly facies 1	clst	221.15	221.40	221.28	29.01.14	09:55	10:08	10:16	10:21		10:23			10:26	20	2	
BDB1-221.50-SQ	OPA	shaly facies 1	clst	221.40	221.60	221.50	29.01.14	09:55	10:08	10:16	10:23		10:24			10:41	21	1	
BDB1-225.18-AQ	OPA	shaly facies 1	clst	225.05	225.30	225.18	29.01.14	12:01	12:08	12:20	12:25		12:27			12:29	14	2	
BDB1-227.43-AQ	OPA	shaly facies 1	clst	227.30	227.55	227.43	29.01.14	12:01	12:10	12:16	12:18		12:20			12:22	13	2	
BDB1-229.68-AQ	OPA	shaly facies 1	clst	229.54	229.82	229.68	29.01.14	15:40	15:56	16:02	16:07		16:10			16:13	24	3	
BDB1-231.18-AQ	OPA	shaly facies 1	clst	231.05	231.30	231.18	29.01.14	17:12	17:21	17:32	17:33		17:36			17:39	13	3	
BDB1-233.63-AQ	OPA	shaly facies 1	clst	233.50	233.75	233.63	29.01.14	17:05	17:10	17:27	17:29		17:30			17:32	8	1	
BDB1-235.14-AQ	OPA	shaly facies 1	clst	235.00	235.28	235.14	29.01.14	18:40	18:49	18:56	19:02		19:04			19:07	17	2	
BDB1-237.88-AQ	STF	Gross Wolf Mb.	arg ma	237.78	237.98	237.88	29.01.14	20:17	20:27	20:34	20:35		20:36			20:39	12	1	
BDB1-243.37-AQ	STF	Gross Wolf Mb.	lst	243.28	243.45	243.37	30.01.14	09:40	09:50	10:10	10:10		10:13			10:15	13	3	
BDB1-245.54-AQ	STF	Rietheim Mb.	bit ma	245.43	245.64	245.54	30.01.14	09:40	09:55	10:15	10:15		10:17			10:20	17	2	
BDB1-246.34-AQ	STF	Rietheim Mb.	bit ma	246.25	246.43	246.34	30.01.14	11:00	11:09	11:27	11:29		11:32			11:33	14	3	
BDB1-246.99-NG	STF	Rietheim Mb.	bit ma	246.94	247.03	246.99	30.01.14	11:00	11:07	11:15	11:21	4	11:27	155	5.7	11:32	19	6	

**Notes:**

AQ = samples for aqueous extraction etc.; NG = samples for noble gas analyses; SQ = samples for high-pressure squeezing. HRST = Hauptrogenstein, PAF = Passwang Formation, OPA = Opalinus Clay, STF = Stafflegg Formation; Lithology according to Hostettler et al. (2017).

## A.4 GROUNDWATER SAMPLING PROTOCOL

RWI Uni Bern, Swisstopo

1

15.12.2013

### MT URL, Borehole DB1: Protocol of Groundwater Sampling

Date	Time	Activity
Fr. 13.12.13	11:00	<p>So far drillcores revealed non-fractured rocks of Hauptrogenstein and Passwang Fm with no indication of water inflow.</p> <p>Based on that DJ, HNW, DR decided to continue drilling until the end of the day and postpone groundwater sampling to Tuesday/Wednesday (17/18. 12.) after the geophysical logging of the borehole. A time slot of about 8-12 hours would be available at this time to not retard casing and sealing of the borehole.</p> <p>D. Traber (Nagra) agreed with this procedure.</p>
	ca. 16:00	<p>COFOR drillteam recognises a minor water inflow in the last core section to be drilled on this day; final depth 59.65 m BHL.</p> <p>The drillcore revealed some small fractures sub-parallel to the core direction.</p> <p>Measurement of observed artesian outflow suggested an inflow of about 5-10 L/min into the borehole.</p> <p>DJ, HNW, DR decided to stop drilling and install the single packer.</p>
	ca. 16:30	COFOR start to remove drill stem.
	17:45	<p>Drill stem removed; borehole is ready for packer installation.</p> <p>Monitoring of E.C., temperature and flow of water flowing out of the borehole (see Table 1); current E.C. 400 <math>\mu</math>S/cm.</p> <p>Increase in E.C. and the continuous, constant flow rate support an inflow that is worth sampling.</p> <p>Based on drill core appearance and flow rate DJ, HNW, DR decided to place the 1 m long packer between 50 m and 51 m BHL. If the inflow occurs in this interval and remains constant, this would allow exchanging the interval volume within ca. 1.5–2 hours.</p>
	ca. 18:15	Packer arrives on place, assembly of the packer system.
	19:00	Start of packer insertion into the borehole by DJ, HNW, DR, MH
	20:15	<p>Packer inserted (top: 50m BHL, bottom 51 m BHL)</p> <p>E.C. of out-flowing water has increased to 723 <math>\mu</math>S/cm (Table 11)</p>
	20:40	Start inflation of packer; artesian water flow starts to cease.
	21:30	Packer pressure stable at 30 bar; pressure in packed-off interval (i.e. 51.0–59.65 m BHL) becomes stable at 7 bar

		<p>No more outflow from borehole.</p> <p>Water starts to flow in water sampling line (inlet at ca. 52.3 m BHL) and N2-gas sampling line (inlet at ca 51.0 m BHL).</p> <p>Flow rate is ca. 1 L/min per line (total ca. 2 L/min); rate is limited by diameter of sampling lines (ca. 6 mm).</p> <p>No need for gas lift of water.</p> <p>Water is turbid; E.C. becomes stable at 730 <math>\mu\text{S}/\text{cm}</math>.</p> <p>Out-flowing water is collected in a 580 L barrel corresponding to about 3.5 interval volumes.</p>
	21:45	All work completed, DJ, HNW, DR; MH leave site
Sa, 14.12.13	15:00	<p>HNW &amp; DR arrive on site for water sampling.</p> <p>Water is still flowing at the same rate; the 580 L barrel is full and overflows.</p> <p>Packer pressure at 24.5 bar; Interval pressure at 7.5 bar.</p> <p>Packer is again inflated to 28.5 bar.</p> <p>Based on flow rate and time about 2100 L of water have flown out of the line corresponding to roughly 13 times the packed-off interval.</p> <p>Water in the upper N2-line is less turbid, water in lower water-sampling line is turbid</p> <p>E.C. is stable at 715–718 <math>\mu\text{S}/\text{cm}</math> and at 13.2° C in both lines (Table 2).</p>
	16:00	Start water sampling; Measurements see Table 2.
	17:45	End water sampling; HNW, DR leave site.
Su, 15.12.13	ca. 19:00	DR will go on-site to collect a second sample.
Mo, 16.12.13	ca. 05:30	<p>Packer will be removed by DJ, DR, MH and the help of COFOR.</p> <p>Drilling activities may continue at about 8 am.</p>

Table 1: Logging data of artesian outflow from borehole BDB1

Date	Time	E.C. ( $\mu\text{S}/\text{cm}$ )	T ( $^{\circ}\text{C}$ )	Comments
Fr, 13.12.12	17:45	401	14.2	drilling fluid
		400	14.1	artesian outflow from borehole
	18:00	399	14.2	artesian outflow from borehole
	19:00	555	14.7	artesian outflow from borehole
	20:15	723	14.4	artesian outflow from borehole after packer installation, but before inflation
	20:40	729	14.4	artesian outflow from borehole just before packer inflation
	21:30	730	13.8	artesian outflow through sampling lines interval pressure 7 bar after packer inflation (30 bar)

Table 2: Logging data of 1<sup>st</sup> groundwater sampling from borehole BDB1

Date	Time	E.C. ( $\mu\text{S}/\text{cm}$ )	T ( $^{\circ}\text{C}$ )	O <sub>2</sub> (mg/L)	Eh (mV)	pH	Comments
Sa, 14.12.12	15:30	718	13.3	-	-	-	upper N2 line, artesian outflow; turbid interval P: 7.5 bar
		715	13.2	-	-	-	lower water line, artesian outflow, very turbid interval P: 7.5 bar
	16:00	715	13.3	1.6	-30	7.24	artesian outflow from upper N2 line; turbid start sampling from upper N2 line for chemistry, $\delta^{18}\text{O}$ , $\delta^2\text{H}$ , $\delta^{13}\text{C}$ , $^{14}\text{C}$ , noble gases samples for cations and $\delta^{13}\text{C}$ filtrated on site (also on set for $\delta^{18}\text{O}$ , $\delta^2\text{H}$ )
	17:45	710	12.8	1.5	-33	7.19	artesian outflow from upper N2 line; turbid after completion of all samples

Staff involved:

DJ: David Jaeggi, Swisstopo

HM: Mauro Hauesler, Swisstopo

DR: Daniel Rufer, RWI, UniBe

HNW: Nick Waber, RWI, UniBe

COFOR drilling team

Protocol by HNW

Bern, 15.12.2



Picture 1: Inspection of last core section where indication of water inflow were observed (Fr, 13.12.2013).



Picture 2: Installation of packer system (Fr. 13.12.2013).



Picture 3: Artesian outflow after installation of packer but before packer inflation (Fr, 13.12.2013).



Picture 4: Artesian outflow from lower water sampling line after packer inflation (Sa, 14.12.2013).



Picture 5: Collection of artesian outflow in 580 L barrel (Sa, 14.12.2013).



Picture 6: Manometer showing interval pressure of 7 bar after packer inflation (Sa, 14.12.2013).



Picture 7: Collection of noble gas sample (Sa, 14.12.2013).



Picture 8: Field measurements devices and collected water samples; copper tubes are for noble gas measurements (Sa, 14.12.2013).



Picture 8: Collected water samples; note difference between samples filtered on-site (glass bottles for  $\delta^{13}\text{C}$  and 2 HDPE bottles in the middle) and unfiltered samples; steel cylinders are for  $^{14}\text{C}$  measurement (Sa, 14.12.2013).

**MT URL, Borehole BDB1: Groundwater sampling / sample 2**

Date: So 15.12.13

Staff involved:

DR: Daniel Rufer, RWI, UniBe

MS: Michèle Suchy, UniBe

Time	Activity / measurements
21:15	<p>Packer pressure: 24.5 bar Intervall pressure: 8.5 bar</p> <p>The lower water-sampling line has ceded to flow The upper N2-line has very low turbidity (almost clear) --&gt; all measurements refer to the water from the N2-line</p> <p>Flow rate: ca 1 L/min The 580 L water tank is full E.C. : 705 <math>\mu\text{S}/\text{cm}</math> at 12.5°C</p>
21:25	<p>DR re-inflated packer to 28.5 bar to verify interval pressure (which is 1 bar higher than on Friday)</p> <p>As a result the N2-line water rapidly turns very turbid (completely opaque) E.C. still at 710 <math>\mu\text{S}/\text{cm}</math> at 12.4°C --&gt; wait approx. 30min to see if it clears (it does not)</p>
22:00	<p>Water still has the same turbidity (visually)</p> <p>DR, MS start on-site measurements --&gt; data see Table 2</p>
22:15	<p>Water still has the same turbidity (visually)</p> <p>DR, MS start water sampling</p>
Ca 23:15	End water sampling. DR, MS leave site

Table 2: Logging data of 2nd groundwater sample from borehole BDB1

Time	E.C. ( $\mu\text{S}/\text{cm}$ )	T ( $^{\circ}\text{C}$ )	O <sub>2</sub> (mg/L)	eH (mV)	pH	Comments
21:15	705	12.5	-	-	-	Clear water from N2 line, artesian outflow; water-line clogged; Interval P: 8.5 bar
21:25	710	12.4	-	-	-	N2-line water very turbid, artesian outflow; water-line clogged; Interval P: 8.5 bar
22:04	704	12.5	1.6	-45 -42	7.20	N2-line water very turbid, artesian outflow; water-line clogged; Interval P: 8.5 bar

**Samples taken:**2x 500 ml unfiltered, no HNO<sub>3</sub>2x 250 ml unfiltered, no HNO<sub>3</sub>1x ca 200 ml filtered, no HNO<sub>3</sub>1x 125 ml filtered, HNO<sub>3</sub>2x glass ampoules, filtered, no HNO<sub>3</sub>2x 75 ml steel containers, unfiltered, no HNO<sub>3</sub>

### MT URL, Borehole BDB1: Groundwater sampling / sample 3

Date: Mo 16.12.13

Staff involved:

DR: Daniel Rufer, RWI, UniBe

DJ: David Jaeggi, swisstopo

COFOR drilling team

Intervall: 51 m - 59.65 m BHL

Time	Activity / measurements
05:30	Packer pressure: 24.5 bar Intervall pressure: 8.4 bar  The lower water-sampling line has still no flow The upper N2-line has very low turbidity (almost clear) --> all measurements refer to the water from the N2-line  Flow rate: ca 1 L/min  DR: Sampling of 3x 500ml and 1x 75 steel vessel; unfiltered, no HNO <sub>3</sub> from N2-line DR Sampling of 500ml of the same water for field measurements
Ca 05:45	DJ re-inflated packer to >28 bar  --> no observable increase in turbidity over >5min  DJ, DR decide to deflate packer and remove it
06:00	DR starts on-site measurements --> data see Table 2
Ca 06:30	Start of packer removal with help of COFOR drilling team
ca 07:15	Packer removed, begin of reinstalling drill stem by COFOR and resuming of normal operation

Table 2: Logging data of 3rd groundwater sample from borehole BDB1

Time	E.C. ( $\mu\text{S}/\text{cm}$ )	T ( $^{\circ}\text{C}$ )	O <sub>2</sub> (mg/L)	eH (mV)	pH	Comments
06:00	689	11.3	2.65	-42	7.22	Clear water from N2 line, artesian outflow; water-line clogged;  Interval P: 8.5 bar  Sample taken from bottle approx. 30 min after sampling of water

All analyses performed on water that was bottled for approx. 30 minutes

**Samples taken (analytical purpose to be defined):**

3x 500 ml unfiltered, no HNO<sub>3</sub>

1x 75 ml steel containers, unfiltered, no HNO<sub>3</sub>

protocol by DR

MT URL, 16.12.13



**APPENDIX B:  
AQUEOUS EXTRACTION DATA**

**CONTENTS**

	<b><u>Page</u></b>
<b>B.1</b>	<b>AQUEOUS EXTRACTION EXPERIMENTAL DATA..... 211</b>
<b>B.2</b>	<b>CHEMICAL COMPOSITION OF AQUEOUS EXTRACT SOLUTIONS..... 213</b>
<b>B.3</b>	<b>GEOCHEMICAL MODEL RESULTS OF AQUEOUS EXTRACT SOLUTIONS..... 215</b>



## B.1 AQUEOUS EXTRACTION EXPERIMENTAL DATA

Sample	Depth	Strati- graphie	Member / Facies	Lithology	Date Extract	Extraction Atmosphere	Extraction Time	Experim. Temp.	Mass wet rock	Mass water added	Mass porewater in leached wet rock	Mass leach solution	S:L Ratio wet rock : water
	m BHL						h	°C	g	g	g	g	
BDB1-36.19	36.19	HRST	Brüggli - Mb.	sa lst	07.01.14	glovebox	48	20	27.998	27.943	0.144	28.087	0.997
BDB1-43.78	43.78	PAF	Waldenburg - Mb.	sa lst	07.01.14	glovebox	48	20	30.288	29.950	1.651	31.601	0.958
BDB1-59.75	59.75	PAF	Waldenburg - Mb.	sa lst	07.01.14	glovebox	48	20	29.755	29.962	0.941	30.903	0.963
BDB1-60.79	60.79	PAF	Waldenburg - Mb.	sa lst	07.01.14	glovebox	48	20	30.110	30.003	1.909	31.912	0.944
BDB1-61.00	61.00	PAF	Waldenburg - Mb.	sa lst	07.01.14	glovebox	48	20	29.735	30.074	1.111	31.185	0.954
BDB1-61.52	61.52	PAF	Waldenburg - Mb.	sa lst	07.01.14	glovebox	48	20	29.070	28.326	1.192	29.518	0.985
BDB1-62.80	62.80	PAF	Waldenburg - Mb.	lst	05.02.14	glovebox	48	20	29.301	30.225	0.483	30.708	0.954
BDB1-63.15	63.15	PAF	Waldenburg - Mb.	lst	08.01.14	glovebox	48	20	29.786	30.260	0.777	31.037	0.960
BDB1-63.80	63.80	PAF	Waldenburg - Mb.	sa lst	08.01.14	glovebox	48	20	30.037	30.268	1.057	31.325	0.959
BDB1-64.11	64.11	PAF	Waldenburg - Mb.	sa lst	08.01.14	glovebox	48	20	29.981	30.074	1.110	31.184	0.961
BDB1-64.88	64.88	PAF	Waldenburg - Mb.	lst	08.01.14	glovebox	48	20	29.734	30.130	0.536	30.666	0.970
BDB1-65.34	65.34	PAF	Waldenburg - Mb.	lst	08.01.14	glovebox	48	20	29.549	30.307	0.577	30.884	0.957
BDB1-65.70	65.70	PAF	Waldenburg - Mb.	sa lst	08.01.14	glovebox	48	20	29.847	30.264	1.097	31.361	0.952
BDB1-66.15	66.15	PAF	Waldenburg - Mb.	sa lst	08.01.14	glovebox	48	20	30.343	29.975	0.667	30.642	0.990
BDB1-66.70	66.70	PAF	Waldenburg - Mb.	sa lst	08.01.14	glovebox	48	20	29.562	30.121	0.719	30.840	0.959
BDB1-67.30	67.30	PAF	Waldenburg - Mb.	sa lst	05.02.14	glovebox	48	20	30.028	30.101	1.223	31.324	0.959
BDB1-67.80	67.80	PAF	Waldenburg - Mb.	sa lst	08.01.14	glovebox	48	20	29.739	30.259	1.446	31.705	0.938
BDB1-68.90	68.90	PAF	Waldenburg - Mb.	sa lst	08.01.14	glovebox	48	20	29.587	30.156	0.634	30.790	0.961
BDB1-72.20	72.20	PAF	Waldenburg - Mb.	sa lst	08.01.14	glovebox	48	20	30.517	30.262	1.461	31.723	0.962
BDB1-76.30	76.30	PAF	Himichopf - Mb.	sa lst	08.01.14	glovebox	48	20	29.720	30.117	0.866	30.983	0.959
BDB1-82.30	82.30	PAF	Himichopf - Mb.	lst	08.01.14	glovebox	48	20	29.932	30.293	1.030	31.323	0.956
BDB1-89.45	89.45	PAF	Himichopf - Mb.	li sst	08.01.14	glovebox	48	20	30.163	30.157	1.276	31.433	0.960
BDB1-93.24	93.24	PAF	Himichopf - Mb.	sa ma	05.02.14	glovebox	48	20	31.128	30.294	1.894	32.188	0.967
BDB1-93.65	93.65	PAF	Himichopf - Mb.	sa ma	08.01.14	glovebox	48	20	29.604	30.255	1.713	31.968	0.926
BDB1-97.10	97.10	PAF	Sissach - Mb.	lst	08.01.14	glovebox	48	20	29.878	30.212	1.032	31.244	0.956
BDB1-98.68	98.68	PAF	Sissach - Mb.	sa lst	03.02.14	glovebox	48	20	30.295	30.132	0.492	30.624	0.989
BDB1-100.63	100.63	PAF	Sissach - Mb.	sa ma	03.02.14	glovebox	48	20	30.215	30.156	1.089	31.245	0.967
BDB1-101.80	101.80	PAF	Sissach - Mb.	sa ma	03.02.14	glovebox	48	20	30.423	30.072	1.161	31.233	0.974
BDB1-102.93	102.93	PAF	Sissach - Mb.	sa ma	03.02.14	glovebox	48	20	29.861	30.083	1.755	31.838	0.938
BDB1-104.78	104.78	PAF	Sissach - Mb.	sa ma	03.02.14	glovebox	48	20	30.056	30.029	1.265	31.294	0.960

## B.1 (cont.)

Sample	Depth	Strati- graphie	Member / Facies	Lithology	Date Extract	Extraction Atmosphere	Extraction Time	Experim. Temp.	Mass wet rock	Mass water added	Mass porewater in leached wet rock	Mass leach solution	S:L Ratio wet rock : water
	m BHL						h	°C	g	g	g	g	
BDB1-108.24	108.24	OPA	sandy facies 2	clst & lst la	03.02.14	glovebox	48	20	29.803	30.054	1.521	31.575	0.944
BDB1-113.88	113.88	OPA	sandy facies 2	clst & lst la	03.02.14	glovebox	48	20	29.956	30.169	1.330	31.499	0.951
BDB1-114.80	114.80	OPA	sandy facies 2	clst & lst la	04.02.14	glovebox	48	20	29.738	29.490	1.239	30.729	0.968
BDB1-119.86	119.86	OPA	sandy facies 2	clst & lst la	04.02.14	glovebox	48	20	30.265	30.173	1.559	31.732	0.954
BDB1-120.68	120.68	OPA	sandy facies 2	clst & lst la	04.02.14	glovebox	48	20	30.461	30.037	1.581	31.618	0.963
BDB1-128.24	128.24	OPA	sandy facies 2	clst & lst la	04.02.14	glovebox	48	20	30.364	30.133	1.598	31.731	0.957
BDB1-132.63	132.63	OPA	sandy facies 2	clst & lst la	04.02.14	glovebox	48	20	29.989	30.051	1.432	31.483	0.953
BDB1-144.17	144.17	OPA	shaly facies 2	silt clst	04.02.14	glovebox	48	20	30.230	30.105	1.802	31.907	0.947
BDB1-161.18	161.18	OPA	shaly facies 2	silt clst	04.02.14	glovebox	48	20	29.430	30.079	1.711	31.790	0.926
BDB1-166.08	166.08	OPA	shaly facies 2	silt clst	04.02.14	glovebox	48	20	30.202	30.110	1.742	31.852	0.948
BDB1-172.70	172.70	OPA	shaly facies 2	silt clst	04.02.14	glovebox	48	20	29.954	30.090	1.427	31.517	0.950
BDB1-175.33	175.33	OPA	sandy facies 1	clst & sst la	04.02.14	glovebox	48	20	29.909	29.770	1.256	31.026	0.964
BDB1-178.73	178.73	OPA	sandy facies 1	clst & sst la	04.02.14	glovebox	48	20	29.803	30.038	1.314	31.352	0.951
BDB1-189.71	189.71	OPA	carb.-rich sandy f.	limestone	04.02.14	glovebox	48	20	30.454	30.039	0.472	30.511	0.998
BDB1-192.68	192.68	OPA	shaly facies 1	clst	04.02.14	glovebox	48	20	29.944	30.068	1.682	31.750	0.943
BDB1-198.13	198.13	OPA	shaly facies 1	clst	04.02.14	glovebox	48	20	30.400	30.192	1.634	31.826	0.955
BDB1-203.68	203.68	OPA	shaly facies 1	clst	04.02.14	glovebox	48	20	30.474	30.035	1.725	31.760	0.960
BDB1-209.00	209.00	OPA	shaly facies 1	clst	04.02.14	glovebox	48	20	30.003	30.084	1.721	31.805	0.943
BDB1-213.85	213.85	OPA	shaly facies 1	clst	05.02.14	glovebox	48	20	30.024	29.958	1.810	31.768	0.945
BDB1-217.98	217.98	OPA	shaly facies 1	clst	05.02.14	glovebox	48	20	30.071	30.112	1.688	31.800	0.946
BDB1-219.49	219.49	OPA	shaly facies 1	clst	05.02.14	glovebox	48	20	30.359	30.082	1.567	31.649	0.959
BDB1-221.28	221.28	OPA	shaly facies 1	clst	05.02.14	glovebox	48	20	29.751	30.065	1.492	31.557	0.943
BDB1-225.18	225.18	OPA	shaly facies 1	clst	05.02.14	glovebox	48	20	29.722	30.076	1.694	31.770	0.936
BDB1-227.43	227.43	OPA	shaly facies 1	clst	05.02.14	glovebox	48	20	29.944	30.107	1.654	31.761	0.943
BDB1-229.68	229.68	OPA	shaly facies 1	clst	05.02.14	glovebox	48	20	29.762	30.142	1.707	31.849	0.934
BDB1-231.18	231.18	OPA	shaly facies 1	clst	05.02.14	glovebox	48	20	30.013	30.069	1.770	31.839	0.943
BDB1-233.63	233.63	OPA	shaly facies 1	clst	05.02.14	glovebox	48	20	30.004	30.166	1.706	31.872	0.941
BDB1-235.14	235.14	OPA	shaly facies 1	clst	05.02.14	glovebox	48	20	29.987	30.144	1.833	31.977	0.938
BDB1-237.88	237.88	STF	Gross Wolf Mb.	arg ma	05.02.14	glovebox	48	20	30.088	30.054	1.687	31.741	0.948
BDB1-243.37	243.37	STF	Gross Wolf Mb.	lst	05.02.14	glovebox	48	20	29.023	30.191	0.201	30.392	0.955
BDB1-245.54	245.54	STF	Rietheim Mb.	bit ma	05.02.14	glovebox	48	20	30.105	30.219	1.649	31.868	0.945
BDB1-246.34	246.34	STF	Rietheim Mb.	bit ma	05.02.14	glovebox	48	20	29.899	30.172	1.514	31.686	0.944

## B.2 CHEMICAL COMPOSITION OF AQUEOUS EXTRACT SOLUTIONS

Sample	Depth	Strati- graphie	Member / Facies	Lithology	Date Analysis	pH	T (°C)	Na	K	NH4	Mg	Ca	Sr	F	Cl	Br	SO4	NO3	Tot. Alk.	Tot. Alk. as HCO3	TDS	CB
	m BHL							mg/L	mg/L	mg/L	mg/L	mg/L	mg/L	mg/L	mg/L	mg/L	mg/L	mg/L	meq/L	mg/L	mg/L	%
BDB1-36.19	36.19	HRST	Brüggli - Mb.	sa lst	09.01.14	8.03	20	8.6	13.0	0.74	11.4	35.5	2.385	0.55	5.1	0.052	41.0	0.04	2.31	140.9	259	2.51%
BDB1-43.78	43.78	PAF	Waldenburg - Mb.	sa lst	09.01.14	8.37	20	17.1	14.5	1.02	8.23	11.7	3.607	7.03	1.1	<0.016	32.0	0.03	2.05	125.1	221	-10.71%
BDB1-59.75	59.75	PAF	Waldenburg - Mb.	sa lst	09.01.14	7.68	20	35.5	8.2	<0.5	14.0	65.5	2.443	0.57	79.5	0.692	42.3	0.02	3.63	221.5	470	-4.31%
BDB1-60.79	60.79	PAF	Waldenburg - Mb.	sa lst	09.01.14	8.21	20	11.8	14.9	0.70	14.4	20.7	3.272	1.42	15.6	0.102	40.5	0.05	2.48	151.3	275	-9.29%
BDB1-61.00	61.00	PAF	Waldenburg - Mb.	sa lst	09.01.14	8.06	20	17.3	18.0	0.73	22.3	33.7	3.682	0.88	22.6	0.152	47.9	0.05	3.56	217.2	384	-4.31%
BDB1-61.52	61.52	PAF	Waldenburg - Mb.	sa lst	10.01.14	8.06	20	13.5	16.1	0.78	13.8	19.8	3.595	1.48	17.9	0.134	50.2	0.04	2.31	140.9	278	-10.25%
BDB1-62.80	62.80	PAF	Waldenburg - Mb.	lst	07.02.14	7.90	20	18.8	10.5	<1	13.1	63.5	1.913	<0.16	34.3	0.280	83.4	<0.16	2.64	161.1	387	0.32%
BDB1-63.15	63.15	PAF	Waldenburg - Mb.	lst	10.01.14	8.05	20	19.9	12.1	0.32	28.6	51.3	2.533	0.25	27.9	0.214	79.6	0.05	4.33	264.2	487	-4.98%
BDB1-63.80	63.80	PAF	Waldenburg - Mb.	sa lst	10.01.14	8.15	20	18.6	13.9	0.77	14.5	32.6	4.178	0.86	14.4	0.108	52.9	0.06	3.29	200.7	354	-8.58%
BDB1-64.11	64.11	PAF	Waldenburg - Mb.	sa lst	10.01.14	7.74	20	8.1	10.5	0.32	12.3	39.4	3.194	0.29	5.2	0.039	76.3	0.04	2.76	168.4	324	-10.32%
BDB1-64.88	64.88	PAF	Waldenburg - Mb.	lst	10.01.14	7.86	20	18.0	13.2	0.69	18.5	33.1	3.595	0.49	13.5	0.098	70.9	0.02	3.42	208.7	381	-9.54%
BDB1-65.34	65.34	PAF	Waldenburg - Mb.	lst	10.01.14	8.11	20	10.7	7.7	0.41	10.1	33.0	1.731	0.14	9.1	0.069	35.0	0.05	2.59	158.0	266	-5.94%
BDB1-65.70	65.70	PAF	Waldenburg - Mb.	sa lst	10.01.14	8.13	20	22.6	18.5	0.93	12.5	23.8	4.531	0.95	12.8	0.098	73.4	0.05	2.38	145.2	315	-6.76%
BDB1-66.15	66.15	PAF	Waldenburg - Mb.	sa lst	10.01.14	8.02	20	13.7	8.6	0.49	8.89	31.0	2.017	0.22	9.1	0.067	41.0	0.06	2.73	166.6	282	-10.15%
BDB1-66.70	66.70	PAF	Waldenburg - Mb.	sa lst	07.02.14	7.86	20	17.7	15.5	0.83	8.92	21.9	3.304	0.75	7.9	0.059	46.6	0.05	2.58	157.4	281	-10.84%
BDB1-67.30	67.30	PAF	Waldenburg - Mb.	sa lst	10.01.14	8.06	20	18.9	17.9	0.87	19.82	41.76	7.217	0.60	13.4	0.049	89.7	0.04	3.16	192.8	403	-2.59%
BDB1-67.80	67.80	PAF	Waldenburg - Mb.	sa lst	10.01.14	8.15	20	24.8	13.9	0.81	11.9	22.1	4.177	0.96	10.6	0.078	48.7	0.04	3.08	187.9	326	-10.32%
BDB1-68.90	68.90	PAF	Waldenburg - Mb.	sa lst	10.01.14	8.14	20	17.6	8.6	0.52	6.58	23.2	2.081	0.42	6.8	0.046	28.9	0.05	2.65	161.7	256	-11.81%
BDB1-72.20	72.20	PAF	Waldenburg - Mb.	sa lst	10.01.14	8.60	20	47.4	10.7	1.12	3.18	5.84	1.859	2.63	10.1	0.064	45.3	0.05	2.28	139.1	267	-10.85%
BDB1-76.30	76.30	PAF	Himichopf - Mb.	sa lst	10.01.14	7.98	20	65.9	21.4	<1	19.8	37.6	5.080	0.75	24.1	0.126	114.5	0.06	4.06	247.7	537	-0.88%
BDB1-82.30	82.30	PAF	Himichopf - Mb.	lst	10.01.14	8.14	20	106.5	18.0	<1.25	10.2	17.7	4.121	2.48	23.9	0.123	61.5	0.04	4.93	300.8	545	-0.80%
BDB1-89.45	89.45	PAF	Himichopf - Mb.	li sst	10.01.14	8.79	20	97.4	13.3	<1.25	1.50	2.99	0.857	3.57	22.6	0.104	61.3	0.05	3.59	219.1	423	-7.78%
BDB1-93.24	93.24	PAF	Himichopf - Mb.	sa ma	07.02.14	8.75	20	104.8	11.3	2.00	0.68	1.35	0.411	9.85	21.5	0.074	55.5	0.09	2.57	156.8	364	1.32%
BDB1-93.65	93.65	PAF	Himichopf - Mb.	sa ma	10.01.14	8.57	20	107.4	7.5	<1.25	0.71	1.42	0.443	7.84	21.2	0.071	30.4	0.07	3.62	220.9	398	-2.54%
BDB1-97.10	97.10	PAF	Sissach - Mb.	lst	10.01.14	8.12	20	81.7	11.8	<1.25	9.36	20.8	1.770	0.76	39.0	0.180	48.3	0.05	4.10	250.2	464	-4.53%
BDB1-98.68	98.68	PAF	Sissach - Mb.	sa lst	06.02.14	8.95	20	133.1	10.1	2.06	0.75	2.1	0.400	7.19	40.5	0.185	86.9	<0.4	3.02	184.3	465	-1.86%
BDB1-100.63	100.63	PAF	Sissach - Mb.	sa ma	06.02.14	8.14	20	118.9	17.1	1.69	7.30	19.2	1.351	0.77	50.0	0.200	76.5	<0.4	4.25	259.3	552	-0.69%
BDB1-101.80	101.80	PAF	Sissach - Mb.	sa ma	06.02.14	8.01	20	104.3	15.7	1.58	28.1	34.3	1.391	0.46	59.5	0.225	70.1	<0.4	5.85	357.0	673	-0.12%
BDB1-102.93	102.93	PAF	Sissach - Mb.	sa ma	06.02.14	9.07	20	135.3	10.0	2.23	0.53	1.46	0.230	4.17	77.3	0.270	84.7	<0.4	2.20	134.2	449	-1.40%
BDB1-104.78	104.78	PAF	Sissach - Mb.	sa ma	06.02.14	8.91	20	164.2	6.6	1.78	0.69	1.86	0.257	3.69	52.8	0.200	88.0	<0.4	2.69	164.1	482	8.58%

## B.2 (cont.)

Sample	Depth	Strati- graphie	Member / Facies	Lithology	Date Analysis	pH	T (°C)	Na	K	NH4	Mg	Ca	Sr	F	Cl	Br	SO4	NO3	Tot. Alk.	Tot. Alk. as HCO3	TDS	CB
	m BHL							mg/L	mg/L	mg/L	mg/L	mg/L	mg/L	mg/L	mg/L	mg/L	mg/L	mg/L	meq/L	mg/L	mg/L	%
BDB1-108.24	108.24	OPA	sandy facies 2	clst & lst la	06.02.14	8.98	20	162.5	6.6	1.78	0.55	1.46	0.192	9.29	58.1	0.200	69.1	<0.4	3.93	239.8	548	-1.44%
BDB1-113.88	113.88	OPA	sandy facies 2	clst & lst la	06.02.14	8.70	20	203.0	11.2	2.17	1.03	2.15	0.319	4.99	71.5	0.240	114.8	<0.4	4.72	288.0	699	-0.42%
BDB1-114.80	114.80	OPA	sandy facies 2	clst & lst la	06.02.14	8.91	20	157.0	8.2	2.28	0.53	1.60	0.177	6.40	71.5	0.240	85.8	<0.4	3.03	184.9	517	-0.61%
BDB1-119.86	119.86	OPA	sandy facies 2	clst & lst la	06.02.14	8.95	20	183.3	8.4	2.03	0.66	1.83	0.204	5.41	86.0	0.280	81.6	<0.4	4.00	244.1	612	-1.00%
BDB1-120.68	120.68	OPA	sandy facies 2	clst & lst la	06.02.14	8.82	20	200.3	8.5	2.06	0.69	1.83	0.210	5.62	99.5	0.330	89.2	<0.4	4.12	251.4	657	-0.51%
BDB1-128.24	128.24	OPA	sandy facies 2	clst & lst la	06.02.14	8.92	20	208.9	7.7	2.11	0.63	1.77	0.179	4.97	118.4	0.390	92.9	<0.4	3.94	240.4	676	-0.76%
BDB1-132.63	132.63	OPA	sandy facies 2	clst & lst la	06.02.14	8.86	20	226.5	9.6	2.21	0.81	1.38	0.264	3.67	124.6	0.420	121.8	<0.4	4.11	250.8	742	-0.59%
BDB1-144.17	144.17	OPA	shaly facies 2	silt clst	06.02.14	8.95	20	247.9	7.6	2.06	0.68	1.28	0.171	3.60	190.2	0.610	111.8	<0.4	3.30	201.4	767	-0.40%
BDB1-161.18	161.18	OPA	shaly facies 2	silt clst	06.02.14	8.69	20	295.6	9.3	<3.85	0.76	1.69	0.171	2.81	233.0	0.740	122.0	<0.4	3.97	242.2	908	0.02%
BDB1-166.08	166.08	OPA	shaly facies 2	silt clst	06.02.14	8.54	20	305.7	8.5	<4.17	0.89	1.79	0.198	2.97	260.2	0.840	131.5	<0.4	3.43	209.3	922	0.02%
BDB1-172.70	172.70	OPA	shaly facies 2	silt clst	06.02.14	8.50	20	287.7	8.8	<3.85	0.83	1.62	0.179	3.02	244.1	0.780	127.3	<0.4	3.14	191.6	866	0.19%
BDB1-175.33	175.33	OPA	sandy facies 1	clst & sst la	06.02.14	8.75	20	280.5	10.8	<3.57	1.06	2.10	0.223	2.40	205.9	0.670	131.2	<0.4	3.94	240.4	875	0.23%
BDB1-178.73	178.73	OPA	sandy facies 1	clst & sst la	06.02.14	8.68	20	309.9	12.4	<4.17	1.19	2.41	0.342	2.35	276.5	0.900	139.3	<0.4	3.12	190.4	936	0.26%
BDB1-189.71	189.71	OPA	carb.-rich sandy f.	limestone	06.02.14	8.18	20	180.0	13.4	1.85	3.54	11.6	0.441	0.58	87.6	0.290	83.9	<0.4	4.64	283.1	666	0.90%
BDB1-192.68	192.68	OPA	shaly facies 1	clst	06.02.14	8.81	20	332.6	9.3	n.a.	1.01	1.99	0.197	4.14	314.4	1.010	131.5	<0.4	2.99	182.4	979	0.21%
BDB1-198.13	198.13	OPA	shaly facies 1	clst	06.02.14	8.83	20	341.1	9.0	2.79	0.96	2.01	0.187	4.14	341.7	1.060	148.7	<0.4	2.66	162.3	1014	-1.22%
BDB1-203.68	203.68	OPA	shaly facies 1	clst	06.02.14	8.78	20	362.3	9.4	2.80	1.00	2.44	0.189	4.28	355.5	1.150	170.3	<0.4	2.57	156.8	1066	-0.54%
BDB1-209.00	209.00	OPA	shaly facies 1	clst	06.02.14	8.80	20	367.9	9.8	2.88	1.02	2.47	0.194	4.17	351.8	1.130	183.3	<0.4	2.66	162.3	1087	-0.50%
BDB1-213.85	213.85	OPA	shaly facies 1	clst	07.02.14	8.83	20	398.3	9.7	<5	1.30	3.03	0.241	3.70	391.9	1.250	187.8	<0.4	2.79	170.2	1167	-0.36%
BDB1-217.98	217.98	OPA	shaly facies 1	clst	07.02.14	8.78	20	375.3	9.0	<4.5	1.08	2.48	0.195	4.26	350.9	1.110	190.5	<0.4	2.90	176.9	1112	-0.67%
BDB1-219.49	219.49	OPA	shaly facies 1	clst	07.02.14	8.87	20	350.6	9.0	2.83	0.95	2.01	0.171	4.71	305.5	0.980	185.5	<0.4	3.06	186.7	1049	-0.45%
BDB1-221.28	221.28	OPA	shaly facies 1	clst	07.02.14	8.84	20	340.1	8.8	2.81	0.97	1.81	0.172	4.81	298.3	0.940	178.5	<0.4	2.98	181.8	1019	-0.60%
BDB1-225.18	225.18	OPA	shaly facies 1	clst	07.02.14	8.72	20	380.7	9.0	<4.5	1.11	2.43	0.191	4.85	354.8	1.100	196.3	<0.4	2.86	174.5	1125	-0.63%
BDB1-227.43	227.43	OPA	shaly facies 1	clst	07.02.14	8.86	20	361.8	9.6	<4.17	1.07	2.10	0.206	5.18	351.5	1.120	183.6	<0.4	2.40	146.4	1063	-0.75%
BDB1-229.68	229.68	OPA	shaly facies 1	clst	07.02.14	8.74	20	382.1	9.2	<4.5	0.98	2.33	0.168	5.20	360.2	1.140	193.4	<0.4	2.68	163.5	1118	-0.27%
BDB1-231.18	231.18	OPA	shaly facies 1	clst	07.02.14	8.83	20	386.8	8.9	<5	1.23	2.52	0.215	4.77	374.0	1.180	190.3	<0.4	2.59	158.0	1128	-0.24%
BDB1-233.63	233.63	OPA	shaly facies 1	clst	07.02.14	8.77	20	392.6	9.4	<5	1.37	2.93	0.242	4.78	375.6	1.210	194.7	<0.4	2.67	162.9	1146	-0.01%
BDB1-235.14	235.14	OPA	shaly facies 1	clst	07.02.14	8.83	20	429.4	9.5	<5	1.39	2.85	0.271	5.24	404.1	1.270	199.1	<0.4	2.55	155.6	1209	2.13%
BDB1-237.88	237.88	STF	Gross Wolf Mb.	arg ma	07.02.14	8.83	20	393.9	9.6	<5	1.23	2.62	0.248	5.39	390.0	1.250	205.9	<0.4	2.09	127.5	1138	-0.17%
BDB1-243.37	243.37	STF	Gross Wolf Mb.	lst	07.02.14	8.28	20	122.8	6.6	1.08	2.01	9.39	0.442	0.21	59.0	0.190	66.2	<0.4	2.22	135.5	402	7.70%
BDB1-245.54	245.54	STF	Rietheim Mb.	bit ma	07.02.14	8.69	20	397.1	7.0	<5	1.01	2.46	0.196	2.95	352.2	1.120	213.3	<0.4	3.01	183.7	1161	0.30%
BDB1-246.34	246.34	STF	Rietheim Mb.	bit ma	07.02.14	8.80	20	374.5	7.2	<4.17	1.22	2.52	0.230	2.55	302.9	0.970	190.5	<0.4	3.37	205.6	1088	2.07%

### B.3 GEOCHEMICAL MODEL RESULTS OF AQUEOUS EXTRACT SOLUTIONS

Sample	Depth m BHL	Strati- graphie	Member / Facies	Lithology	Water Type	MODELLED USING MEASURED pH				MODELLED USING pH ADJUSTED FOR CALCITE SATURATION														
						pH	TIC calc.	log P CO <sub>2</sub> (g)	SI calcite	pH	Ionic Strength	Alkalinit y	TIC	log P CO <sub>2</sub> (g)	SI calcite	SI aragonite	SI dolomite	SI dolomite(d)	SI magnesite	SI anhydrite	SI gypsum	SI celestite	SI strontianite	SI fluorite
						mmol/L				mol	meq/l	mmol/L												
BDB1-36.19	36.19	HRST	Brüggli - Mb.	sa lst	Ca-Mg-HCO <sub>3</sub> -SO <sub>4</sub>	8.08	2.322E-03	-2.98	0.26	7.81	4.920E-03	2.301	2.354	-2.70	0.00	-0.15	-0.21	-0.78	-0.78	-2.43	-2.19	-1.66	-0.69	-1.71
BDB1-43.78	43.78	PAF	Waldenburg - Mb.	sa lst	Na-Mg-Ca-HCO <sub>3</sub> -SO <sub>4</sub>	8.39	2.025E-03	-3.34	0.05	8.34	3.620E-03	2.038	2.008	-3.29	0.00	-0.15	0.13	-0.44	-0.44	-2.98	-2.75	-1.55	-0.03	0.05
BDB1-59.75	59.75	PAF	Waldenburg - Mb.	sa lst	Ca-Na-HCO <sub>3</sub> -Cl	7.75	3.742E-03	-2.46	0.36	7.39	8.770E-03	3.632	3.937	-2.09	0.00	-0.15	-0.38	-0.96	-0.95	-2.23	-1.99	-1.72	-0.95	-1.47
BDB1-60.79	60.79	PAF	Waldenburg - Mb.	sa lst	Ca-Mg-HCO <sub>3</sub> -SO <sub>4</sub>	8.21	2.475E-03	-3.08	0.19	8.02	4.822E-03	2.471	2.490	-2.88	0.00	-0.15	0.13	-0.44	-0.44	-2.66	-2.42	-1.52	-0.32	-1.12
BDB1-61.00	61.00	PAF	Waldenburg - Mb.	sa lst	Mg-Ca-HCO <sub>3</sub>	8.05	3.584E-03	-2.76	0.37	7.67	6.906E-03	3.552	3.688	-2.38	0.00	-0.15	0.10	-0.47	-0.46	-2.44	-2.20	-1.46	-0.48	-1.37
BDB1-61.52	61.52	PAF	Waldenburg - Mb.	sa lst	Mg-Ca-HCO <sub>3</sub> -SO <sub>4</sub>	8.04	2.332E-03	-2.93	-0.03	8.07	4.904E-03	2.300	2.306	-2.97	0.00	-0.15	0.13	-0.45	-0.44	-2.59	-2.35	-1.39	-0.26	-1.11
BDB1-62.80	62.80	PAF	Waldenburg - Mb.	lst	Ca-Mg-HCO <sub>3</sub> -SO <sub>4</sub>	7.91	2.683E-03	-2.75	0.36	7.54	7.731E-03	2.641	2.792	-2.38	0.00	-0.15	-0.40	-0.97	-1.94	-1.70	-1.52	-1.04	-	
BDB1-63.15	63.15	PAF	Waldenburg - Mb.	lst	Ca-Mg-HCO <sub>3</sub> -SO <sub>4</sub>	8.05	4.351E-03	-2.69	0.60	7.44	9.036E-03	4.328	4.648	-2.06	0.00	-0.15	0.03	-0.54	-0.54	-2.09	-1.85	-1.45	-0.83	-2.33
BDB1-63.80	63.80	PAF	Waldenburg - Mb.	sa lst	Ca-Mg-HCO <sub>3</sub> -SO <sub>4</sub>	8.16	3.290E-03	-2.91	0.43	7.71	6.094E-03	3.281	3.392	-2.46	0.00	-0.15	-0.07	-0.64	-0.64	-2.39	-2.15	-1.34	-0.41	-1.39
BDB1-64.11	64.11	PAF	Waldenburg - Mb.	sa lst	Ca-Mg-HCO <sub>3</sub> -SO <sub>4</sub>	7.74	2.854E-03	-2.55	0.03	7.71	5.925E-03	2.756	2.854	-2.53	0.00	-0.15	-0.22	-0.79	-0.79	-2.14	-1.90	-1.29	-0.61	-2.25
BDB1-64.88	64.88	PAF	Waldenburg - Mb.	lst	Ca-Mg-HCO <sub>3</sub> -SO <sub>4</sub>	7.87	3.493E-03	-2.60	0.16	7.70	6.708E-03	3.413	3.531	-2.43	0.00	-0.15	0.03	-0.54	-0.54	-2.27	-2.03	-1.29	-0.49	-1.89
BDB1-65.34	65.34	PAF	Waldenburg - Mb.	lst	Ca-Mg-HCO <sub>3</sub> -SO <sub>4</sub>	8.08	2.606E-03	-2.92	0.29	7.79	4.768E-03	2.585	2.658	-2.63	0.00	-0.15	-0.23	-0.80	-0.80	-2.52	-2.28	-1.86	-0.80	-2.92
BDB1-65.70	65.70	PAF	Waldenburg - Mb.	sa lst	Ca-Mg-Na-HCO <sub>3</sub> -SO <sub>4</sub>	8.16	2.382E-03	-3.04	0.16	8.00	5.573E-03	2.368	2.384	-2.88	0.00	-0.15	0.00	-0.57	-0.57	-2.37	-2.13	-1.14	-0.24	-1.43
BDB1-66.15	66.15	PAF	Waldenburg - Mb.	sa lst	Ca-Mg-HCO <sub>3</sub> -SO <sub>4</sub>	8.05	2.753E-03	-2.87	0.25	7.79	4.834E-03	2.724	2.798	-2.61	0.00	-0.15	-0.26	-0.83	-0.83	-2.47	-2.24	-1.72	-0.71	-2.56
BDB1-66.70	66.70	PAF	Waldenburg - Mb.	sa lst	Ca-Mg-Na-HCO <sub>3</sub> -SO <sub>4</sub>	7.85	2.644E-03	-2.69	-0.12	7.97	4.628E-03	2.570	2.596	-2.82	0.00	-0.15	-0.11	-0.68	-0.67	-2.57	-2.33	-1.45	-0.34	-1.64
BDB1-67.30	67.30	PAF	Waldenburg - Mb.	sa lst	Ca-Mg-SO <sub>4</sub> -HCO <sub>3</sub>	8.05	3.179E-03	-2.82	0.39	7.65	7.501E-03	3.150	3.273	-2.41	0.00	-0.15	-0.04	-0.61	-0.61	-2.09	-1.86	-0.91	-0.28	-1.63
BDB1-67.80	67.80	PAF	Waldenburg - Mb.	sa lst	Ca-Mg-Na-HCO <sub>3</sub> -SO <sub>4</sub>	8.16	3.085E-03	-2.93	0.25	7.90	5.337E-03	3.071	3.120	-2.67	0.00	-0.15	0.02	-0.55	-0.55	-2.57	-2.33	-1.35	-0.24	-1.44
BDB1-68.90	68.90	PAF	Waldenburg - Mb.	sa lst	Ca-Mg-Na-HCO <sub>3</sub>	8.07	2.672E-03	-2.90	0.15	7.92	4.111E-03	2.644	2.689	-2.75	0.00	-0.15	-0.26	-0.83	-0.83	-2.73	-2.49	-1.83	-0.57	-2.10
BDB1-72.20	72.20	PAF	Waldenburg - Mb.	sa lst	Na-HCO <sub>3</sub> -SO <sub>4</sub>	8.70	2.208E-03	-3.61	0.08	8.62	3.948E-03	2.267	2.201	-3.53	0.00	-0.15	0.02	-0.55	-0.54	-3.14	-2.90	-1.68	-0.01	-1.12
BDB1-76.30	76.30	PAF	Himichopf - Mb.	sa lst	Na-Cg-Ma-HCO <sub>3</sub> -SO <sub>4</sub>	7.98	4.111E-03	-2.64	0.36	7.61	9.364E-03	4.062	4.256	-2.27	0.00	-0.15	0.01	-0.57	-0.56	-2.06	-1.82	-0.99	-0.39	-1.51
BDB1-82.30	82.30	PAF	Himichopf - Mb.	lst	Na-HCO <sub>3</sub>	8.15	4.949E-03	-2.72	0.31	7.83	8.226E-03	4.932	5.060	-2.40	0.00	-0.15	0.04	-0.53	-0.52	-2.61	-2.37	-1.30	-0.15	-0.76
BDB1-89.45	89.45	PAF	Himichopf - Mb.	li sst	Na-HCO <sub>3</sub> -SO <sub>4</sub>	8.96	3.416E-03	-3.70	0.16	8.77	6.077E-03	3.591	3.482	-3.49	0.00	-0.15	-0.01	-0.58	-0.57	-3.34	-3.10	-1.92	-0.05	-1.20
BDB1-93.24	93.24	PAF	Himichopf - Mb.	sa ma	Na-HCO <sub>3</sub> -SO <sub>4</sub>	8.78	2.467E-03	-3.65	-0.47	9.37	5.620E-03	2.555	2.242	-4.32	0.00	-0.15	0.01	-0.56	-0.56	-3.80	-3.56	-2.33	0.01	-0.69
BDB1-93.65	93.65	PAF	Himichopf - Mb.	sa ma	Na-HCO <sub>3</sub>	8.67	3.542E-03	-3.38	-0.39	9.15	5.689E-03	3.621	3.365	-3.90	0.00	-0.15	0.00	-0.57	-0.56	-3.98	-3.75	-2.51	0.02	-0.86
BDB1-97.10	97.10	PAF	Sissach - Mb.	lst	Na-HCO <sub>3</sub>	8.12	4.123E-03	-2.77	0.29	7.83	7.169E-03	4.102	4.211	-2.47	0.00	-0.15	-0.06	-0.63	-0.63	-2.62	-2.38	-1.74	-0.59	-1.70
BDB1-98.68	98.68	PAF	Sissach - Mb.	sa lst	Na-HCO <sub>3</sub> -SO <sub>4</sub>	9.13	2.761E-03	-3.97	0.04	9.07	7.225E-03	3.005	2.784	-3.90	0.00	-0.15	-0.15	-0.72	-0.72	-3.41	-3.18	-2.16	-0.21	-0.79
BDB1-100.63	100.63	PAF	Sissach - Mb.	sa ma	Na-HCO <sub>3</sub> -SO <sub>4</sub>	8.19	4.250E-03	-2.83	0.31	7.87	8.497E-03	4.231	4.297	-2.51	0.00	-0.15	-0.14	-0.71	-0.70	-2.50	-2.26	-1.71	-0.67	-1.75
BDB1-101.80	101.80	PAF	Sissach - Mb.	sa ma	Na-Mg-HCO <sub>3</sub>	8.03	5.894E-03	-2.54	0.52	7.50	1.113E-02	5.836	6.184	-2.00	0.00	-0.15	0.20	-0.37	-0.37	-2.35	-2.11	-1.80	-0.91	-1.99
BDB1-102.93	102.93	PAF	Sissach - Mb.	sa ma	Na-HCO <sub>3</sub> -SO <sub>4</sub> -Cl	9.27	1.933E-03	-4.28	-0.13	9.45	7.279E-03	2.187	1.864	-4.50	0.00	-0.15	-0.13	-0.71	-0.70	-3.60	-3.37	-2.42	-0.28	-1.43
BDB1-104.78	104.78	PAF	Sissach - Mb.	sa ma	Na-HCO <sub>3</sub> -SO <sub>4</sub> -Cl	9.14	2.452E-03	-4.04	-0.05	9.20	7.811E-03	2.678	2.427	-4.11	0.00	-0.15	-0.13	-0.70	-0.70	-3.47	-3.23	-2.36	-0.35	-1.43

## B.3 (cont.)

Sample	Depth m BHL	Strati- graphie	Member / Facies	Lithology	Water Type	MODELLED USING MEASURED pH				MODELLED USING pH ADJUSTED FOR CALCITE SATURATION														
						pH	TIC calc.	log P CO <sub>2</sub> (g)	SI calcite	pH	Ionic Strength	Alkalinit y	TIC	log P CO <sub>2</sub> (g)	SI calcite	SI aragonite	SI dolomite	SI dolomite(d)	SI magnesite	SI anhydrite	SI gypsum	SI celestite	SI strontianite	SI fluorite
						mmol/L	mmol/L	mmol/L		mol	meq/l	mmol/L	mmol/L	mmol/L	mmol/L	mmol/L	mmol/L	mmol/L	mmol/L	mmol/L	mmol/L	mmol/L	mmol/L	mmol/L
BDB1-108.24	108.24	OPA	sandy facies 2	clst & lst	Na-HCO <sub>3</sub> -SO <sub>4</sub> -Cl	8.98	3.61E-03	-3.86	-0.01	9.15	8.265E-03	3.919	3.602	-3.88	0.00	-0.15	-0.12	-0.72	-0.70	-3.68	-3.44	-2.58	-0.38	-0.75
BDB1-113.88	113.88	OPA	sandy facies 2	clst & lst	Na-HCO <sub>3</sub> -Cl-SO <sub>4</sub>	8.70	4.52E-03	-3.44	-0.05	8.88	1.056E-02	4.704	4.463	-3.51	0.00	-0.15	-0.02	-0.70	-0.65	-3.31	-3.08	-2.18	-0.38	-1.14
BDB1-114.80	114.80	OPA	sandy facies 2	clst & lst	Na-HCO <sub>3</sub> -Cl-SO <sub>4</sub>	8.91	2.79E-03	-3.92	-0.12	9.23	8.121E-03	3.015	2.715	-4.09	0.00	-0.15	-0.18	-0.99	-0.87	-3.52	-3.29	-2.51	-0.56	-1.02
BDB1-119.86	119.86	OPA	sandy facies 2	clst & lst	Na-HCO <sub>3</sub> -Cl-SO <sub>4</sub>	8.95	3.72E-03	-3.75	0.01	9.02	9.278E-03	3.986	3.720	-3.74	0.00	-0.15	-0.14	-0.69	-0.70	-3.52	-3.28	-2.49	-0.43	-1.13
BDB1-120.68	120.68	OPA	sandy facies 2	clst & lst	Na-HCO <sub>3</sub> -Cl-SO <sub>4</sub>	8.82	3.85E-03	-3.71	-0.01	9.02	1.006E-02	4.106	3.831	-3.72	0.00	-0.15	-0.12	-0.72	-0.70	-3.49	-3.25	-2.46	-0.44	-1.10
BDB1-128.24	128.24	OPA	sandy facies 2	clst & lst	Na-HCO <sub>3</sub> -Cl-SO <sub>4</sub>	8.92	3.66E-03	-3.76	-0.02	9.07	1.047E-02	3.926	3.636	-3.80	0.00	-0.15	-0.15	-0.76	-0.74	-3.49	-3.26	-2.51	-0.51	-1.23
BDB1-132.63	132.63	OPA	sandy facies 2	clst & lst	Na-HCO <sub>3</sub> -Cl-SO <sub>4</sub>	8.86	3.86E-03	-3.67	-0.19	9.22	1.166E-02	4.097	3.699	-3.95	0.00	-0.15	0.08	-0.88	-0.69	-3.50	-3.26	-2.25	-0.40	-1.61
BDB1-144.17	144.17	OPA	shaly facies 2	silt clst	Na-Cl-HCO <sub>3</sub> -SO <sub>4</sub>	8.95	3.07E-03	-3.81	-0.27	9.39	1.244E-02	3.289	2.849	-4.26	0.00	-0.15	0.04	-1.10	-0.82	-3.57	-3.33	-2.48	-0.64	-1.66
BDB1-161.18	161.18	OPA	shaly facies 2	silt clst	Na-Cl-HCO <sub>3</sub> -SO <sub>4</sub>	8.69	3.81E-03	-3.53	-0.24	9.13	1.467E-02	3.973	3.659	-3.87	0.00	-0.15	-0.04	-1.11	-0.86	-3.43	-3.20	-2.47	-0.74	-1.77
BDB1-166.08	166.08	OPA	shaly facies 2	silt clst	Na-Cl-HCO <sub>3</sub> -SO <sub>4</sub>	8.54	3.36E-03	-3.34	-0.49	9.18	1.519E-02	3.433	3.130	-4.00	0.00	-0.15	0.00	-1.57	-1.08	-3.37	-3.13	-2.37	-0.96	-1.68
BDB1-172.70	172.70	OPA	shaly facies 2	silt clst	Na-Cl-HCO <sub>3</sub> -SO <sub>4</sub>	8.50	3.06E-03	-3.47	-0.49	9.28	1.437E-02	3.143	2.810	-4.15	0.00	-0.15	0.01	-1.54	-1.05	-3.41	-3.18	-2.42	-0.95	-1.71
BDB1-175.33	175.33	OPA	sandy facies 1	clst & sst	Na-Cl-HCO <sub>3</sub> -SO <sub>4</sub>	8.75	3.75E-03	-3.62	-0.08	9.01	1.413E-02	3.943	3.701	-3.74	0.00	-0.15	0.00	-0.74	-0.65	-3.31	-3.07	-2.32	-0.56	-1.81
BDB1-178.73	178.73	OPA	sandy facies 1	clst & sst	Na-Cl-HCO <sub>3</sub> -SO <sub>4</sub>	8.68	2.98E-03	-3.70	-0.15	9.07	1.553E-02	3.123	2.902	-3.90	0.00	-0.15	-0.01	-0.89	-0.73	-3.23	-2.99	-2.12	-0.50	-1.77
BDB1-189.71	189.71	OPA	carb.-rich sandy f.	limestone	Na-HCO <sub>3</sub> -Cl-SO <sub>4</sub>	8.18	4.62E-03	-2.88	0.20	8.08	1.002E-02	4.620	4.627	-2.68	0.00	-0.15	-0.23	-0.40	-0.60	-2.68	-2.45	-2.16	-0.74	-2.24
BDB1-192.68	192.68	OPA	shaly facies 1	clst	Na-Cl-HCO <sub>3</sub> -SO <sub>4</sub>	8.81	2.83E-03	-3.78	-0.20	9.20	1.635E-02	2.993	2.713	-4.08	0.00	-0.15	0.01	-0.98	-0.77	-3.35	-3.11	-2.39	-0.71	-1.37
BDB1-198.13	198.13	OPA	shaly facies 1	clst	Na-Cl-SO <sub>4</sub>	8.83	2.46E-03	-3.89	-0.23	9.28	1.693E-02	2.644	2.314	-4.24	0.00	-0.15	-0.02	-1.06	-0.83	-3.30	-3.06	-2.37	-0.76	-1.37
BDB1-203.68	203.68	OPA	shaly facies 1	clst	Na-Cl-SO <sub>4</sub>	8.78	2.37E-03	-3.90	-0.17	9.20	1.796E-02	2.553	2.267	-4.16	0.00	-0.15	-0.09	-1.01	-0.83	-3.17	-2.93	-2.32	-0.79	-1.27
BDB1-209.00	209.00	OPA	shaly facies 1	clst	Na-Cl-SO <sub>4</sub>	8.80	2.48E-03	-3.82	-0.21	9.18	1.833E-02	2.642	2.355	-4.12	0.00	-0.15	-0.09	-1.08	-0.87	-3.14	-2.90	-2.28	-0.82	-1.29
BDB1-213.85	213.85	OPA	shaly facies 1	clst	Na-Cl-SO <sub>4</sub>	8.83	2.66E-03	-3.73	-0.15	9.04	1.986E-02	2.793	2.595	-3.93	0.00	-0.15	-0.07	-0.95	-0.79	-3.05	-2.81	-2.19	-0.76	-1.32
BDB1-217.98	217.98	OPA	shaly facies 1	clst	Na-Cl-SO <sub>4</sub>	8.78	2.76E-03	-3.73	-0.20	9.13	1.890E-02	2.903	2.662	-4.01	0.00	-0.15	-0.07	-1.04	-0.84	-3.12	-2.89	-2.27	-0.81	-1.28
BDB1-219.49	219.49	OPA	shaly facies 1	clst	Na-Cl-SO <sub>4</sub>	8.87	2.85E-03	-3.79	-0.21	9.22	1.757E-02	3.043	2.704	-4.10	0.00	-0.15	-0.03	-1.02	-0.81	-3.22	-2.98	-2.33	-0.78	-1.28
BDB1-221.28	221.28	OPA	shaly facies 1	clst	Na-Cl-SO <sub>4</sub>	8.84	2.77E-03	-3.81	-0.25	9.29	1.708E-02	2.964	2.593	-4.20	0.00	-0.15	0.03	-1.06	-0.80	-3.27	-3.04	-2.34	-0.78	-1.30
BDB1-225.18	225.18	OPA	shaly facies 1	clst	Na-Cl-SO <sub>4</sub>	8.72	2.72E-03	-3.76	-0.20	9.15	1.919E-02	2.863	2.613	-4.05	0.00	-0.15	-0.04	-1.02	-0.82	-3.12	-2.89	-2.27	-0.81	-1.18
BDB1-227.43	227.43	OPA	shaly facies 1	clst	Na-Cl-SO <sub>4</sub>	8.86	2.25E-03	-3.96	-0.23	9.32	1.828E-02	2.402	2.113	-4.33	0.00	-0.15	0.01	-1.04	-0.80	-3.20	-2.97	-2.25	-0.75	-1.17
BDB1-229.68	229.68	OPA	shaly facies 1	clst	Na-Cl-SO <sub>4</sub>	8.74	2.52E-03	-3.86	-0.19	9.21	1.915E-02	2.683	2.420	-4.14	0.00	-0.15	-0.08	-1.04	-0.85	-3.15	-2.91	-2.33	-0.84	-1.13
BDB1-231.18	231.18	OPA	shaly facies 1	clst	Na-Cl-SO <sub>4</sub>	8.83	2.45E-03	-3.85	-0.19	9.18	1.934E-02	2.593	2.351	-4.13	0.00	-0.15	-0.02	-0.97	-0.78	-3.12	-2.88	-2.23	-0.76	-1.17
BDB1-233.63	233.63	OPA	shaly facies 1	clst	Na-Cl-SO <sub>4</sub>	8.77	2.53E-03	-3.79	-0.15	9.08	1.962E-02	2.673	2.466	-4.00	0.00	-0.15	-0.04	-0.91	-0.76	-3.05	-2.81	-2.17	-0.74	-1.11
BDB1-235.14	235.14	OPA	shaly facies 1	clst	Na-Cl-SO <sub>4</sub>	8.83	2.41E-03	-3.85	-0.16	9.13	2.085E-02	2.553	2.332	-4.08	0.00	-0.15	-0.02	-0.92	-0.75	-3.06	-2.83	-2.13	-0.69	-1.05
BDB1-237.88	237.88	STF	Gross Wolf Mb.	arg ma	Na-Cl-SO <sub>4</sub>	8.83	1.95E-03	-4.02	-0.21	9.28	1.980E-02	2.092	1.852	-4.34	0.00	-0.15	-0.03	-1.03	-0.82	-3.07	-2.84	-2.14	-0.74	-1.05
BDB1-243.37	243.37	STF	Gross Wolf Mb.	lst	Na-HCO <sub>3</sub> -Cl-SO <sub>4</sub>	8.28	2.19E-03	-3.35	-0.02	8.45	6.571E-03	2.209	2.162	-3.38	0.00	-0.15	-0.38	-0.99	-0.97	-2.80	-2.57	-2.18	-0.86	-3.15
BDB1-245.54	245.54	STF	Rietheim Mb.	bit ma	Na-Cl-SO <sub>4</sub>	8.69	2.86E-03	-3.73	-0.19	9.12	1.983E-02	3.013	2.762	-4.00	0.00	-0.15	-0.09	-1.04	-0.85	-3.09	-2.86	-2.23	-0.79	-1.61
BDB1-246.34	246.34	STF	Rietheim Mb.	bit ma	Na-Cl-SO <sub>4</sub>	8.80	3.21E-03	-3.67	-0.13	9.04	1.837E-02	3.374	3.141	-3.85	0.00	-0.15	-0.02	-0.85	-0.72	-3.12	-2.88	-2.20	-0.67	-1.72